İSTANBUL TECHNICAL UNIVERSITY ★ INSTITUTE OF SCIENCE AND TECHNOLOGY

CYCLIC BEHAVIOR OF THIN STEEL PLATE SHEAR WALLS WITH SEMI-RIGID BEAM-TO-COLUMN CONNECTIONS

Ph.D. Thesis by

Cüneyt VATANSEVER, M.Sc.

Department : Civil Engineering

Programme: Structural Engineering

FEBRUARY 2008

İSTANBUL TECHNICAL UNIVERSITY ★ INSTITUTE OF SCIENCE AND TECHNOLOGY

CYCLIC BEHAVIOR OF THIN STEEL PLATE SHEAR WALLS WITH SEMI-RIGID BEAM-TO-COLUMN CONNECTIONS

Ph.D. Thesis by

Cüneyt VATANSEVER, M.Sc.

(501002105)

Date of submission : 1 November 2007

Date of defence examination: 15 February 2008

Supervisor (Chairman): Prof. Dr. Nesrin YARDIMCI

Members of the Examining Committee Prof.Dr. Hasan BODUROĞLU (ITU)

Prof.Dr. Erdoğan UZGİDER (ITU)

Prof.Dr. Gülay ALTAY (BU)

Prof.Dr. Tuncer ÇELİK (Beykent U.)

FEBRUARY 2008

<u>İSTANBUL TEKNİK ÜNİVERSİTESİ ★ FEN BİLİMLERİ ENSTİTÜSÜ</u>

YARI RİJİT KİRİŞ-KOLON BİRLEŞİMLİ İNCE LEVHALI ÇELİK PERDELERİN ÇEVRİMSEL DAVRANIŞI

DOKTORA TEZİ

Y. Müh. Cüneyt VATANSEVER
(501002105)

Tezin Enstitüye Verildiği Tarih : 1 Kasım 2007
Tezin Savunulduğu Tarih : 15 Şubat 2008

Tez Danışmanı :	**Prof.Dr. Nesrin YARDIMCI**
Diğer Jüri Üyeleri	**Prof.Dr. Hasan BODUROĞLU (İ.T.Ü.)**
	Prof.Dr. Erdoğan UZGİDER (İ.T.Ü.)
	Prof.Dr. Gülay ALTAY (B.Ü.)
	Prof.Dr. Tuncer ÇELİK (Beykent Ü.)

ŞUBAT 2008

FOREWORD

In Turkey, unstiffened thin steel plate shear walls are relatively new system to resist lateral loads induced by earthquake and winds. With this research project, I hope the structural engineers in Turkey will take an opportunity to know the steel plate shear wall systems. This study which was performed to provide powerful information about these systems as well includes an experimental research and numerical investigation.

I would like to express my sincere gratitude to my thesis supervisor, Prof. Dr. Nesrin Yardımcı, for her continuous guidance, support and encouragement that she provided throughout the preparation of this thesis.

I would like to also thank Prof. Dr. Gülay Altay, Prof. Dr. Hasan Boduroğlu, Assoc. Prof. Dr. Cavidan Yorgun, Assoc. Prof. Dr. Oğuz Cem Çelik and Assist. Prof. Dr. Ercan Yüksel for their valuable suggestions.

I would like to acknowledge Assist. Prof. Konuralp Girgin, Research Assist. Yavuz Durgun and Research Assist. M. Günhan Aksoylu for their valuable opinions.

I would like to also special thanks Prof. Dr. Dursun Z. Şeker, Research Assist. E. Özgür Avşar and Research Assist. Umut Aydar for their contributions to photogrammetric sections of the thesis.

The experimental section of this thesis was conducted at the Structural and Earthquake Engineering Laboratory of ITU. This phase of this research would not have been possible without the assistance of the laboratory technicians. A special thanks goes to Mahmut Şamlı, Zeki Sivrikaya and Hakan Saruhan, C.E., M. Sc. for their help with machining, test setup and welding. I would like to thank Research Assist. Kıvanç Taşkın for his devoted help during the tests.

This research project was also supported by the following companies which made this investigation possible.

- Arcelor International Çelik Dış Tic. A. Ş.
- ROZAK DEMİR PROFİL TİC. A. Ş.
- ATAÇELİK YAPI ÜRETİM A. Ş.
- TAŞDİLDİREN ÇELİK KONSTRÜKSİYON SAN. TİC. LTD. ŞTİ.
- degussa. Consruction Chemicals Yapkim Yapı Kimya Sanayi A. Ş.
- TABOSAN MÜHENDİSLİK İMALAT VE MONTAJ A. Ş.
- SÖNMEZ İNŞAAT SANAYİ VE TİCARET LTD. ŞTİ.
- YÜKSEK YAPI İNŞAAT TAAHHÜT TURİZM TİC. SAN. LTD. ŞTİ.

I would like to thank the executive officers and workers of these companies for their unlimited supports and efforts.

Heartfelt thanks are also due to my wife Gülşah Vatansever, my son Efe Berke Vatansever, my mother Ayşe Vatansever and my father Fikret Vatansever for their morale support and assistance during my difficult times.

February 2008 Cüneyt VATANSEVER

TABLE OF CONTENTS

ABBREVIATIONS

AISC	: American Institute of Steel Construction
ASTM	: American Society for Testing and Materials
ATC	: Applied Technology Council
BF	: Bare Frame
DSC	: Double Skin Composite
DSPW	: Ductile Steel Plate Wall
EC3	: Eurocode 3
FEM	: Finite Element Model
IPFI	: Improved Plate-Frame Interaction
ITU	: Istanbul Technical University
LYP	: Low Yield Point
MTS	: Material Test System
PFI	: Plate-Frame Interaction
SEAOC	: Structural Engineers Association of California
SPSW	: Steel Plate Shear Wall
STEEL	: Structural and Earthquake Engineering Laboratory
TS	: Turkish Standard
TSPSW	: Thin Steel Plate Shear Wall
UB	: University of Buffalo

LIST OF TABLES

LIST OF FIGURES

LIST OF SYMBOLS

$\mathbf{A_b}$	: Area of the beam section
$\mathbf{A_c}$	: Area of the column section
$\mathbf{C_1, C_2}$	: Modification factors
G	: Shear modulus of the infill plate material
h	: Distance between top and bottom beam centers
$\mathbf{I_c}$	: Moment of inertia of the column section
$\mathbf{K_\varphi}$	: Initial joint rotational stiffness
$\mathbf{K_{\varphi,p}}$	: Plastic rotational stiffness
$\mathbf{K_{\varphi,y}}$	: Post-yielding rotational stiffness
$\mathbf{K_e}$	: Elastic stiffness
$\mathbf{K_f}$	: Stiffness of the frame
$\mathbf{K_p}$	: Stiffness of the infill plate
$\mathbf{K_{p,1}}$	: Inial stiffness of the infill plate
$\mathbf{K_{p,2}}$	: Reduced stiffness of the infill plate
L, l	: Distance between column centers
$\mathbf{l_{eff}}$	: Effective infill plate width
M	: Bending moment
$\mathbf{M_{con}}$	: Bending moment at connection section
$\mathbf{M_{j,p}}$	: Plastic flexural resistance
$\mathbf{M_{j,y}}$	: First yield moment
$\mathbf{M_{pcon}}$	: Plastic moment of the beam-to-column connection
$\mathbf{M_o}$	: Reference bending moment
n	: Shape factor
P	: Shear force
$\mathbf{P_{cr}}$	: Critical shear force
$\mathbf{P_{fu}}$	: Shear strength of the frame
$\mathbf{P_p}$	: Shear force of the infill plate
$\mathbf{P_{pcr}}$	: Critical shear force of the infill plate
$\mathbf{P_{pu}}$	: Shear strength of the infill plate
$\mathbf{P_{pu,1}}$	: Initial shear strength of the infill plate
$\mathbf{P_{pu,2}}$	: Post-yield shear strength of the infill plate
$\mathbf{Q_y}$	: Yield force
$\mathbf{t, t_p}$	: Thickness of the infill plate
Δ	: Lateral displacement of frame
α	: Orientation angle of the strips to the vertical
θ	: Principal angle of tension field direction
φ	: Rotation
τ	: Shear stress
δ^*	: Control deformation
τ_{cr}	: Critical shear stress
Δ_{fe}	: Limiting elastic shear displacement of frame

φ_o	: Permanent rotation
Δ_p	: Shear displacement of the infill plate
Δ_{pcr}	: Critical shear displacement of the infill plate
Δ_{pe}	: Limiting elastic shear displacement of infill plate
$\Delta_{pe,1}$	: Initial yield displacement of infill plate
$\Delta_{pe,2}$	: Post-yield displacement of infill plate
Δ_{ppb}	: Shear displacement of postbuckled component of shear force
σ_t	: Stress in tension field
σ_x	: Tensile stress in x direction
τ_{xy}	: Shear stress in y direction
σ_y	: Tensile stress in y direction
δ_y	: Yield deformation
τ_{yx}	: Shear stress in x direction

CYCLIC BEHAVIOR OF THIN STEEL PLATE SHEAR WALLS WITH SEMI-RIGID BEAM-TO-COLUMN CONNECTIONS

SUMMARY

An experimental research which mainly includes three, 1/3 scale, one-storey, single bay test specimens, was performed under cyclic loading in order to compare the cyclic response of thin steel plate shear wall specimens that were different from each other. One more bare frame specimen was also tested to show the performance of the semi-rigid beam-to-column connections with flush end plates. Additionally, the existing simplified method which was called Plate Frame Interaction to use for predicting the response of thin steel plate shear walls and characteristic values of the systems such as base shear and displacements corresponding to yield point and ultimate strength was improved taking the beam-to-column joint behavior into account.

The main test specimens used for this purpose consist of one bare frame representing the baseline case for the shear wall tests, a traditional thin steel plate wall including the infill plate connected to boundary frame on all edges and an innovative one with the panel attached to the frame beams only. All infill plates were 0.50mm thick and had a height of 900mm and width of 1520mm. Self drilling screws were utilized to provide the connection between the infills and surrounding frame members. Also, a fish plate welded to the flange of each frame member was used.

In this experimental study, all of the specimens were tested in accordance with the ATC-24, Guidelines for Cyclic Seismic Testing of Components of Steel Structures, by Applied Technology Council.

Several numerical analyses using the models of the specimens that were previously tested by other researchers were also carried out to verify the analytical models of test specimens. One of them was selected as a preliminary model to develop strip and finite element models. The parallel strip model which is simpler than the finite element model was developed using computer software SAP2000 that is able to conduct nonlinear pushover analysis. For the complicated nonlinear finite element models of thin steel plate shear walls ABAQUS, very detailed computer program, was also employed.

In addition to main experimental study, several ancillary investigations were carried out to complement the shear wall tests. Firstly, in order to determine the actual yield and ultimate stresses of the infill panels and beam end-plates, tension coupon tests were conducted. Then, another test to determine the failure modes and the ultimate tensile force of the self-drilling screw connection type were also performed. The

results which were obtained by the latter test were used to determine the number of screws to provide the connection between the infill panel edges and fish plates.

To provide the useful information about the test procedure before the experiments to be conducted both the simplified strip and nonlinear finite element models of the specimens were also developed. Beam-to-column connection behavior was also taken into account in the structural analyses of the models. The initial stiffness and moment carrying capacity of the connection, designed as semi-rigid and partial strength connection type, were determined in accordance with the Eurocode 3. For the representation of semi-rigid beam-to-column connection behavior, four-parameter nonlinear representation of the moment-rotation curve was employed. This was subsequently added to the nonlinear finite element models of the specimens.

After the experimental observations during testing of the specimens were described, the data from the measurement devices such as strains, displacements and loads were evaluated to generate the information about the behavior of the specimens and response of the infills. Therefore, several properties of systems are extracted from the experimental data, namely, initial stiffness, yield base shear and displacements, cumulative energy dissipation and displacement ductility. Furthermore, the orientation and the magnitude of the principal stresses and strains in the infill plate during linear and nonlinear portions are examined and the variation of the strain magnitude and energy dissipation across the infills is investigated.

Consequently, the results obtained from both the tests and the analytical models of the specimens were comparatively discussed and some recommendations for the further research were also made.

YARI RİJİT KİRİŞ-KOLON BİRLEŞİMLİ İNCE LEVHALI ÇELİK PERDELERİN ÇEVRİMSEL DAVRANIŞI

ÖZET

Birbirinden farklı ince levhalı çelik perde numunelerin tekrarlı yükler altında davranışlarını karşılaştırmak amacıyla, esas olarak 1/3 ölçekli, tek katlı ve açıklıklı üç adet test numunesinden oluşan bir deneysel çalışma yürütülmüştür. Ayrıca, kiriş yüksekliği boyunca uç levhalı yarı-rijit kiriş-kolon birleşimlerinin davranışını görmek üzere bir adet çelik çerçevenin de testi gerçekleştirilmiştir. Buna ek olarak, Panel Çerçeve Etkileşimi adı verilen mevcut basit bir metot, ince levhalı çelik perdelerin davranışlarını ve bu sistemlere ait, akma durumuna karşı gelen yer değiştirme ve taban kesme kuvveti ile dayanım gibi karakteristik değerleri tahmin edebilmek amacıyla, kiriş-kolon birleşimlerinin davranışları da esas alınarak genişletilmiştir.

Ana deney numuneleri, perdelere temel teşkil eden bir adet çelik çerçeve, panelin çerçeve elemanlarına dört kenarından bağlandığı geleneksel ince levhalı çelik perde ve panelin sadece çerçeve kirişlerine bağlandığı özel ince levhalı çelik perdelerden oluşmaktadır. Tüm paneller 0.50mm kalınlıklı ve 900mm yükseklik ile 1520mm genişliğe sahiptir. Çelik panelin çerçeve elemanlarına birleşiminde matkap uçlu vidalardan yararlanılmıştır. Ayrıca bu birleşim için her bir çerçeve elemanının başlığına kaynaklı birer birleşim levhası kullanılmaktadır.

Bu deneysel çalışmada, tüm numuneler ATC-24 (Guidelines for Cyclic Seismic Testing of Components of Steel Structures, by Applied Technology Council) esas alınarak test edilmiştir.

Deney numunelerinin analitik modellerini doğru bir yaklaşımla oluşturabilmek amacıyla, daha önce başka araştırmacılar tarafından test edilen numunelerin kullanıldığı pek çok sayısal analiz gerçekleştirilmiştir. Bunlardan biri çubuk ve sonlu eleman modeller oluşturmak üzere örnek olarak seçilmiştir. Perdenin paralel çubuk modelleri doğrusal olmayan statik itme analizlerinin gerçekleştirildiği SAP2000 bilgisayar yazılımı kullanılarak geliştirilmiştir. Perdenin daha karmaşık olan doğrusal olmayan sonlu eleman modelleri için de geniş kapsamlı bir bilgisayar programı olan ABAQUS'ten yararlanılmıştır.

Ana deneysel çalışmaya ek olarak, bu deneyleri tamamlayıcı birkaç yardımcı araştırma da gerçekleştirilmiştir. İlk olarak, panel ve kiriş uç levhalarına ait malzemelerin gerçek akma ve çekme dayanımlarını tespit etmek amacıyla çekme testleri, ikinci olarak da, matkap uçlu vidaların kullanıldığı birleşimlerin göçme modlarını ve taşıyabileceği en büyük kesme kuvvetini tespit etmek üzere bir seri test yürütülmüştür. İkinci olarak yürütülen deneyler sonunda elde edilen sonuçlar, panel kenarları ile birleşim levhalarının bağlantısı için vida sayısının belirlenmesinde kullanılmıştır.

Deneylere başlamadan önce test prosedürü ile ilgili gerekli bilgileri sağlayabilmek için numunelerin hem basit çubuk modelleri hem de doğrusal olmayan sonlu eleman modelleri oluşturulmuştur. Yapısal analizlerde kiriş-kolon birleşiminin davranışı da dikkate alınmıştır. Yarı-rijit ve kısmi dayanımlı olarak tasarlanan birleşimin başlangıç rijitliği ve moment taşıma kapasitesi Eurocode 3'e göre belirlenmektedir. Yarı-rijit kiriş-kolon birleşim davranışının temsil edilmesinde, dört parametreli doğrusal olmayan moment-dönme eğrisinden yararlanılmıştır. Bu birleşim modeli aynı zamanda numunelerin doğrusal olmayan sonlu eleman modellerinin oluşturulmasında da yer almıştır.

Numunelerin testleri sırasında yapılan deneysel gözlemlerin ardından panel ve numunelerin davranışları ile ilgili bilgilerin elde edilmesi amacıyla, ölçüm aletleri vasıtasıyla alınan bilgiler, örneğin şekil değiştirmeler, yer değiştirmeler ve yük değerleri değerlendirilmiştir. Böylece, sistemlere ait, başlangıç rijitliği, akma durumuna karşı gelen taban kesme kuvveti ve yer değiştirmeler, toplam enerji sönümleme miktarı ve yer değiştirme sünekliği gibi özellikler deneysel veriler kullanılarak elde edilmiştir. Bununla birlikte, doğrusal ve doğrusal olmayan deney bölümlerinde paneldeki asal gerilme ve şekil değiştirme miktarları ile yönleri incelenmiş ve enerji sönümleme durumu değerlendirilmiştir.

Sonuç olarak, numunelerin hem testleri hem de analitik modellerden elde edilen sonuçlar karşılaştırmalı olarak irdelenmiş ve gelecek araştırmalar için bazı öneriler yapılmıştır.

1. INTRODUCTION

Thin steel plate shear walls (TSPSWs) are very effective and economical lateral load-resisting systems.

A thin steel plate shear wall is composed of vertical steel plates which are named as infill panels and columns and beams connected to steel panels. The beam-to-column connections may be either moment-resisting and semi-rigid joint types or simple joint type. Infill steel panels are generally attached to the surrounding frames by either fillet welds or bolts. Epoxy has also been used for the connection between the infills and the fish plates welded to the flanges of beams and columns **(Berman and Bruneau, 2005)**.

The panels themselves have been able to either stiffened or unstiffened, depending on the design philosophy.

Actually, the most important reason why the steel plate shear walls have been prefered as a lateral load-resisting system is that they have superior ductility, a robust resistance to degradation under cyclic loading, high initial stiffness, and when moment-resisting beam-to-column connections are present, inherent redundancy and a capacity for significant energy dissipation.

Most existing buildings with steel plate shear walls were designed such that shear panels should not be out-of-buckled. Thus, steel panels were stiffened in different ways such as vertically and/or horizontally using angles or steel bars. **Wagner (1931)**, however, demonstrated that buckling does not necessarily represent the limit of useful behaviour and that the post-buckling strength of an unstiffened shear panel can be considerable. At the point of buckling, the load resisting mechanism changes from in-plane shear to an inclined tension field action that develops along the elongated diagonal. When the panel is thin, buckling will occur at very low loads and resistance of the panel is dominated by tension field action.

It is believed that full or partial moment-resisting (semi-rigid beam-to-column connections) joints would increase the energy absorption characteristic of infilled frames by reducing pinching in the load-deformation hysteresis loops. Either some previously proposed analytical models and analysis methods would not take the effect of beam-to-column connections types in the steel plate shear walls into account or some would consider this effect in any way. In some researches that were conducted, this effect was considered in the analytical models using coefficients to need to be developed by reference to available experimental results **(Sabouri-Ghomi et al., 2005)** or frame models with semi-rigid beam-to-column connections such as bounding surface model that is originally formulated by Dafalias and Popov (1976) **(Berman and Bruneau, 2005)**. At this point, therefore, additional experimental and analytical investigations would be useful to better predict the behaviour of steel infilled frames during unloading and reloading regions. Additionally, there is no any available experimental data for thin steel plate shear walls with infill panels which are connected to beams only due to that conventional TSPSWs have usually been used in all experimental studies that have been carried out until now. More detailed experimental and analytical data from new innovative specimens are needed to ascertain that the presence of full or partial moment-resisting (semi-rigid beam-to-column connections) joints remarkably improve the overall load-deformation behaviour of these structural systems and to clearly understand the differences between the load-deformation behaviors of two different type of TSPSWs.

1.1 Objectives and Scope

The research reported herein deals with unstiffened TSPSWs which are composed of beams, columns and infill panels.

The primary objective of this research is to investigate the behavior of two types of the unstiffened thin steel plate shear walls under cyclic lateral in-plane loading, considering the post-buckling behavior of infill panels with two different panel-to-boundary frame connection types. For this purpose, six specimens were designed in total. While the infill plates in two TSPSW specimens are connected to the surrounding frame on all sides, infills in other two specimens have a connection on upper and lower edges only (connected to beam flanges only). Two bare frame specimens are also included. Two different beam-to-column connections, with flush end plate and header plate, were employed. For fastener the most applicable to thin infill panel-to-boundary frame connection, self-drilling screws are selected.

Actually, four objectives will be considered in this study. The first one is to evaluate an existing analytical model used for estimating the shear capacity of steel plate shear walls under lateral loads. The second objective is to assess how the storey shear forces are shared between the panels and the partial moment-resisting frame for two types of TSPSWs. The third one is to develop a nonlinear finite element model of TSPSWs which includes the effect of the rigidity of beam-to-column connections on the behaviour of steel infilled frames. The ability of the shear wall to dissipate energy during inelastic cyclic loading, and the contribution of partially moment-resisting frame thereto, are also of interest.

The fourth objective of this research is, in parallel with the experimental work, to develop an analytical tool for predicting the behaviour of steel plate shear wall subjected to lateral loading up to the ultimate capacity. Also, a numerical investigation will be made to verify test results.

1.2 Organization of the Thesis

This section provides a description of the manner in which the remainder of the manuscript is organized.

Chapter 2 includes a chronological review of the previously published researches on steel plate shear wall behaviour. Both analytical and experimental investigations are summarized in this chapter.

The aim of the Chapter 3 is to provide a preliminary investigation into developing both the nonlinear finite element model and simplified strip model of the steel plate shear walls. Finite element model is developed using ABAQUS 6.4 Student Edition which is very complicated finite element analysis program limited to 1000 nodes. SAP2000 structural analysis program which is simpler than ABAQUS and more useful in structural engineering field in practice is employed for developing the strip model of the TSPSWs. For this purpose, the specimens which were tested in previous experimental studies are considered. One of the specimens used in the tests conducted at University of Maine by **Chen (1991)** is selected as a preliminary model and presented in this section. The results from experimental studies and those from both finite element and strip model analyses are compared and discussed. The studies performed in this section should be assessed as a beginning level for clearly understanding ABAQUS and the behavior of the TSPSWs.

An overview of the experimental programme is provided in Chapter 4. The objectives of the tests, a description of the specimens' details, and the test design considerations and the limitations are described. The semi-rigid beam-to-column connection design and rigidity of the joint are defined. The moment-rotation curve of the joint employed in finite element models of steel plate shear wall specimens is determined. The assumptions made in this stage are also presented. Instrumentation, photogrametric measurements data acquisition are defined in detail.

In Chapter 5, the results of tension coupon tests for determining the properties of infill panel materials and beam end plates are summarized in a tabular form. Self-drilling screws which were used in the connection between the infill panels and fish plates were described and tested for their failure modes under pure shear force. The results of the tests are presented.

Chapter 6 consists of preliminary numerical analyses of test specimens and their results. In order to properly design the experimental research, two types of analytical models of the specimens such as strip and finite element models are utilized. ABAQUS, a nonlinear general-purpose program is used for finite element models of the specimens while SAP2000 which is commonly used in the field of the structural engineering is utilized in developing the strip models of the specimens. A summary of the results from the preliminary numerical analyses are also presented.

Chapter 7 deals with the experimental studies. This section begins with a discussion of the estimation of yield displacements and the loading protocol used for quasi-static testing. Then, complete descriptions of observations made during the testing of each specimen are given, accompanied by several photos taken during the testing.

Chapter 8 is composed of evaluation of strain data obtained from the tests performed using cyclic loading. Strain data from each specimen is evaluated and the results are presented. An existing simplified method which is called plate-frame interaction (PFI) method that originated by **Sabouri-Ghomi et al. (2005)** is also improved. Then, a method which can be used for the prediction of the behavior of TSPSWs is proposed.

In Chapter 9, conclusions based on the information obtained previous chapters are presented. Recommendations for further research program are given.

2. LITERATURE REVIEW

Utilization of steel plate shear walls began in early 1970's. Initially, stiffened steel shear walls were used in Japan in new construction and in the USA for seismic retrofit of the existing buildings as well as in new buildings **(Astaneh, 1989)**. Early steel shear walls have been designed such that shear buckling of the infill plate should not be occurred. Thus, in order to prevent the shear buckling of the steel panels vertical and horizontal stiffener members attached to the surfaces of the steel infills were used. In that design philosophy, post-buckling behavior of the steel panel was neglected.

For many years, it has been known that lateral load carrying capacity of the infill panels are not limited to elastic shear buckling of them. When they are designed properly, after buckling, the load-resisting system of the steel plate changes from in-plane shear to an inclined tension fields. A theory utilizing the post-buckling strength which develops in thin panels subjected to a shear force was firstly presented by Wagner in 1931 **(Wagner, 1931)**. Wagner showed that a thin web does not fail when it buckles and after buckling, the panel continues to carry the shear forces by means of a series of the inclined tension fields. After works of **Wagner (1931)**, **Kuhn et al. (1952)** proposed a theory of "incomplete diagonal tension". They studied the intermediate cases between the pure diagonal tension and pure shear resistant. This theory is based on the assumption that the shear capacity of the panels results from both pure shear and tension field action. In 1961, Basler was firstly considered the post-buckling strength of the steel plates normally used in plate girders **(Basler, 1961)**. With the considering this post-buckling strength, a theory to evaluate the ultimate shear capacity of a steel plate girder web by superimposing the state of stress up to the point of buckling and the post-buckling benefit was developed by Basler. Basler's theory has been widely accepted and has formed the basis for the design of steel plate shear walls in many modern design standards.

A chronological review of the previously published research on steel plate shear wall behaviour is presented. Both analytical and experimental investigations are summarized below.

2.1 Takahashi et al. (1973)

In early 1970's, **Takahashi et al. (1973)** conducted a series of experimental and finite element analytical studies on stiffened thin steel plate shear walls. The objective of the research was to investigate the behaviour of thin stiffened steel plate shear wall systems having various configurations of stiffened infill panels as an alternative solution to the stiff concrete shear walls commonly designed as lateral load-resisting structures in the buildings.

The experimental programme can be divided into two parts. In the first series of tests, twelve one-storey specimens with overall dimensions of 2100 mm width by 900 mm height were tested. The parameters investigated were the strength, hysteresis curve and post-buckling behaviour of steel panels together with the spacing and width of stiffeners on both sides of steel panels.

The first test results demonstrated that all the specimens underwent large deformations exhibiting a very stable and ductile behaviour. Some of the panels buckled elastically because the heights of the transverse stiffeners were small. Partial buckling also occurred in the specimens that had relatively large spacing between stiffeners. In some other specimens, plastic buckling occurred. In general, the hysteresis curves were S-shaped for most specimens, except in a few cases where the specimens were heavily reinforced with wide stiffeners.

In the second series of tests, two full-scale one-bay two storey steel plate shear wall specimens, taken from a proposed 32-storey building design were tested under cyclic horizontal load. The test specimens differed from one another in that one was built without openings and the other with an opening in each storey. To provide similar shear rigidity and strength, the specimen with openings was made of 6.00 mm thick steel plate while the specimen without opening was made of 4.50 mm thick panels.

Both full-scale specimens show robust and stable hysteresis loops and large energy absorption capacity. As the applied lateral load approached the yielding strength of the specimens partial buckling of the infill plates was observed at several points. However, the influence of these partial buckles on the rigidity of the specimens was very small. A theoretical finite element analysis of the specimens was carried out under the assumptions of no out-of-plane buckling for infill plates and bi-linear stress-strain relationship for the steel material. The experimental load-deflection graphs agreed reasonably well with analytical results. The yielding shear stress obtained from the Von Mises equation was in good agreement with experimental results. Tearing of the welds at the base of the columns occurred at the final stage of loading.

The authors concluded that the equations presented for the design of stiffeners for thin steel plate shear walls are satisfactory provided that plate buckling would not occur until the plates develop their shear yield strength. Furthermore, they concluded that the conventional shear theory, wherein the horizontal shear is transferred by beam action alone, can be conveniently used to calculate the stiffness and yield strength of the stiffened shear panels.

2.2 Mimura and Akiyana (1977)

After the work by Takahashi et al., Mimura and Akiyana conducted a research similar to previous work by developing general expressions for predicting the monotonic and cyclic behaviour of steel plate shear walls. The main objective was to study the load-deflection behaviour of a steel plate shear wall frame in which the shear buckling load of the plates was considerably less than their shear yield strength.

In their derivation, they assumed that the overall strength of a steel plate shear wall frame is determined by a load required to induce elastic buckling of the infill panels plus the post-buckling strength of the shear panels and boundary frame. Elastic-plastic behaviour was assumed to establish the monotonic load-deflection curve of the frame. They also developed a theoretical hysteresis model.

2.3 Agelidis and Mansell (1982)

Agelidis and Mansell (1982) performed a feasibility study of analysis and design of tall service cores for multi-storey buildings constructed from orthotropically stiffened steel plate shear walls. The investigation also included cost estimation of details for stiffeners, plate and stiffener splices, floor beam and slab supporting systems, core corners and connections between core panels and connecting beams.

A two-dimensional linear plane-stress finite element analysis was carried out to acquire stresses and maximum deflections of the core under dead, live and wind load combinations. The geometric orthotropy of the stiffened steel plates was modeled by material orthotropy, so that the stiffeners were assumed to be "smeared" throughout the panels' width, giving different moduli of elasticity in the two principal directions. The cross walls forming the flanges of the core were modelled by beam elements with the same cross-sectional area and material properties.

The maximum lateral deflection of the core computed from finite element analysis agreed well with the results obtained by a manual method used first for a preliminary design. The effects of connecting beam stiffness and plate cross-section on the maximum longitudinal stresses in the flange walls and web walls as well as maximum bending moments in the beams and maximum lateral deflection of the core were also investigated.

2.4 Thorburn, Kulak and Montgomery (1983)

Thorburn et al. (1983) performed an experimental study on the use of steel plates framed by structural columns and beams to form a shear wall system. The main purpose of this experimental work was to briefly review the steel shear wall systems in use in that time and to develop an analysis technique suitable for studying the transfer of forces in steel wall subjected to shear.

Thorburn et al. (1983) developed an analytical method to study the shear resistance of thin unstiffened steel plate shear walls. The model was based on the theory of pure diagonal tension by **Wagner (1931)** which did not account for any shear carried by the infill plates prior to shear buckling. The so-called strip model represented the shear panels as a series of inclined strip members, capable of transmitting tension forces only, and oriented in the same direction as the principal tensile stresses in the panel. Each strip was assigned an area equal to the product of the strip width and the plate thickness.

The derivation of the angle of inclination of the tension strips was based on the Principle of Least Work. A one-storey one-bay steel panel, surrounded by beams and columns, was subjected to pure shear. The columns were assumed to be continuous while the beam-to-column connections were considered to be pinned. This assumption ensured that no moment was transferred from the rigid joints to the beams. The effect of column bending was also excluded from the derivation. The storey beams were assumed to be infinitely rigid in bending. This was due to the assumption that tensionfield forces for any two adjacent storeys differ very little and oppose one another, therefore the net vertical forces acting on the beam would be negligible. Two extreme cases were considered for the column elements:

1) columns with infinite bending stiffness ensuring a uniformly distributed tension zone over the entire panel,

2) completely flexible columns where no anchorage to the inclined strip tensile forces through the columns was considered.

Thorburn et al. (1983) also conducted a parametric study to investigate the effects of infill plate thickness, storey height, storey width and column stiffness on the strength and stiffness characteristics of a thin unstiffened steel plate shear panel. The relationships obtained for each parameter can be given as a following summary:

- The panel stiffness increased linearly with increasing infill plate thickness. The slope of the line was a function of the panel geometry.

- As the panel height was increased, the lateral stiffness of the panel decreased. The relationship between the log of the storey height and panel stiffness was linear.

- Panel stiffness increased linearly as the panel length increased until the aspect ratio, L/h, was 1.0. After this point the panel stiffness increased with increasing panel width.

There was a linear relationship between the panel stiffness and the log of column rigidity.

2.5 Timler and Kulak (1983)

In order to investigate the adequacy of the strip model proposed by Thorburn et al. in 1983, **Timler and Kulak (1983)** tested a large scale, single storey steel plate shear wall specimen under cyclic loading to the serviceability limit and pushover loading to failure. No external axial pre-loading was induced to the columns prior to the test. The main objectives of this investigation were to observe the tension field in a test specimen subjected to shear force, compare the results from experimental study and those from proposed analytical model and recommend additional design and fabrication techniques.

The derivation of the angle of inclination for diagonal tension strips developed by **Thorburn et al. (1983)** was re-evaluated. A revised formula for calculating the angle of inclination of tension strips in multi-storey buildings considering the bending effects of columns. The simplified analytical model, strip model, developed by **Thorburn et al. (1983)** was found to be satisfactory in predicting the overall load-deflection response of the specimen, although the predicted elastic stiffness of the specimen was slightly stiffer than the measured value.

The measured axial strains in the columns were in good agreement with the predicted values. Less satisfactory correlation was obtained between measured and computed bending strains. In each case, the measured strains were lower than those predicted.

2.6 Tromposch and Kulak (1987)

A single-storey full-scale unstiffened steel plate shear wall specimen which is similar to the one used in the experimental study by **Timler and Kulak (1983)** was tested by Tromposch and Kulak in 1987. The objective of the test was to verify the inclined tension bar model proposed by **Thorburn et al. (1983)** under quasi static, fully reversed cyclic loading. To consider the effects of gravity loads applied to a structure, an axial pre-load was applied to the columns through high strength prestressing bars anchored at both ends of the columns.

The inclined tension bar model was found to be adequate in predicting the strength and ultimate capacity of the unstiffened steel plate shear wall specimen. The effects of beam-to-column connections, initial column axial loads and residual stress induced in the infill plate due to the welding process were found to be significant in predicting the load deflection response of the steel plate shear wall panel.

The hysteresis loops developed in the specimen were pinched, but they were stable. An analytical method based on the model described by **Mimura and Akiyana (1977)** was proposed to predict the hysteresis behaviour of and unstiffened steel plate shear wall panel.

Further parametric studies showed that frames with fixed beam-to-column connections can dissipate as much as three times more energy as that dissipated by frames with simple pinned beam-to-column connections. The beneficial post-buckling strength and the relatively stable hysteretic characteristics of unstiffened thin steel panels were amply demonstrated.

2.7 Roberts and Sabouri-Ghomi (1991)

A nonlinear analysis of the dynamic response of thin steel plate shear walls, with fixed beam-to-column connections, based on a finite difference solution of the governing differential of motion was performed by Sabouri-Ghomi and Roberts. The hysteretic characteristics of steel plate shear walls, incorporated in the analysis, included the influence of shear buckling and plastic yielding of the web plate and plastic yielding of the surrounding frame **(Sabouri-Ghomi and Roberts, 1991)**.

The thin steel plate shear wall was idealized as a vertical cantilever plate girder, in which the columns and cross-beams of the shear wall act as the flanges and transverse stiffeners of the plate girder respectively. Overall bending deformations of the shear wall were assumed to be negligible compared with the shear deformations due to the fixed beam-to-column connections and continuity of the relatively stiff cross-beams through adjacent bays of the structural frame.

The results obtained from these solutions validate the analysis for the elastic response of shear walls and also demonstrate the effectiveness of the hysteretic characteristics in inhibiting resonance.

2.8 Caccese, Elgaaly and Chen (1993)

1/4 scale six specimens, which include a moment-resisting frame, three specimens with varying plate thickness and moment-resisting beam-to-column connections, and two specimens with shear beam-to-column connections, were used in the cyclic testing.

In order to assess the feasibility of using the thin-plate shear wall system in seismic zone and to make recommendations for further studies were aimed in this research. Two major parameters, the beam-to-column connection and panel slenderness ratio (the ratio of centerline column spacing to the thickness of the plate), were studied in the experimental investigations.

In conclusion, the author expresses that effective use of thin steel plate shear walls to resist seismic forces is possible. Addition of an unstiffened thin steel plate to a steel frame gives the system a substantial increase in stiffness, load-carrying capacity and energy absorption. When a slender plate is used, inelastic behavior commences by yielding of the plate and the system strength is governed by plastic hinge formation in the columns. When relatively thick plates are used, the failure mode is governed by the column instability. Once the failure mode is governed by the column, only a negligible increase in the system strength is achieved when the plate is thickened.

2.9 Elgaaly, Caccese and Du (1993)

The analytical models, which are capable of accurately predicting the behavior of the steel plate shear wall in the postbuckling domain under monotonic and cyclic loads, are described.

A nonlinear finite element program which combines the effects of large displacements and material nonlinearities was used to investigate the postbuckling behavior of thin steel plate shear walls. A simple analytical model that ignores the strength of the plate prior to buckling was developed. In this model the plate is replaced by inclined tension members. The stress-strain characteristics of these members were developed based on test results **(Caccese et al., 1993)**.

A nonlinear finite element analysis, which includes both material and geometric nonlinearities, was used to investigate the postbuckling behavior of steel plate shear wall specimens under monotonic loading. The frame members (beams and columns) were allowed to deflect in-plane only and the plates were allowed to deflect and rotate in any direction, except at the edges where it is connected to the beams and columns. The connections between the beams and columns were considered to be rigid connections. At the top of the model very stiff beam elements were used to represent the top panel of the specimen that was used to anchor the tension field in the third story plate panel.

The finite element analysis overestimates the stiffness of the wall by 30% and 40% and strength by 26% and 18% for two specimens. It was shown that the initial shape of the plate, out-of-plane deformations of the frame in the test, the postbuckling shape of the specimen and the coarse finite element mesh used to depict complex postbuckling shape are the possible reasons of these overestimations.

For modeling the postbuckling behavior of the steel panels, based on the test behavior, a tri-linear stress-strain relationship for the truss member was developed. Also, to predict the hysteretic behavior of a steel plate shear wall, a symmetric cross-strip model that uses a hysteretic stress-strain relationship was developed.

The authors concluded that thin plates that are adequately supported along their edges have a postbuckling strength that can be several times their elastic buckling strength. The capacity of the shear walls where the plate panels are designed based on elastic buckling strength of the plate panels will be limited by yielding and buckling of the columns prior to reaching a fraction of the postbuckling strength of the plate panels. For a specified column section there is an optimum plate thickness that if exceeded, indicates there will be no increase in the ultimate capacity of the wall, and the wall will fail due to column yielding and buckling.

2.10 Xue and Lu (1994a)

An analytical investigation was conducted on four thin-steel plate shear wall configurations **(Xue and Lu, 1994a)**. In each case, a 12 storey three-bay frame with moment-resisting beam-to-column connections in the exterior bays and with steel infill panels in the interior bay was used. The primary parameter studied in this research was the lateral stiffness of the frame systems with a varied lateral load carrying system. A total of four combinations were done using frames with either moment-resisting or simple beam-to-column connections which were combined with the infill plates connected either on four sides or only to the beams. For comparison, two types of boundaries were determined. A frame with all moment-resisting connections and with an infill panel connected on all sides and prevented from buckling was studied as an upper bound case. The lower bound was defined as a frame with simple beam-to-column connections in the interior bay and no infill plate. The ground storey had the height of 4572 mm and the upper ones had the height of 3658 mm. The thickness of the infill plates varied from 2.8mm at the bottom of the shear walls to 2.2 mm at the top.

The six mixed structures (frame-shear wall) described above were modelled using finite element method. Elastic beam elements were used for beams and columns in the FEM model. For steel panels, elasto-plastic shell elements were used. An initial out-of-plane deformation configuration was specified for the infill plates based on several shear buckling modes.

Monotonically increasing load was applied on the structures at each floor level. There was no any gravity load applied on the structures.

The results of the analyses, the base shear versus top displacement, demonstrated that the presence of the infill plates increased significantly the lateral stiffness of the system, but the effect of the type of beam-to-column connection used in the bay with infill panels on the lateral stiffness of the entire frame was found to be negligible. The stiffness of the frame systems with infill panels attached to both beams and columns were as high as the lateral stiffness of the frame system predicted using the upper bound solution. The stiffness, also, were slightly higher than that of the frame with infill panels connected only to the beams. A number of factors led to the conclusion that the frame system with the simple beam-to-column connection in the interior bay and the infill plates connected only to the beams exhibited the best performance.

2.11 Xue and Lu (1994b)

Xue and Lu (1994b) also carried out a parametric investigation to study the effect of the width / thickness ratio of the panel and the panel aspect ratio (width / height) on the load versus deformation characteristics of a single storey, single bay steel plate shear wall with simple beam-to-column connections and with the infill panel attached to the beams only.

These parameters, width / thickness and width / height ratios, were investigated by the finite element analysis of 20 different cases. The authors found that the influence of the width/thickness ratio on the response was negligible. Simplified empirical equations were also proposed to predict the yield strength, yield displacement and the post-yield stiffness of the system.

Xue and Lu (1994b) also performed a cyclic finite element analysis on a single panel of the twelve-storey, three bay structure described before **Xue and Lu (1994a)**. Six cycles of gradually increasing deflections were applied up to a storey drift of 1.68%. The panel demonstrated significant energy dissipation capacity when the non-dimensionalized load versus deflection response was examined.

The merit of the approach presented by the researchers, compared to the conventional approach for the frame-shear wall system, should be further investigated. In this research the numerical analyses were only conducted on several frame-shear wall systems. No any experimental study was performed to confirm the cyclic behavior of the proposed system and the results from the analytical investigation.

2.12 Elgaaly and Liu (1997)

In general, two analytical models were developed considering steel panels welded to surrounding beams and columns and those connected to boundary frames by bolts. In order to predict the behavior of steel plate shear walls under seismically-induced loads the panels were modeled using equivalent tension-only truss members.

The plate panels in a shear wall would be replaced by a series of equivalent truss elements in the diagonal tension direction.

Because the thickness (stiffness) of the plate was small relative to the stiffness of the surrounding beams and columns and to simplify the analysis, the inclination angle of the equivalent truss members was assumed to be 45^o.

In welded shear walls, it would be assumed that the stress-strain relationship for the equivalent truss element is elastic, elasto-plastic and perfectly plastic.

Four shear wall test specimens with welded plates were analyzed and tested. Three of the specimens were 1/4 scale models and the fourth was 1/3 scale. The specimens were first analyzed under monotonic loads. The comparison between the analytical and test results indicates that the analytical model depicts the behavior of the specimens, under displacement controlled cyclic loading, to a good degree of accuracy.

As for the bolted thin-steel-plate shear walls, the author explained that the differences between the welded and bolted plate shear walls behavior were in the elastic stiffness, the initial yielding load and the stiffness after initial yielding. The bolted plate shear walls, therefore, differ from welded plate shear walls that bolted plate shear walls have smaller elastic stiffness and lower initial yielding load.

The specimens were first analyzed under monotonic loads. The comparison between the analytical and test results indicates that the analytical model depicts the behavior of the specimens, under displacement controlled cyclic loading, to a good degree of accuracy. The specimens were also analyzed under cyclic load. The load-elongation characteristics for loading and unloading which was developed are used in this analysis.

In conclusion, the authors mentioned that the ultimate capacity of welded and bolted walls is comparable provided that no premature failure of the columns or the connections occurs. Finally, it has to be noted by the authors that the columns attached to the walls have to be designed such that they will not yield or buckle before the plate develops its full capacity by yielding of the diagonal tension field.

2.13 Elgaaly (1998)

To investigate the behavior of bolted shear walls and to compare it with that of welded shear walls were the main objective of the research. Seven specimens were totally tested, but five specimens out of them were presented and discussed. The specimens have single bay and two storeys.

In order to obtain out-of-plane displacement configuration of the lower panel, an array of displacement transducers were used. Topmost transducer to control the displacement of the specimen and electrical straingages were used.

The specimens were tested under cyclic load acting at the top of the shear wall. Each of the eight displacement levels changing from about 3.175mm to 50.8mm consist of three complete cycles.

The test results including maximum load reached and yield stress for each specimen were presented in a table. Two analytical models, also, were developed. More detailed information about these numerical models was given in **Elgaaly and Liu (1997)**.

The research showed that the behavior of thin steel plate shear walls was governed by the tension field action and controlled by the boundary conditions. Because of slippage and local deformations at the connection initial yielding could occur at a lower load and a bolted shear wall could have lower stiffness. The ultimate capacity of welded and bolted walls, however, was comparable provided that premature failure of the columns or the connections did not occur.

The analytical models in which the equivalent truss members were used to represent the steel panel were able to depict the test results to a good degree of accuracy. In bolted shear walls eccentricities at the connection between the panel and boundary beams and columns were considered in the analysis by reducing the stiffness of the wall in the elastic range before the initiation of yielding. In conclusion, the author has demonstrated that the columns attached to the steel panels have to be designed such that they will not yield or buckle before the plate reaches its full capacity by yielding of the diagonal tension field.

2.14 Driver, Kulak, Elwi and Kennedy (1998a)

The modeling studies related to the shear wall test conducted by **Driver et al. (1998a)** were described. The test specimen was a large-scale four story steel plate shear wall that has unstiffened panels and moment-resisting beam-to-column frame connections. During the test, both vertical and lateral loads were applied. The vertical loads were kept constant and lateral loads were cycled with gradually increasing intensities and displacements until the structure failed. The test specimen showed great ductility, considerable energy dissipation, and robust resistance to degradation.

Two different modeling techniques were investigated: a finite element model and a simple, ultimate strength model. An associated hysteresis model is also described.

The authors explained that the behavior of thin plates in real structures subjected to in-plane membrane forces can be significantly affected by initial out-of-plane deformations, which, must be taken into account in the analytical model. However, a series of trial initial plate configurations showed that the overall load versus deflection behavior is largely independent of the geometry selected. The effects of the residual stresses, which were measured at various locations on the cross section of each type of member in the shear wall frame, were taken into account in the finite element model.

Because of the complexity of the model, geometric nonlinearities were omitted for the case of monotonic loading up to the ultimate capacity.

An ultimate strength analysis that excluded geometric non-linearities was performed on the steel plate shear wall model. The ultimate load is accurately predcited by the finite element model.

The gradual post-ultimate strength degradation exhibited by the test specimen is not seen in the finite element results because plate tearing and local buckling observed near the end of the test were not included in the model.

Strip model analyses of the test specimen were also carried out to compare the results with the behavior exhibited during the phsical test. Models with two different angles were used to examine the effect of varying the angle of inclination the tension strips. The analysis included P-Δ effects. The two different angles of inclination examined of 42^o and 50^o gave essentially the same response.

The strip model represents well the load versus deflection envelope behavior of the test specimen, and in particular its ultimate strength.

A hysteresis model which was based, in part, on the previous study of both **Mimura and Akiyama (1977)** and **Tromposch and Kulak (1987)** was proposed to predict the cyclic behavior of the steel plate shear walls.

The hysteresis model identified the different phases of the loading cycles well and gave a good prediction of the amount of energy dissipated.

2.15 Driver, Kulak, Elwi and Kennedy (1998b)

The objective of this research was to study the behavior of steel plate shear walls when subjected to extreme cyclic loading. In this manner, a large-scale, four story, single bay steel plate shear wall specimen with unstiffened panels was tested using controlled cyclic loading to determine its behavior under and idealized severe earthquake event. The shear wall had moment-resisting beam-to-column connections, resulting in a lateral load-resisting system that possesses an inherent redundancy. Gravity loads were applied at the top of the wall and equal horizontal loads were applied at the four floor levels.

The shear wall specimen failed by sudden fracturing of the west column at its base. Although failure mode of the column occurred at a very large frame deflection and after many inelastic reversals, the failure mode is nevertheless of importance in assessing the suitability of any structural system for seismic application. Certainly, the failure mode of sudden fracture of the column is not desirable and should be avoided. Therefore, it is recommended that in all cases precautions to prevent local buckling at the column bases be pursued.

The four story steel plate shear wall test specimen exhibited excellent performance. The hysteresis behavior indicates that the shear wall configuration tested possesses an extremely high degree of ductility. The hysteresis curves were very stable throught the response and did not show any sudden reductions in strength. Furthermore, the amount of energy dissipated during the loading cycles was significantly greater than that shown by similar shear walls but with shear-type beam-to-column connections.

2.16 Timler, Ventura, Prion and Anjam (1998)

The objective of this study, generally, was to make a comparison between the cost of a selected building with steel plate shear walls and that of the same building with reinforced concrete shear walls. In this research, also, two large-scale test groups were described.

In the first test group the specimen with one bay and four stories was used to verify existing theories and design formulae that were based on a limited number of tests on two panel specimens with shear loads only at the University of Alberta **(Driver, 1997)**.

In addition, ancillary tests were conducted to determine the performance of connection details between the shear panel and boundary frame members, using corner detail specimens.

It was mentioned that, briefly, a stable ductile response could be achieved over a large number of cycles, even after stretching and buckling of the shear panel had occurred.

In the second test group, quasi-static and shake-table tests were carried out at the University of British Columbia on single and multi-storey steel plate shear wall specimens. In quasi-static tests performed, good energy dissipation and ductility capacities were realized. The strengths generated from the analytical models were found in agreement with the experimental results in the post-yield region. In some cases the analytical models, however, did not accurately predict the elastic stiffnesses of the specimens.

The dynamic behavior of a multi-storey specimen under simulated earthquake motions was investigated. Parallel analytical studies were also conducted to compare analytical predictions with shake-table test results and to produce design recommendations. To monitor the formation of diagonal tension field action combined with diagonal compression buckling and frame action was an important part of the experimental research. The stability of the hysteresis curves under intense seismic loadings was of primary concern.

Both before and after the application of external vertical and lateral loadings complementary vibration measurements were performed on all the multi-storey specimens. With these measurement data obtained, to provide information needed for calibration of the analytical models of the steel plate shear wall specimens was aimed. The primary purpose was also to detect the lower modes of vibration of each frame at three stages: undamaged specimen with no masses; undamaged specimen with storey masses; and damaged specimen with storey masses.

Small shifts in the longitudinal fundamental frequency of the frames were found out due to yielding of columns and the first storey shear panel and global out-of-plane buckling of the base columns. A good correlation between the analytical and experimental fundamental frequencies was observed. One of the most important findings from the studies was the sensitivity of the frame behavior with respect to aspect ratio. The frame behavior would be closer either to a bending beam or a shear beam depending on the aspect ratio of the frame. It is mentioned that this circumstance significantly affected the effectiveness of simplified models.

2.17 Lubell, Prion, Ventura and Rezai (2000)

Experimental testing was conducted on two single and one four-story steel shear wall specimens, under cyclic quasi-static loading. Each specimen consisted of a single bay with column-to-column and floor-to-floor dimensions of 900mm, representing a quarter-scale model of a typical office building core.

The primary objectives of the testing program were identification of load-deformation characteristics and the stresses induced in the structural components.

During the test program the main issues investigated were the overall strength, elastic postbuckling stiffness, formation of diagonal tension field action combined with diagonal compression buckling of the infill plates, stability of tha panel hysteresis curves, effects of beam and column rigidities, and the interaction between the frame action and the shear panel behavior.

Well-defined elastoplastic load deformation envelopes were achieved for each specimen. Hysteresis loops were S-shaped, stable and full. Increased energy dissipation was achieved with each displacement level increment in the postyield region. Some decrease in energy dissipation between subsequent cycles at the same load level was noted, due to local damage.

The principal sequence of significant inelastic action in the single-panel specimens consisted of yielding of the infill panel followed by yielding of the boundary frame. The columns of the multi-story specimen yielded before significant inelastic action occured in the infill panel, resulting in a state of global instability.

A series of numerical models were also generated of the three test specimens to assess the ability of current simplified analysis techniques. The strip model used for analysis of the three specimens is based on the theory of pure diagonal tension by **Wagner (1931)**, which does not account foe any shear carried by the thin plates prior to shear buckling.

The derivation of the angle of the inclination of the tension strips is based on a shear mode deformation of an infill panel, using least work principles **(Timler and Kulak 1983)**.

In all cases the numerical models were reasonably accurate at predicting the postyield strengths and stiffnesses of the respective specimens. However, the elastic stiffness was significantly overpredicted for some specimens.

In conclusion, the experimental and analytical components of this study have shown that steel plate shear walls exhibit many desirable characteristics for structures in areas of high seismic risk. Numerical modeling using current simplified analysis techniques provided good correlation with the specimen postyield strengths but did not accurately predict the elastic stiffnesses under certain conditions.

2.18 Rezai, Ventura and Prion (2000)

A numerical study using different strip models to compare with test results of two single-storey and one four-storey specimens tested at the University of British Columbia was reported in this paper. Two different strip models were considered in comparison with test results.

Parallel strip model, a simplified model in the Canadian Steel Design Code (CAN/CSA-S16-01) is based on the theory of pure diagonal tension by **Wagner (1931)**, were described. In this method used to model infill panels, shear carried by the thin steel plates prior to shear buckling is not taken into account since buckling generally occurs at low lateral load levels because of large panel width to thickness ratio and fabrication induced out-of-flatness imperfections. The shear panels represented as a series of inclined tension only strip members with the same cross-sectional area equal to the product of the strip width and the panel thickness. These members are oriented in the same direction as the principal tensile stresses in panel.

Multi-angle model, the method of modelling to utilize a series of strip elements which are placed at different angles instead of the infill panels. Because the degree of magnification and inclination of the infill plate principal tension stresses are different at various locations in the plate, the tension strips are placed at different angles. To simplify the modelling, the tension-only truss members are placed diagonally between opposite corners and from the corners to the mid-span of boundary members.

The cross-sectional area of the strips was determined based on the degree of interaction between the infill wall and boundary frame. The configuration of these members and detailed information are presented in the dissertation by **Rezai (1999)**.

Four different strip models (three with parallel strips at angles 45^o, 37^o and 55^o and one multi-angle strip model) were created of the single storey specimens. To study the effects of various modelling assumptions on the analytical results was the main reason for creating three different angles of inclination of the strips.

Using four-storey specimen, four different parallel strip models at different angles were created to demonstrate the effect of varying the angle of inclination of strips on the load-deflection behavior of the test specimen. These angles were 45^{o}, 37^{o}, 55^{o} and 22^{o}.

The two important characteristics of the UBC four-storey specimen were low stiffness and high yield strength values that were not properly captured by the analytical strip models. The stiffening effect of infill panels in increasing the overall elastic stiffness of the bare frame is primarily governed by the formation of a diagonal tension field. The extent of which tension field action can be effectively generated in a panel is significantly influenced by the storey height and width of the panel. It has been shown that as the ratio of overall height of a multi-storey steel plate shear wall frame to its width increases, the strip model tends to overestimate the elastic stiffness of the structure **(Rezai, 1999)**.

In conclusion, the strip models generally overpredicted the elastic stiffness the test specimens. The load-deformation bahaviour of the specimens was considerably affected by a change of 10° in the angle of inclination of tension strips. The discrepancies between the analytical and experimental results were more dramatic for the four-storey specimen compared to the single storey specimens. It has been said that the reason of this was mainly related to the small overall aspect ratio of the four-storey specimen and, thereby, increased moment to base shear ratio, which resulted in a dominance of flexural deformation (or chord drift) compared to shear behaviour.

An improved analytical model was proposed for simplified analysis. The proposed model predicted reasonable results for pushover analyses. Even though the proposed analytical model was in closer agreement with the experimental results, compared to the 37° strip model predictions, the elastic stiffness and the yield strength of the four-storey specimen were overpredicted and underpredicted by the proposed model, respectively.

2.19 Bruneau and Bhagwagar (2002)

Non-linear inelastic analyses are conducted to investigate how structural behaviour is affected when thin infills of steel, low yield steel, or Shearfill fabric, a brand name fabric which is an anisotropic material, are used to seismically retrofit steel frames located in regions of low and high seismicity. A typical three bay frame extracted from an actual 20-story hospital building in New York City is considered for this purpose. Fully rigid and perfectly flexible frame connection rigidities are considered to capture the extremes of frame behaviour.

It is found that the use of even very thin steel infill panels can significantly reduce story drifts without significant increases in floor accelerations, and that low yield steel behaves slightly better than standard constructional grade steel under extreme seismic conditions but at the cost of some extra material. It is also concluded that Shearfill membranes may not have the necessary strength and stiffness to be an effective retrofit solution, unless a thick membrane having multiple layers can be constructed.

2.20 Berman and Bruneau (2003)

A revised procedure for the design of steel plate shear walls is proposed. In this procedure the thickness of the infill plate is found using equations that are derived from the plastic analysis of the strip model, which is an accepted model for the representation of steel plate shear walls.

The use of plastic analysis as an alternative for the design of steel plate shear walls is investigated using the strip model as a basis. Fundamental plastic collapse mechanisms are described for single and multistory steel plate shear walls with either simple or rigid beam-to-column connections. Ultimate strengths predicted from these collapse mechanisms are compared with existing experimental results, and used to assess the CAN/CSA S16-01 design procedure.

Note that it is assumed that column hinges will form instead of beam hinges at the roof and base levels. Sizable beams are usually required at these two locations to anchor the tension field forces from the wall plate and hence plastic hinges typically develope in columns there.

Also, a comparison is made with results obtained experimentally by others using the equations expressed above. It is noted that the ultimate strengths of the steel plate shear walls that are calculated by simple equations and those from experimental studies by others are in reasonable agreement.

2.21 Berman and Bruneau (2004)

The strip model developed by others and implemented in a Canadian Standard to model steel plate shear walls is used to develop, investigate, and quantify, through plastic analysis, the various possible collapse mechanisms of steel plate shear walls. Comparisons of experimentally obtained ultimate strengths of steel plate shear walls and those predicted by plastic analysis are given and reasonable agreement is observed. Modifications are proposed to a section of an existing codified procedure for the design of steel plate shear walls which is shown could lead to designs with less-than-expected ultimate strength. In addition to the above, the results of an experimental study to determine the feasibility of light-gauge steel plate shear walls for use in the seismic retrofit of buildings are also described. Three specimens were constructed and tested under quasi-static loading, one using a corrugated infill and epoxy connection to the surrounding frame, one using a flat infill with an epoxy connection to the surrounding frame, and one using a flat infill with a welded connection to the frame.

In conclusion, light-gauge steel plate shear walls have been shown to be a viable seismic retrofit option for buildings. Substantial ductility and stiffness can be achieved with these types of infills. From the experimental results for three specimens, there is no substantial advantage to using infills with corrugated steel sheets in spite of their enhanced buckling strength. The failure mode for the specimen utilizing a corrugated infill was determined to fracture of the infill at locations of repeated local buckling, while for the specimen with a flat infill and welded connection to the boundary frame, fracture of the infill occurred at a drift of $12\delta_y$. Moreover, there was no strength degradation which shows these systems can be stable up to large drifts until the drift level of $12\delta_y$ was reached. The moments in the beams and columns were shown to be small for all specimens and the variation of the strain across the infills was insignificant.

2.22 Berman and Bruneau (2005)

The prototype design, specimen design, experimental setup, and experimental results of three light-gauge steel plate shear wall concepts are described in this paper. Prototype light-gauge steel plate shear walls are designed as seismic retrofits for a hospital structure in an area of high seismicity, and emphasis is placed on minimizing their impact on the existing framing. Three single-storey test specimens are designed using these prototypes as a basis, two specimens with flat infill plates having thickness of 0.9mm and a third using a corrugated infill plate with thickness of 0.7mm. Connection of the infill panels to the boundary frames is achieved through the use of bolts in combination with industrial strength epoxy or welds, allowing for mobility of the infills if desired.

Additionally, in order to represent the behavior of the bare-boundary frame which has beam-to-column connections partially transmitting moments the bounding surface model with internal variables, originally formulated by **Dafalias and Popov (1976)** is used. The hysteretic behavior of semi-rigid frames, therefore, is depicted.

Testing of the systems is done under quasi-static conditions. It is shown that one of the flat infill plate specimens, as well as the specimen utilizing a corrugated infill plate, achieved significant ductility and energy dissipation while minimizing the demands placed on the surrounding framing. Also, experimental results are compared to monotonic pushover predictions from computer analysis using a simple model and good agreement is observed.

The ultimate failure mode of the specimen which utilized a corrugated infill was found to be fracture of the infill at locations of repeated local buckling and an industrial strength epoxy was found to be an adequate material to connect the infill to the boundary frame in this case. For the specimen using the flat infill and an epoxy connection to the boundary frame, failure occurred in the epoxy prior to yielding of the infill. The specimen utilizing a flat infill and a welded connection to the boundary frame was significantly more ductile than the other two and failure was the result of fractures in the infill adjacent to the fillet weld used to connect the infill to the boundary frame.

2.23 Sabouri-Ghomi, Ventura and Kharrazi (2005)

In this paper, an analytical model of the ductile steel plate walls (DSPW) that responds to characterize the structural behavior of the configurations including DSPWs with thin or thick steel plates, and with or without stiffeners and openings is presented and discussed.

For the analysis and design of the steel plate shear walls a method, Plate-Frame Interaction (PFI) Method is proposed. This method can be applied step by step and frame and infills are considered separately. The steps used for the analysis are summarized in the following.

- Calculate and draw the shear load-displacement diagrams. For this purpose, some equations are given in related paper. In this step, Load versus displacement diagrams are obtained independently from each other for boundary frame and infill panel only. The shear wall force-deformation diagram is obtained by superposition of the infill panel and frame force-deformation diagrams.

- Check for columns to ensure that the columns can sustain the normal boundary stresses associated with the tension field.

- Check for the end beams to ensure that these can sustain the normal boundary stresses associated with the tension field.

- In order to ensure that the steel plate dissipates more energy than the boundary frame, the steel plate shear walls should be designed in such a way that the yield displacement belonging to the infill panel only will be larger than that of the boundary frame only.

The proposed model provides a good understanding of how the different components of the system interact, and is able to properly represent the system's overall hysteretic characteristics, which can be readily incorporated in practical nonlinear analyses of buildings with DSPWs. The effectiveness of the method is demonstrated by comparing the predicted response with results from experimental studies performed by different researchers.

2.24 Shishkin, Driver and Grodin (2005)

The parallel strip method for analysis of steel plate shear wall, originally developed by **Thorburn et al. (1983)**, was refined to create a detailed model based on phenomena observed during the test using a four-storey specimen **(Driver et al., 1998b)** in order to obtain a more accurate prediction of nonlinear behavior of steel plate shear walls.

The modifications that were made in the model were based largely on experimental observations of test specimens during loading. The beam-to-column joint panel zone was stiffened to reflect the small inelastic deformations. Multilinear rigid-inelastic flexural and axial hinge were used to model the pushover behavior of steel plate shear walls. A compression-only diagonal strut was modelled to represent the small contribution of compressive resistance in each infill plate. The tearing of the infill panel corners was modelled using deterioration axial hinge that were located on the strips that came closest to the corners of each panel.

The pushover analysis was performed on the detailed model of the four-storey specimen tested by **Driver et al. (1998b)** using SAP2000. The pushover curve generated by the detailed model was found to be in very good agreement with the test specimen envelope curve.

2.25 Sheng-Jin Chen and Chyuan Jhang (2006)

This paper includes both experimental and numerical investigation. In order to examine the stiffness, strength, deformation capacity and energy dissipation capacity of low yield point (LYP) steel shear wall under cyclic load a series of experimental studies in which five specimens were totally tested were carried out. In numerical studies, a two-force strip method was proposed to simulate the elastic and inelastic behavior of shear wall system. Infill panels used in the shear walls were 6mm and 8mm thick. It was reported that good energy dissipation capacities were obtained for all specimens. The authors also indicated that excellent deformation capacities were obtained from both rigid frame-shear wall system and simple frame shear wall system. It was also reported in this study good correlations were found between experimental and analytical results.

2.26 Other Related Studies

Nakashima et al. (1994) presented the results of a pilot test conducted for evaluating the energy dissipation behavior of shear panels made of low yield steel whose 0.2% offset yield stress was 120 MPa.

The loading condition, stiffener spacing and magnitude of axial force were determined as test variables. In the research, a total of six full-scale specimens were tested. Shear panels with both horizontal and vertical stiffeners exhibited stable hysteresis and large energy dissipation.

The authors proposed that the frames made of high strength structural steels could be combined with the steel panels made of low strength structural steels to minimize structural damage under earthquake.

Nakashima (1995) conducted an experimental investigation on the hysteretic behavior of shear panels made of low-yield steel whose nominal 0.2% offset yield stress is 120 MPa. Six shear panels were tested. Loading conditions and width-to-thickness ratio were determined as the test parameters.

The hysteretic behavior that involves drastic strain hardening could be simulated accurately by the multisurface model if the associated parameters were chosen properly. It was found that strain hardening during cycles with the same deformation amplitude as well as under increasing deformations was significant. Energy dissipated by the hysteresis was larger in the tested shear panels than in the equivalent linearly elastic and perfectly plastic model.

Elgaaly (2000) investigated the post-buckling behavior of thin steel plates using computational models. The computational model includes the effects of geometric and material nonlinearities because the failure of such structures is usually due to large out-of-plane deflections, yielding, and rupture. The nonlinear finite element analysis program NONSAP and ANSR-III used for analysis were modified, adding new elements, thin shell element, and new material properties to the programs since these programs did not include the suitable elements and material properties to conduct the study. In order to calculate the post-buckling strength of stiffened and unstiffened plates subjected to uniaxial compression, and plates subjected to in-plane bending or shear the modified programs were used.

Crippling of plates subjected to in-plane or eccentric edge compressive loads was also examined. The results from the computational models were compared with test results and reasonable agreements were obtained. In addition to this, a computational model was developed for a multi-story thin steel plate shear wall subjected to cyclic loading. The results from the model were compared with experimental results, and again agreement was achieved.

Hitaka and Matsui (2003) carried out an experimental study on steel plate shear wall with vertical slits. The proposed design method was also described. The test results were presented for 42 wall plate specimens of roughly one-third of full scale, which were subjected to static monotonic and cyclic lateral loading. The dimensions of the steel plate were typically 4250 mm (width)×3120 mm (height)×14 mm (thickness), located in the bays with 6900 mm beam spans. The design of the slit is varied along the height of the structure according to the strength and stiffness demand.

In conclusion, all specimens showed large ductility. The hysteresis response of the shear wall was roughly predicted by models based on the mechanisms of link bending and shear plate deformation prior to the onset of out-of-plane deformations. Strength degraded only after the initiation of the plate’s out-of-plane buckling. Two modes of transverse deformation were observed depending on slit configurations. One mode is characterized by lateral-torsional buckling of shear links, and the other resembles a shear buckling mode.

Vian et al. (2003) performed an experimental study to investigate cyclic performance of low yield strength steel panel shear walls. In this research, the specimens utilizing low yield strength steel for the infill panel and reduced beam sections at the ends of the beams were tested. Two specimens in the experimental program make allowance for penetration of the wall panel by utilities. The first, consisting of multiple holes, or perforations, in the steel panel. The second such specimen has quarter-circle cutouts in the top corners of the frame.

The lower yield strength and thickness of the tested plates result in a reduced stiffness and earlier onset of energy dissipation by the panel as compared to currently available hot-rolled plate. The perforated panel specimen showed promise towards alleviating stiffness and over-strength concerns using conventional hot-rolled plates. The author said that use of the reduced beam section details may result in more economical designs for beams "anchoring" a steel plate shear wall system at the top and bottom of multi-story frame.

Berman and Bruneau (2004) performed the investigation whose purpose is to review the shear strengths of both SPSW and vertical cantilevering plate girders, compare them with results from experimental studies, and show that the tension field inclination angles for SPSW and plate girders are substantially different (due to their different associated boundary conditions) which leads to different tension field strengths.

The authors have concluded that steel plate shear walls designed to buckle in shear and develop a diagonal tension field are similar to vertical plate girders in a qualitative manner only. They have also indicated that the analogy that the vertical boundary elements of a SPSW are similar to the flanges of a plate girder, the horizontal boundary elements are similar to stiffeners, and the infill plate of a SPSW is similar to the web of a plate girder, is useful in developing a general understanding of SPSW behavior, but it does not fully represent the behavior of this structural system. Consequently, they have stated that the major difference is the stiffness of the boundary elements.

Zhao and Astaneh-Asl (2004) have carried out the experimental studies of three-story composite shear wall specimens consisting of a steel plate shear wall with a reinforced concrete wall attached to one side of it using bolts. The test results were presented and discussed. Two half-scale specimens were tested and both showed highly ductile behavior and cyclic postyielding performance. The bolts connecting the reinforced concrete wall to steel plate shear walls were able to ensure the composite action by bracing the steel plate shear wall to the reinforced concrete shear wall and preventing the overall buckling of steel plates. During late cycles and after shear yielding of steel plate, inelastic local buckling of steel plate shear wall occurred in the areas between the bolts.

Liang et al. (2004) have studied the local and postlocal buckling strength of steel plates in double skin composite (DSC) panels under biaxial compression and in-plane shear by using finite element method. A DSC panel is formed by placing concrete between two steel plates welded with headed stud shear connectors at a regular spacing. Critical local buckling interaction relationships are presented for steel plates with various boundary conditions that include the shear stiffness effects of stud shear connectors. A geometric and material nonlinear analysis is employed to investigate the postlocal buckling interaction strength steel plates in biaxial compression and shear. The initial imperfections of steel plates, material yielding, and the nonlinear shear-slip behavior of stud shear connectors are considered in the nonlinear analysis. Design models for critical buckling and ultimate strength interactions are proposed for determining the maximum stud spacing and ultimate strength of steel plates in DSC panels.

Berman et al. (2005) has conducted an experimental research to compare hysteretic behavior of light-gauge steel plate shear walls and braced frames. For this purpose, six specimens were tested under cyclic loading. Four specimens of these were concentrically braced frames (two with cold-formed steel studs for in-plane and out-of-plane restraint of the braces and two without). The rest of the specimens were light-gauge steel plate shear walls (SPSW) (one with a flat infill plate and one with a corrugated infill).

In conclusion, the largest initial stiffness was provided by a braced frame specimen with cold-formed steel studs and the largest ductility was achieved with a steel plate shear wall with flat infill. It was also found that both the energy dissipated per cycle and the cumulative energy dissipation were similar for flat plate SPSW and braced frames with two tubular braces, up to a ductility of four after scaling the hysteretic results to the same design base shear. After that the tubular braces fractured while the

SPSW with a flat infill reached a ductility of nine before the energy dissipation per cycle decreased.

Alinia and Dastfan (2006) have investigated the effects of surrounding members (i.e. beams and columns) on the overall behavior of thin steel plate shear walls (TSPSWs) in theoretical manner only. The results have showed that the flexural stiffness of surrounding members has no significant effects, either on elastic shear buckling or on the post-buckling behavior of shear walls. But, the torsional rigidity of supporting members has a significant effect only on the elastic buckling load, and the extensional stiffness slightly affects the post-buckling capacity. In addition, it has mentioned that the beam-to-column connection type has no significant effect on the panel's behavior.

Alinia and Dastfan (2007) have performed a numerical research to compare the behavior of unstiffened panels with that of heavily stiffened panels. Therefore, the effect of stiffening upon the ultimate strength of shear panels was investigated. For this purpose, four nonlinear finite element models considering nonlinearity of material and geometry were developed using ANSYS. Additionally, in order to investigate the required amount of stiffeners to prevent pinching, eight more panels with different geometries and stiffeners were also modelled and analyzed. The panels' dimensions that considered in this research changed from 300mm to 3000mm. The thicknesses of the panels in the models were 0.50mm, 1.00mm and 10.00mm. Large-deflection effects were also taken into account in the analyses.

It was reported that the unstiffened steel shear panels had a very ductile behavior and buckle during the early stages; consequently they did not have great energy dissipation capacity. With the use of stiffeners in mild steel panels, pinching of the hysteresis curves was prevented and energy dissipation capacity increased. The authors also indicated that an optimum amount of stiffeners should be used to achieve both sufficient rigidity and deformability since too much stiffening leads to a loss of structural deformability.

3. PRELIMINARY STUDIES ON MODELLING OF THIN STEEL PLATE SHEAR WALLS

Two different models as well as methods were considered to clearly understand the nonlinear behavior of the TSPSW systems. The parallel strip model which is simpler than the other was developed using SAP2000 that is able to conduct nonlinear pushover analysis. For the complicated nonlinear finite element model of TSPSW ABAQUS, very detailed computer program, was employed. In order to be able to properly develop a finite element model, prior to designing the test specimens several studies were performed considering the existing steel plate shear walls tested by other researchers. The shear wall specimen M14 tested by Chen was selected as a preliminary model to develop strip and finite element model **(Chen, 1991)**.

The specimen M14, one-quarter scale model, is a single-bay, three-storey steel frame with thin unstiffened infill panels directly welded to the flanges of the beams and columns. The shear wall frame which is made of ASTM A36 steel is comprised of S3×5.7 horizontal members and W4×13 columns. The specimen is shown in Figure 3.1

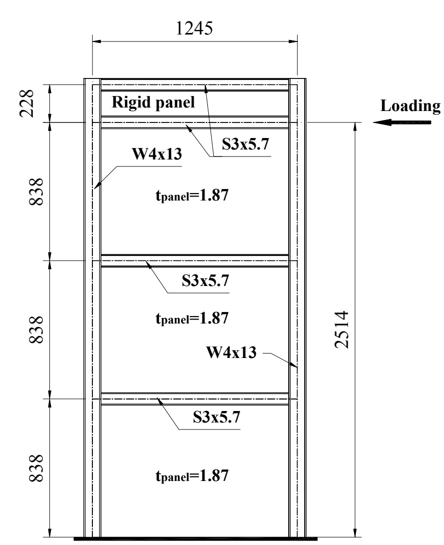

Figure 3.1: Shear Wall Specimen M14 Tested by Chen (dimensions are in mm)

Pushover curves for the specimen which is shown in Figure 3.1 were obtained under monotonically increasing load, to a maximum displacement of 50mm.

3.1 Finite Element Model

The finite element model was previously developed using the general purpose program ABAQUS 6.4 Student Edition which is going to be utilized for nonlinear analyses of the steel plate shear wall specimens including the postbuckling behavior of the infill panels. In order to take the postbuckling behaviour of the infill panels into account, an investigation on finding the eigenbuckling modes of the infill plates under lateral loading has firstly been carried out in the preliminary analyses. The finite element model, shown in Figure 3.2, also includes both material and geometric nonlinearities.

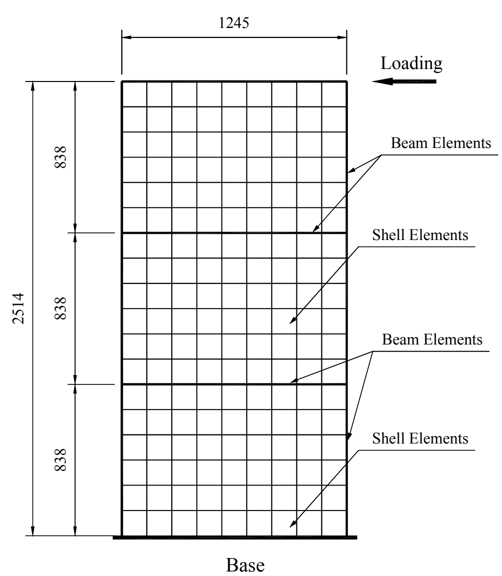

Figure 3.2: Finite Element Model of Specimen M14

3.1.1 Elements

For modeling the beams and columns, three-node quadratic beam elements (ABAQUS element B32) are used. This element allows axial stretching, biaxial bending and warping of the cross section. The beam element B32 using linear and quadratic interpolation is based on a formulation also allowing “transverse shear strain”; that is, the cross-section may not necessarily remain normal to the beam axis.

This leads to Timoshenko beam theory **(Timoshenko, 1956)** and is generally considered useful for thicker beams, whose shear flexibility may be important. However, this element is formulated so that it is efficient for thin beams—where Euler-Bernoulli theory is accurate—as well as for thick beams. Because of this it is the most effective beam element in ABAQUS. In this formulation of the beam element, large axial strains are also considered. The cross section is described with 13 mid-surface integration points, five in each flange and five in the web, with two common locations at the intersections.

The shear wall infill panels are modeled using ABAQUS element S8R5; eight-node doubly curved thin shell, reduced integration indicated by "R" in its name. This element five degrees of freedom per node, although a sixth (rotation about the out-of-plane axis) is included automatically under particular circumstance, for example in case it is attached to a beam or to a shell element that uses six degrees of freedom at all nodes. Thus, all degrees of freedom per node are activated for the plate in the model.

3.1.2 Material properties

All material is modeled as isotropic with rate-independent elastoplastic behavior. The effects of strain hardening are taken into account. The properties are identical in tension and compression. The von Mises yield surface is considered as the yield criterion.

For the stress versus strain relation for both infill panels and boundary frames measured material properties from the coupon tests **(Caccese et al., 1993)** were used. But, the material properties of the beams are considered as identical to the columns because of that any test result from tension coupons cut from the beams is not reported in the relating paper **(Caccese et al., 1993)**. The bilinear stress versus strain response selected extended from the origin to the mean value of the measured yield point and then to the mean measured ultimate stress and corresponding strain. The initial slope is equal to the modulus of elasticity which is assumed to be value of 200kN/mm^2.

3.1.3 Initial conditions

Initial imperfection, out-of-plane deformations in the thin infill panel, accentuated by effects such as floor beam deflections, fish plate connection eccentricity, distortion due to welding process is unavoidable phenomena to be present. This effect, therefore, must be considered in the the analytical model. In order to take this significant effect into account, the infill panel was taken to have an initial out-of-flatness corresponding to the second panel buckling mode of the steel plate shear wall which was loaded in the same manner as in the subsequent pushover analysis. This mode occurred at an applied lateral load of 19.12 kN acting on the top.

Two analyses are also performed for two different amplitudes of the initial imperfection of the steel panels to see that how the changes in initial deformed shape configurations affect the behavior of the TSPSW.

3.1.4 Method of solution

Nonlinearities, material nonlinearity, and/or boundary nonlinearities such as contact and friction, can arise from large-displacement effects. The most efficient method to achieve successive solutions along the equilibrium path in the nonlinear problems is to utilize a method using an iteration scheme. ABAQUS generally uses Newton-Raphson scheme with a load control as a default solution strategy. However, this method tends to diverge as unstable response is approached. The local instabilities of the infill thin panel make it extremely difficult to obtain a complete solution up to ultimate capacity using a load control strategy. Therefore, the modified Riks Method by **Riks (1979)**, **Crisfield (1981)**, **Ramm (1981)**, and **Powell and Simons (1981)**, which includes the load magnitude as an additional unknown in the problem formulation is used.

This approach gives solutions regardless of whether the response is stable or unstable. The benefit of the modified Riks algorithm is that the equilibrium states during an unstable phase of the load-deflection response can be found.

3.1.5 Finite element model analysis of Chen specimen M14

The analytical model for the three-story steel plate shear wall specimen M14 was developed using the general-purpose nonlinear program ABAQUS. A 6×9 element mesh was used for all panels. This is resulted in a total of 4218 variables, which includes degrees of freedom and any Lagrange multiplier variables. The model was loaded with horizontal point loads distributed along the beam at the uppermost floor level. There is no any vertical load acting on the columns as in the test **(Chen, 1991)**.

Three different finite element analyses were carried out. In the first analysis, shear wall specimen M14 is fully fixed at base and the initial out-of-plane deformation configuration is based on the second buckling mode with the scale factor of $30 \times t_p$, resulting in 56.1mm, which is the maximum out-of-plane deformation value. In second, joints at base are pinned and the initial out-of-plane deformation shape is similar to that in the first analysis. The specimen is again fully fixed at base and the infill panel is taken to have an initial out-of-flatness corresponding to the second buckling mode with the scale factor of $5 \times t_p$, resulting in the maximum out-of-plane deflection value of 9.35mm in the third analysis.

3.1.6 Results of finite element analyses

Three ultimate strength analyses that include both material and geometric nonlinearities were performed on the steel plate shear wall specimen M14, previously tested by Chen **(Chen, 1991)**. Figure 3.3 shows a comparison between the experimental and analytical top displacement versus base shear curves for specimen M14. It should be noted that, there is no noticeable change of the specimen stiffness at the theoretical buckling load of the infill panel as stated in the paper by **Elgaaly et al. (1993)**.

As can be seen from the Figure 3.3, the finite element analyses overestimate the initial stiffness of the wall by 23% and the ultimate strength by 15% for the specimen M14 when the model used in the second analysis is considered. The differences can be attributed to the following causes. The initial shape of the infill panel does affect the initial stiffness of the shear wall specimen. The actual initial out-of-plane deformation configuration of the panel may be different from that taken into account in the analyses. The eccentricities in the connection between the infill plates and boundary frame (beams and columns flanges) due to fabrication is certain to be present. Residual stresses due to welding process are not included in the finite element model. For representing the postbuckling shape of the plates, more elements need to be used in the model.

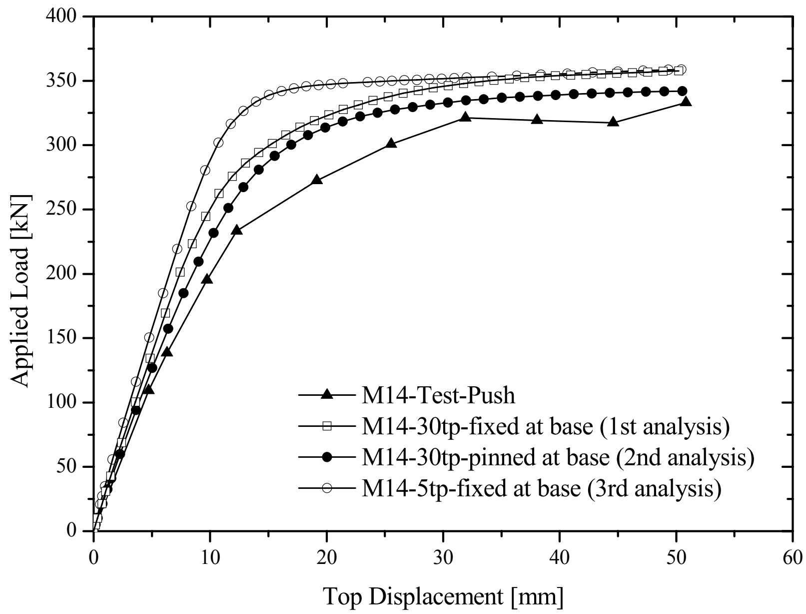

Figure 3.3: Pushover Curves from Finite Element Models of Specimen M14

The results which are obtained from the finite element analyses and the test are summarized in Table 3.1.

Table 3.1: Summary of the Results from Finite Element Analyses

M14	Results from the test	Results from the first analysis	Results from the second analysis	Results from the third analysis
Initial stiffness	22065 kN/m	27129 kN/m	24721 kN/m	30505 kN/m
Load at 12.7mm	231 kN	283.0 kN	265.5 kN	325.0 kN
Load at 25.4mm	289 kN	337.9 kN	326.8 kN	349.8 kN
Ultimate shear strength	333 kN	357.7 kN	341.9 kN	358.8 kN

The buckle shape shown in Figure 3.4 is consistent in orientation with that in the test. The deformed configuration of the specimen model considered in the second analysis when loaded to base shear of approximately 358 kN is shown in Figure 3.4.

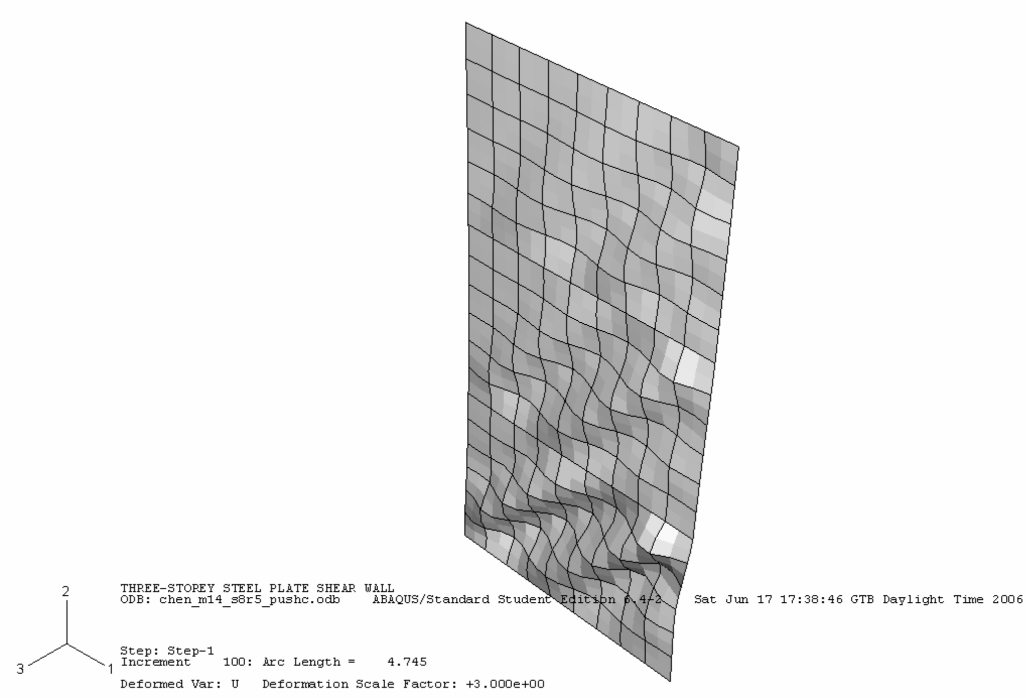

Figure 3.4: Deflected Shape of Specimen M14 (magnified 5 times)

As seen from the Figure 3.3, as the peak amplitude of out-of-plane deformation to which is set in the models increases the general behavior of a shear wall changes slightly for Chen specimen M14. In this case, while the initial stiffness particularly increases as the peak amplitude of deformation decreases, there is an insignificant increase in ultimate strength of the shear wall. However, the numerical investigation conducted by **Driver et al. (1998a)** showed that different initial deformed geometry of infill panel exhibited that the overall load versus deflection behavior is largely independent of the geometry selected.

3.2 Strip Model

The finite element method provides a powerful technique for modeling the behavior of complex structures. However, it is either very difficult or impossible to reach the resources for performing such an analysis. In the case of routine analysis of structures, structural designers require simpler methods that use commonly available computing resources.

A simplified method for analyzing thin steel plate shear walls – the strip model – was presented originally by **Thorburn et al. (1983)**. Thus, the model can be analyzed using any commercially available computer program package. For the purpose of developing the strip model, SAP2000, which is very common structural analysis program in structural engineering field, is used.

The fundamental assumption in the strip model is that dominant action that resists the story shear is the diagonal tension field that develops after thin unstiffened infill panel buckles. The lateral load carrying capacity of thin unstiffened infill panels before buckling elastically is relatively low and, therefore, insignificant to be considered because of the large size of the plate with respect to the thickness and because of the inevitable initial out-of-plane imperfection due to fabrication and /or installing process of the panel. Due to the dominance of tension field action in the behavior, the infill panel is represented by a series of discrete, pin-ended - tension only - strip members inclined with the same orientation as the tension field. Therefore, the compression in the orthogonal direction is negligible and the angle of the inclination of the tension field can be predicted reasonably well. All strip members have the same area equal to the plate thickness multiplied by width of the strip for an infill panel. According to the investigation conducted by **Thorburn et al. (1983)**, ten strips per panel was found to be adequate to represent the tension field action for thin unstiffened steel plate shear walls.

3.2.1 Description of SAP2000 strip models of Chen specimen M14

Four different SAP2000 strip models in which the inclination angles of the strips vary from 35° to 50° are developed to clearly understand the general behavior of this type of shear wall and the effect of the inclination angle of strips on the behavior of TSPSWs. While the angles, 35°, 45°, 50° are selected in an arbitrary manner, 40.18° is calculated using below equation **(Timler and Kulak, 1983)**. Ten pin-ended strips are employed in the models to depict the behavior of the infill panel. Because the beam-to-column connection is developed by a continuous fillet weld of the entire beam section to the column flange, these types of joints are considered as the rigid connections in the models.

$$\tan\alpha^4 = \frac{1+\dfrac{Lt_p}{2A_c}}{1+\dfrac{ht_p}{A_b}+\dfrac{h^4 t_p}{360 I_c L}} \quad \textbf{(3.1)}$$

3.2.2 Strip model analyses of Chen specimen M14

The specimen M14 was modeled using SAP2000 under monotonically increasing load acting on the top in horizontal direction as in the test. The analysis of the shear wall has been performed utilizing the strip model, that is, the thin infill panel was replaced by a series of inclined tension-only bars with the same orientation. The SAP2000 strip models used in the prediction of the behavior (ultimate strength and initial stiffness) is given in Figure 3.5.

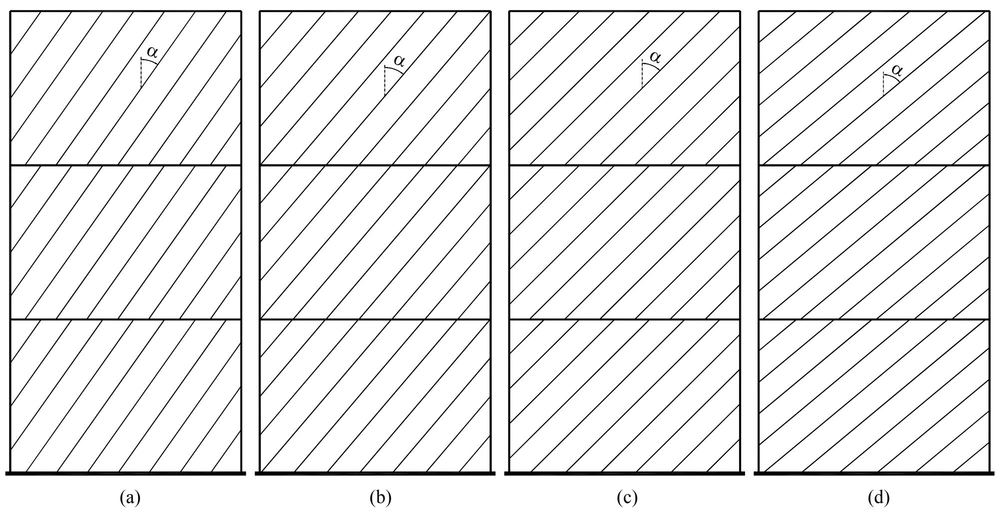

Figure 3.5: SAP2000 Strip Models of Specimen M14; (a), (b), (c), (d), inclination angle values of 35°, 40.18°, 45° and 50°, respectively

Beams, columns and strips – tension-only truss members - are modeled using SAP2000 frame member.

In practice, the strips are often modeled as spanning from the center lines of the beams and columns. However, in this case, due to the depths of the boundary frame members (beams and columns), this leads to strip lengths that are longer in the models than in the actual test specimen, resulting in an overprediction of the yield displacement. Because of this reason, to more accurately predict the behavior of the specimen M14, actual strip lengths are used in the pushover analyses of the strip models.

The material properties used are taken from the paper by **Caccese et al. (1993)**. The behaviors of the plastic hinges to use for representing the plastic deformations of the frame sections under axial forces and moments are based on the actual material properties, mean yield stresses and mean ultimate stresses. For the columns and beams, moment plastic hinges, M3 are defined, while axial plastic hinges, P are used for the strips. The actual strip lengths are taken into account in defining of axial plastic hinges for the strips. Because there is no any gravity load directly acting on the columns in the test and for the simplicity as well, the influence of the axial force on moment versus curvature behavior of the columns is neglected for the plastic hinges definition used for the columns.

3.2.3 Results of strip model analyses

The four strip models with different inclination angles of the strips varying from 35° to 50° were examined. The results obtained from the SAP2000 pushover analyses and the results from the test performed by Chen are given in Table 3.2. The pushover curves for each strip model and the response of the specimen M14 in test are shown in Figure 3.6. As can be seen from the Figure 3.6, the strip model analysis including inclination angle of 35° is ended at lateral displacement of 40mm due to P-Δ effect, while other analyses continue up to lateral displacement of 50mm.

Table 3.2: Summary of the Results from Strip Model Analyses

M14	Results from the test	Results from the model with 35°	Results from the model with 40.18°	Results from the model with 45°	Results from the model with 50°
Initial stiffness	22065 kN/m	22527 kN/m	23847 kN/m	20536 kN/m	21767 kN/m
Load at 12.7mm	231 kN	285.1kN	302.8 kN	260.8 kN	276.3 kN
Load at 25.4mm	289 kN	355.3 kN	369.5 kN	342.1 kN	361.9 kN
Ultimate shear strength	333 kN	374.4 kN	390.9 kN	350.7 kN	384.8kN

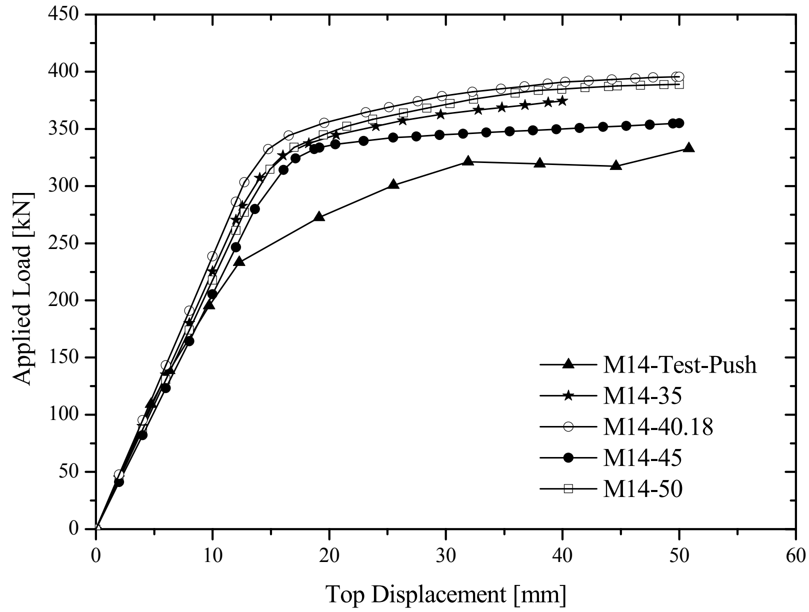

Figure 3.6: Pushover Curves from Strip Models of Specimen M14

3.3 Comparison of the Results

For the simplicity, instead of that all results from finite element and strip models analyses are compared with each other, second finite element analysis and the strip model analysis including the inclination angle of 45° are considered to make comparison. The comparison of the results is given in Table 3.3. As seen from the following table, in general, all results obtained from the analyses considered in Table 3.3 are in agreement with the test results. The strip model which is composed of the equivalent tension-only strips with the inclination angle of 45° predicted the initial stiffness of the shear wall well. However, the second finite element model gave a good prediction of the ultimate strength. While the strip model also gave a good prediction of the applied load at 12.7mm, the finite element model predicted the applied load at 25.4mm well.

Table 3.3: Comparison of the Results

M14	Results from the test (1)	Results from second finite element analysis (2)	Results from the strip model with 45° (3)	Comparison between 1st and 2nd column [%]	Comparison between 1st and 3rd column [%]
Initial stiffness	22065 kN/m	24721 kN/m	20536 kN/m	+12.0	-6.9
Load at 12.7mm	231 kN	265.5 kN	260.8 kN	+14.9	+12.9
Load at 25.4mm	289 kN	326.8 kN	342.1 kN	+13.1	+18.4
Ultimate shear strength	333 kN	341.9 kN	350.7 kN	+2.7	+5.3

3.4 Summary

The preliminary studies on modeling of TSPSWs which were carried out in this section are considered specimen M14 previously tested by Chen as a preliminary model to understand the behavior of TSPSWs under lateral loads using finite element models and strip models. The results obtained from the analyses employing both finite element and strip models are given and compared. For other analytical studies including different samples of TSPSWs that were previously tested by other researchers, it can be refered to **Vatansever and Yardımcı (2005)**, **Vatansever and Yardımcı (2007a)**, **Vatansever and Yardımcı (2007b)** and **Vatansever and Yardımcı (2007c)**.

4. EXPERIMENTAL DESIGN AND SETUP

This section describes the design, setup and instrumentation of six specimens that can be divided into two groups having three specimens with respect to beam-to-column connection types. Two different beam-to-column joint types, flush end plate and header plate semi-rigid connections were provided. One group, therefore, is composed of specimens with flush end plate beam-to-column connections and the other has those having header plate beam-to-column connections. Two bare frames (BF), two thin steel plate shear walls (TSPSWs) having the panels attached to the boundary frames on all their edges and two innovative TSPSWs with the steel plates connected to the beams only are designed for quasi-static testing. All properties of the specimens are given in Table 4.1.

Table 4.1: Properties of the Specimens

Specimens	Beam-to-column connection type	Panel-to-frame connection type
BF-F	Flush end plate connection	Bare frame (without steel panel)
SW-A-F	Flush end plate connection	Steel panel connected to boundary frame on all edges
SW-B-F	Flush end plate connection	Steel panel connected to beams only
BF-H	Header plate connection	Bare frame (without steel panel)
SW-A-H	Header plate connection	Steel panel connected to boundary frame on all edges
SW-B-H	Header plate connection	Steel panel connected to beams only

The experiments are conducted in the Structural and Earthquake Engineering Laboratory (STEEL) of Istanbul Technical University (ITU). This facility is equipped with a 750kN capacity reinforced concrete reaction wall that has dimensions in vertical plane of 4.55m by 5.57m and a thickness of 0.60m. Load is provided through a computer-controlled MTS hydraulic testing system using actuator which is capable of producing up to 250kN.

Detailed information about design of the specimens, test-setup and instrumentation of the specimens will be given in the following sections.

4.1 Objectives

Previous experimental works which have been carried out are generally on the conventional thin steel plate shear walls in which infill panels have been attached to the boundary frames on their all edges as mentioned in Chapter 2.

Although previous experimental and analytical investigations provide much powerful and useful information about the behavior of TSPSWs, no tests on the shear walls with infill panels connected to beams only have ever been conducted. Also, there is no any comparison between the conventional shear wall and that with the panel attached to beams only. However, an analytical study was performed considering these types of steel plate shear walls **(Xue and Lu, 1994a)**.

The objective of the tests is to provide information about the behavior of steel plate shear walls composed of infill plates with no connection to the columns and to compare the behavior of innovative TSPSW with that of the conventional one under lateral quasi-static load. Aspects of prime interests are initial stiffness, load level at which yielding first occurs, ductility, energy absorbtion, cyclic stability and the failure mode of the shear walls.

In fact, the effect of the behavior of the beam-to-column connection type on that of TSPSWs was initially aimed. Because the load capacity of the actuator was exceeded during the pilot test unless the ultimate strength of BF-F was reached, TSPSW specimens with flush end plate beam-to-column connections could not be tested to prevent the actuator system from any possible damage. However, the specimens that were not tested are described in the following section. These specimens will be tested when the new actuator system that is purchased within the project of The Scientific & Technological Research Council of Turkey is installed.

The test results and hysteresis behavior of the specimen BF-F are given in Appendix A.

4.2 Test Design Considerations

The design of the specimens was influenced by a number of factors. The actuator which will be used in the tests is capable of producing up to 250 kN. Because of this low loading capacity the scale of the specimens were selected to be 1 / 3. In addition to this, in the design of the infill panels since the thickness of the infills directly affected the lateral load carrying capacity of the specimens, actuator capacity were also considered while determining the infill plates' thicknesses. Due to this issue, the thicknesses of the infill panels used in the tests were 0.50mm. The material yield and ultimate stresses of all steel panels were 187.7 MPa and 317.2 MPa, respectively. The test results of the coupons cut from the panel in two orthogonal directions are given in Chapter 5 in detail.

The column spacing and storey height were constrained by the location of anchor holes in the laboratory strong floor and reaction wall. The column spacing and the spacing of the additional frame which was used to prevent out-of-plane deformation of the specimens were selected to be as close to equal as this constraint permitted.

The specimens were to be constructed of elements and materials commonly available in Turkey and fabricated using industry-standard details and methods.

4.3 Design of Test Specimens

The thin steel plate shear walls and bare frames are shown in Figure 4.1, Figure 4.2 and Figure 4.3 respectively. All test specimens are one-story and single-bay systems. TSPSWs are composed of steel frame (two columns and two beams) and one thin steel infill plate which is produced by cold-formed process. BFs are the steel frames with semi-rigid beam-to-column connections without infill panels. During the design of test specimens, limitations of the equipment available for quasi-static testing in the STEEL of ITU are also considered. Due to the load capacity (250 kN) of the actuator utilized in the tests and to space restrictions, one-third scale models are tested. Figure 4.4, a schematic of entire setup, is presented to aid in the description of the design of the surrounding frames and test setup.

Although TSPSW specimens with flush end plate semi-rigid beam-to-column connections could not be tested they are defined in this section.

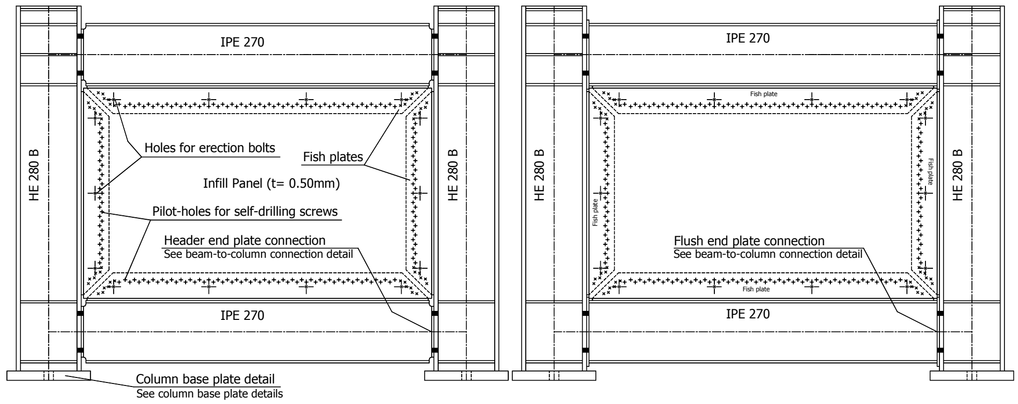

Figure 4.1: Test Specimens of TSPSWs with Panels Connected to Boundary Frames

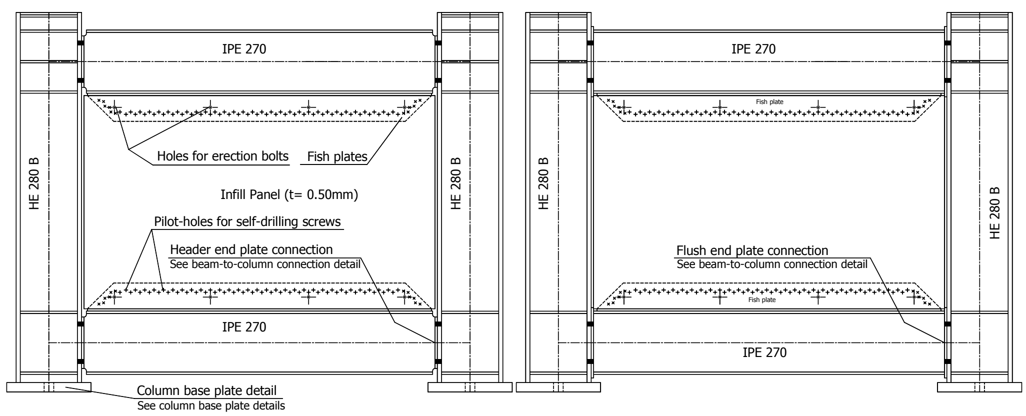

Figure 4.2: Test Specimens of TSPSWs with Panels Connected to Beams Only

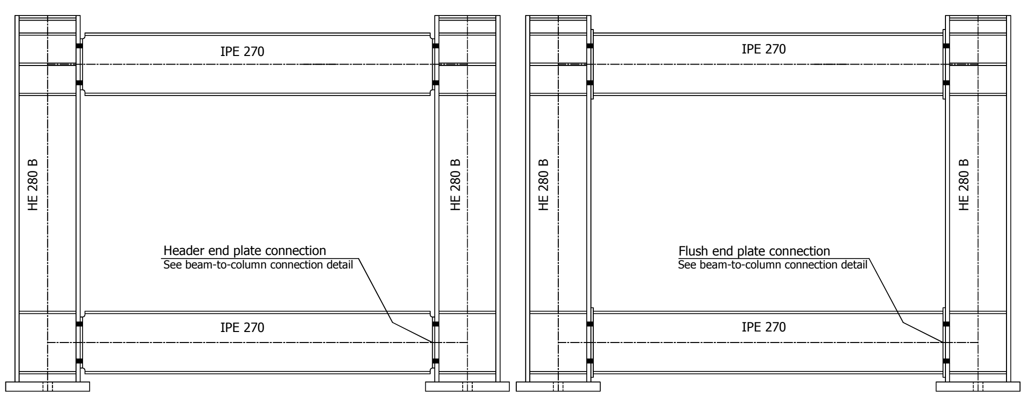

Figure 4.3: Test Specimens of BFs without Panels

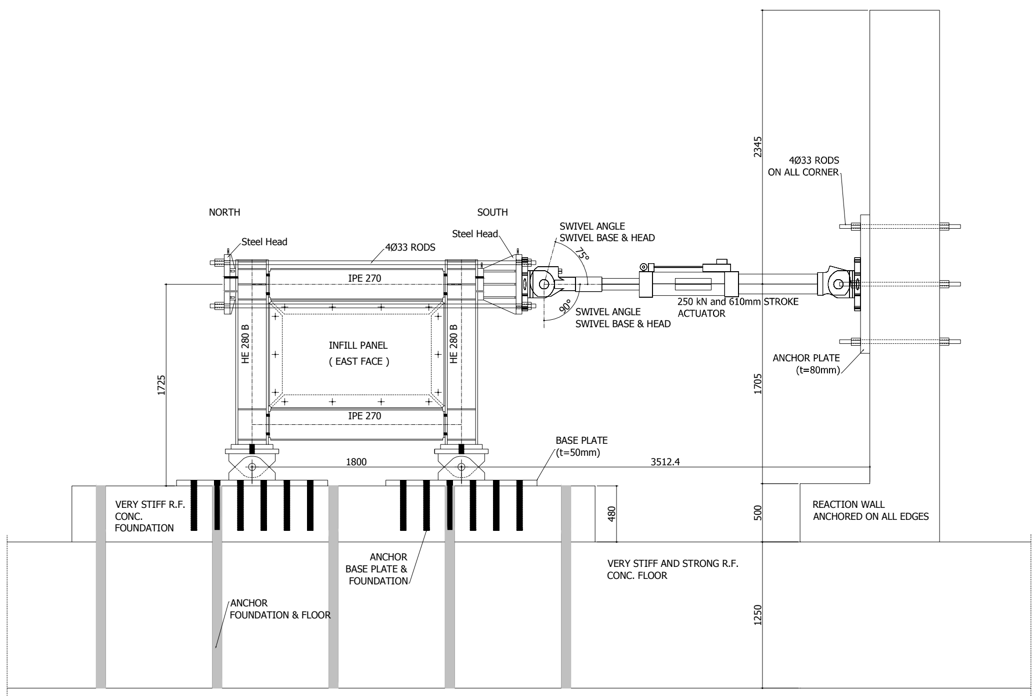

Figure 4.4: Test Setup

Two different types of boundary frame-to-infill panel connections were designed. One of TSPSW specimens has a connection between their all edges of infill panels and fish plates welded to flanges of the frame members while the infill plate in the other type of them is connected to the fish plates welded to upper and lower beams only. Infill panel-to-fish plate connection is provided through self drilling screws together with a few erection bolts.

The TSPSW specimens were designed such that the frame members would remain elastic under the maximum possible loading. This was done to insure the safety of the test and so that the same boundary frame could be re-used in future experiments. To account for the possibility of obtaining infill panel materials with larger yield stress than the 235 MPa initially assumed, and to take any possible strain hardening, the boundary frame was designed as if the infill plates could develop three times the full capacity of the actuator (250 kN) to be able to re-use the surrounding frame in the further tests by new actuator that is capable of producing up to 1000 kN. The thickness of the infill panel (0.50mm) is also determined such that the lateral load carrying capacity of TSPSW specimens will not exceed the capacity of actuator.

Two steel heads that are different from each other for each column are also designed to safely push and pull the specimens. Due to presence of steel heads attached to the column flanges at the level of the top beam to prevent local deformations of the column flanges, the stiffeners were used in the panel zones of beam-to-column connections.

4.3.1 Design of boundary beams and columns

SAP2000 pushover analyses of strip models and ABAQUS nonlinear finite element analyses of the test specimens were used to determine the maximum moments, shear forces, and axial forces in the boundary frame. The beams and columns were then designed to remain elastic under these maximum actions with the safety of factor of 3.0.

These design actions and some practical considerations (i.e. providing commonly available profiles and materials) resulted in the selection of HE280B columns and IPE270 beams. Steel for the boundary frame members is specified to be Fe44. Due to the need to re-use the boundary frames for additional testing in the further research, coupon tests of the frame material were not performed. However, because of that the failure in beam-to-column connections will occur by yielding of beam end plate is expected coupon tests of the beam end plate material were performed and their results are given in Chapter 5. Overall dimensions and section sizes of the boundary frame are shown in Figure 4.5.

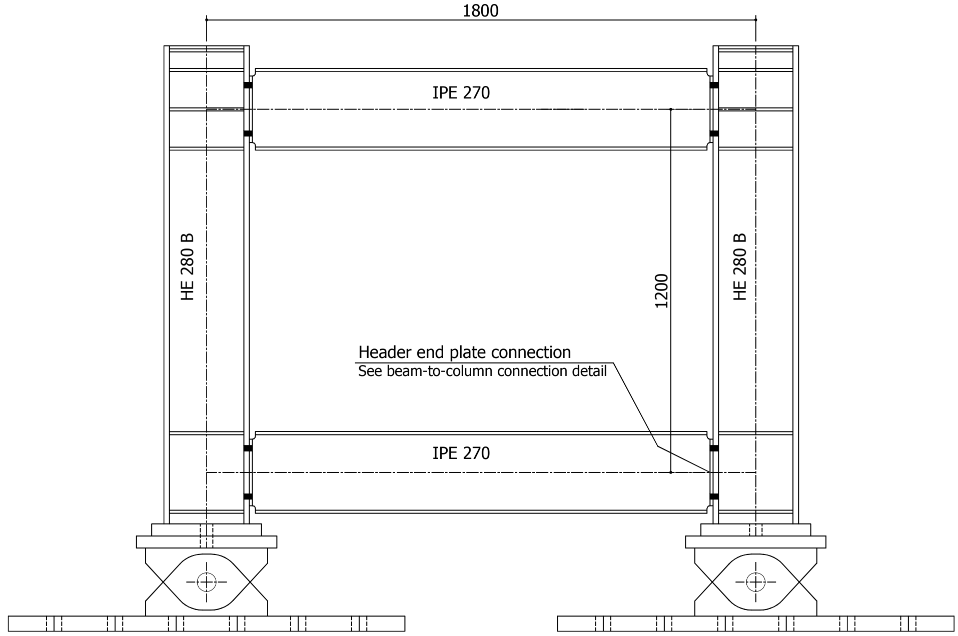

Figure 4.5: Boundary Frame Detail

4.3.2 Beam-to-column connections

TSPSWs may use either full moment-resisting or simple beam-to-column connections. In these systems, semi-rigid and partial-strength connections are employed. It is well known that when a TSPSW has full or partial moment-resisting beam-to-column connections pinching in the load-deformation hysteresis loops is reduced and the energy absorption characteristic of infilled frames are therefore increased. In this study, semi-rigid beam-to-column joints with header plate and flush end plate connections are used in the specimens separately.

Beam-to-column connection behavior was also taken into account in the structural analyses. The initial stiffness and moment carrying capacity of the connection, designed as semi-rigid and partial strength connection type, were determined in accordance with the Eurocode 3 (EC3).

In TSPSWs specimens, beams are attached to the flanges of the columns through the end plates by four bolts. Beam-to-column connection details are given in Figure 4.6 and Figure 4.7.

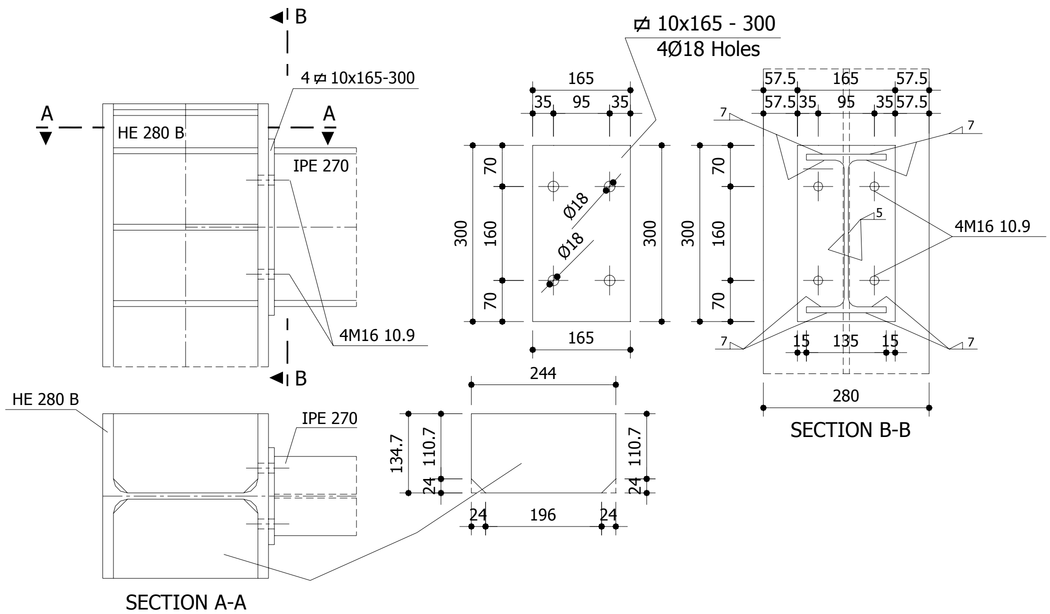

Figure 4.6: Beam-to-Column Joint Detail with Flush End Plate (dimensions in mm)

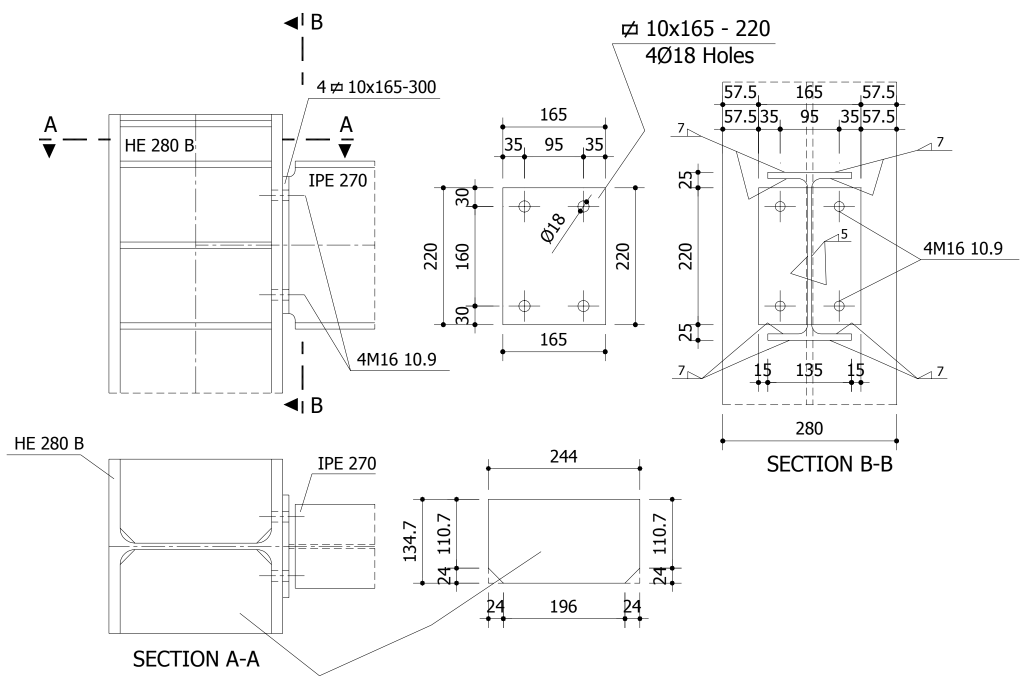

Figure 4.7: Beam-to-Column Joint Detail with Header Plate (dimensions in mm)

4.3.2.1 Modelling of beam-to-column connections behavior

The methods for predicting the beam-to-column joint behavior can be divided into five different categories such as empirical models, analytical models, mechanical models, finite element models and experimental testing **(Faella et al., 2000)**.

As the aim of the joint modelling is to account for the joint rotational behavior in the steel plate shear wall analyses, it is evident that the prediction of joint behavior by means of one of the methods mentioned before has to be generally accompanied by a mathematical representation of the moment-rotation curve, which is necessary to be utilized as input data in computer programs for the structural analyses of steel plate shear walls with semi-rigid beam-to-column connections.

Each method for predicting the joint rotational behavior has therefore to be combined with mathematical reperesentation of moment-rotation curve. The relationships to represent the M-φ curve can be split into two groups such as stiffness, resistance and shape factor based formulations and curve fitting by regression analysis **(Faella et al., 2000)**.

In the method using stiffness, resistance and shape factor based formulations, there are four different mathematical representations of the moment-rotation curve which are called linear, bilinear, multilinear and nonlinear representations shown in Figure 4.8.

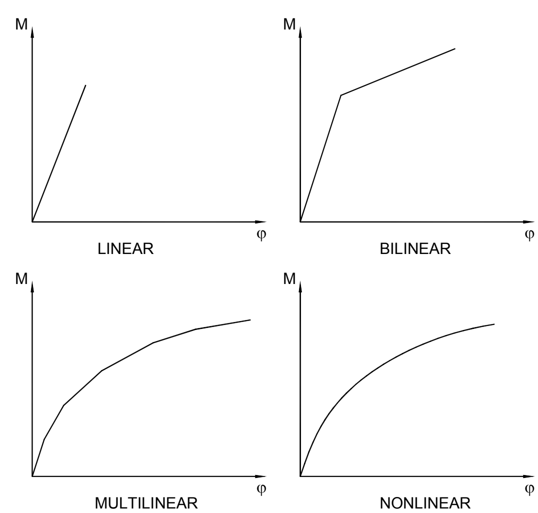

Figure 4.8: Mathematical Representations of the Moment-Rotation Curve **(Faella et al., 2000)**.

The linear representation, the simplest one, requires a single parameter, the joint rotational stiffness K_φ. The initial rotational stiffness K_φ, the plastic flexural resistance $M_{j,p}$ and the plastic (hardening) rotational stiffness $K_{\varphi,p}$ are necessary for the bilinear representation while five parameters, namely, the initial rotational stiffness K_φ, the first yielding moment $M_{j,y}$, the post-yielding rotational stiffness $K_{\varphi,y}$, the plastic moment $M_{j,p}$ and the plastic (hardening) rotational stiffness $K_{\varphi,p}$, are required for the trilinear representation of the moment-rotation curves **(Moncarz and Gerstle, 1981)** given in Figure 4.9.

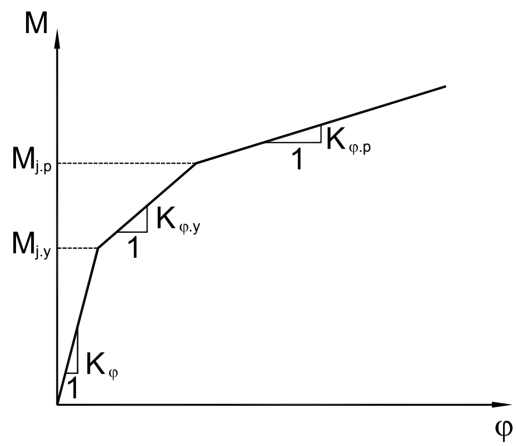

Figure 4.9: Trilinear Model of Moncarz and Gerstle **(Faella et al., 2000)**.

A very simple nonlinear representation of the moment-rotation curve is obtained by means of the Ramberg-Osgood relationship depending on the three parameters, the initial rotational stiffness of the joint K_φ, the rotational stiffness, K corresponding to the ratio of M_o to a permanent rotation φ_o, the shape factor n **(Ramberg and Osgood, 1943)**.

In this study, four parameter nonlinear representation of the moment-rotation curve, expressed by the Eq. 4.1, is utilized **(Goldberg and Richard, 1963 and Abbott and Richard, 1975)**.

$$M = \frac{(K_\varphi - K_{\varphi,p})\varphi}{\left(1 + \left|\frac{(K_\varphi - K_{\varphi,p})\varphi}{M_o}\right|^n\right)^{1/n}} + K_{\varphi,p}\varphi \qquad \textbf{(4.1)}$$

Where K_{φ}, $K_{\varphi,p}$, M_o, M and n are initial and plastic stiffness, a reference bending moment, computed bending moment and a shape factor, respectively.

One advantage of Eq. 4.1 over the Ramberg–Osgood is that it has ability to allow for positive, zero and negative value of $K_{\varphi,p}$. Therefore, Eq. 4.1 can be used also for moment-rotation curves exhibiting a softening or hardening branch. The post-buckling behavior of the column web in compression can be given as an example for the case of a softening branch **(Faella et al., 2000)**.

4.3.2.2 Design of beam-to-column connections

In the modelling of the semi-rigid beam-to-column connection behavior, for the representation of the moment-rotation curve nonlinear approximation obtained by using Eq. 4.1 is employed.

In order to be able to apply the Eq. 4.1 to get the moment-rotation curve of beam-to-column joint, initial and plastic stiffness and the reference bending moment of the connection have first to be calculated. In addition to this, the rotation values of φ should also be known. These parameters except for plastic stiffness and rotations are then initially obtained based on the provisions of Eurocode 3.

In above formula given in Eq. 4.1, $K_{\varphi,p}$ is taken to be equal to zero for the simplicity and because of that failing due to the buckling of the compressed zone of column web panel is not expected. It is also assumed that reference value M_o equals the plastic moment capacity of the connection. Therefore, the moment-rotation curve that is considered in the structural analyses has a straight branch continuing in horizontal direction after the moment capacity of the connection is reached. The rotation values varying from 0.00rad to 0.05rad with the interval of 0.005 are arbitrarily determined.

Two different moment-rotation curves, shown in Figure 4.10 and Figure 4.11, are separately achieved for beam-to-column connections with flush end plate and header plate. The calculation procedures which were performed in accordance with EC3 for these two type connections are given in Appendix B in detail. Briefly, yield strength of the beam end plates material using in determining the moment-rotation curves was obtained by the coupon tests. The moment capacities of the connections were increased by 50% in order to account for possible overstrength due to, for example, strain-hardening. The shape factor, n was assumed to be equal to 3.0 for header plate, 2.5 for flush end plate connection type.

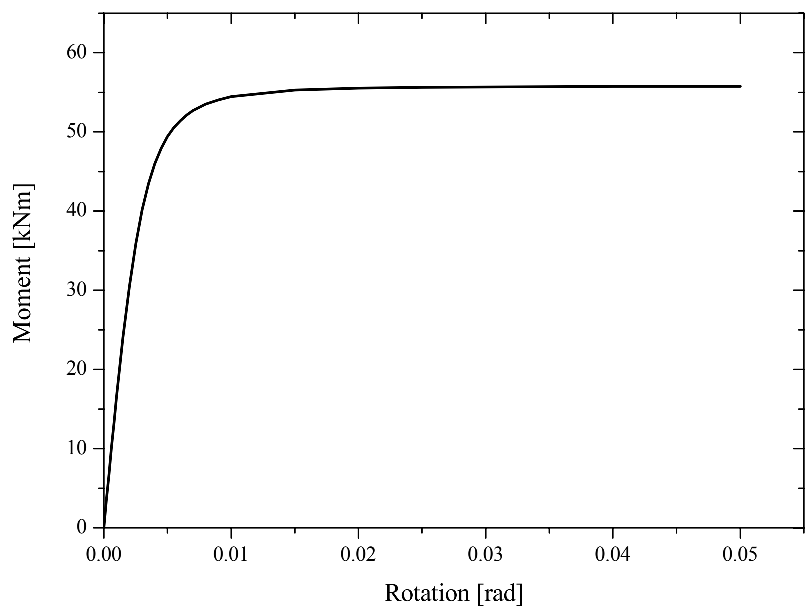

Figure 4.10: Moment-Rotation Curve for Flush End Plate Connection

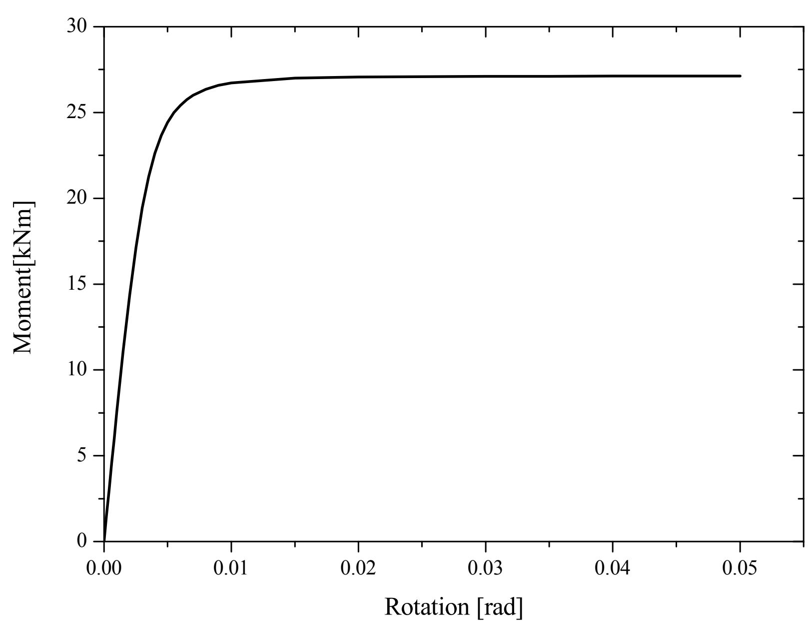

Figure 4.11: Moment-Rotation Curve for Header Plate Connection

4.3.3 Infill panel-to-fish plate connection

In fact, the use of two types of connections was initially decided to attach the infill panel to the fish plates welded to flanges of the columns and beams. Epoxy (Concresive 1406) which is made of two components would have been utilized as a fastener, but to properly apply the epoxy to the surfaces within the duration of 50min. given in its specification was found to be impractical and too difficult in the sites, for example, in case of strengthening of a steel building, epoxy application can not be practical solution for providing infill panel-to-fish plate connection. Furthermore, in the test conducted using epoxy at UB (New York State University at Buffalo) it was observed that the epoxy which connected the infill panel to the boundary frame failed across entire length of the top beam connection while the specimen still exhibited mostly linear behavior. The resistance of the epoxy against the fire which is needed to be investigated, but not considered within this research, is the most significant phenomena for the structural systems that are especially providing the lateral support with the buildings against earthquake and wind.

Since it must be necessary to connect the infill panels to the fish plates such that infill plate develops full capacity of tension field, connection design was totally changed. Instead of using epoxy for attaching the infills to surrounding beams and columns, self drilling screws whose diameter were 5.50mm, the capacity of drill thickness was 12mm and mostly employed in the cladding works to fix metal sheets to flanges of purlins were used. Infill panel-to-fish plate connection detail is shown in Figure 4.12.

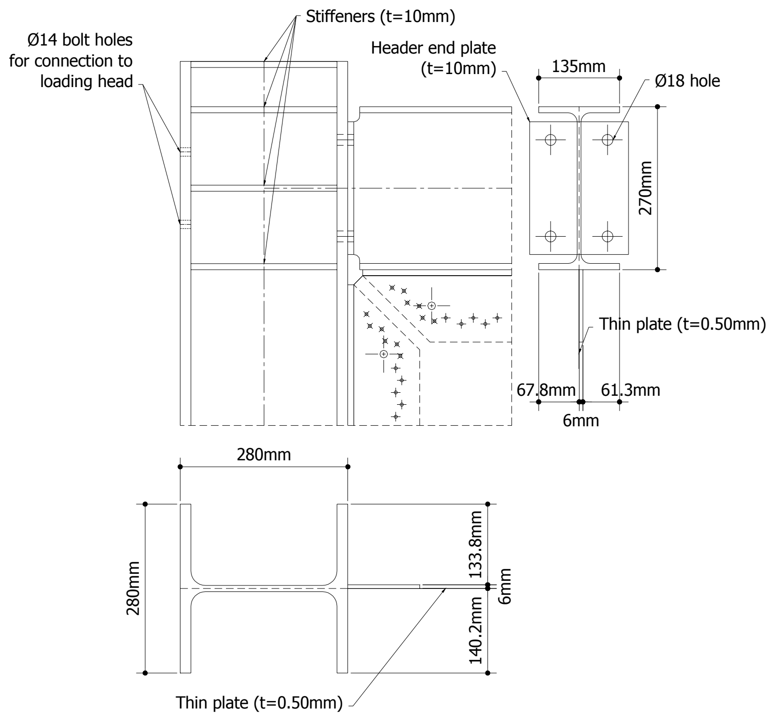

Figure 4.12: Infill Panel-to-Fish Plate Connection Detail

4.3.3.1 Design of infill panel-to-fish plate connections

In the design of infill panel-to-fish plates, the results of the pushover analyses of the strip models of the specimens were considered. The connection was designed such that any significant failure would not occur in the connection until the full tension capacity of gross section of the strips was reached. This results in safe factor of 1.5 using in determining the number of screws at each strip end.

In order to obtain the performance and the ultimate load of the screw connections, a series of test was done using five specimens whose details and test results are given in Chapter 5. Each specimen has one screw and two strip plates that represent the infill panel (0.50mm) and fish plates (6.00mm). The screw material is 1022 steel, which is typically used for moderate strength structural applications such as cold formed fasteners and bolts. It is often used in the case hardened condition. The minimum yield and tensile strength of 1022 steel are approximately 310MPa and 410MPa, respectively.

In addition to this, the ultimate load which is controlled by the total yielding of the plate strip (equivalent truss element), were also taken into account. In the first step, the number of self drilling screws was determined at the end of the each strip. After obtaining the total number of screws, spacing between the screws was selected. Two screw lines whose arrangement is shown together with the erection bolts in Figure 4.13 in detail, were used to avoid premature tearing of the infill panels in net sections. The distance between two lines was selected to be 10mm due to the holes of erection bolts which were used for properly installation of the infill panels. The horizontal distance between the two screws was designated so as not to exceed three times the diameter of the screw.

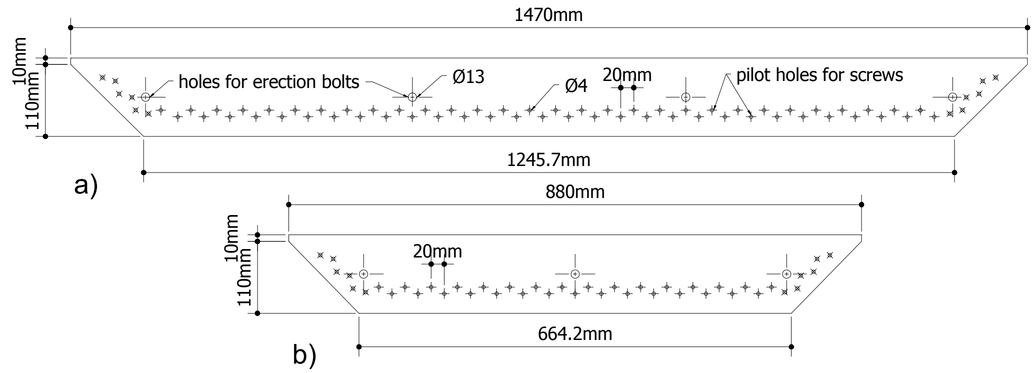

Figure 4.13: Fish Plates Details, a) for beams, b) for columns

4.4 Design of Foundation Plates and Clevises

Anticipated support reactions from the two thin steel plate shear wall specimens were found to be as small as they were carried by reinforced concrete foundation and slab. Therefore, no additional arrangement was needed for these existing systems. Also, the holes on the foundation slab were not at the proper locations for the desired specimen dimensions. This warranted the design of a new foundation made from steel plate, with the added benefit that it could more easily accommodate different specimen dimensions in the future. In order to create the pinned connection at the column bases, steel clevises were also designed so as to support the anticipated loads. The overall dimensions of the foundation plate and clevis are given in Figure 4.14.

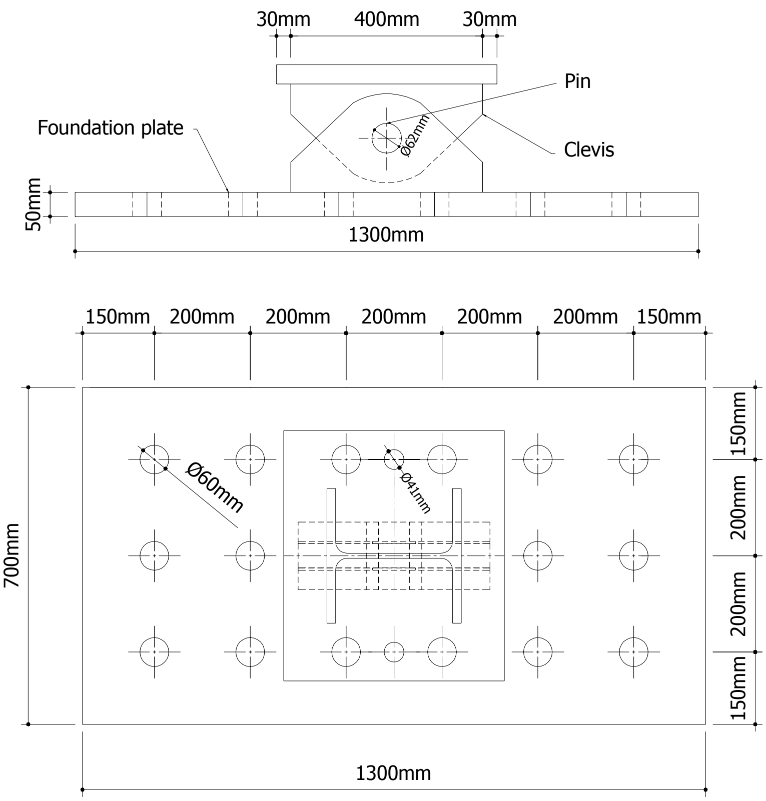

Figure 4.14: Foundation Plate and Clevis

4.4.1 Design loads

The new foundation plates and clevises were meant to become permanent parts of the available equipment in the STEEL of ITU. In anticipation of future possible loading scenarios, it was found that the support reactions of the TSPSW specimens were the largest anticipated. For further research that will be performed by using the new actuator which is capable of producing up to 1000kN but, the load carrying capacity of the reaction wall that the actuator will be mounted is 750kN. So, it was deemed appropriate to design the foundation plates and clevises for 2.0 times the maximum support reactions for these specimens assuming the loading actuator was developing its full capacity. This meant that each clevis would be designed for a horizontal force of ±500kN.

4.4.2 Foundation plate configuration

Each foundation plate was secured to the 480mm thick reinforced concrete strong slab using 12 bolts with 40mm diameter. This concrete slab was also anchored to the

1250mm thick reinforced concrete floor of the STEEL of ITU by 16 prestressed, 33mm diameter bars. The resulting friction between the slab and plates in the maximum uplift condition was deemed sufficient to resist horizontal sliding based on the previous tests. The overall configuration of one foundation plate with the two clevis parts is shown in Figure 4.15.

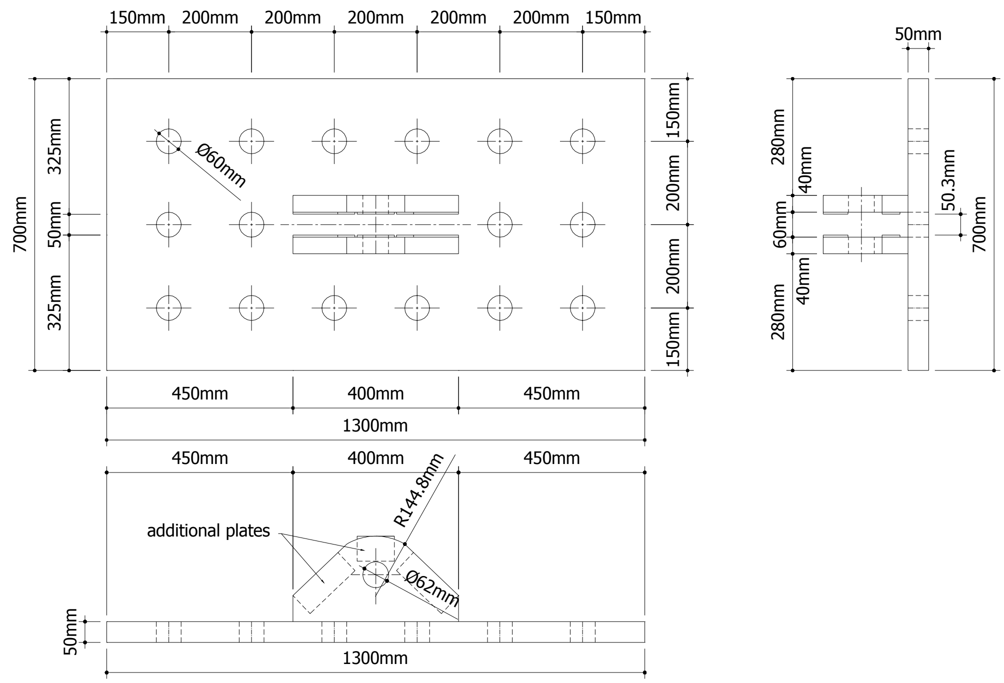

Figure 4.15: Foundation Plate Details with Clevis Parts

4.4.3 Design of clevises

The design loads for the clevises are the same as in the the design of the foundation plates. A clevis, shown in Figure 4.16, is composed of two 40mm thick vertical plates fixed to the foundation plate with groove weld and one 50mm thick vertical plate and 40mm thick horizontal plate. These two plates were also welded to each other. A 61.7mm diameter bar (pin) was used to provide a pinned connection between two parts from column base and foundation plate in each clevis.

Six additional plates (~4.9mm) in each clevis were welded to inside surfaces of the plate parts of the clevis connected to the foundation plate to fill the gab which was occured when the other clevis part attached to the column base was placed between two clevis members.

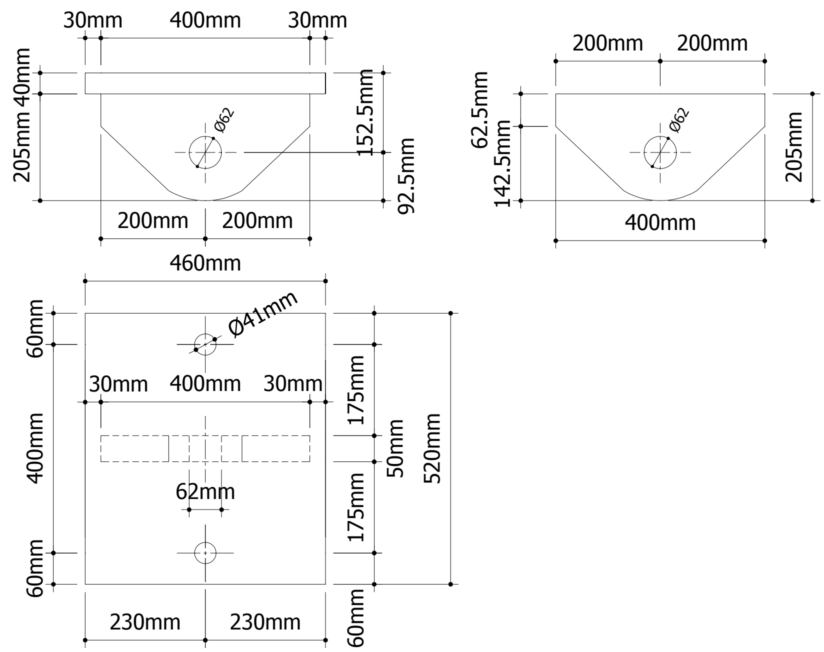

Figure 4.16: Schematic View of Clevis Parts Attached to Column Bases

4.4.4 Design of steel heads for loading

In the tests, the half of the stroke of the actuator was used because of quasi-static cyclic loading. Due to the distance approximately 380mm between the south column outside flange and outside face of the actuator head and to properly apply the pulling force on the specimens as well it was required to design two steel heads, shown in Figure 4.17, mounted to each upper end of the columns. These members are attached to each other through four high strength rods with diameter of 33mm. In order to properly install the steel heads at the top end of the columns two bolts with 12mm diameter attaching outside column flanges to steel heads are used for each connection.

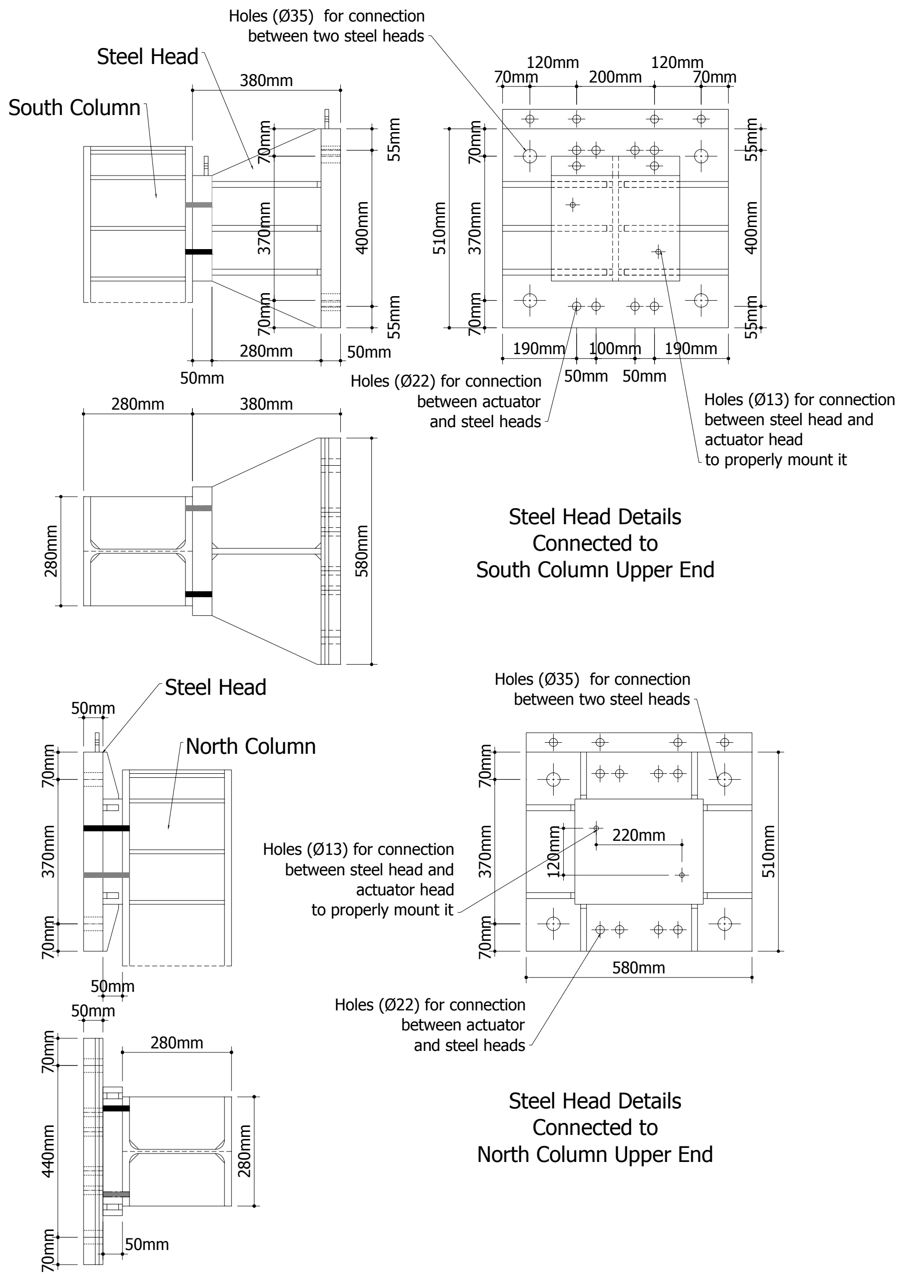

Figure 4.17: Schematic View of Steel Heads

4.5 Test Setup

In this section, test specimens, BF-H, SW-A-H and SW-B-H, shown in Figure 4.18, Figure 4.19 and Figure 4.20, respectively prior to testing and test setup are described giving detail information as well.

4.5.1 Mounting of specimens

Testing was performed in the STEEL of ITU. The foundation plate was fixed to the very stiff foundation slab connected to the strong floor as described in Section 4.3. Each specimen was mounted on the clevises that were designed together with foundation plates. Two 40.7mm diameter 10.9 bolts were used to attach each column base to the corresponding clevis part, and then to attach each clevis part to the foundation plate 61.7mm diameter Fe52 pin was utilized. All bolts except for pin were tightened to their specified internal tension.

Figure 4.18: Specimen BF-H Prior to Testing

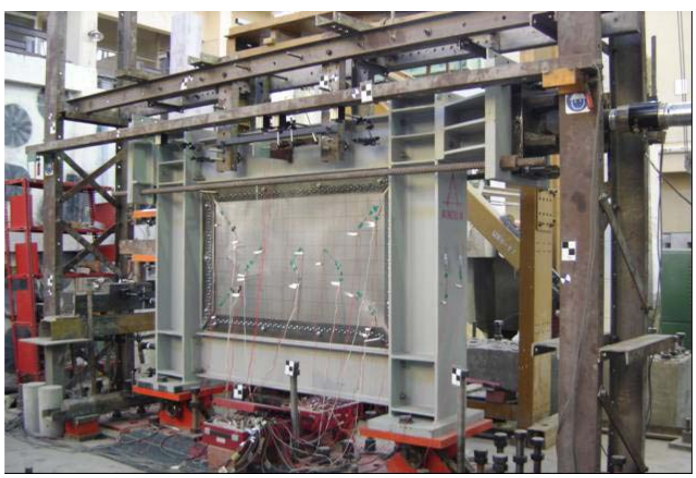

Figure 4.19: Specimen SW-A-H Prior to Testing

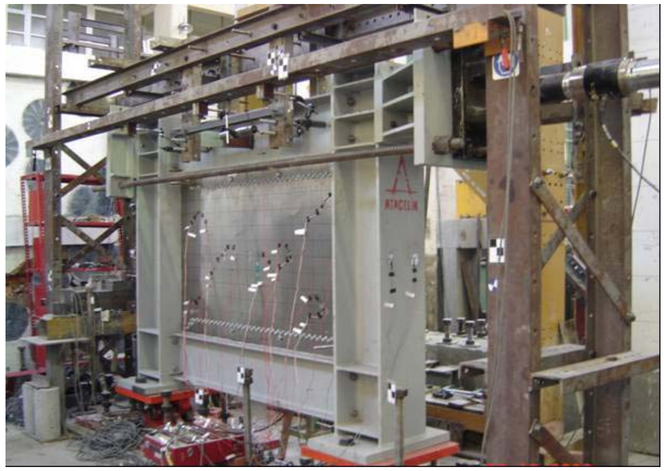

Figure 4.20: Specimen SW-B-H Prior to Testing

4.5.2 Actuator mounting

The actuator, manufactured by MTS Systems Corporation, with a load capacity of 250kN, and an available stroke of 600mm was mounted, as shown in Figure 4.21, to the reaction wall using four 33mm diameter high strength threaded rods. Eight high strength bolts with diameter of 22mm were used to connect the actuator to the test specimen. The actuator is equipped with swivels at each end and end-plates (heads) with holes to accept the rods. The reaction wall, actuator, specimen, clevises, foundation slab and strong floor were shown previously in Figure 4.4.

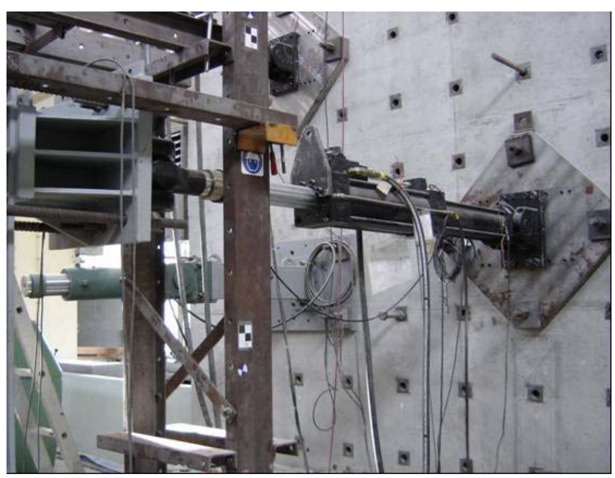

Figure 4.21: Mounting of the Actuator

4.5.3 Lateral bracing system

Lateral bracing was provided to the specimen through the use of steel rollers (Figure 4.22) cantilevering from frames mounted on the east and west side of the specimen and set to roll along the half of the web of the specimen's upper beam. A gab of approximately 2.0mm was left between the beam web and each roller so that the roller would only be engaged if the ouf-of-plane deflection closed that gab. In order to support the rollers four vertical cantilever beams which were connected to third of two horizontal beams were used. These two horizontal beams were supported at each end by two frames cantilevering from foundation slab. The connection of each two frames to the foundation slab was provided by six bolts with diameter of 33mm.

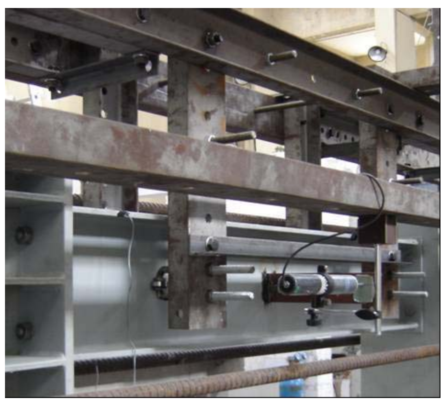

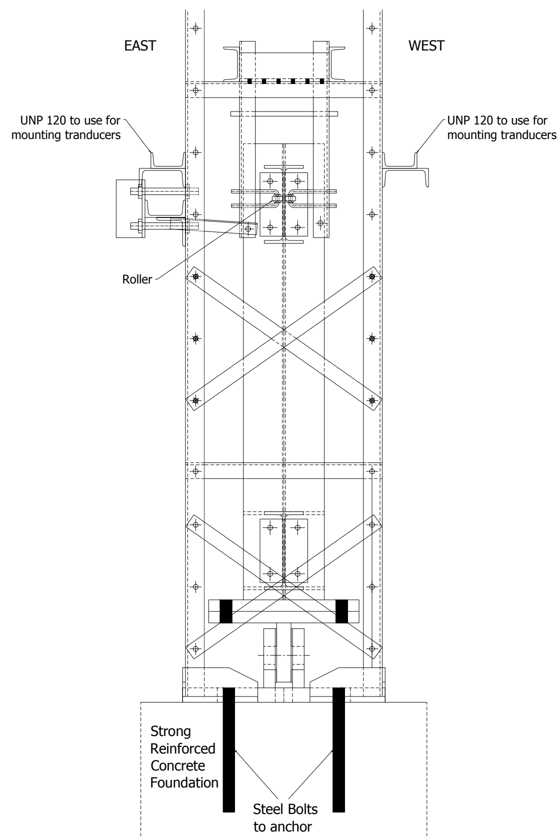

Schematic View of Lateral Bracing System

Figure 4.22: Lateral Bracing of Specimen

4.6 Instrumentation and Data Acquisition

All specimens with the exception of BF-H which is representing the reference bare frame and that is instrumented with transducers only were instrumented with KFG-3-120-C1-11L1M2R, KFG-3-120-D16-11L1M2S and KFG-3-120-D17-11L1M2S strain-gauges manufactured by Kyowa Electronic Instruments Co., Ltd. C1, D16 and D17 indicate uniaxial strain-gauge, biaxial and triaxial strain rosettes, respectively. The length of the strain-gauges is 3.0mm and their gauge resistances are given as nearly 120Ω. A total of 53 strain-gauges with the strain rosettes that were located on both steel panel and boundary frame members were affixed to each TSPSW specimen separately.

Additionally, 12 transducers whose stroke capacities vary from 10mm to 200mm were used.

65 data acquisition channels except two channels used for loading system were required to read the input from the electronic devices. For this purpose, the use of a switch box, shown in Figure 4.23, was needed on test site. The data was processed using a software program, namely TestWare-SX using Operating System (OS/2) Version 2.1, to display the load versus deflection curves for all specimens during the test on PC monitor.

Figure 4.23: Switch Box Used on Test Site

4.6.1 Strain-gauges

A total of 23 uniaxial strain-gauges, 12 biaxial and 2 triaxial strain-rosettes in total were used to measure strains in infill panel and at the mid-heigth of the top beam and south column during testing for all TSPSW specimens. Biaxial rosettes were placed on east and west faces of the infill plates such that the orientation of the strain-gauges would be in vertical and horizontal directions. The gauges which were oriented at 45^o from the horizontal were also added to obtain the angle of the principle stresses at the corners and the center of the panel. In order to also identify the any variation in the magnitude of the tension field strains along a path 45° from the horizontal, these gauges could be utilized. Apart from the other regions triaxial rosettes were employed at the center of infill plates with the additional one uniaxial strain-gauge mounted at 45^o from the horizontal on each face. Thus, there are three major clusters of gauges at mid-height on each face of the infill plates. The first cluster is at the centerline, the second and third are 304mm to the north and south of the centerline. Therefore, any variation in the magnitude of tension field strains across the infill plate can be recorded.

Hence, each face of the panel had six biaxial, one triaxial strain rosettes and seven uniaxial strain-gauges. All gauges on each face were directly opposite to each other. One strain-gauge bounded on the steel bar, which is one of the four bars utilized for the connection between two steel heads, was also used to measure the axial strains during the test. With this measurement, it was checked whether the steel bars remained elastic or not throughout the test.

No strain-gauge was used in specimen BF-H whose instrumentation was shown in Figure 4.24.

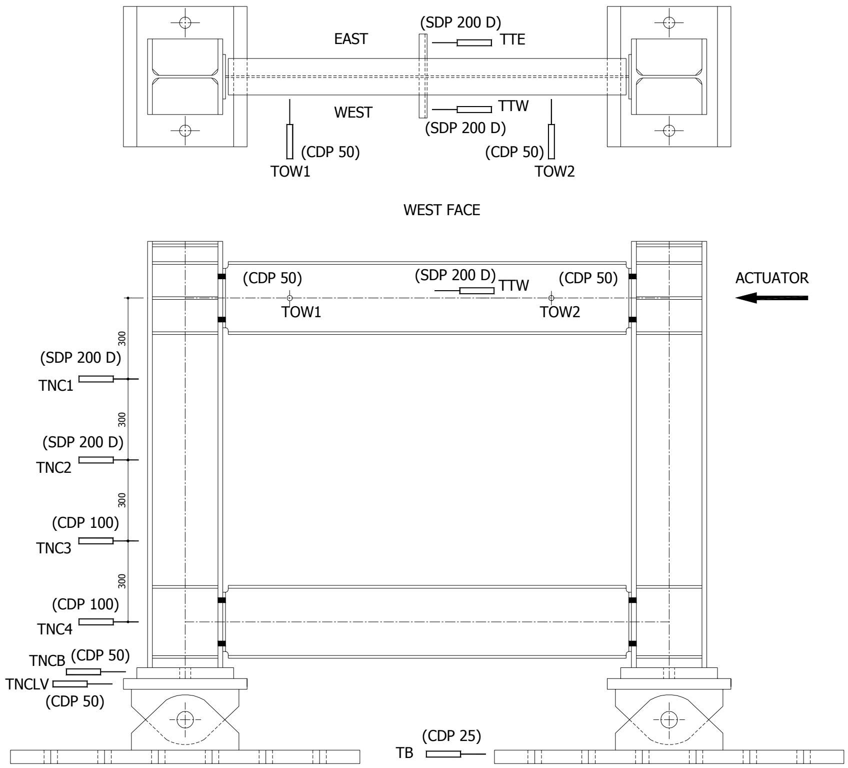

Figure 4.24: Instrumentation for Specimen BF-H

A total of eight strain-gauges, four by four, were bounded on south end of the top beam and bottom beam to record the variation of axial strains along the width of beam flanges in the beam-to-column connections of specimen BF-F. The configuration of its instrumentation is given in Figure 4.25. Furthermore, it was also able to be possible to monitor the beam-to-column connection behavior during the test.

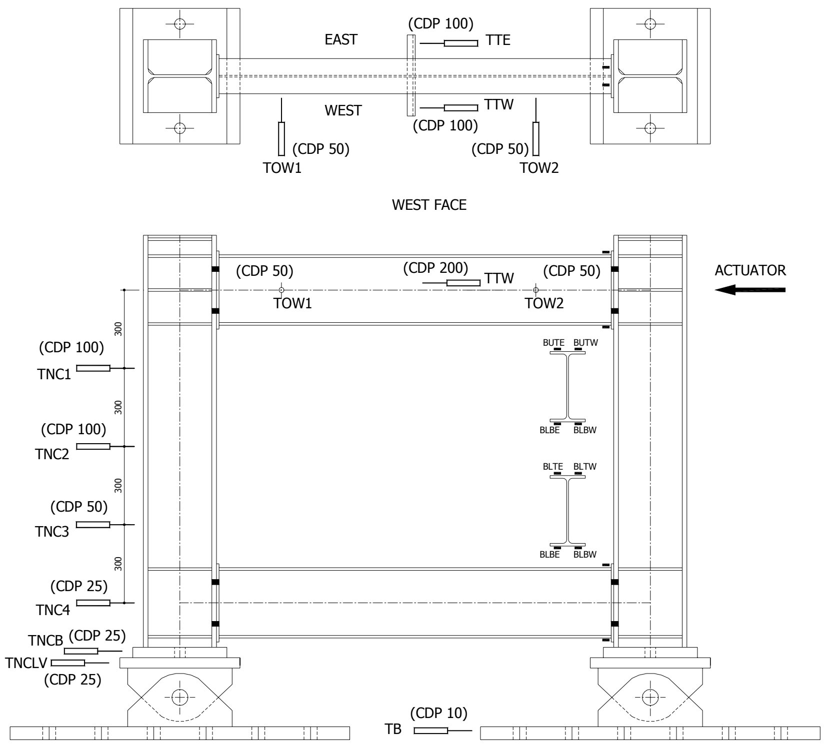

Figure 4.25: Instrumentation for Specimen BF-F

Instrumentation for the test specimens SW-A-H, SW-B-H is also given in Figure 4.26, Figure 4.27, Figure 4.28 and Figure 4.29 for each specimen face, respectively.

In addition to the strain gauges on the infill panels, a total of eight strain gauges were placed at the midpoint of top beam and south column to monitor the moments and axial forces there.

As a result, specimen SW-A-H and SW-B-H each had 53 strain gauges in total with those mounted on the top beam and south column while there were no any strain gauges mounted on specimen BF-H. Specimen BF-F, however, had eight strain-gauges at the south ends of the upper and lower beams.

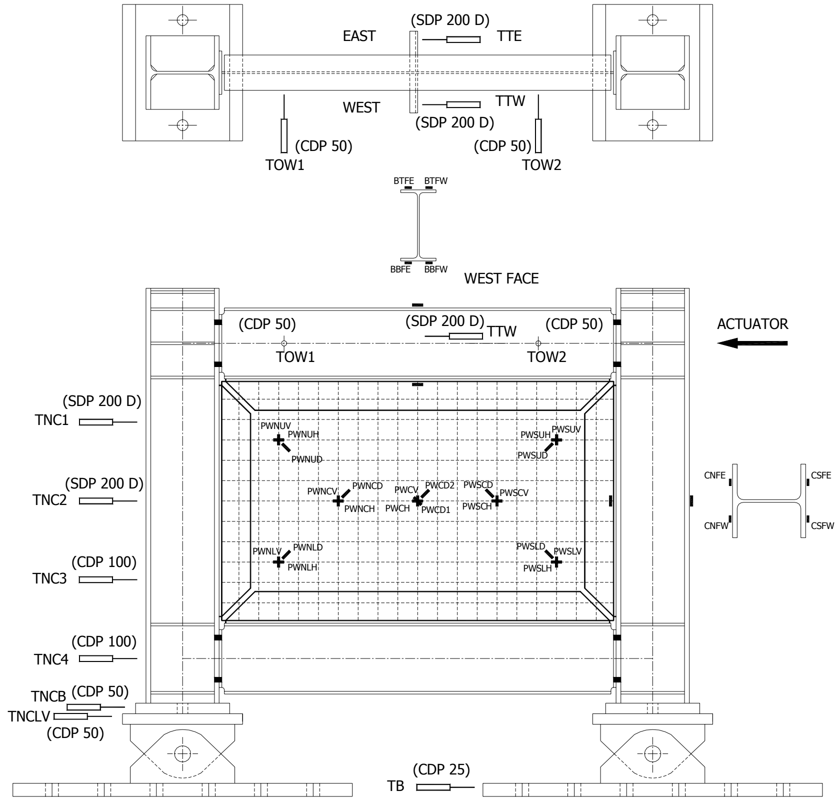

Figure 4.26: West Face Instrumentation for Specimen SW-A-H

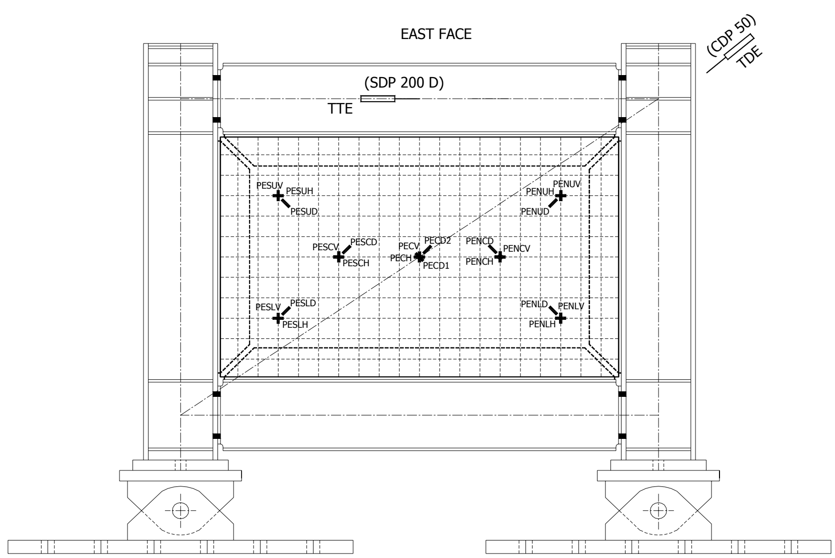

Figure 4.27: East Face Instrumentation for Specimen SW-A-H

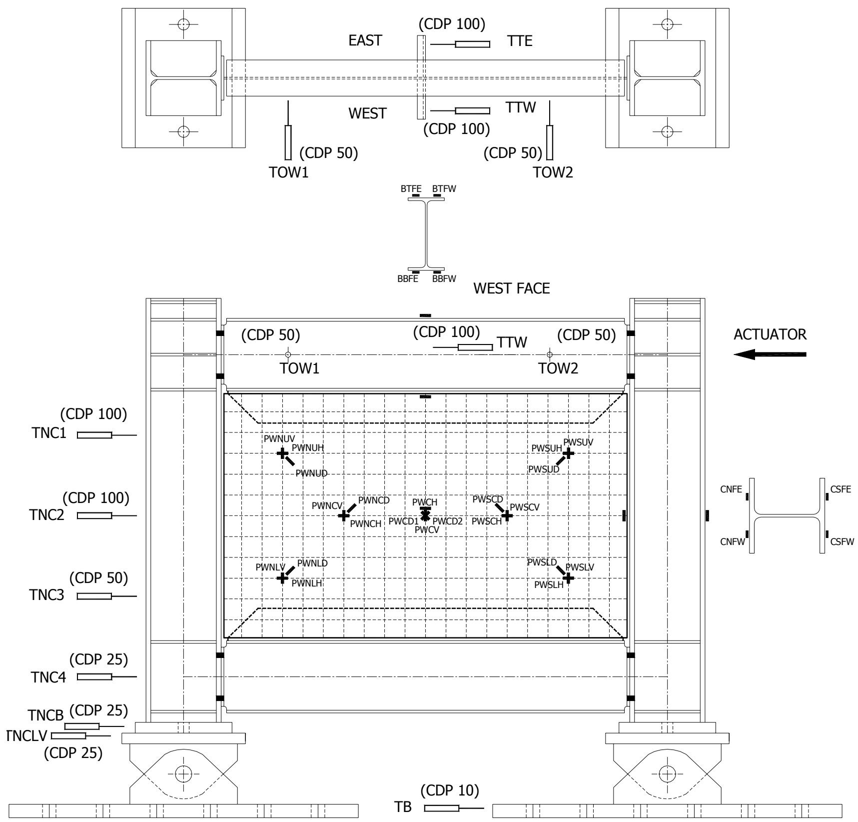

Figure 4.28: West Face Instrumentation for Specimen SW-B-H

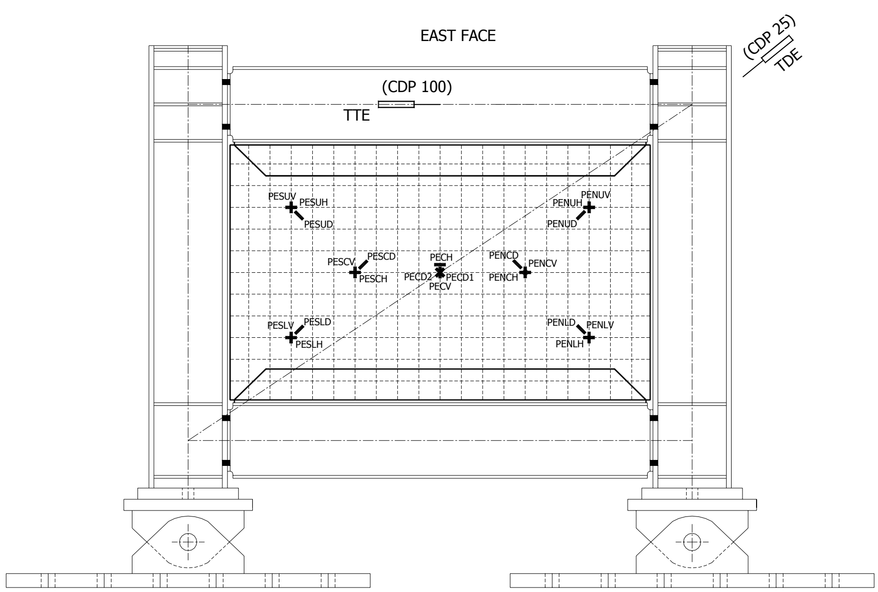

Figure 4.29: East Face Instrumentation for Specimen SW-B-H

4.6.2 Transducers

A total of 12 transducers were additionally utilized to measure and control in-plane and out-of-plane displacements in all TSPSW specimens. However, BF-H and BF-F use eleven transducers due to absence of that mouted in diagonal direction in TSPSWs.

The layout of the transducers was the same for all four specimens except for their stroke capacities and is shown in Figures 4.24, 4.25, 4.26 and 4.28. Since the most important measurement was determined to be the horizontal displacement of the frame TTW and TTE were used as the control for the top displacement during testing. TDE was also added to provide an additional instrument from which the horizontal displacement can be found and to obtain the global displacement in diagonal direction. The stroke capacity of the TTW and TTE was 100mm in specimen SW-B-H and BF-F while in other specimens those capable of measuring 200mm were used for TTW and TTE. The stroke capacities of all other transdusers were shown in Figures 4.24~4.28. TNC1, TNC2 and TNC3 are placed at the quarter points of the north column to measure any pull-in of that column by the yielding infill plates and also to achieve the deformed configuration of the specimens. TNC4 was utilized to acquire the relative displacements (drifts) between the top and bottom beams in the cycles. TNCB and TNCLV were used to measure any global movement of the specimens (also including slippage of the bolts). TB was placed at the foundation plates to take the measurements for the control of whole movement of the test setup with respect to reinforced concrete foundation slab. In addition to these transducers used for only measuring in-plane deflections of the specimens, TOW1 and TOW2 were employed to control the out-of-plane deformations of the top of the specimens throughout the tests. The out-of-plane measurements also monitored the effectiveness of the lateral bracing system.

4.6.3 Photogrammetric measurement and data acquisition

Photogrammetry is the art and science of defining the position and shape of objects from photographs. The results of photogrammetric measurements may be number

(3D coordinate of object points), drawings (maps and plans with planimetric detail and contour lines) or images (orthophotos) **(Kraus, 1993)**.

The significance of the contents of the photographs is at least as important as the geometric reconstruction of objects. The result of such photo-interpretation is the classification of objects by various features. Photogrammetry permits the reconstruction of the objects and it's the determination of some of their features without touching the objects.

The main use of photogrammetry is in the production of topographic maps. It can also be used to create dense fields of fixed points which can serve as a basis for ground surveys. The required accuracy of the coordinates can be ensured by proper selection of the scale of the photographs. A further application lies in close-range Photogrammetry, with object distances in the range from 1m to 100m. Particular uses are found in architecture, precision surveys of building and engineering objects, supervision of building operations and documentation of damage to buildings, measurement of artistic and technical models, deformation surveys, kinematic measurements and many others.

Photogrammetry is a technique that aims at obtaining the position, shape and geometric features of objects indirectly, that is, from one or more photographs. The advantage of the indirect measurement is very crucial for projects, as the photos can be taken remotely and the objects do not have to be entered.

The aim of the photogrammetric measurement in this research is to obtain the deflected shape configuration of the infill panels and also to see whether we can acquire the maximum and minimum value of out-of-plane deformations or not in order to obtain the initial imperfect configurations of the infill panels to impose on finite element models.

Photogrammetry is an efficient tool in monitoring of spatial objects with respect to location, form and shape. It's main advantage to other measuring techniques lie in the fact that the measurement is done on the images. This method has a wide range of application due to advantage of indirect measurement possibility. Thus, the recorded images contain a great extend of information so that many of the detailed acquisition of deformation can be done afterwards.

In this study, a photogrametric measurement was also performed to acquire the out-of-plane deformation configurations of infill panels. For this purpose, each face of infill plates were previously squared by permenant marker to create the intersection points to evaluate the deformed shape of the panels.

To evaluate the deformation of a steel panel, three-dimensional coordinates of control points mounted on the object must be known. In order to measure characteristic points which indicated the deformation must be projected at least in two image.

With known camera calibration parameters (interior orientation parameters) the unknown 3D-object coordinates (XYZ) can be computed by measuring their image coordinates of the object (in this case of the steel block) points. Their values can be determined with an adjustment procedure (bundle adjustment). The faulty measurements will be eliminated by this way and a precise measuring capability can be reached. In order to relate the determined XYZ coordinates to an overall coordinate system, control points with known coordinates are used.

Today in addition to so called classical, analog ways of photogrammetric data handling, digital methods are also used. This enables an automation of data processing by means of image analysis and matching techniques. 3D-object reconstruction techniques, classification or image detection and their integration into a deformation analysis procedure using information system technology can also be used.

In order to determine the deformation of a panel as a whole system, the 3D-shape of it must be reconstructed. This reconstruction procedure must be based on the determined coordinate of the building characteristic points. 18 control points were mounted on the object and surrounding environment. It is assumed that, after the tests, places of control points are not changed. Prior measurement was done on these control points using total station.

Using the digital technology, the photographic processing has disappeared. In this, a digital camera by Samsung 210 has been used. In order to use this camera for photogrammetric purposes, it is necessary to take the deviations of the camera and lens system from the central perspective via additional parameters into consideration.

These additional parameters for the calibration are realized in the Photogrammetry laboratory before the images were taken.

Images were taken at the beginning of the tests and also at the end cycle of each displacement level. At least 5 photos which are suitable for the photogrammetric evaluation were taken. The processing and evaluation of the images was done with a photogrammetric software package PICTRAN. For more detailed information, it can be reffered to **Vatansever et al. (2007)**.

4.7 Summary

A test programme was planned to investigate and to compare the behaviors of two thin steel plate shear walls subjected to lateral quasi-static loading. Shear wall test specimens consisted of partial moment-resisting frames with thin steel infill panels. Two specimens which were composed of bare frames were also designed. Hence, it would be possible to obtain the contribution of the thin infill panels as a lateral load-resisting member to the behavior of the shear wall system.

Before the tests, to be able to use in the future experimental researches as well, test setup members such as foundation plates and clevises, steel heads and lateral bracing system were designed.

The test specimens and other additional members were fabricated using standard industry procedure. Infill panels and hot-rolled sections are commonly available in Turkey.

Consequently, the phases of experimental design and test setup were described and test specimens and their instrumentation were defined in detail in this chapter.

5. ANCILLARY TESTS

Several ancillary investigations were carried out to complement the shear wall tests. In order to determine the actual yield and ultimate stresses of the infill panels and beam end-plates, tension coupon tests were conducted. These values were also used for the finite element models to be described in Chapter 6. Another test to determine the failure modes and the ultimate tensile force of the self-drilling screw connection type were performed. The values which were obtained by the latter test were used to determine the number of screws to provide the connection between the infill panel edges and fish plates. The standards and procedures to consider and the tests that were conducted are described in detail in the following sections.

5.1 Standards and Procedures

Testing of the tension coupons followed the requirements of TS 138 EN 10002-1 (Metallic materials-Tensile testing-Part 1: Method of test at ambient temperature). The coupons from infill panel materials were cut to meet requirements for "sheet-type" specimens that may have a thickness of between 0.10mm and 3.0mm. The coupons cut from the beam end-plates were proportioned as the same specimens that are required to have a minimum thickness of 3.0mm.

All coupon tests were conducted in a testing machine of 200 kN capacity. Strains were recorded using a mechanical extensometer with a gauge length of 100mm. In order to determine the modulus of elasticity, approximately 5 readings were taken in the elastic region.

5.2 Tension Coupon Tests

All tension coupon tests conducted are described in this section. Nine coupons in total were tested to determine the material behaviors of infill plates and beam end-plates.

A total of six tension coupons, shown with their dimensions in Figure 5.1, from the infill plates (all panels were cut from the same plate) were tested in uniaxial tension to determine the stress versus strain behavior. While three coupons were taken in horizontal direction, the rest were cut in vertical direction.

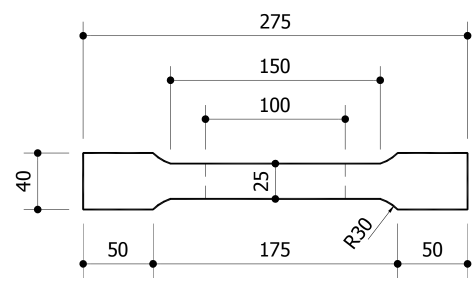

Figure 5.1: Detail of Tension Coupons for Infill Panel (dimensions in mm)

A total of three coupons, given with their dimensions in Figure 5.2, from beam end-plates (all plates were cut from the same plate) were also tested in uniaxial tension to determine the stress versus strain behavior.

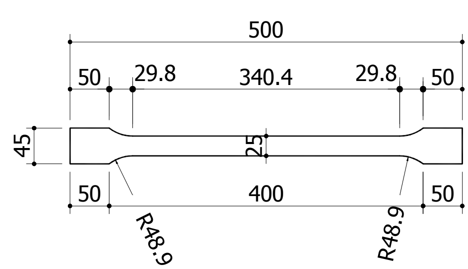

Figure 5.2: Detail of Tension Coupons for Beam End Plate (dimensions in mm)

Tension coupon tests were not performed for surrounding frame members and fish plates as the beams, columns and fish plates were designed to remain elastic during the tests. Steel for the boundary frame members (beams and columns) was specified to be St 44. Beam end-plates, column base plates, fish plates and foundation plates were specified to be St 37.

5.2.1 Test results

All tensile tests were performed at the Constructional Material Laboratory of ITU. The tensile test results are separately summarized for both infill panels and beam end-plates in the following sections.

The results of the tensile tests for the infill panels are shown in Table 5.1. The mean, standard deviation and coefficient of variation are given for all characteristic stress and strain values for panels. All specimens displayed extremely ductile behavior, with failure strains in excess of 40%.

Table 5.1: Infill Panel Tension Coupon Test Results

Coupon Mark	Width [mm]	Thickness [mm]	Elastic Modulus [MPa]	Yield Stress [MPa]	Ultimate Stress [MPa]	Failure Stress [MPa]	Failure Strain [%]
PV1	24.8	0.52	209121	186.3	304.2	243.3	49.0
PV2	24.7	0.51	194623	180.2	311.4	241.3	41.8
PV3	24.65	0.50	194939	191.0	318.3	278.5	45.5
PH1	24.8	0.51	189961	183.2	317.9	232.6	41.5
PH2	24.7	0.49	202567	194.5	332.2	247.1	43.0
PH3	24.7	0.51	194623	190.7	319.2	268.6	42.8
Mean			197639.0	187.7	317.2	251.9	43.9
St. Dev.			6936.22	5.38	9.31	17.71	2.85
Coeff. Var. (%)			3.5	2.9	2.9	7.0	6.5

The beam end-plate tension coupon test results are shown in Table 5.2. As shown in the table, three coupons were cut from the plates. The mean, standard deviation and coefficient of variation are given for all characteristic stress and strain values for panels. As can be seen in the table, the elastic modulus and failure stress of BEP3 are somewhat lower than those of the other specimens although yield stress and ultimate stress are similar. All specimens exhibited ductile behavior, with failure strains in excess of 20%.

Table 5.2: Beam End-Plate Tension Coupon Test Results

Coupon Mark	Width [mm]	Thickness [mm]	Elastic Modulus [MPa]	Yield Stress [MPa]	Ultimate Stress [MPa]	Failure Stress [MPa]	Failure Strain [%]
BEP1	24.75	10	188208	301.1	425.9	320.9	26.0
BEP2	25.1	10.1	210825	301.7	421.6	328.8	23.7
BEP3	24.9	9.9	179019	302.3	423.7	294.4	23.7
Mean			192684.0	301.7	423.7	314.7	24.5
St. Dev.			16368.61	0.60	2.15	18.02	1.33
Coeff. Var. (%)			8.5	0.2	0.5	5.7	5.4

5.3 Screw Connection Test Specimens

In order to determine the failure modes and the ultimate tensile capacity of the screw connection a series of test was conducted. For this purpose, five test specimens whose details are shown in Figure 5.3 were designed. The strips with 6.0mm and 0.50mm thick represent the fish plate welded to columns and beams flanges and the infill panel, respectively. One self-drilling screw was used in all test specimens. The size of the screws is 5.5-24×38. Drill diameter and drill length of the screws are given as 4.90mm~4.92mm and 14.52mm~14.66mm, respectively. The length of screws is between 37.12mm and 37.56mm.

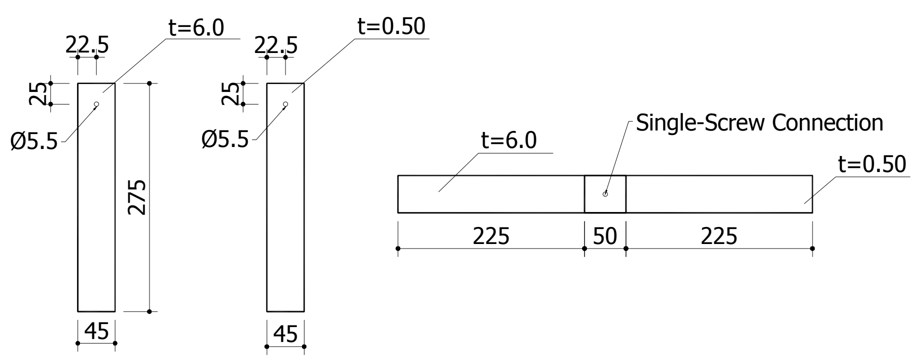

Figure 5.3: Details of Strips for Screw Connection Specimens (dimensions in mm)

5.3.1 Test results

The results of the screw connection tests are summarized in Table 5.3. In this table, ultimate bearing stresses are calculated dividing the ultimate load by the bearing surface area of the sheet with the thickness of 0.52mm. The actual thicknesses were given in the table. Figure 5.4 shows the test setup and placement of the specimens.

The type of longitudinal shear failure of the sheet along two parallel lines, shown in Figure 5.5, occurred in all screw connection specimens.

Table 5.3: Screw Connection Test Results

Specimen Mark	Thickness of the Plates		Screw Nom. Dia. [mm]	Ultimate Load [N]	Ultimate Bearing Stress [MPa]
	Fish Plate [mm]	Infill Plate [mm]			
S1	6.04	0.52	5.5	1863.3	651.5
S2	6.03	0.52	5.5	3040.1	1063.0
S3	6.03	0.52	5.5	2451.7	857.2
S4	6.03	0.52	5.5	2059.4	720.1
S5	6.03	0.52	5.5	2255.5	788.6
Mean				2334.0	816.1
St. Dev.				451.54	157.88
Coeff. Var. (%)				19.3	19.3

Figure 5.4: Test Setup and Photographic View of Typical Specimen

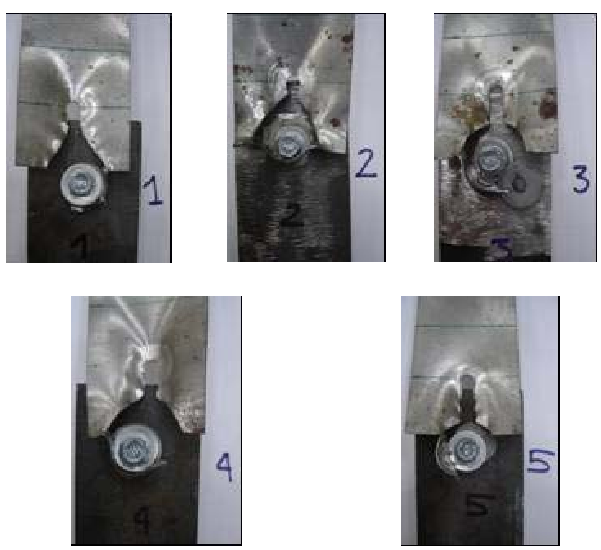

Figure 5.5: Failure Modes for All Screw Connection Specimens

5.4 Summary

The results of the tension coupon tests give detailed information on stress vs. strain relations of the materials of the infill panels and beam end-plates. This information is included in the beam-to-column joints model and finite element model of the shear wall and bare frame specimens so as to enable the computer program (ABAQUS) to simulate the material behavior that was present in the test specimens.

In determining the number of screws to connect the infill panel edges to the fish plates, screw connection test results were used. The mean value of ultimate load was considered for the design of this connection.

6. PRELIMINARY NUMERICAL ANALYSES OF TEST SPECIMENS

Three specimens in total, one bare frame and two thin steel plate shear walls were designed to individually examine the behaviors of the specimens and to compare the behaviors of two different TSPSWs as the lateral load-resisting systems under cyclic loading. Prior to conducting the experimental studies, a method of analysis was required in order to be able to predict the behaviors of the specimens so that the tests could be properly designed. Additionally, some control parameters to be used to develop the displacement histories during the cyclic tests such as ultimate lateral load capacity, yield strengths of the specimens and deformations corresponding to the yield strengths have also to be estimated.

Some preliminary studies on modelling of the TSPSW are described in Chapter 3. For both finite element and the strip models, basic features such as types of elements, initial panel imperfections and method of solutions are discussed in that chapter. Both the strip and finite element model approaches are applied to the all TSPSW test specimens. In developing the strip models, SAP2000 that is commonly available structural analysis package is used to obtain load versus relative top displacement curves of the specimens. ABAQUS, which is the general-purpose nonlinear program is utilized to develop the nonlinear finite element models of the test specimens.

Based on nominal dimensions (as given on the design drawings), the preliminary strip and finite element models of the shear wall specimens are described and analyses results are given in the following sections. These results also include those from analyses of the bare frames.

6.1 Simplified Model Analyses of the Specimens

Four analytical models, shown in Figure 6.1~6.3, including SW-A-H, SW-B-H, BF-H and BF-F were created with the aim of predicting the parameters previously mentioned. SAP2000 is employed to develop these models. In modelling the thin steel panels, parallel strip model approach whose details were given in Chapter 3 was utilized. Therefore, these panels are represented by a series of discrete, pin-ended strips inclined with the same orientation as the tension field. 10 tension-only strips were found to be adequate to model the panels as given in the investigation conducted by **Thorburn et al. (1983)**. As the inclination angle of the strips for the panel connected to beams only was expected to be distinct from 45°, the inclination angles of the pin-ended strips were initially assumed to be 28° in SW-B-H specimen. The latter value was calculated considering the incomplete diagonal tension field approach **(McGuire, 1968)**. The inclination angle value of 45° was used for the representative of the panel in SW-A-H.

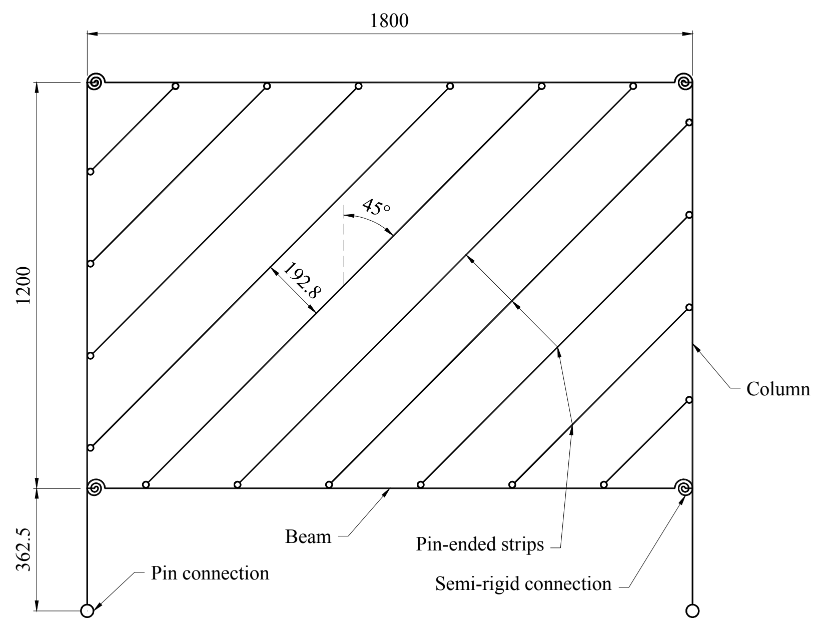

Figure 6.1: Parallel Strip Model of Specimen SW-A-H

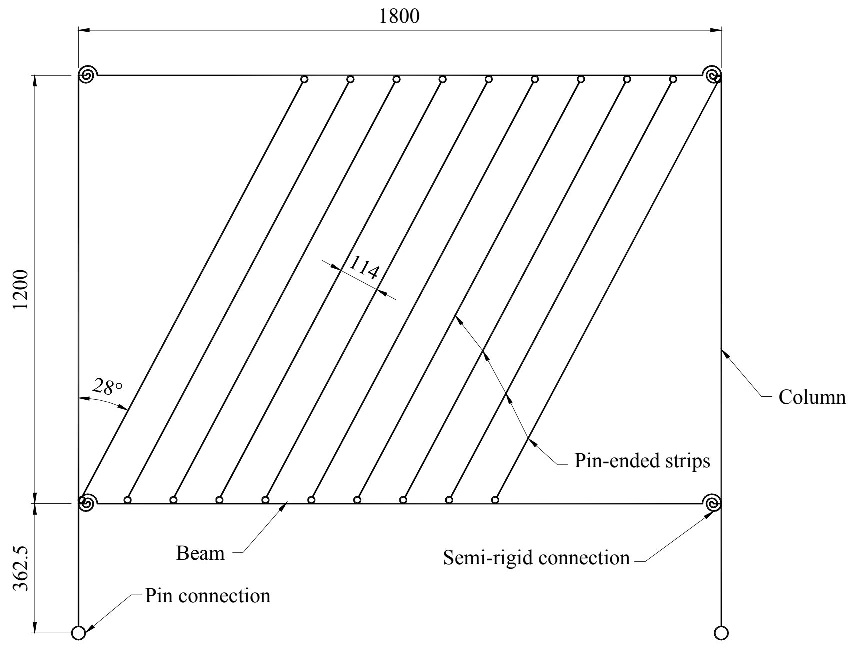

Figure 6.2: Parallel Strip Model of Specimen SW-B-H

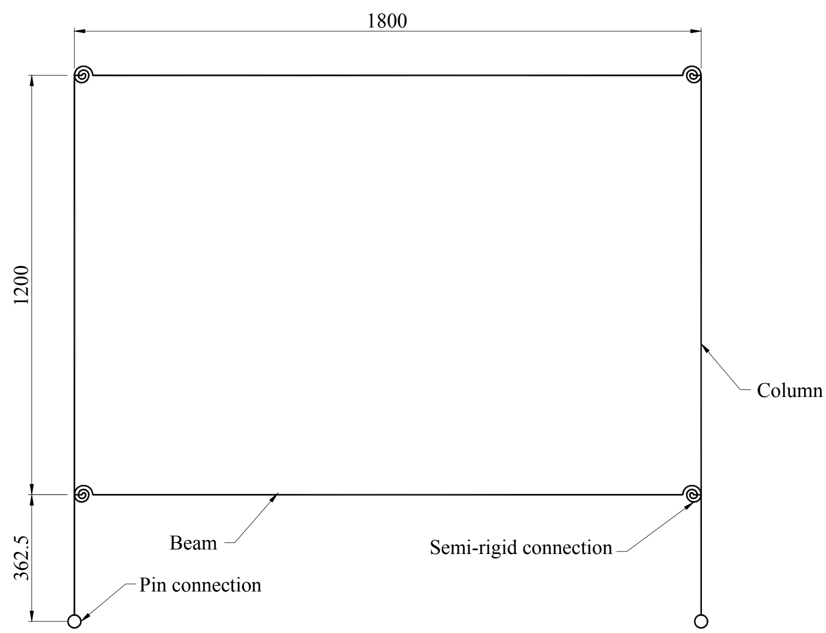

Figure 6.3: Simplified Model of Specimen BF-H and BF-F

Actual material properties were used in these preliminary models. Also, in the moment-rotation curves of the beam-to-column joints, the yield stress and modulus of elasticity of the beam end plates that were obtained from coupon tests was included. The tension tests were carried out using the coupons cut from the infill panel in two orthogonal directions. The material behavior of both the boundary members and infill panels is assumed to be linearly elastic-perfectly plastic, with linear strain-hardening. It should be noted that the boundary frame members are designed to remain elastic throughout the tests.

The behaviors of the plastic hinges to use for representing the plastic deformations of the frame sections under axial forces and moments are based on the nominal material properties, minimum yield stresses and minimum ultimate stresses. For the columns and beams, moment plastic hinges, M3 (SAP2000 definition) are defined, while axial plastic hinges, P (SAP2000 definition) are used for the strips. The actual strip lengths are taken into account in defining the axial plastic hinges for the strips as also stated in **Berman and Bruneau (2003)**. Because there is no any gravity load directly acting on the columns in the test and for the simplicity as well, the influence of the axial force on moment versus curvature behavior of the columns is neglected for the plastic hinges definition used for the columns. The pushover analyses did not include P-Δ effect due to absence of the gravity load applied on the columns.

The nonlinear behaviors of the beam-to-column connections are again represented by plastic hinges, M3 based on moment-rotation curves given in Section 4.3.2.2. Hence, the semi-rigidity and the partial-strength of the joints are taken into account. These plastic hinges are assigned to each frame member (beam) end connected to the column flanges.

Using these models, the required actuator strokes and capacities, movements of measuring devices could also be estimated.

The predicted load-deflection curves for SW-A-H, SW-B-H and BF-H are shown in Figures 6.4~6.6.

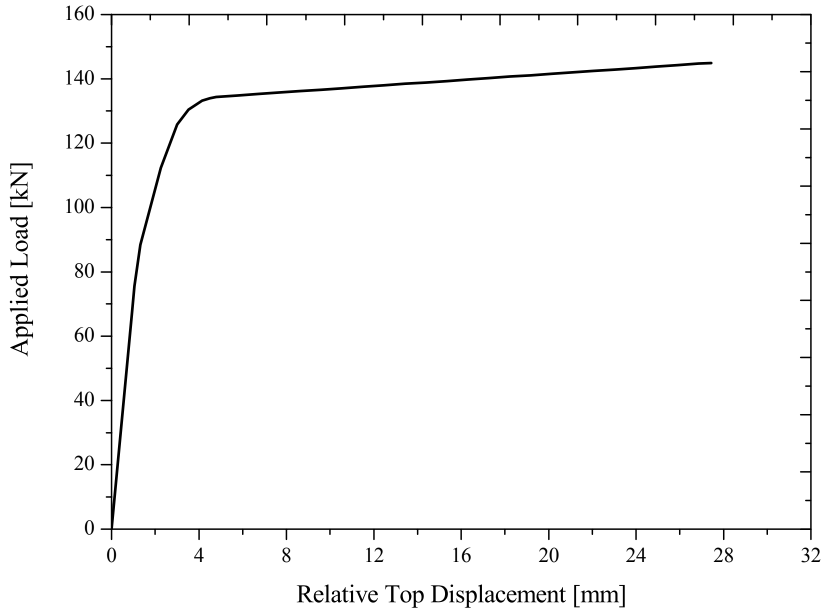

Figure 6.4: Predicted Load-Deflection Curve of Specimen SW-A-H

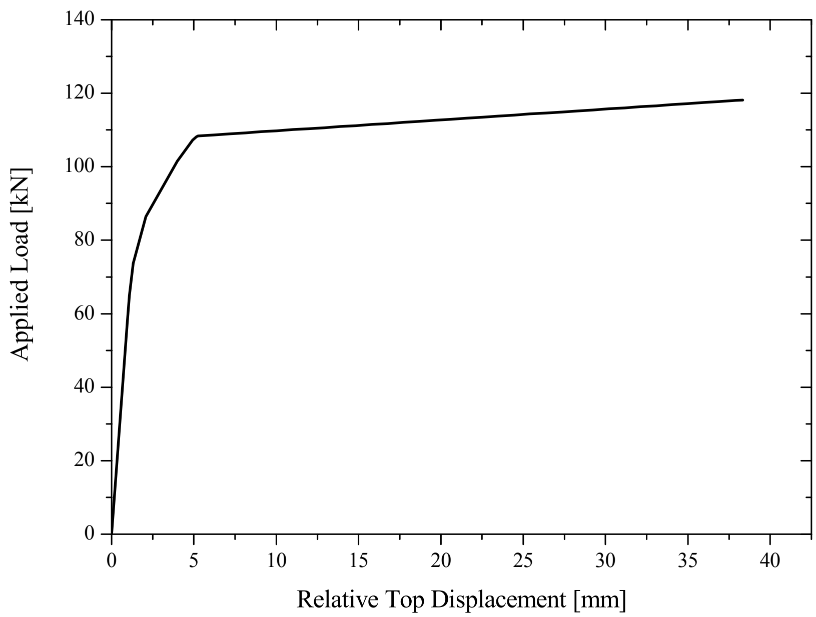

Figure 6.5: Predicted Load-Deflection Curve of Specimen SW-B-H

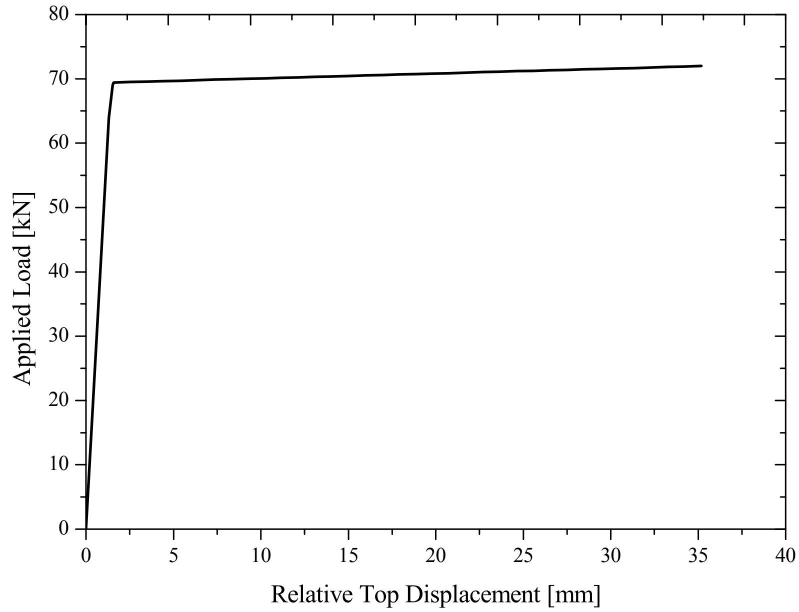

Figure 6.6: Predicted Load-Deflection Curve of Specimen BF-H

6.1.1 Analyses results and comparison

The preliminary predicted load-deflection curves that were separately given in above section are compared with each other. All curves, shown in Figure 6.7, gave essentially the expected response.

The response of the partial-moment-resisting frame (bare frame) acting alone serves to demonstrate the significant contribution of the infill plates in resisting the story shears and the increasing the stiffness of the shear walls. The ultimate base shear from the model of SW-A-H is more than two times that from the model of BF-H. As for the specimen SW-B-H the increase in the maximum lateral force to that from bare frame is approximately 70%.

The initial stiffnesses of the specimens, SW-A-H, SW-B-H and BF-H, are approximately 71.7 kN/mm, 61.2 kN/mm and 48.9 kN/mm, respectively. The base shears corresponding to the yield displacements which were determined by judgment are also nearly 146 kN, 95 kN and 69 kN, respectively.

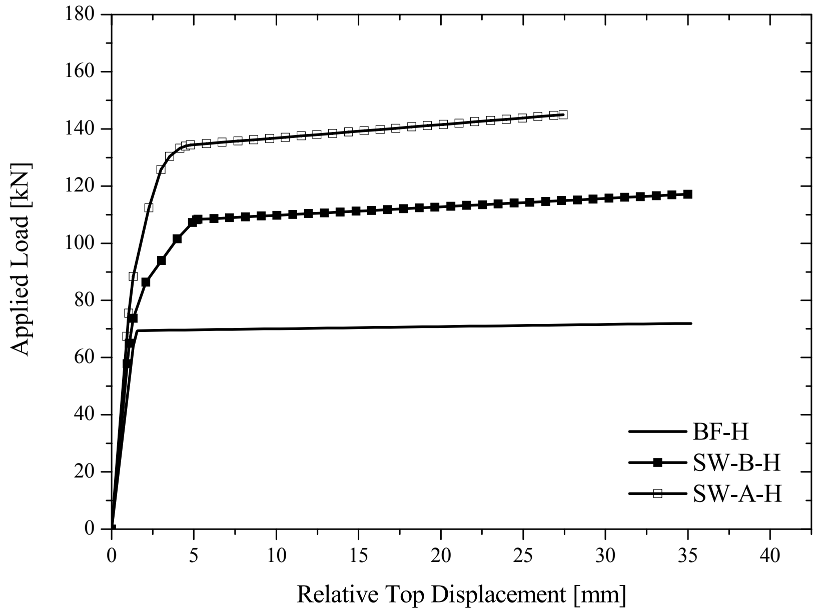

Figure 6.7: Predicted Load-Deflection Curve of Test Specimens

6.2 Finite Element Models Analyses of the Specimens

Four nonlinear finite element models, shown in Figure 6.8~6.10, including SW-A-H, SW-B-H, BF-H and BF-F were created with the aim of more accurately predicting the test parameters that were previously mentioned. ABAQUS is employed to develop these models with both geometric and material nonlinearities. This software is well suited for the solution of higly nonlinear engineering problems. It contains an extensive library of elements that can model virtually all geometric boundary conditions.

As stated in **Behbahanifard (2003)**, ABAQUS consists of two main analysis modules; ABAQUS/Standard and ABAQUS/Explicit. In ABAQUS/Standard, an implicit method, equilibrium is achieved through an iterative procedure, from which the deformed configuration of the structure is obtained. ABAQUS/Explicit uses a nonlinear explicit dynamic formulation and can be used for analysis of systems under both dynamic and quasi-static conditions. In dynamic explicit method the unbalanced forces between the internal and external forces at the beginning of the increment is considered as a driving force acting on a mass, from which the deformed state after a very small time increment using central difference method, thus no iteration is involved in this technique.

Because some of the elements, for example ABAQUS element JOINTC used for the connection model in this study, in ABAQUS library are not supported by the explicit analysis technique the steel plate shear wall specimens were analysed with the static implicit method implemented in ABAQUS/Standard.

Because the beams and columns are modeled as line elements, rigid outriggers extending from centerline of the boundary frame members to the infill panel edges are used, as shown in Figure 6.8 and 6.9, to allow the eccentricity at the connection between the surrounding frames and plate edges to consider in the analyses of TSPSW specimen models.

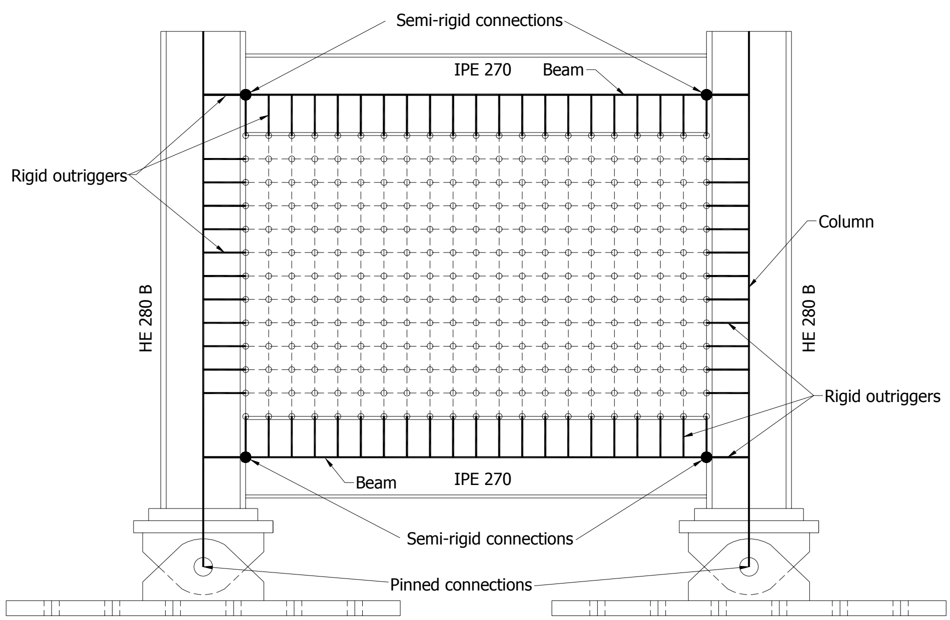

Figure 6.8: Finite Element Model of Specimen SW-A-H

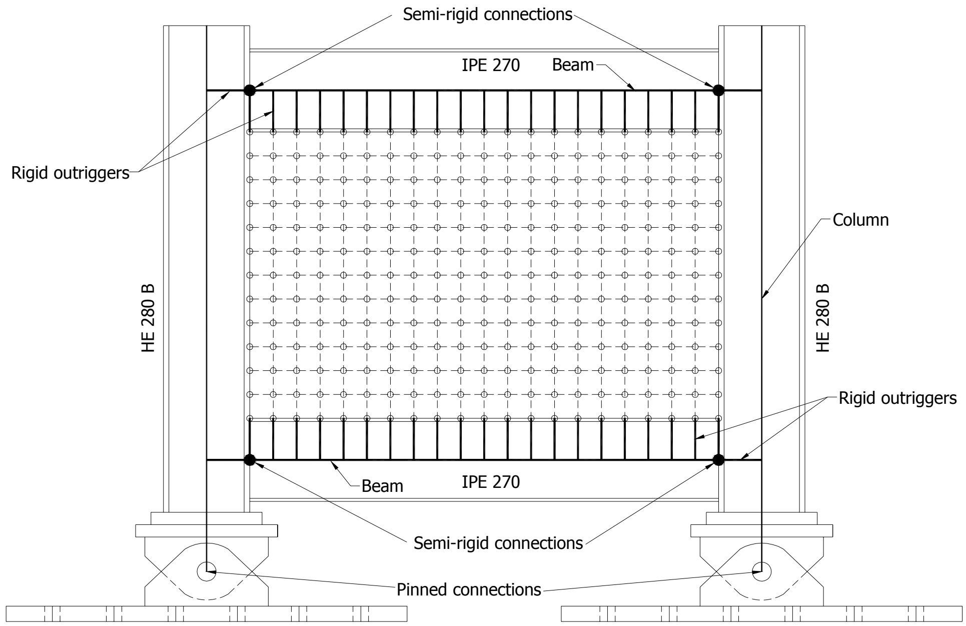

Figure 6.9: Finite Element Model of Specimen SW-B-H

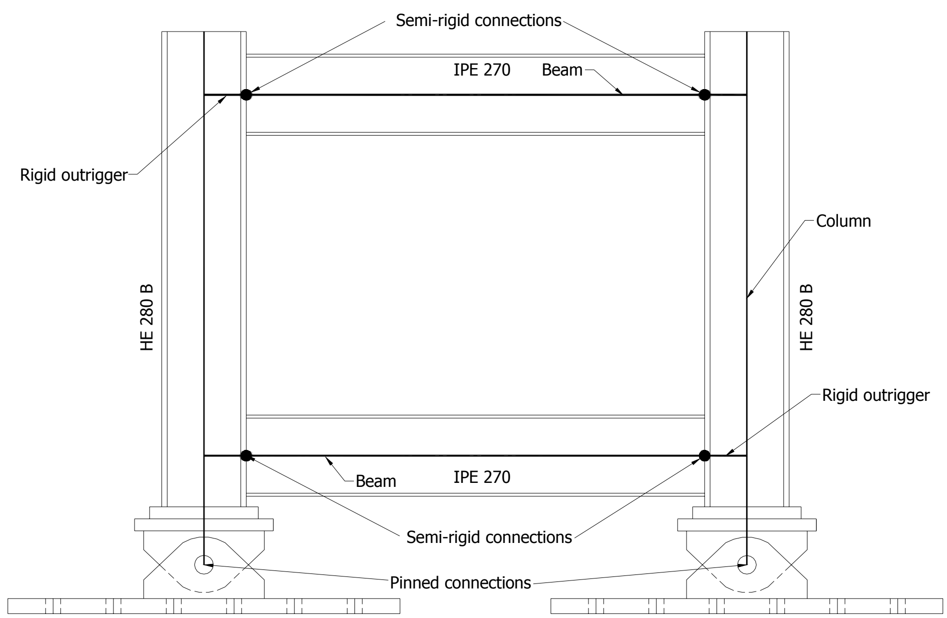

Figure 6.10: Finite Element Model of Specimen BF-H and BF-F

In these models, the nonlinear behavior of the beam-to-column connections is taken into account using the spring element which is defined with the moment-rotation relation of the connection type that was achieved based on the assumptions expressed in the Section 4.3.2.1.

The columns are pinned at their bases. Since all specimens were braced to prevent out-of-plane deformation using lateral bracing system in the tests the out-of-plane deformations of the nodes on the top beam were restricted in the models' analyses. Hence, at the top of the specimen a guide was provided to allow only in-plane movement.

Actual material properties that were obtained from the tension coupon tests' results whose details were given in Chapter 6 are used in the models. The material behavior of the boundary members is assumed to be linearly elastic-perfectly plastic, with linear strain-hardening. However, the boundary frame members are designed to remain elastic throughout the tests.

The influence of the fish plates welded to flanges of boundary frame members is ignored because their contributions are found to be negligible. The models, then, did not include the fish plates. Moreover, it was shown by **Driver (1997)** that omitting the fish plates in the shear wall models was unlikely to cause any significant change in the overall behavior.

Initial panel imperfections are specified that the infill panels are taken to have an initial out-of-flatness corresponding to the related buckling modes of the steel infill plates which are loaded in the same manner as in the subsequent pushover analyses. The peak amplitudes are set to values of 10mm and 15mm in order to depict a reasonable maximum out-of-flatness for SW-A-H and SW-B-H, respectively.

A 12×20 element mesh is used for panels in all shear wall specimens. The beams and columns are modeled using three-node quadratic beam elements (ABAQUS element B32). Detailed information about this element was given in Section 3.1.1.

The shear wall infill panels are modeled using 4-node doubly curved general-purpose shell elements (ABAQUS element S4). Element type S4 is a fully integrated, general-purpose, finite-membrane-strain shell element available in ABAQUS/Standard. The element's membrane response is treated with an assumed strain formulation that gives accurate solutions to in-plane bending problems. This element has six degrees of freedom per node. Thus, out-of-plane behavior of the plate is included in the models.

The predicted load-deflection curves and deformed shapes of the specimens are given in the following section.

6.2.1 Analyses results and comparison

All pushover curves for the FEMs of the test specimens are shown in Figure 6.11. As can be seen from the figure, the behaviors of the specimens are generally similar to those from the strip models.

From Figure 6.11, it can be observed that the contribution of the infill panel to the initial stiffness of the system is considerable. The ultimate base shear from the model of SW-A-H is about two times that from the model of BF-H. As for the specimen SW-B-H the contribution of the infill panel to ultimate lateral force which was attained is approximately 55%.

The initial stiffnesses of the specimens, SW-A-H, SW-B-H and BF-H, are approximately 65.8 kN/mm, 49.8 kN/mm and 19.5 kN/mm, respectively. The base shears corresponding to the yield displacements which were determined by judgment are also nearly 174.7 kN, 141.9 kN and 91.5 kN, respectively.

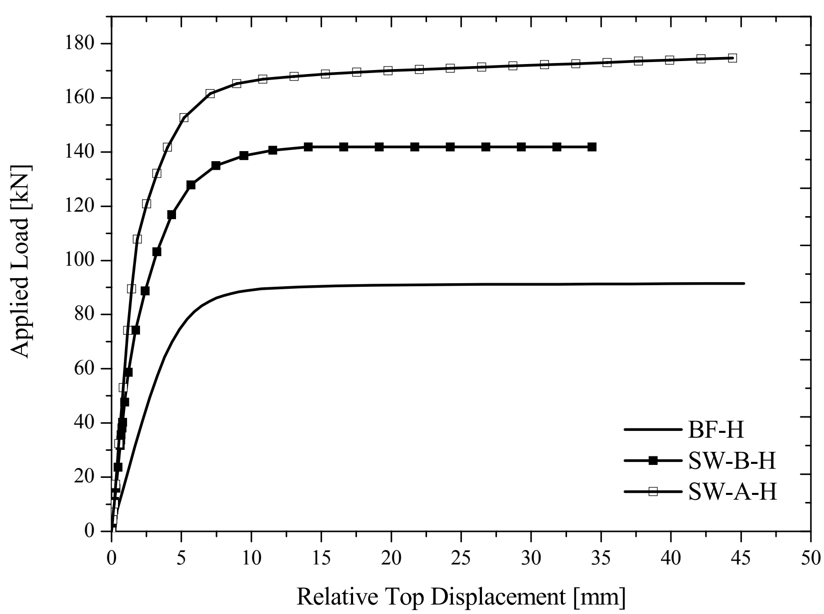

Figure 6.11: Predicted Pushover Curves of FEMs of All Specimens

6.3 Summary

The strip models for the shear wall specimens and frame model for the bare frame specimen that are loaded cyclically into the inelastic region provide a relatively simple means of predicting the envelope of load versus deflection curves. The analysis procedure can be conveniently performed using a personal computer and any commercial structural analysis computer package.

The basis of the model is the representation of the tension field in the thin infill plates as a series of discrete, pin-ended diagonal tension strips. Initially, while the angle of inclination of the tension strips have been selected to be 45° in the model of SW-A-H, 28° has been used in the model of SW-B-H to depict the partial-tension field action. It can be noted that the latter value can be changed considering the test records from the strain gauges. In contrast to this, it is expected that the inclination value of 45° will not significantly be altered. Plastic hinges are also modelled at the possible joints that plastic deformations may occur so as to simulate inelastic behavior of the structural elements.

7. EXPERIMENTAL PROGRAM AND OBSERVATIONS

This section describes the loading programs and experimental observations for the two steel plate shear wall specimens and one bare frame specimen discussed in Chapter 4. Methods applied to estimate the yield base shears and displacements prior to testing are discussed, along with the loading protocol used, and the recorded cyclic displacement histories. After this discussion, the testing of each specimen is described in detail, and observations made during testing regarding the behavior of each specimen are defined.

7.1 Loading Program

Loading of the test specimens consisted of quasi-static cycles using displacement control only although ATC-24 procedure requires force control loading to a level of 0.75 times yield force. No axial compression forces were applied on the columns in the tests. It was reported by **Elgaaly and Liu (1997)** that, in the tests performed by **Elgaaly et al. (1993)**, the columns in the shear wall specimens were subjected to constant axial compression as high as 50% of their American Institute of Steel Construction (AISC) calculated nominal strength; it was found that the effect of the presence of axial compression in columns with such magnitudes is small. It was observed that the lateral load carrying capacity of the shear walls with no axial compressive loads acting on their columns was more than that of those with axial compressive loads by nearly 15%.

Although very complicated finite element models using actual material properties were used to predict the yield base shears and displacements, there is a typical uncertainty for these critical values to determine the displacement histories followed in the tests. Therefore, the elastic cycles in the tests were increased. Once the yield displacement had been identified experimentally, the subsequent cycles were done using displacement control.

7.1.1 Estimation of yield force and displacement

For all specimens, the yield base shears are predicted analytically in accordance with the ATC-24. For the purpose of this detailed analytical investigation, the nonlinear finite element models which will be described in Chapter 8 were developed to consistently predict the yield base shears. ABAQUS was used to develop the nonlinear finite element models for pushover analyses. Therefore, the preliminary strip models discussed in the Chapter 6 were not used for this purpose. In order to avoid greater confidence in the predicted values for the yield base shears, the nonlinear behavior of semi-rigid beam-to-column joints, initial imperfection of the infill panels (initial out-of-plane deformation configuration) and stress-strain relationship of the materials from tension coupon tests are taken into account in the models. The configuration of initial out-of-plane deformation was accounted for the models based on the infill panels' buckling modes following the method that was stated in Section 3.1.3.

ABAQUS was successfully employed to predict the overall envelope curve of the specimen behavior. Since the cyclic analyses were not able properly to follow the pinched shape of the hyteresis curves which was resulted from the stretching and buckling of the infill plates, monotonic finite element analyses were performed for preferable solution. However, the most complicated finite element analysis was performed by **Behbahanifard (2003)** using a kinematic material model for cyclic simulation of three-story steel plate shear wall.

ATC-24 specifies that the characteristic values may be either determined experimentally (from a monotonic load test) or predicted analytically. In this study, analytical method for prediction of these parameters was choosen. It is recommended to estimate the yield force Q_y and to use the procedure given in Figure 7.1 to deduce the yield deformation δ_y and the elastic stiffness K_e. This procedure requires force control loading to a level of $0.75Q_y$, measurement of the corresponding control deformation δ^*, and prediction of δ_y and K_e as shown in the Figure 7.1.

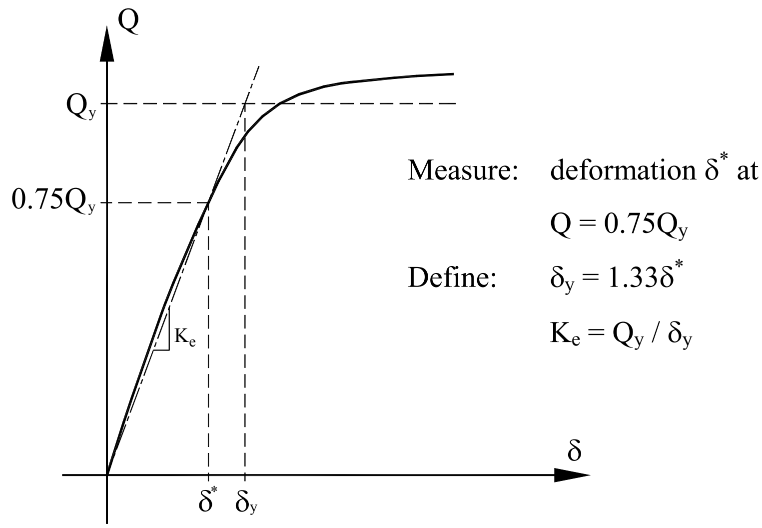

Figure 7.1: Determination of Yield Values Q_y and δ_y and Elastic Stiffness K_e **(ATC-24, 1992)**

However, the displacement control loading was preferred in the application of the procedure that is recommended in the ATC-24 while increasing the elastic cycles applied prior to yield displacement. Due to small increments in the displacements resulting in larger number of cycles up to the yield displacement level, these critical variables were easily determined during the tests monitoring the load-displacement curves of each specimen as well.

Resulting pushover curves predicted for the three different test specimens were shown in Figure 6.11, to a maximum relative displacement of 45mm for SW-A-H and BF-H, and 35mm for SW-B-H.

7.1.2 Loading protocol in ATC-24

Quasi-static cyclic testing was carried out in accordance with the ATC-24 loading protocol **(ATC-24, 1992)** except for the force control loading section up to a level of $0.75Q_y$ which is recommended in the procedure.

This document specifies that specimens should be subjected to three cycles at each displacement step up to three times the yield displacement, following this step only two cycles are necessary. The first displacement step should be 1/3 of the yield displacement, the second should be 2/3 of the yield displacement, the third should be the yield displacement (δ_y), and the increment applied in every subsequent step should be the yield displacement resulted in $2\delta_y$, $3\delta_y$, etc. cycles of deformations. This procedure followed in the tests is also graphically given in Figure 7.2.

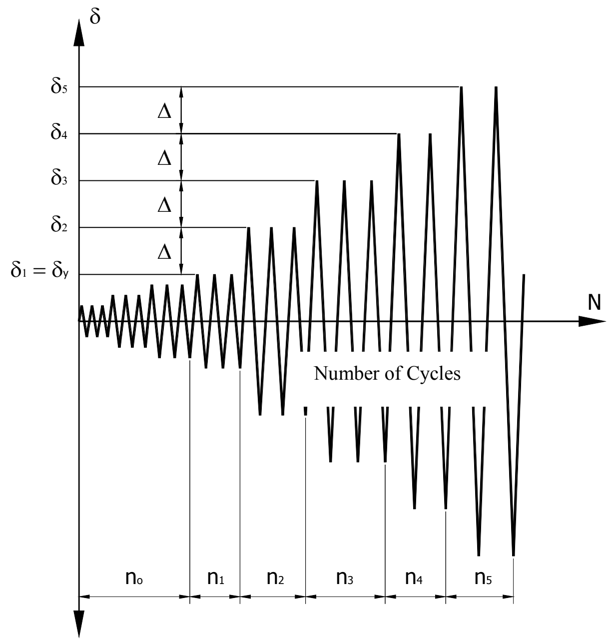

Figure 7.2: Deformation History for Multiple Step Test **(ATC-24, 1992)**

7.1.3 Displacement histories in cycles

Since the yield forces and displacements, as described in Section 7.1.1, are predicted from numerical simulation, there is slightly variation in what was observed and used during the experiments. Therefore, the actual displacement histories used for each specimen are given in Tables 7.1~7.3. As can be seen in the histories for the specimens, the number of displacement steps prior to yield is larger than those of which is recommended in ATC-24. It should be noted that the relative displacements referred to in this section are obtained by taking the difference between average of transducers TTW and TTE and TNC4, shown in Figure 4.26~4.29. The displacement values listed in Tables 7.1~7.3 are achieved for pushing direction. Moreover, while the figures used in Section 7.2 are called, although some of the figures are used for expression of phonemona occurred at pulling stage they are called according to the values in Tables 7.1~7.3.

Table 7.1: Cyclic Displacement History for BF-H

Disp. Step	Number of Cycles	Cumulative No. of Cycles	Relative Disp. Ratio to δ_y (Δ/δ_y)	Relative Disp. [mm]	Top Disp. [mm]	Drift (%)
1	3	3	0.17	1.42	1.94	0.12
2	3	6	0.34	2.78	3.88	0.23
3	3	9	0.51	4.15	5.85	0.35
4	3	12	0.67	5.49	7.79	0.46
5	3	15	0.83	6.84	9.74	0.57
6	3	18	1	8.21	11.70	0.68
7	3	21	2	16.61	23.39	1.38
8	3	24	3	25.17	35.09	2.10
9	2	26	4	33.69	46.79	2.81
10	2	28	5	42.21	58.53	3.52
11	2	30	6	50.77	70.20	4.23
12	2	32	7	59.74	81.81	4.98

Table 7.2: Cyclic Displacement History for SW-A-H

Disp. Step	Number of Cycles	Cumulative No. of Cycles	Relative Disp. Ratio to δ_y (Δ/δ_y)	Relative Disp. [mm]	Top Disp. [mm]	Drift (%)
1	3	3	0.14	0.93	1.13	0.08
2	3	6	0.27	1.82	2.18	0.15
3	3	9	0.40	2.72	3.27	0.23
4	3	12	0.54	3.63	4.42	0.30
5	3	15	0.71	4.84	5.89	0.40
6	3	18	0.87	5.89	7.21	0.49
7	3	21	1	6.77	8.41	0.56
8	3	24	2	12.82	16.79	1.07
9	3	27	3	18.98	25.19	1.58
10	2	29	4	25.28	33.72	2.11
11	2	31	5	31.40	41.97	2.62
12	2	33	6	37.66	50.39	3.14
13	1	34	7	44.00	58.80	3.67

Table 7.3: Cyclic Displacement History for SW-B-H

Disp. Step	Number of Cycles	Cumulative No. of Cycles	Relative Disp. Ratio to δ_y (Δ/δ_y)	Relative Disp. [mm]	Top Disp. [mm]	Drift (%)
1	3	3	0.13	0.78	0.89	0.07
2	3	6	0.25	1.52	1.79	0.13
3	3	9	0.37	2.26	2.71	0.19
4	3	12	0.47	2.89	3.59	0.24
5	3	15	0.58	3.56	4.48	0.30
6	3	18	0.69	4.24	5.39	0.35
7	3	21	0.79	4.88	6.29	0.41
8	3	24	0.89	5.53	7.20	0.46
9	3	27	1	6.18	8.09	0.52
10	3	30	2	12.07	16.20	1.01
11	3	33	3	17.95	24.29	1.50
12	2	35	4	23.74	32.40	1.98
13	2	37	5	30.45	40.51	2.54
14	1/2	37.5	6	37.65	50.61	3.14

7.2 Experimental Observations

This section describes, in detail, the experimental testing and observations of the three specimens. Observations made regarding the performance of the specimens during regions of both linear and nonlinear behavior will be given.

7.2.1 Specimen BF-H

The moment-resisting frame with semi-rigid/partial strength beam-to-column joints represents the baseline case for the TSPSW tests, and the cyclic response of the specimen is characterized by an open stable hysteretic behavior as shown in Figure 7.3.

During the first three cycles of loading (1.94mm top displacement, 0.12% drift) specimen BF-H exhibited completely linear behavior. Up to the top displacement of 7.79mm corresponding to 0.46% drift and approximately 58.50kN load, there is no any noticeable failure occurred in the beam-to-column connections. At the Cycle 10, about 1.00mm gap between the upper edge of the north end plate of the bottom beam and the column flange occurred. At the lower edge of the south end plate of the top beam the similar gap was also observed. In the second half of Cycle 13, paint cracks were occurred on the north end plate of the bottom beam. At the beginning of the Cycle 14, the gap of 1.00mm became 2.00mm.

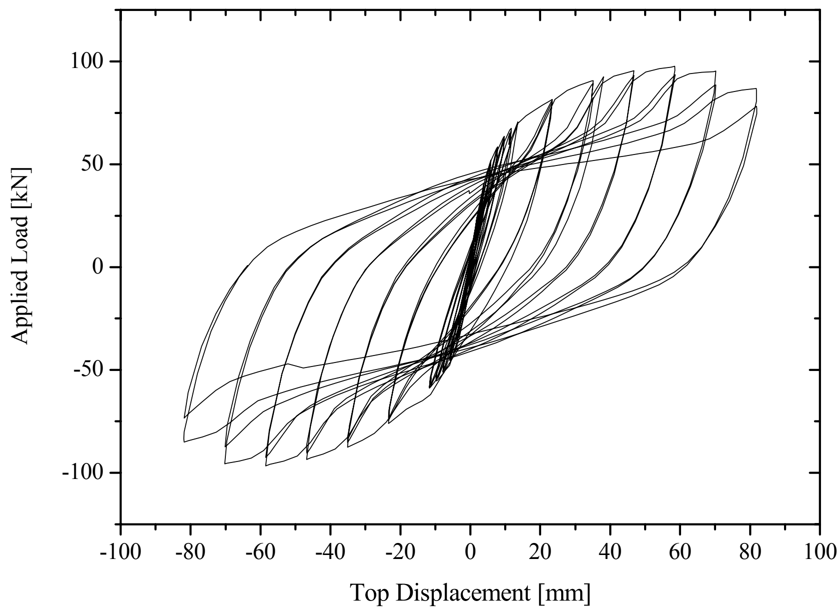

Figure 7.3: Hysteresis Curves for BF-H

During the first half of Cycle 16, cracks in the paint were observed on the beam end plates in the beam-to-column connections. Based on the extrapolation of the shape of the force-displacement hysteresis curve obtained at a top displacement of 11.70mm (0.68% drift) and load of 67.50kN, and visually using an equal energy approach, this displacement was determined to be the experimentally obtained yield point for the specimen BF-H at this cycle. Following the three cycles, the applied load and top displacement was reached 81.6kN and 23.39mm, respectively. No failure or fracture was observed until this cycle. However, new paint cracks were noticed on the beam end plates. The gap between the beam end plates and column flanges were progressed to nearly 3.00mm (Figure 7.4)

At Cycle 25 (46.79mm top displacement, 2.81% drift), the gap of 3.00mm was reached 6.00mm (Figure 7.5). The maximum base shear was 95.5kN and occurred at $+4\delta_y$ of Cycle 25 (the first cycle at $\pm 4\delta_y$). No significant strength degradation occurred subsequent cycles. In the second half of Cycle 25, paint cracks were observed near the fillet welds connecting the end plates to the beam webs.

At Cycle $\pm 5\delta_y$, the distance between the beam end plates and column flanges became 8.00mm. Paint flaking on the beam end plates continued at this cycle. The load and drift were 95.60kN and 3.52%, respectively. A small fracture near the fillet weld connection, shown in Figure 7.6, between the end plate and the beam web was noticed in upper north corner. On the web of the north end of the top beam paint flaking which is usually an indication of yielding occurred.

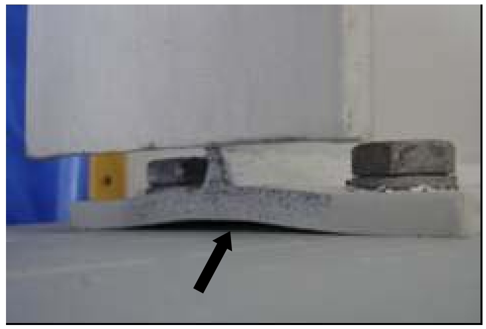

Figure 7.4: Gap between the Beam End Plate and Column Flange
(Specimen BF-H, Cycle 19 and Top Disp. of 23.39mm)

Figure 7.5: Gap between the Beam End Plate and Column Flange
(Specimen BF-H, Cycle 25 and Top Disp. of 46.79mm)

Figure 7.6: Fracture Near the Fillet Weld Connection
(Specimen BF-H, Cycle 27 and Top Disp. of 58.53mm)

During the first half of Cycle 29 (70.20mm top displacement, 4.23% drift), the noticable fracture as shown in Figure 7.7 was observed in upper north connection between the end plate and the beam web. At this point, the north beam end displaced to east. During the second excursion of Cycle 30, the gap between the beam end plate and column flange in the upper north beam-to-column connection became approximately 15mm.

(a) (b)

Figure 7.7: The Fracture in Beam-to-End Plate Connection; (a) from East Side and (b) from West Side (Specimen BF-H, Cycle 29 and Top Disp. of 70.20mm)

At the first $\pm 7\delta_y$ (81.81mm top displacement, 4.98% drift), the general view is given in Figure 7.8. The fracture length of 60mm was observed in upper south connection between the end plate and the beam web (Figure 7.9). The similar tears which were 60mm and 55mm long were also occurred in lower south and north connections respectively. The gaps between the beam end plates and column flanges reached about 30mm (Figure 7.10)

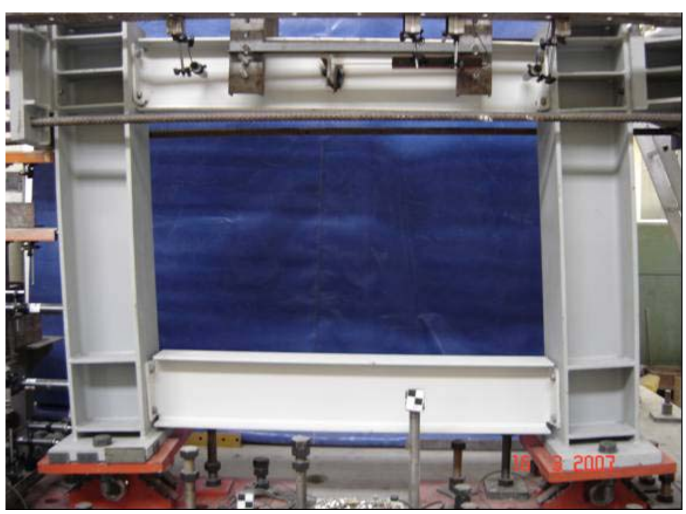

Figure 7.8: General View (Specimen BF-H, Cycle 31 and Top Disp. of 81.81mm)

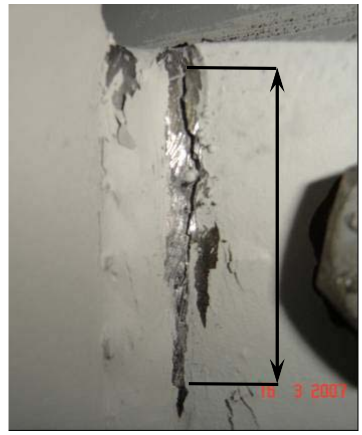

Figure 7.9: End Plate Fracture
(Specimen BF-H, Cycle 31 and Top Disp. of 81.81mm)

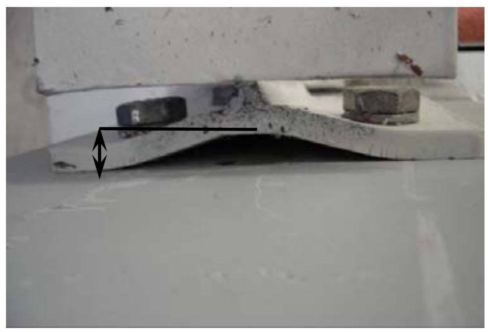

Figure 7.10: Gap between the Beam End Plate and Column Flange
(Specimen BF-H, Cycle 31 and Top Disp. of 81.81mm)

At the last cycle, Cycle 32, with loud sound coming from upper north beam-to-column connection, the fracture length at the north end of the top beam became 90mm from the bottom to the top and similar fracture that was 40mm long from the top to the bottom were suddenly appeared (Figure 7.11). The second excursion to -$7\delta_y$ caused these fractures to again propagate substantially, which in turn, caused the resistance of the wall to degrade to 49.00kN or 48% of the maximum base shear achieved, thus the test was terminated at this point. The north end of the top beam also displaced towards east as shown in Figure 7.12.

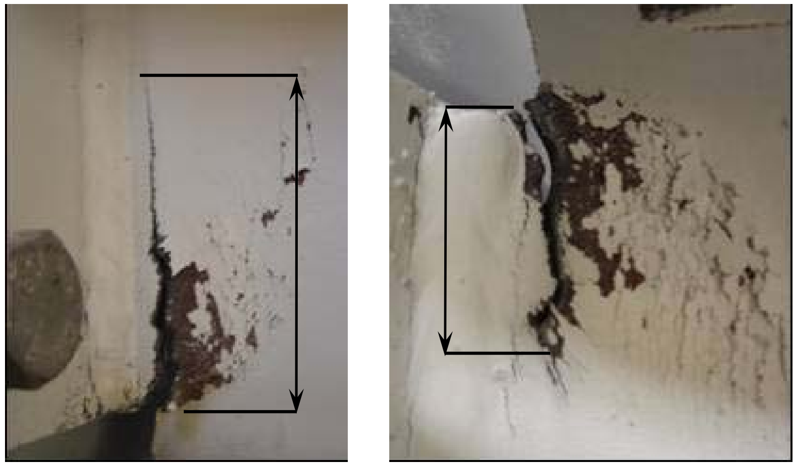

Figure 7.11: Beam Web Fracture
(Specimen BF-H, Cycle 32 and Top Disp. of 81.81mm)

Figure 7.12: Movement of the North End of the Top Beam
(Specimen BF-H, Cycle 32 and Top Disp. of 81.81mm)

7.2.2 Specimen SW-A-H

The specimen SW-A-H exhibited a cyclic response as shown in Figure 7.13. It behaved elastically during the first 9 cycles of testing. After this point, some insignificant nonlinear behavior was observed. Up to Cycle 4, there had been audible buckling sounds beginning from the second cycles from infill panel and magnitude of the buckling waves along the infill plate was small. During Cycles 4, 5 and 6, the audible sounds got a little louder and the magnitude of the buckling waves grew to what is shown in Figure 7.14.

As can be seen from the Figure 7.13, prior to yield point there are pinched loops. This is attributed to local buckling of the infill panel, initial out-of-flatness of the infill and the bearing of the panel in front of the screws in the corners (Figure 7.15).

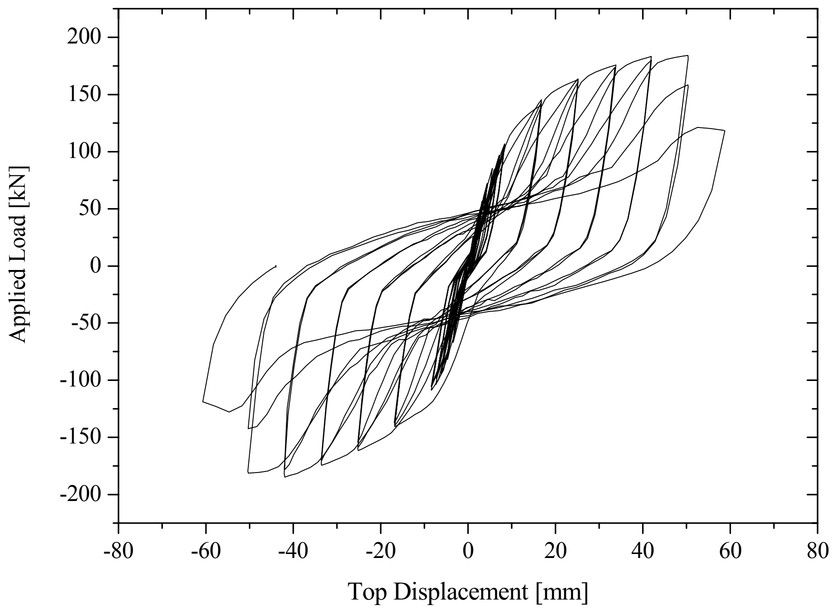

Figure 7.13: Hysteresis Curves for SW-A-H

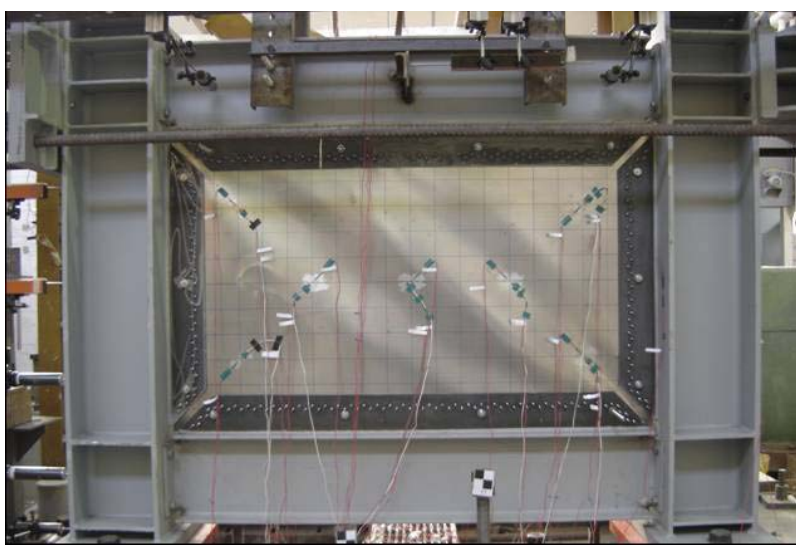

Figure 7.14: Infill Panel Buckling Waves
(Specimen SW-A-H, Cycle 6 and Top Disp. of +2.18mm)

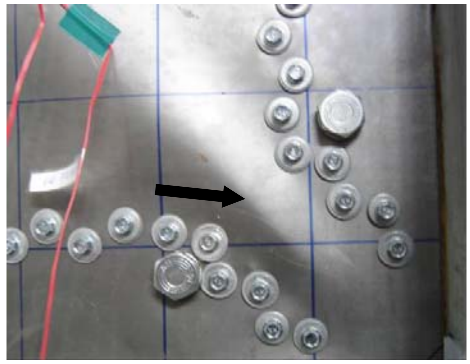

Figure 7.15: Local Buckling of the Infill in Lower North Corner
(Specimen SW-A-H, Cycle 5 and Top Disp. of -2.18mm)

During the three cycles just before yield point (Cycles 16, 17 and 18), the top displacement was 7.21mm and drift was 0.49%. At this stage, the buckling sounds grew louder and the magnitude of the buckling waves on the infill panel grew larger as well.

At the top displacement of 8.41mm (0.56% drift) and load of 107kN during the first half of Cycle 19 some nonlinear behavior that was getting clear was noticed. Based on visual extrapolation of the force-displacement curve this was deemed to be the yield point for this specimen. Figure 7.16 shows the buckling of the infill plate at this stage. No strength degradation was observed during these three cycles at $\pm 1\delta_y$ and maximum base shear was 105kN.

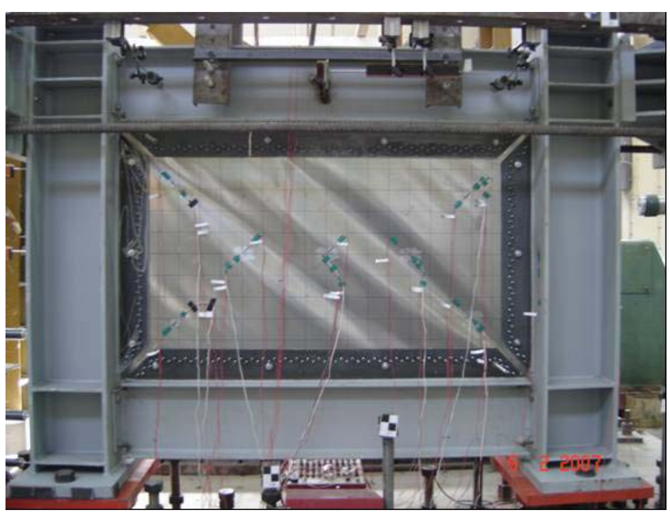

Figure 7.16: Buckling of the Infill Panel
(Specimen SW-A-H, Cycle 19 and Top Disp. of +8.41mm)

In Cycle 22, Figure 7.17 shows the bearing of the plate in front of the erection bolts in upper south corner being opened up and plastic folds in upper north corner being closed up when displacement was applied to the north ($+2\delta_y$). The load of 141 kN and the top displacement of 16.79mm ($\pm2\delta_y$) were achieved in this cycle. No fracture and strength degradation were occurred in the three cycles 22, 23 and 24.

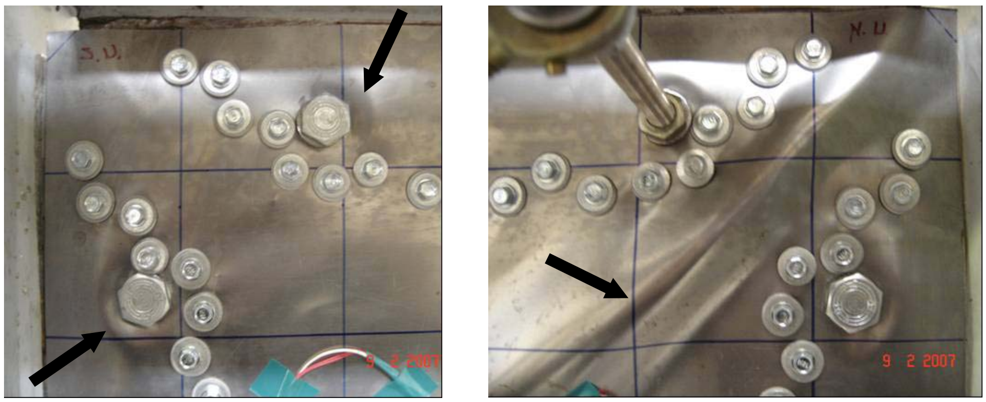

(a) (b)

Figure 7.17: The Bearing of Plate and Plastic Folds in; (a) Upper South Corner and (b) Upper North Corner (Specimen SW-A-H, Cycle 22 and Top Disp. of +16.79mm)

The specimen was then subjected to three cycles at $\pm3\delta_y$ (25.19mm top displacement, 1.58% drift). Again the noise of the tension field reorienting itself grew louder compared to the previous displacement step. The magnitude of the buckling waves during Cycle 25 is shown in Figure 7.18, and it can be seen that more waves appeared over the infill panel than in the previous displacement step.

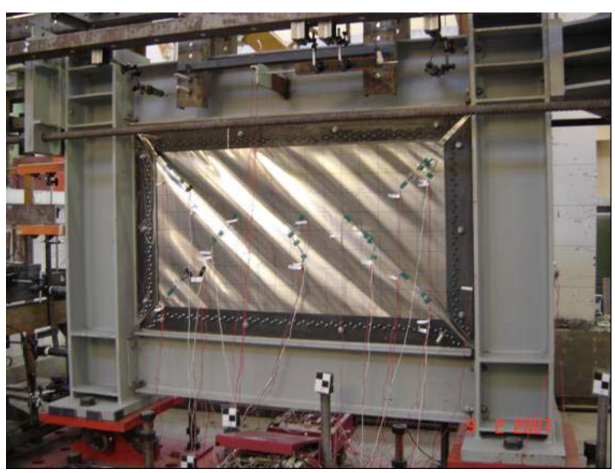

Figure 7.18: Infill Plate Buckling
(Specimen SW-A-H, Cycle 25 and Top Disp. of +25.19mm)

In addition to this, it is apparent from the square grid that the buckling waves, and hence the tension field, are oriented at approximately 45° from vertical. Additionally, plastic folds and residual deformations were beginning to form at the corners of the infill plate. Figure 7.19 shows the folds and plastic deformations forming from the corners. Again there was no degradation of strength during these three cycles and the peak force attained was 163kN.

Following the Cycle 27, only two cycles were performed at $\pm 4\delta_y$ corresponding to 33.72mm top displacement and 2.11% drift, and every subsequent displacement step, in accordance with ATC-24 **(ATC, 1992)**. Figure 7.20 shows the magnitude of infill plate buckling during this stage and it is again apparent that the tension field is oriented at approximately 45° from vertical. The plastic folds forming from the corners became more pronounced during these cycles as shown in Figures 7.21. Again there was no degradation of strength during these two cycles and the maximum base shear was 175kN.

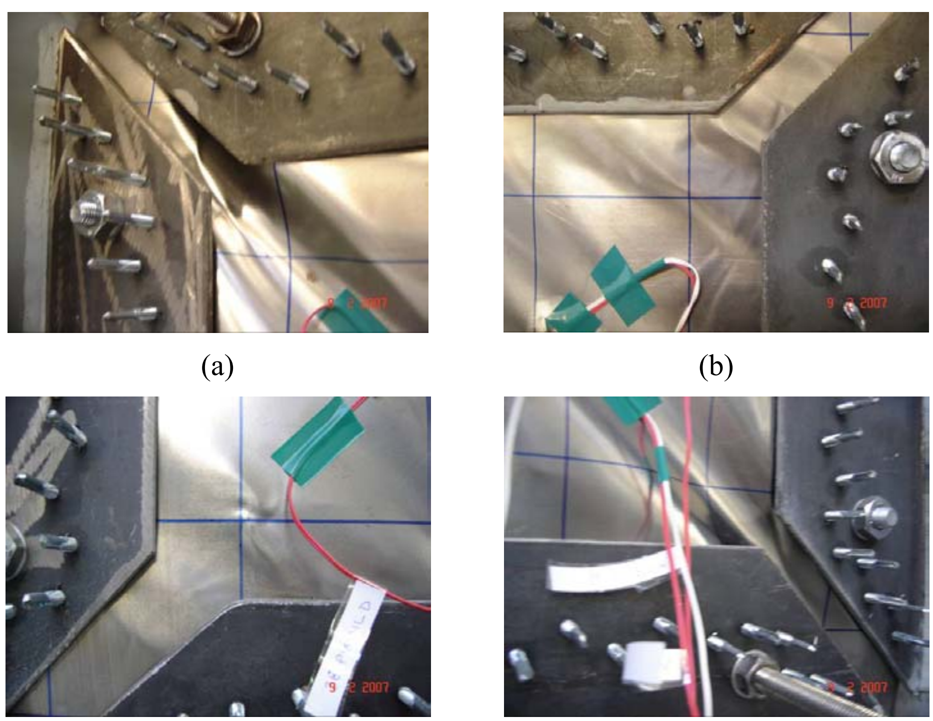

(a) (b)

(c) (d)

Figure 7.19: Plastic Folds and Residual Deformations in; (a) Upper North Corner, (b) Upper South Corner, (c) Lower North Corner and (d) Lower South Corner (Specimen SW-A-H, Cycle 25 and Top Disp. of +25.19mm)

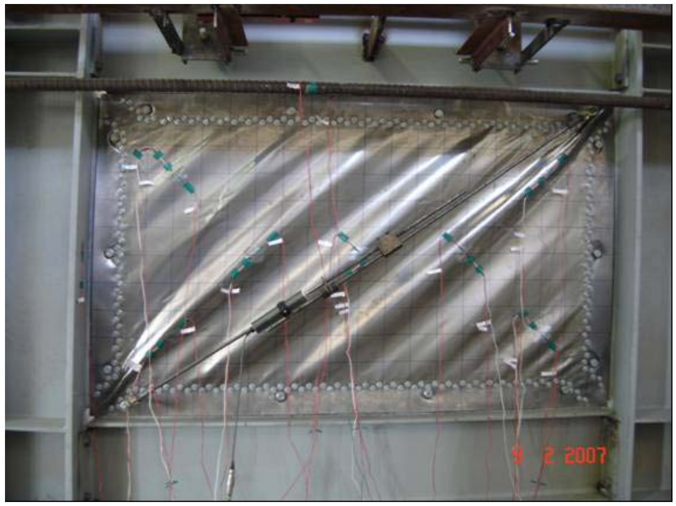

Figure 7.20: Infill Plate Buckling
(Specimen SW-A-H, Cycle 28 and Top Disp. of +33.72mm)

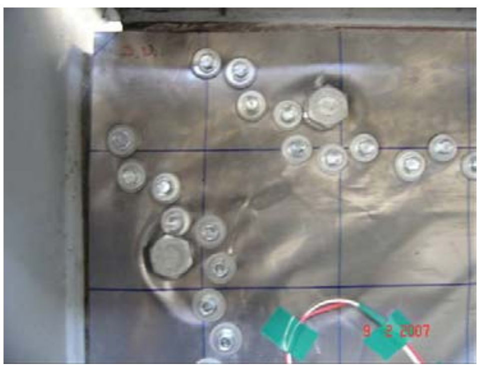

(a)

(b)

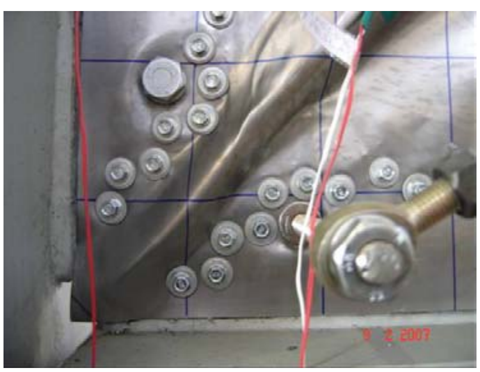

(c)

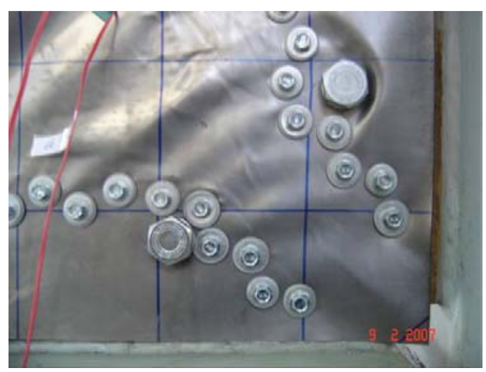

(d)

Figure 7.21: Plastic Folds and Residual Deformations in ; (a) Upper South Corner, (b) Upper North Corner, (c) Lower South Corner and (d) Lower North Corner
(Specimen SW-A-H, Cycle 28 and Top Disp. of +33.72mm)

Figure 7.22 shows the buckling of the infill panel during Cycle +5δ_y (41.97mm top displacement and 2.62% drift). Plastic folds and residual deformations were grown and became more noticable. At -5δ_y, an infill tear approximately 4.00mm in length, shown in Figure 7.23, was observed in upper north corner. Still no degradation in the strength of the shear wall was observed and the maximum base shear reached 183kN at Cycles 30 and 31.

Figure 7.22: Infill Plate Buckling
(Specimen SW-A-H, Cycle 30 and Top Disp. of +41.97mm)

Figure 7.23: Infill Tear in Upper North Corner
(Specimen SW-A-H, Cycle 30 and Top Disp. of +41.97mm)

During the two cycles at ±6δ_y (50.39mm top displacement and 3.14% drift) there were eleven distinct buckling waves in the infill plate as shown in Figure 7.24 and they still appear to be oriented at 45° from vertical. At +6δ_y, infill tear at net section in upper north corner grew to what is shown in Figure 7.25. The length of the tear was about 75mm.

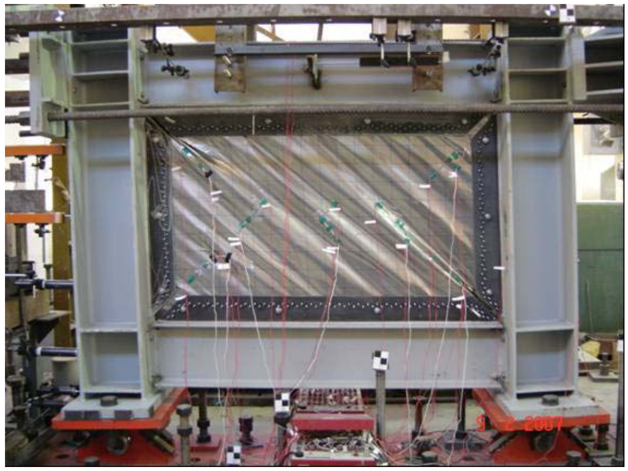

Figure 7.24: Infill Plate Buckling
(Specimen SW-A-H, Cycle 32 and Top Disp. of +50.39mm)

Figure 7.25: Infill Tear in Upper North Corner
(Specimen SW-A-H, Cycle 32 and Top Disp. of +50.39mm)

In the second excursion to $-6\delta_y$, the tear in the corner continued to propagate and its length grew to 140mm as shown in Figure 7.26. Despite of this fracture, the maximum base shear observed during the first cycle at $\pm 6\delta_y$ was 180kN and there was no strength degradation. In the first half of Cycle 33, the length of the tear became approximately 560mm and the way of propagation of the tear is shown in Figure 7.27. While the maximum base shear was 180kN at the end of the Cycle 32, the maximum base shear of 157kN at $+6\delta_y$ in Cycle 33 and that of 142kN at $-6\delta_y$ in Cycle 33 were achieved. There was an average drop of 30kN between the first and second cycles. Additionally, in the second half of Cycle 33 the fracture at net section was about 640mm long in the upper north corner and approximately 320mm in upper south corner as shown in Figure 7.28.

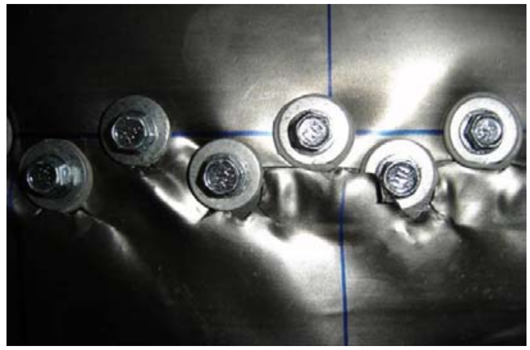

Figure 7.26: Infill Tear in Upper North Corner
(Specimen SW-A-H, Cycle 32 and Top Disp. of -50.39mm)

Figure 7.27: Propagation of Infill Tear in Upper North Corner
(Specimen SW-A-H, Cycle 33 and Top Disp. of +50.39mm)

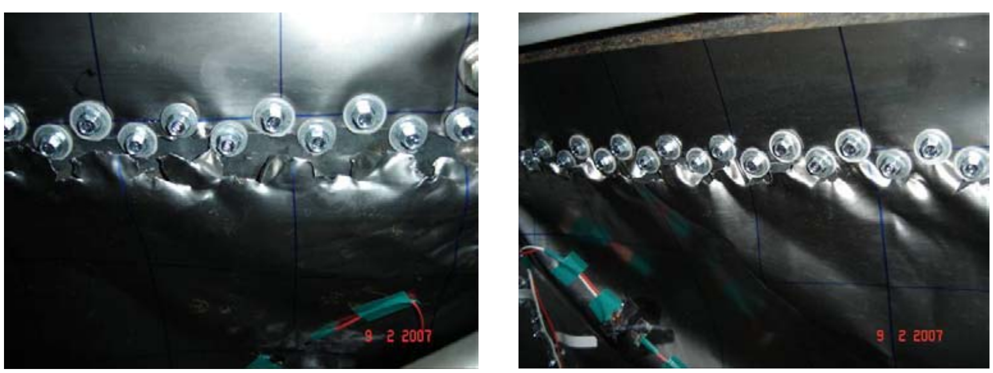

(a) (b)

Figure 7.28: Propagation of Infill Tear in; (a) Upper North Corner and (b) Upper South Corner (Specimen SW-A-H, Cycle 33 and Top Disp. of -50.39mm)

The buckling waves and the bulging of infill panel were also shown in Figure 7.29 at the end of the Cycle 32 and Cycle 33. It can be seen that the residual buckling was dramatic from the out-of-plane deformation configurations of the infills in Figure 7.29 (b).

(a) (b)

Figure 7.29: (a) Buckling of Infill at -6δ_y in Cycle 32 and (b) Buckling of Infill at -6δ_y in Cycle 33 (Specimen SW-A-H, Cycle 32 and Cycle 33 Top Disp. of -50.39mm)

Figure 7.30 shows the buckling of infill panel at the final displacement step, ±7δ_y, which corresponds to 58.80mm top displacement and 3.67% drift. Large residual buckles were also visible in this figure. This indicated that the plate had undergone significant plastic elongation. The specimen was subjected to 1 cycle at this displacement step because the net section failure, as shown in Figure 7.31, on upper edge of infill occurred at the end of the first excursion, +7δ_y.

Figure 7.30: Buckling of Infill Plate
(Specimen SW-A-H, Cycle 34 and Top Disp. of +58.80mm)

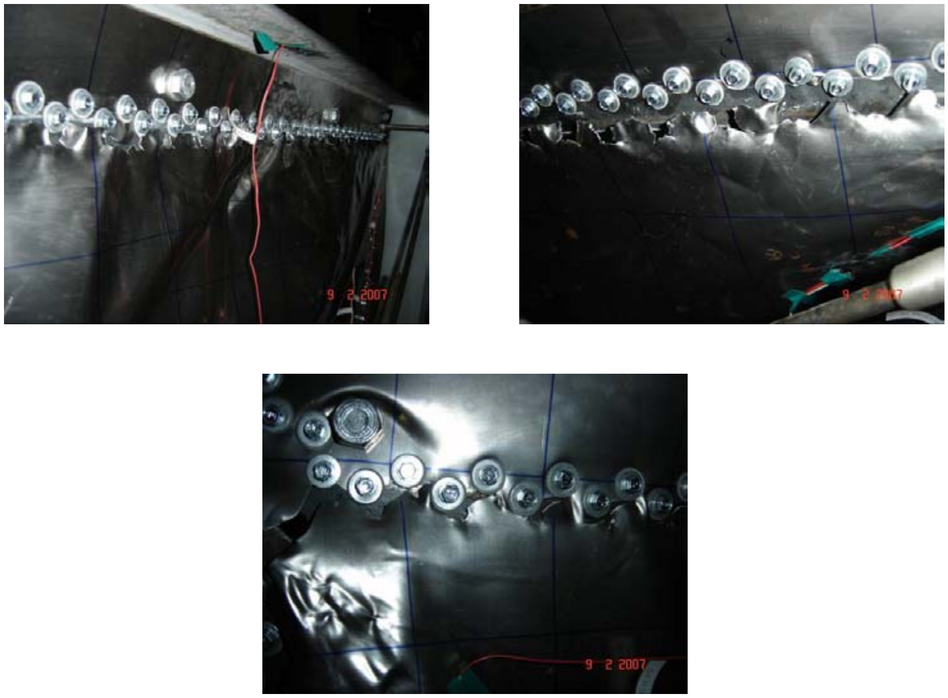

Figure 7.31: Net Section Failure of Infill Plate on Upper Edge
(Specimen SW-A-H, Cycle 34 and Top Disp. of +58.80mm)

During the final cycle at $\pm 7\delta_y$ the maximum base shear was 118kN. Hence, this value reduced at about 34% of its value at Cycle 32. No fracture was observed in the beam-to-column connections at the end of the test. Figure 7.32 shows the failure of the plate in north upper corner.

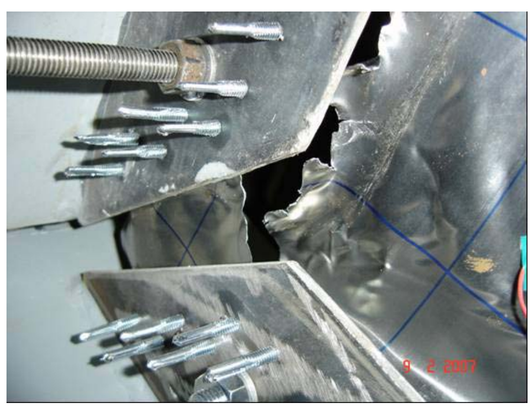

Figure 7.32: Net Section Failure in North Upper Corner
(Specimen SW-A-H, Cycle 34 and Top Disp. of -58.80mm)

7.2.3 Specimen SW-B-H

The specimen SW-B-H exhibited a hysteretic behavior as shown in Figure 7.33. During the first 3 cycles of testing at 0.89mm (0.07% drift) its response was completely elastic. After this point, the hysteresis loops slightly began to pinch and the pinched loops that were not noticeable continued up to yield point which was determined experimentally during testing. Pinched loops that occurred at small displacement steps before the yield are attributed to the initial out-of-straightness, local buckling of infill panel and bearing of the panel in front of some screws especially used in the corners. Therefore, due to these phenomena some insignificant nonlinear behavior was observed.

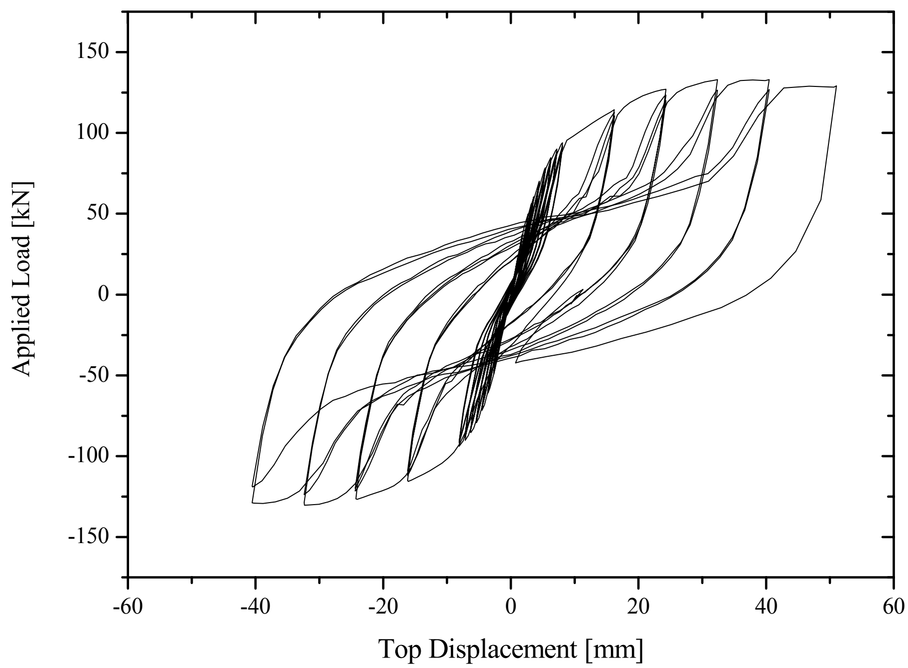

Figure 7.33: Hysteresis Curves for SW-B-H

At Cycle 4, some popping noises from infill panel began to hear and magnitude of the buckling waves along the infill plate was small. During Cycles 4, 5 and 6 there were three buckling waves observed as shown in Figure 7.34. The maximum base shear was 37kN (corresponding top displacement of 1.79mm) at this stage.

During Cycle 7, 8 and 9 additional small pops were heard and three buckling waves became pronounced. A peak force of 49.8 kN is required to initially attain the 0.19% drift or 2.71 mm top displacement limits.

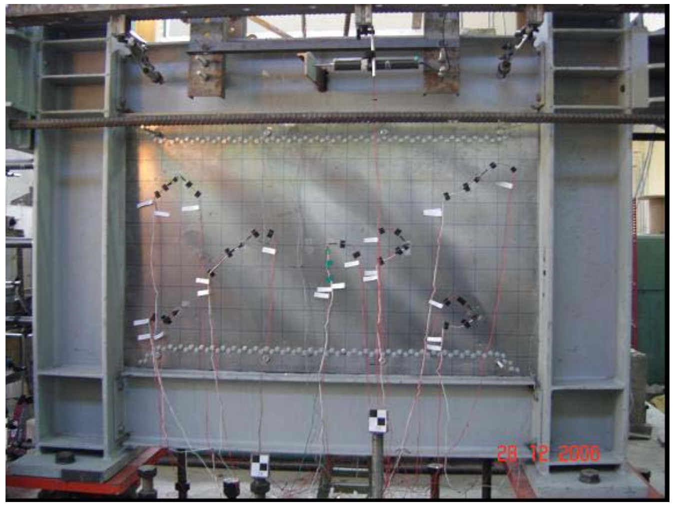

Figure 7.34: Infill Plate Buckling
(Specimen SW-B-H, Cycle 4 and Top Disp. of +1.79mm)

At Cycle 10, 11 and 12 the top displacement and drift was 3.59mm and 0.24% respectively. The audible buckling sounds grew louder and the magnitude of the buckling waves on the infill panel grew larger as well. The load was approximately 60kN.

Four buckling waves for pushing and pulling direction were observed as shown in Figure 7.35 and 7.36 during Cycles 13. Figure 7.37 shows plastic deformations occurred in upper south corner in the second excursion to -0.58δ_y. Plastic folds similar to those before were also noticed in upper north corner at the beginning of Cycle 15. The base shear obtained was approximately 70kN.

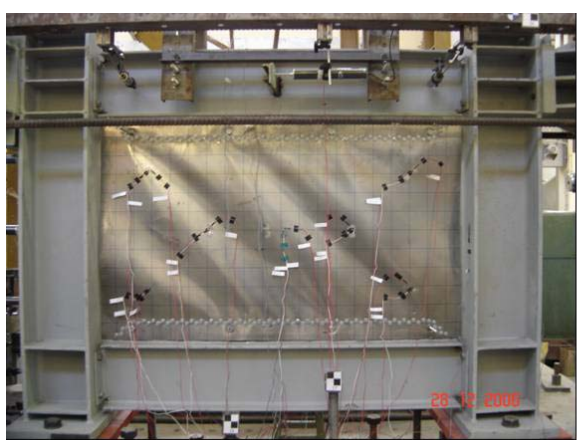

Figure 7.35: Infill Plate Buckling
(Specimen SW-B-H, Cycle 13 and Top Disp. of +4.48mm)

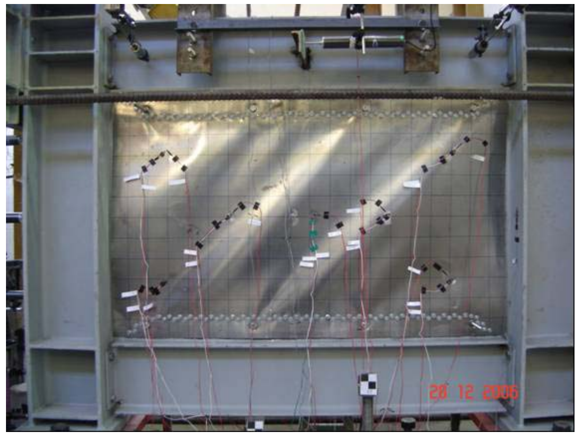

Figure 7.36: Infill Plate Buckling
(Specimen SW-B-H, Cycle 13 and Top Disp. of -4.48mm)

Figure 7.37: Plastic Folds in Upper South Corners
(Specimen SW-B-H, Cycle 13 and Top Disp. of -4.48mm)

At Cycles 16, 17 and 18, some insignificant nonlinear behavior was observed due to plastic folds in the corners. The audible buckling sounds grew a little bit louder and the magnitude of the buckling waves on the infill panel grew again larger as well. The top displacement of 5.39mm and corresponding base shear of 77kN were achieved.

During Cycles 19, 20 and 21 the buckling wave pattern was what is shown in Figure 7.38 at the first excursion to $+0.79\delta_y$. The plastic kinks and the bulgings of plate forming from the upper north and south corners became much clearer as shown in Figure 7.39.

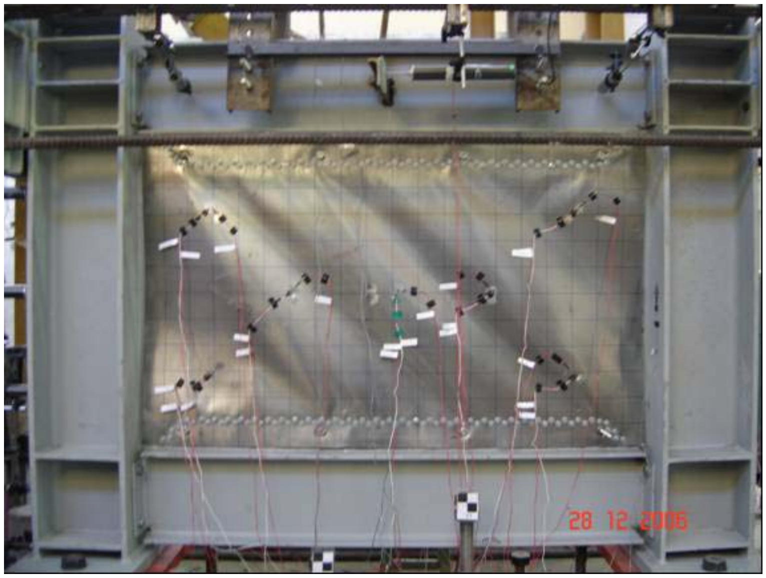

Figure 7.38: Infill Plate Buckling
(Specimen SW-B-H, Cycle 19 and Top Disp. of +6.29mm)

The maximum base shear of 84kN was observed. The top displacement was also 6.30mm. Additionally, from the square grid drawn by marker on the infill it is apparent that the buckling waves, and hence the tension field, are oriented at approximately 40° from vertical.

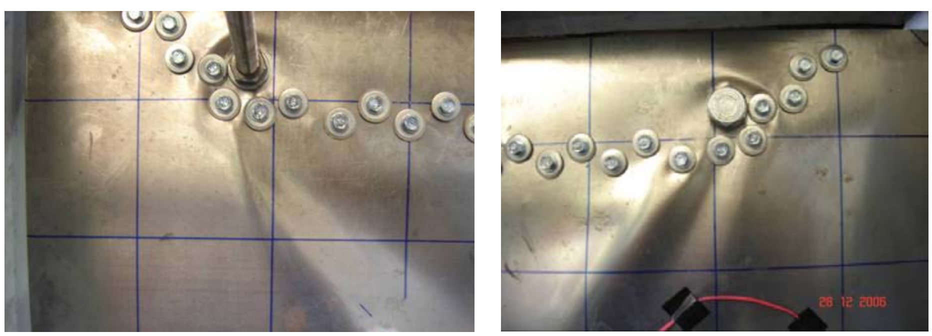

(a) (b)

Figure 7.39: Plastic Kinks and Bulging of Infill Panel; (a) Upper North Corner and (b) Upper South Corner (Specimen SW-B-H, Cycle 19 and Top Disp. of ±6.29mm)

The specimen was then subjected to three cycles at $\pm 0.89\delta_y$ (7.20mm top displacement, 0.46% drift). Again the noise of tension field reorienting itself grew louder compared to the previous displacement step at Cycle 22, 23 and 24. Figure 7.40 shows the buckling waves configuration of infill panel at this stage.

Figure 7.40: Infill Plate Buckling
(Specimen SW-B-H, Cycle 22 and Top Disp. of +7.20mm)

The magnitude of the plastic folds formed in the corners grew to what is shown in Figure 7.41. The maximum base shear was approximately 89kN at the last three cycles applied just before the yield.

(a)

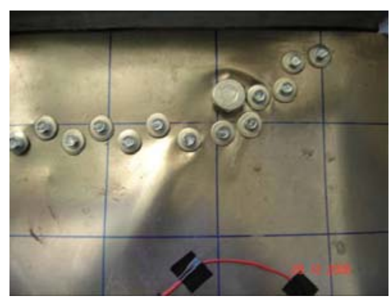

(b)

(c)

Figure 7.41: Plastic Folds and Bearing of Infill Panel; (a) Upper North Corner, (b) Upper South Corner and (c) Lower South Corner
(Specimen SW-B-H, Cycle 22 and Top Disp. of +7.20mm)

Following the previous cycles, again three cycles, Cycle 25, 26 and 27, were applied to the specimen. At the top displacement of 8.09mm (0.52% drift) and load of 94kN during the first half of Cycle 25 some nonlinear behavior getting clear was noticed. Hence, based on the extrapolation of shape of the force-displacement hysteresis curve, this displacement was determined to be the experimentally obtained yield point for this specimen. Figure 7.42 shows the buckling of the infill plate at this stage. There was no change in the maximum base shear obtained during these three cycles at $\pm 1\delta_y$, indicating that the infill was still in good condition and maximum base shear averaging 92kN was observed.

Figure 7.42: Infill Plate Buckling
(Specimen SW-B-H, Cycle 25 and Top Disp. of +8.09mm)

Furthermore, from the square grid drawn by marker on the infill given in Figure 7.42 it is apparent that the buckling waves, and hence the tension field direction, are again generally oriented at about 40° from vertical.

At Cycle 28, during the first excursion to $\pm 2\delta_y$ (corresponding top displacement of 16.20mm and drift of 1.01%), the buckling sounds grew louder and the magnitude of the buckling waves on the infill plate grew larger as well as in Figure 7.43.

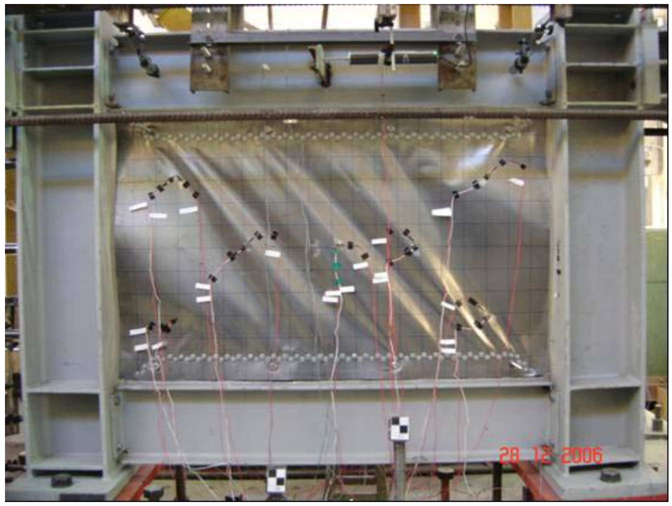

Figure 7.43: Infill Plate Buckling
(Specimen SW-B-H, Cycle 28 and Top Disp. of +16.20mm)

While the maximum base shear was about 114kN at beginning of Cycle 28, in Cycle 30 the maximum base shear of 110kN was observed. Plastic folds which were formed in the corners continued to propagate as shown in Figure 7.44. There was no significant degradation in strength during the three cycles.

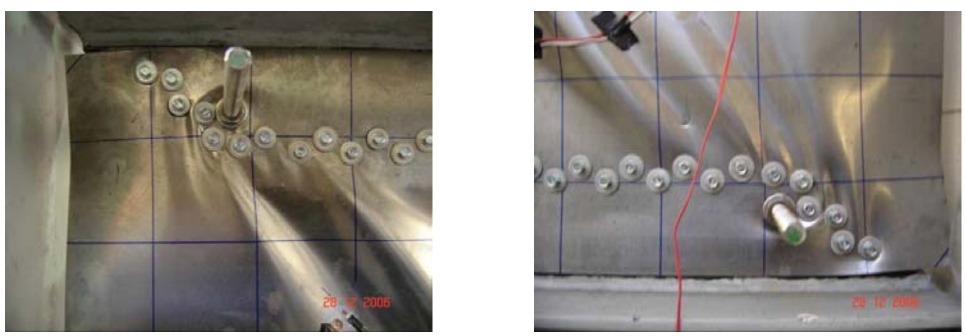

(a) (b)

Figure 7.44: Plastic Folds and Bearing of Infill Panel; (a) Upper North Corner and (b) Lower South Corner (Specimen SW-B-H, Cycle 22 and Top Disp. of +16.20mm)

Figure 7.45 shows the magnitude of residual buckles and the bulging of infill plate in Cycle 28 and 30 at $-2\delta_y$.

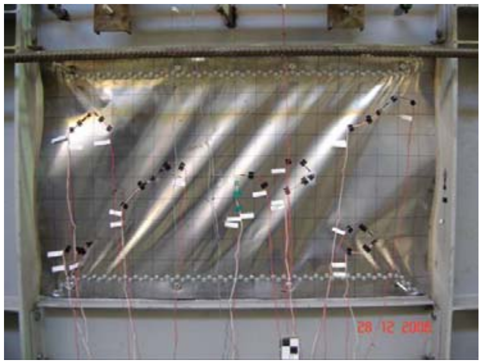

(a)

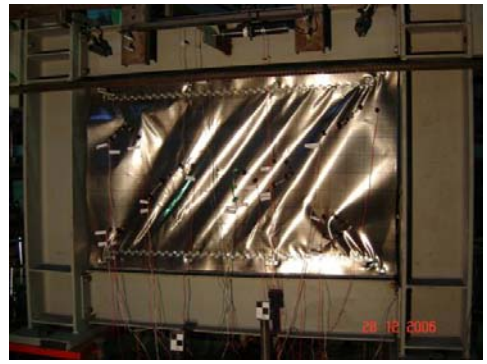

(b)

Figure 7.45: Residual Buckles and Bulging of Infill Panel; (a) Cycle 28 at -2δ_y and (b) Cycle 30 at -2δ_y (Specimen SW-B-H, Top Disp. of -16.20mm)

Following the three cycles at ±2δ_y, specimen SW-B-H was again subjected to three cycles at ±3δ_y (24.29mm top displacement, 1.50% drift). The orientation of the buckling waves, hence tension field direction, was slightly different from previous displacement steps. The orientation angle of less than 40° from vertical was also observed at this stage. The pattern of buckling waves over the infill panel is shown in Figure 7.46. The maximum base shear was 127kN obtained at the first half of Cycle 31. There was a 7 kN drop (from 127 kN to 120 kN) in the base shear between Cycle 31 and Cycle 33. There was no any fracture observed at net section in the panel-to-beam connections.

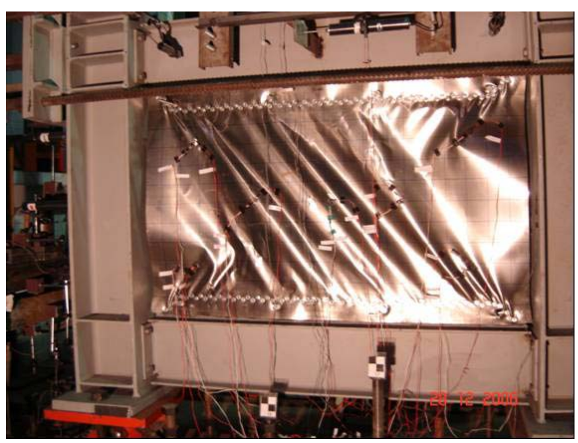

Figure 7.46: Infill Plate Buckling Waves Configuration
(Specimen SW-B-H, Cycle 31 and Top Disp. of +24.29mm)

(a) (b)

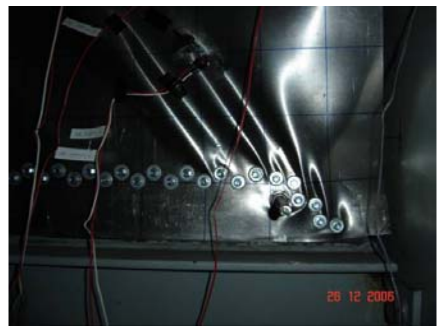

(c) (d)

Figure 7.47: Plastic Folds and Residual Deformations in the Corners; (a) Upper North, (b) Upper South, (c) Lower North and (d) Lower South (Specimen SW-B-H, Cycle 31 and Top Disp. of +24.29mm)

Figure 7.47 shows propagation of the plastic folds and the bearing of the plate in the corners.

After the cycles at $\pm3\delta_y$, only 2 cycles were performed at $\pm4\delta_y$ and every subsequent displacement step, in accordance with ATC-24 **(ATC, 1992)**. Figure 7.48 shows the magnitude of infill buckling during this stage and it can be seen that the tension field is generally oriented at less than 40° from vertical apart from the previous displacement steps.

Figure 7.48: Infill Plate Buckling Waves Configuration
(Specimen SW-B-H, Cycle 34 and Top Disp. of +32.40mm)

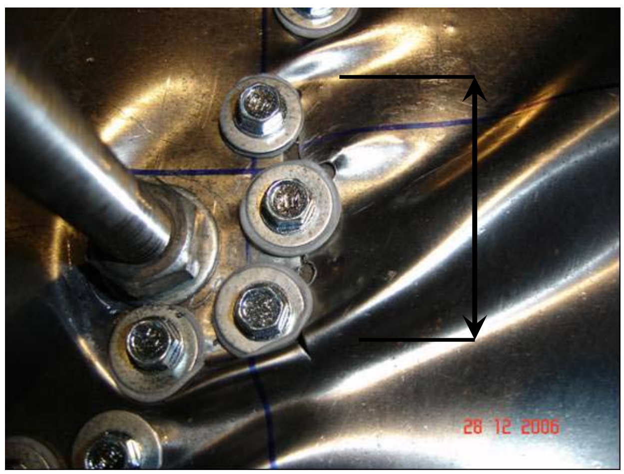

Figure 7.49: Infill Tear in Upper North Corner
(Specimen SW-B-H, Cycle 34 and Top Disp. of +32.40mm)

At Cycle 34, a 45 mm tear in length at net section of infill plate in upper north corner was observed. This fracture occurred at the load of 133 kN is shown in Figure 7.49.

During the second excursion to -4δ_y, fractures at net sections in upper south and lower north corners were observed. Both of them, given in Figure 7.50, were approximately 40mm in length. There was a 7 kN drop (from 133 kN to 126 kN) in the base shear between Cycle 34 and Cycle 35. Therefore, the maximum base shear decreased by 5%.

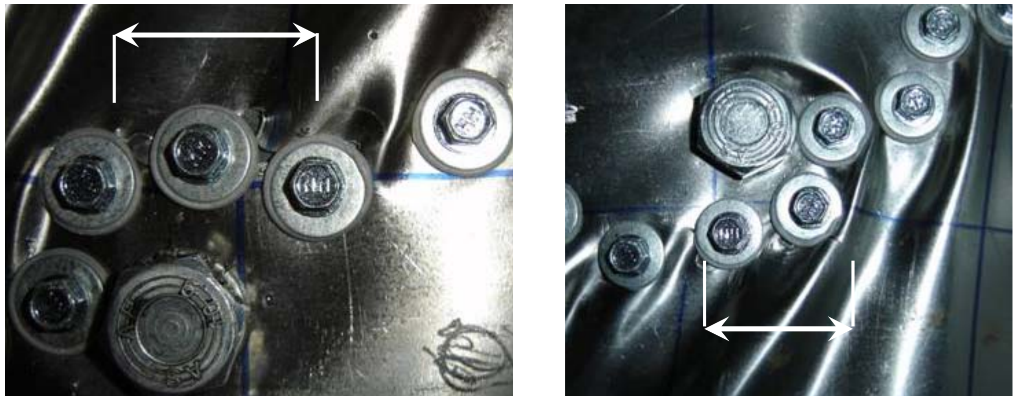

(a) (b)

Figure 7.50: Infill Tears in; (a) Lower North Corner and (b) Upper South Corner
(Specimen SW-B-H, Cycle 34 and Top Disp. of -32.40mm)

Figure 7.51: Infill Plate Buckling Waves Configuration
(Specimen SW-B-H, Cycle 36 and Top Disp. of +40.51mm)

In Cycle 36 at $\pm 5\delta_y$, Figure 7.51 shows the buckling waves pattern, residual bulging of infill plate and the panel regions which remained inactive in energy dissipation.

Additionally, the fracture lengths grew to about 65mm in upper north and lower south corners. The propagation of these fractures is shown in Figure 7.52. There was no any significant reduction in maximum base shear between Cycle 34 and Cycle 36.

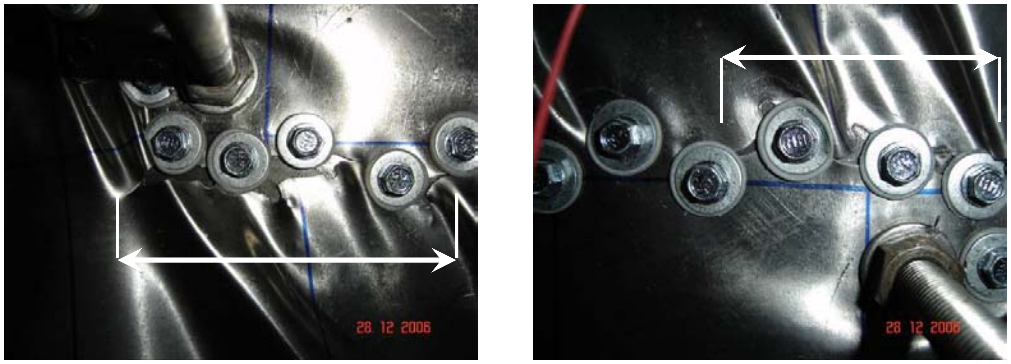

(a) (b)

Figure 7.52: Infill Fracture in; (a) Upper North Corner and (b) Lower South Corner
(Specimen SW-B-H, Cycle 36 and Top Disp. of +40.51mm)

During the first half of Cycle 37, the fractures in lower south and upper north corners became approximately 75mm and 100mm long, respectively. Despite these large fractures no significant strength degradation was observed. The maximum base shear was 127 kN at $+5\delta_y$.

Figure 7.53 shows the buckling of the infill panel at the final displacement step, $\pm6\delta_y$. At this step, because the displacement was suddenly increased by 50.61mm instead of 48.60mm and to prevent test devices from damage in case of entirely failure of the infill plate test was terminated at this point. Hence, the specimen was subjected to a half cycle in this displacement step.

Figure 7.53: Infill Plate Buckling Waves Configuration
(Specimen SW-B-H, Cycle 38 and Top Disp. of +50.61mm)

At the final displacement step, infill tears in the corners grew to what is shown Figure 7.54. The fracture in upper north corner was 185mm long while that in lower south corner was 150mm long. Maximum base shear of 128 kN was achieved at $+6\delta_y$ of Cycle 38.

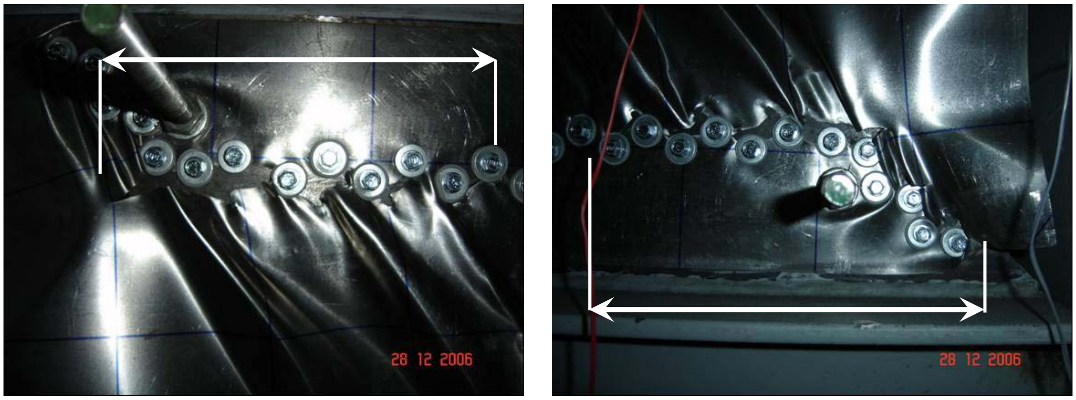

(a) (b)

Figure 7.54: Infill Fracture in; (a) Upper North Corner and (b) Lower South Corner (Specimen SW-B-H, Cycle 38 and Top Disp. of +50.61mm)

7.2.4 Deflected shape configuration of infill panels by photogrammetry

Following the evaluation of the photographs which were taken at $\pm1\delta_y$ during the tests, the configurations of the deflected shapes of the specimens, SW-A-H and SW-B-H were given in Figures 7.55 and 7.56. Deformations are in "m" in the legends.

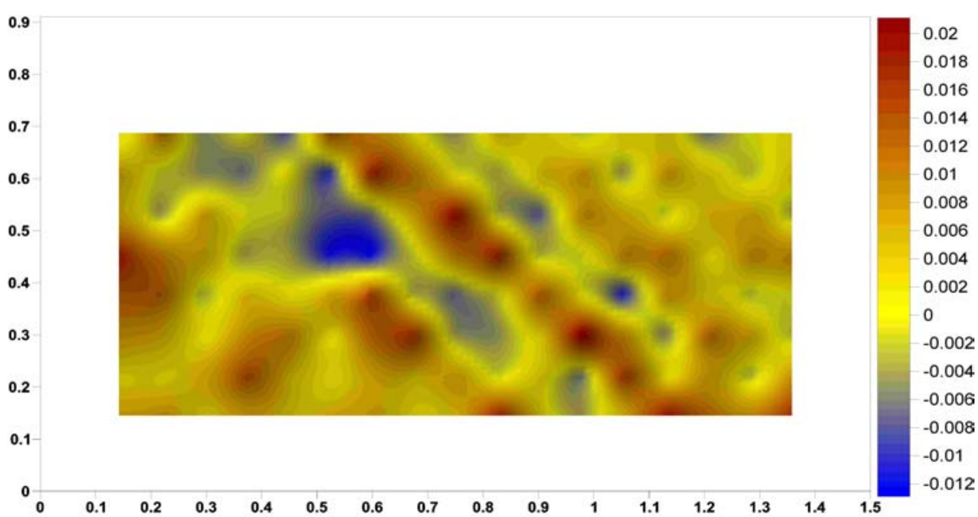

Figure 7.55: Deflected Shape of Infill Panel from Photogrametric Evaluation (Specimen SW-A-H, Cycle 21 and Top Disp. of +8.41mm)

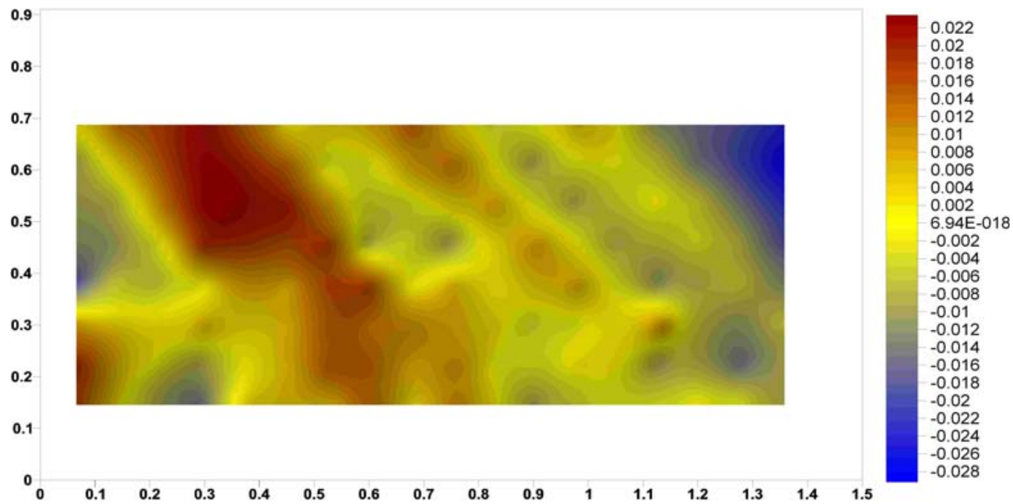

Figure 7.56: Deflected Shape of Infill Panel from Photogrametric Evaluation (Specimen SW-B-H, Cycle 27 and Top Disp. of +8.09mm)

7.3 Summary

Three specimens, two TSPSWs that were called SW-A-H and SW-B-H, and one frame without infill plate that was named as BF-H, were successfully tested under quasi-static loading.

Specimen BF-H was successfully tested to a maximum top displacement of 81.81mm which is corresponding to $\pm 7\delta_y$, 4.98% drift and 59.74mm relative displacement. The maximum base shear of 95 kN occurring at $\pm 5\delta_y$, 3.52% drift and 58.53mm top displacement. Failure of the specimen was from fractures of the connections between the beam webs and the end plates, which developed as a result of the occurrence of stress concentration regions at the fillet weld ends.

Specimen SW-A-H was successfully tested to 58.80mm of the top displacement ($\pm 7\delta_y$, 3.67% drift) and the maximum base shear of 183 kN occurring at $\pm 5\delta_y$, 2.62% drift and 41.97mm top displacement. Failure of the specimen was due to large fractures at the corners of the infill panel that propagated along the net section formed by the self-drilling screw connections. Net section failure across the entire length of the top beam connection was concluded the testing of the specimen.

Specimen SW-B-H performed well and tested to a maximum top displacement of 50.61mm. The maximum base shear was 133 kN and occurred at $\pm 4\delta_y$, 1.98% drift and 32.40mm top displacement were achieved. Failure of the specimen was from fractures at the corners of the infill plates. Apart from SW-A-H, the test was terminated prior to entirely net section failure as in specimen SW-A-H to prevent the measurement devices from damage.

8. EVALUATION AND COMPARISON

This chapter quantitatively describes the test results for one bare frame and two TSPSWs specimens, BF-H, SW-A-H and SW-B-H. The results from the test of bare frame specimen, BH-F, are also discussed in Appendix A.

In all cases load-displacement loops are presented in terms of load versus relative displacement. These hysteretic results are then compared to the predicted pushover curves from the finite element models. Additionally, several properties of systems are extracted from the experimental data, namely, initial stiffness, yield base shear and displacements, cumulative energy dissipation and displacement ductility. Furthermore, the orientation and the magnitude of the principal stresses and strains in the infill plate during linear and nonlinear portions are examined and the variation of the strain magnitude and energy dissipation across the infills is investigated. A method to predict the characteristic values of steel shear walls with very thin infill panels and semi-rigid/partial moment-resisting beam-to-column connections is also proposed.

8.1 Specimen BF-H

The specimen BF-H is a frame without an infill plate and the purpose of testing this specimen was to establish a basis for comparison. The cyclic response for specimen BF-H is shown in Figure 8.1, which is characterized by an open stable hyteresis behavior.

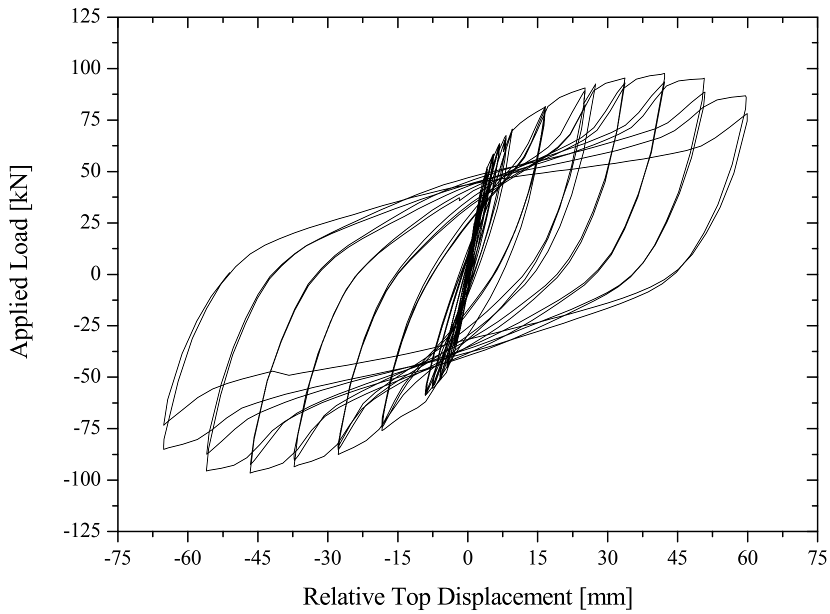

Figure 8.1: Hysteresis Loops (BF-H)

To examine the load capacity, the load-deflection envelopes of the specimen for pushing and pulling direction are plotted in Figure 8.2. The values of load and corresponding relative displacements in the envelope curves were calculated taking the average of peak values at each three cycle. The required forces in the pushing direction for the specimen at various drift levels are summarized in Table 8.1. In this table, for comparison purpose, the required loads at the specified drift levels are calculated using linear interpolation.

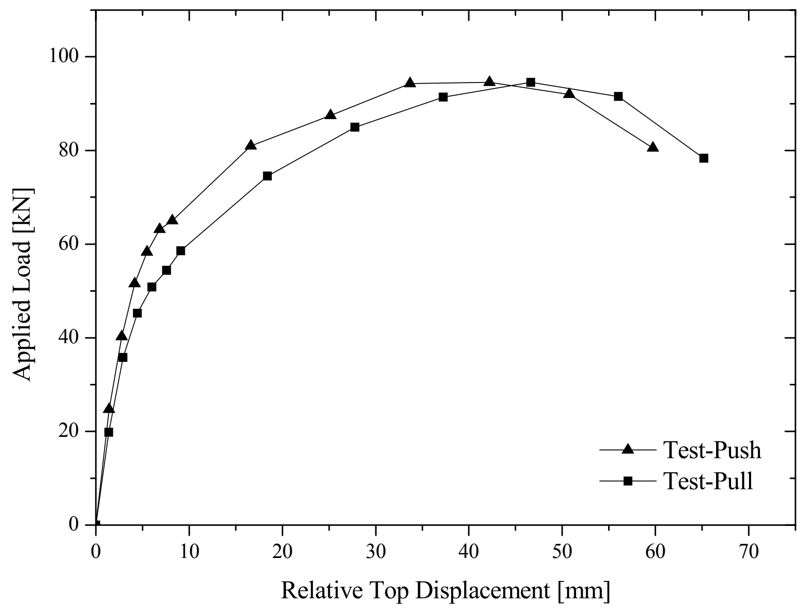

Figure 8.2: Envelopes of Specimen in Pushing and Pulling Direction (BF-H)

As can be seen from the Figure 8.2, the ultimate load capacity of specimen BF-H is obtained as the average of 94.55 kN.

Table 8.1: Required Load at Each Drift Level in Pushing Direction (BF-H)

Drift [%]	Required Load [kN]
0.25	42.12
0.50	60.07
0.75	66.63
1.00	72.33
1.25	78.03
1.50	82.08
2.00	86.60

The initial stiffness at the beginning of the first cycle is indicative of the stiffness of the structure in the undamaged state. As the reversal displacement cycles are imposed, the initial stiffness at the beginning of each new displacement level depicts the stiffness after the damage due to the previous loading. The variation of the initial stiffness at each displacement level is given in Table 8.2 for pushing direction. Initial stiffness is calculated using a polynomial curve fit through the appropriate data set. In this computation, initial half cycle at each displacement step is only considered.

Table 8.2: The Variation of Initial Stiffness in Pushing Direction (BF-H)

Cycles	Δ/δ_y	Initial Stiffness [kN/mm]	Cycles	Δ/δ_y	Initial Stiffness [kN/mm]
1	0.17	21.113	16	1	7.792
4	0.34	16.956	19	2	7.471
7	0.51	15.002	22	3	3.131
10	0.67	12.631	25	4	1.798
13	0.83	9.870	28	5	1.368

The energy dissipation per cycle at each displacement level is also given in Table 8.3. The energy dissipation is calculated using each complete cycle at each displacement increment and is the area enclosed by the load-relative displacement curve.

Table 8.3: Energy Dissipation per Cycle (BF-H)

Cycles	Dissipated Energy [kN×mm]	Cycles	Dissipated Energy [kN×mm]
1	6.250	19	1488.181
2	7.659	20	1178.426
3	7.514	21	1091.613
4	45.380	22	2729.978
5	25.220	23	2740.252
6	23.404	24	2335.255
7	94.581	25	4137.757
8	51.707	26	3996.663
9	46.617	27	5876.644
10	158.390	28	5665.532
11	91.058	29	7473.989
12	84.275	30	7252.388
13	215.860	31	8602.876
14	154.043	32	7739.922
15	135.458		
16	292.867		
17	314.570		
18	207.671		

The cumulative energy dissipation of the specimen BF-H is plotted versus the cumulative number of cycles in Figure 8.3. In calculating the cumulative dissipated energy, the areas enclosed by each load-relative displacement loop were continuously added together.

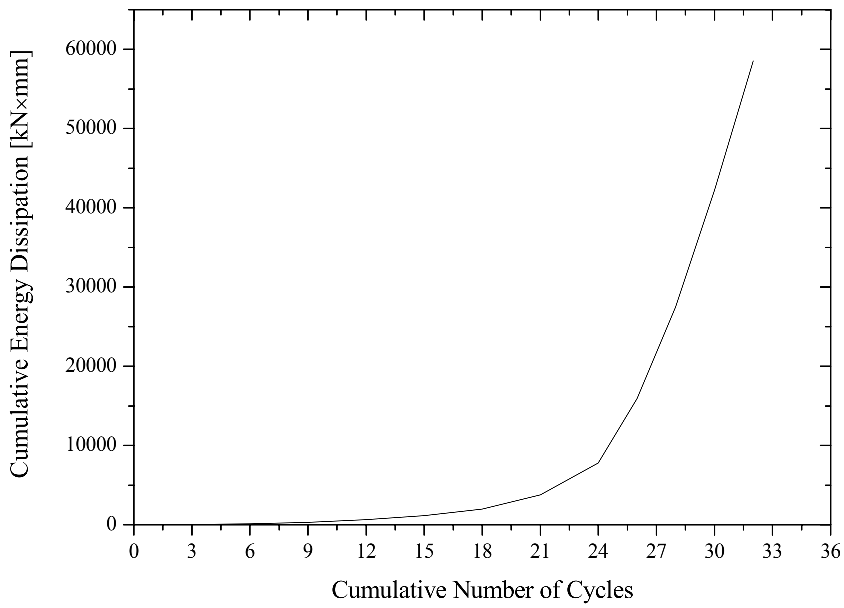

Figure 8.3: Cumulative Energy Dissipation (BF-H)

As can be noted from Figure 8.3, no appreciable energy is dissipated until Cycle 15 that corresponds to the first yielding in the beam end plates. Energy dissipation of the frame increases slightly after this point as yielding progresses to other regions of the frame. Following the Cycle 25, the energy dissipated increased sharply due to the contribution of yielding of the beam webs in the beam-to-column connections.

Also, the variation of energy dissipated per cycle is graphically given in Figure 8.4. As can be noted from the figure, energy dissipation is rapidly increased after Cycle 18, corresponding to $\pm 1\delta_y$ displacement step. After this cycle, as long as the yielding propagates across the beam end plate and along the beam webs, the amount of energy dissipated increased rapidly as expected.

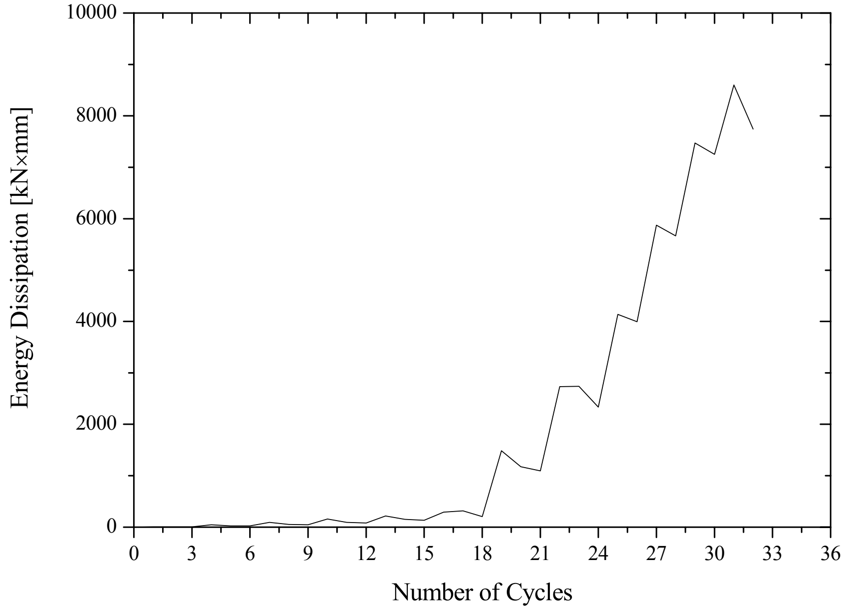

Figure 8.4: Energy Dissipation per Cycle (BF-H)

Figure 8.5 shows the four cycles of the hysteretic response at the displacement steps, 1, 4, 6 and 9, corresponds to Cycle 1, 10, 16 and 25, respectively. These load-displacement curves indicate a linear-elastic behavior in the first cycles. In the fourth cycle, when the drift level 0.23% corresponding to 2.80mm relative top displacement the frame was able to resist an applied lateral load of approximately 39kN in the pushing direction and 36kN in the pulling direction.

The relative top displacement of 8.22mm was assumed to be yield displacement for the frame. After three cycles at this displacement level, the increments for each three cycle were taken to be equal to yield displacement as in the ATC-24.

Additionally, Figure 8.5 shows the change of the initial tangent stiffness of the specimen BF-H with the specified cycles progressed. Initial stiffness is 21.113 kN/mm in the first pulling half cycle. In the first half of Cycle 25, the initial stiffness decreases to 1.798 kN/mm, about a 91% degradation.

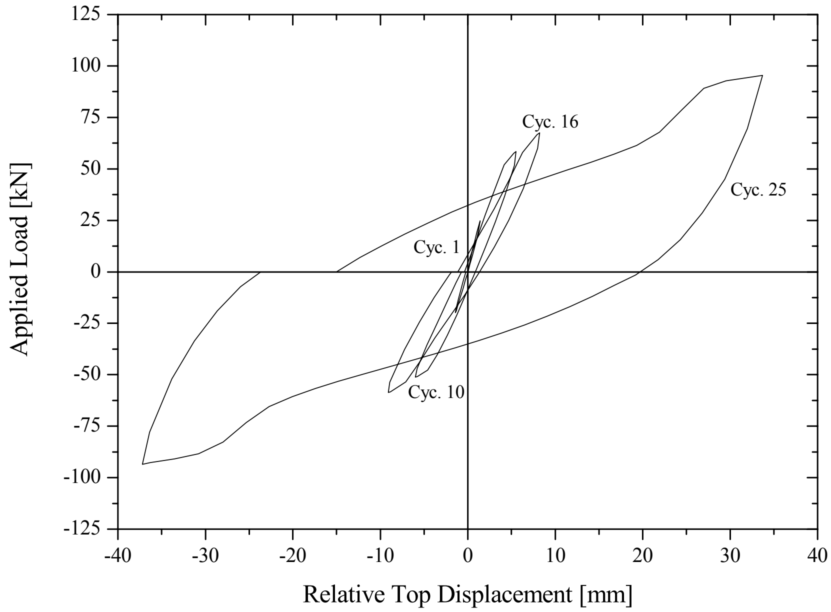

Figure 8.5: Hysteresis Loops at Cycle 1, 10, 16 and 25 (BF-H)

8.1.1 Comparison of the test and numerical analyses results

The cyclic response for specimen BF-H is shown in Figure 8.6, superimposed with the pushover curves of BF-H from preliminary numerical model and finite element model.

As can be noted that both finite element and numerical model analyses overestimate the stiffness of the frame. However, the finite element model gave a good prediction of the ultimate strength of the frame whereas the strip model underestimated the ultimate strength. The differences can be attributed to the assumptions made in determining the nonlinear behavior of the beam-to-column joint.

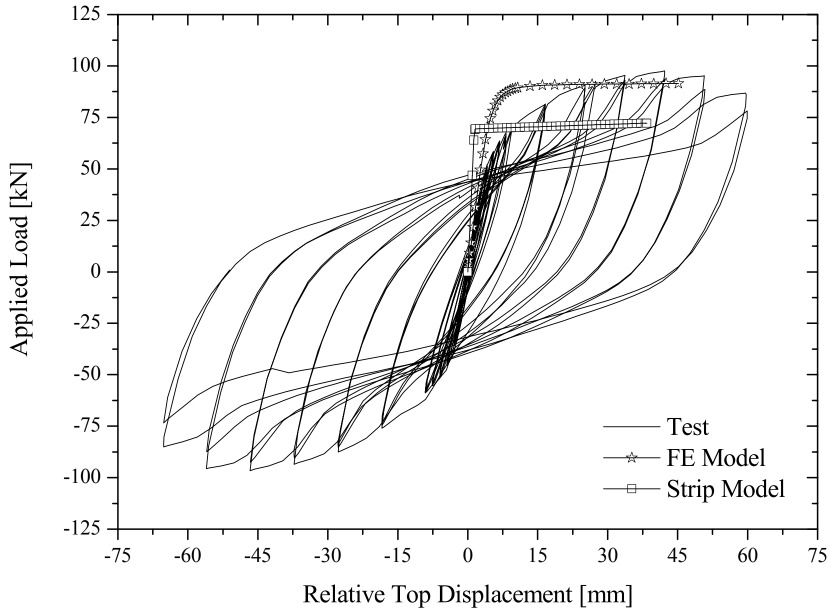

Figure 8.6: Comparison between Experimental and Numerical Results (BF-H)

Figure 8.7 also shows load-displacement envelope curves of the specimen for both pushing and pulling direction with the pushover curves from the numerical models.

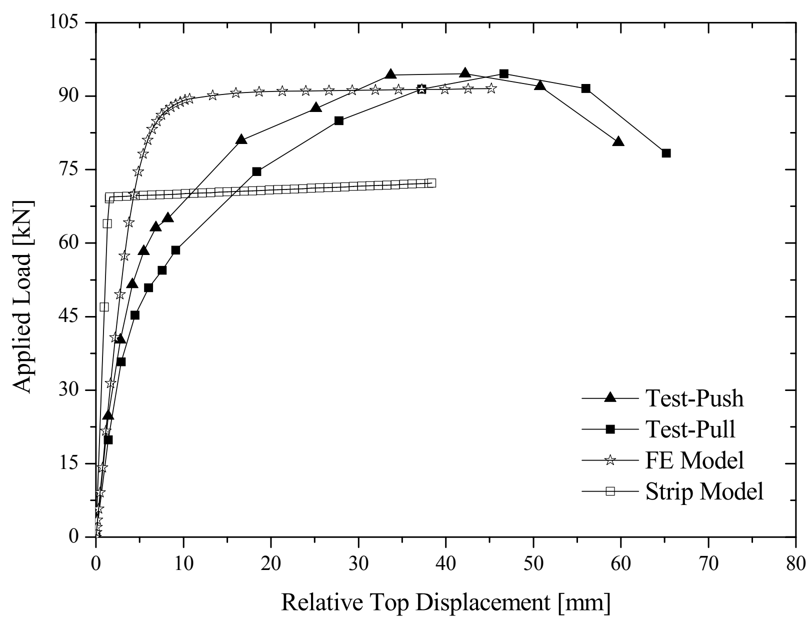

Figure 8.7: Comparison between Envelope of Cyclic Response and Numerical Results Curves (BF-H)

The shape factor, n which governs the shape of the moment-rotation curve of the connection is the most important parameter affecting the behavior of the frame. In addition to this, the assumptions made in the method to consider in calculating the moment capacity and the initial stiffness of the joint have also a significant effect on the frame behavior. As it was mentioned in Section 4.3.2.2, n was taken to be equal to 3.0. If n is equal to 1.5 and the moment capacity of beam-to-column joints is computed using the ultimate load achieved in the test, the finite element model gives a very good prediction of the envelope of the cyclic test curves as shown in Figure 8.8.

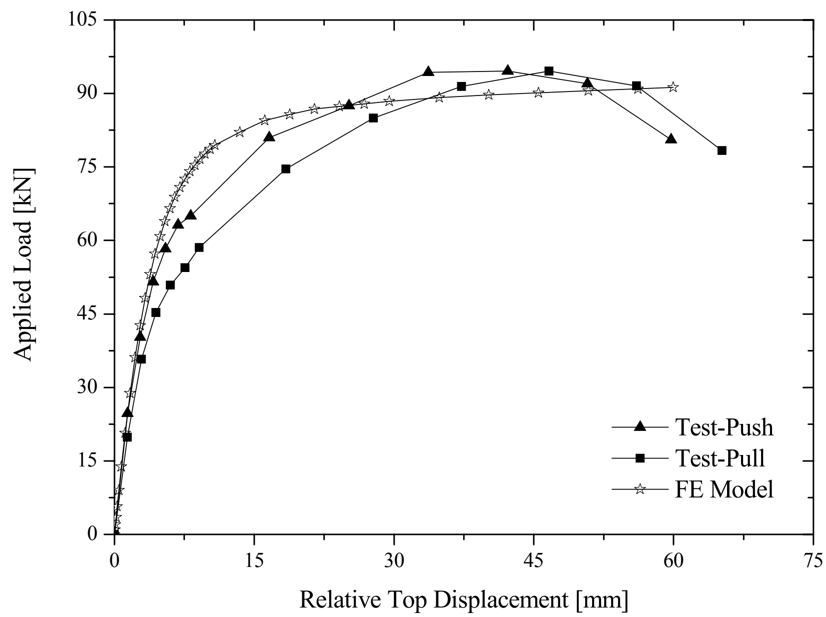

Figure 8.8: Comparison between Envelope of Cyclic Response and FEM Results (n=1.5) Curves (BF-H)

8.2 Specimen SW-A-H

The hysteresis for specimen SW-A-H is shown in Figure 8.9, superimposed with the hysteresis of BF-H. The cyclic response of specimen SW-A-H is ductile and stable up to large drift levels, although significant pinching is apperant in the hysteretic loops. As can be noted from the figure, the peak force attained in the test of SW-H-A is nearly twice times that of specimen BF-H. Furthermore, the infill panel significantly contributed to the energy dissipation capability of the system. However, considering the failure of the specimens SW-A-H and BF-H, while the ultimate load rapidly decreased to 118 kN, about 64% of the maximum load in SW-A-H, the maximum load of 77.2 kN which is about 81% of the ultimate base shear attained was observed in specimen BF-H. The peak load obtained in specimen SW-A-H is approximately two times that in specimen BF-H.

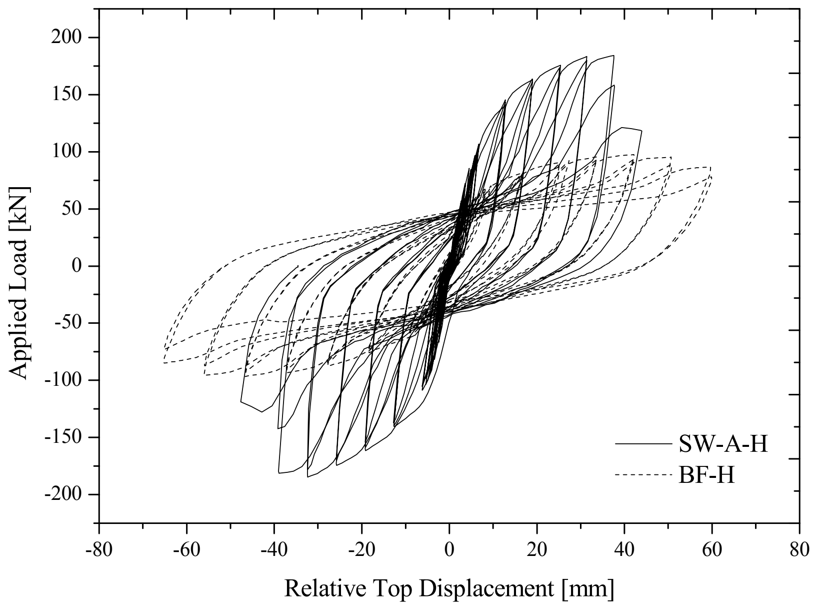

Figure 8.9: Comparison of Specimen SW-A-H and BF-H Hystereses

In order to examine the load capacity, the load-displacement envelopes of the specimen for pushing and pulling direction are plotted in Figure 8.10. In calculating the load and corresponding relative top displacements, the same method expressed in Section 8.1 was emloyed. The required forces in the pushing direction for the specimen at various drift levels are listed in Table 8.4. In this table, for comparison purpose, linear interpolation is utilized in computing the required loads at the specified drift levels.

Table 8.4: Required Load at Each Drift Level in Pushing Direction (SW-A-H)

Drift [%]	Required Load [kN]
0.25	60.72
0.50	97.56
0.75	119.80
1.00	138.14
1.25	150.05
1.50	159.46
2.00	172.12

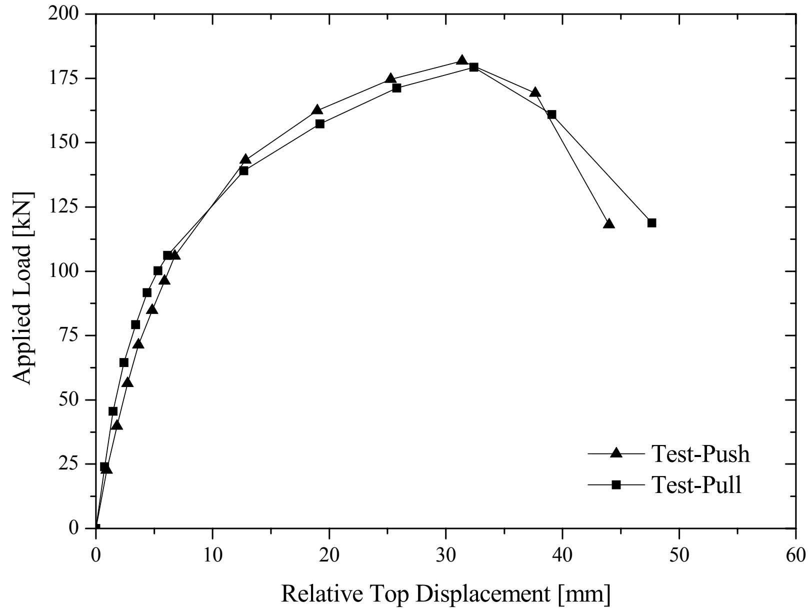

Figure 8.10: Envelopes of Specimen in Pushing and Pulling Direction (SW-A-H)

The change of the initial stiffness with each displacement level is listed in Table 8.5 for pushing direction. Initial stiffness was again calculated using a polynomial curve fit through the appropriate data set. Initial half cycle at each displacement step was also considered in this computation.

Table 8.5: The Variation of Initial Stiffness in Pushing Direction (SW-A-H)

Cycles	Δ/δ_y	Initial Stiffness [kN/mm]	Cycles	Δ/δ_y	Initial Stiffness [kN/mm]
1	0.14	29.865	19	1	9.320
4	0.27	22.058	22	2	7.073
7	0.40	19.788	25	3	4.010
10	0.54	15.701	28	4	3.114
13	0.71	11.997	30	5	1.297
16	0.87	11.316			

The energy dissipation per cycle at each displacement level is also given in Table 8.6. The energy dissipation was computed using each complete cycle of each displacement increment and is the area enclosed by the load-relative displacement curve. At the last displacement step, only one cycle, called Cycle 34, was able to be performed due to the net section failure on the top edge connection of the infill plate. Cycle 34, therefore, consists of one hysteresis loop.

Table 8.6: Energy Dissipation per Cycle (SW-A-H)

Cycles	Dissipated Energy [kN×mm]	Cycles	Dissipated Energy [kN×mm]
1	9.348	19	318.465
2	6.589	20	263.031
3	5.714	21	250.549
4	28.478	22	1987.687
5	20.378	23	1520.391
6	18.524	24	1190.611
7	65.581	25	3387.052
8	45.984	26	2811.625
9	42.234	27	2338.351
10	117.054	28	4759.921
11	87.824	29	4137.418
12	80.893	30	6363.609
13	168.281	31	5731.552
14	137.880	32	7852.829
15	130.748	33	6682.094
16	246.226	34	7232.533
17	192.513		
18	171.281		

Figure 8.11 shows the cumulative energy dissipation of the specimen versus the cumulative number of cycles curve. The cumulative dissipated energy was computed as stated in Section 8.2.

Additionally, to show the change of dissipated energy with number of cycle Figure 8.12 is also given. As can be seen from the figure, energy dissipation is sharply increased after Cycle 21, corresponding to $\pm 1\delta_y$ displacement step. Before this cycle, the amount of energy dissipated does not seem to be considerable.

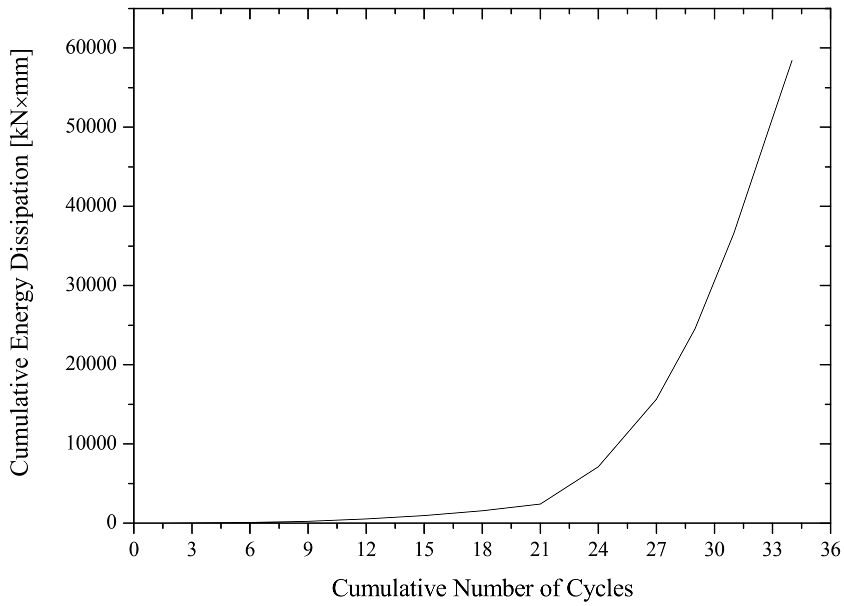

Figure 8.11: Cumulative Energy Dissipation (SW-A-H)

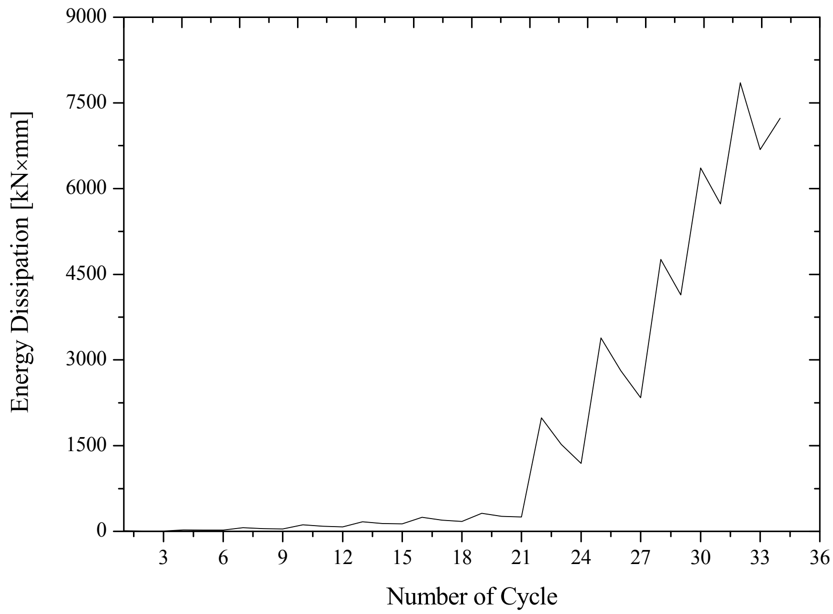

Figure 8.12: Energy Dissipation per Cycle (SW-A-H)

Table 8.7 lists the magnitudes of the tensile principal strains and stresses, and their orientation with respect to vertical for three different levels, as calculated from the strain gauges at the center cluster of the infill panel.

When the Table 8.7 is examined, the angles calculated from the strain gauges, PWCV, PWCH and PWCD1, in the middle of the infill panel are generally larger than those near two vertical sides. However, that the initial predicted orientation of the principal stresses in the infill was 45° is in agreement with the angles obtained from the strain gauges, PWNCH, PWNCD and PWNCV on north and PWSCV, PWSCD and PWSCV on south sides from the infill center. All strain gauges that considered in this table were mounted on west face of the infill plate. In Table 8.7, the minus sign in front of some drift values indicates the pulling direction.

Table 8.7: Principal Directions, Strains and Stresses (SW-A-H)

Strain gauges Considered	Drift [%]	α [°]	Principle Strain [mm/mm]	Principle Stress [MPa]
PWNCH PWNCD PWNCV	0.08	46	0.000315	63.19
	-0.07	-47	0.000287	41.37
	0.15	45	0.000489	108.26
	-0.13	-47	0.000543	100.70
	0.23	46	0.000710	165.59
	-0.20	-47	0.000815	174.00
PWCV PWCH PWCD1	0.08	58	0.000310	64.39
	-0.07	-61	0.000319	85.19
	0.15	58	0.000486	93.62
	-0.13	-54	0.000560	139.55
	0.23	57	0.000705	138.41
	-0.20	-52	0.000837	202.07
PWSCV PWSCH PWSCD	0.08	44	0.000134	1.21
	-0.07	-45	0.000197	10.74
	0.15	45	0.000317	27.19
	-0.13	-46	0.000561	70.23
	0.23	47	0.000499	53.57
	-0.20	-47	0.001033	156.96

The orientation of the principal stresses at the center of the infill during elastic cycles is found to be different than the 45° as also reported by **Berman and Bruneau (2003)**. However, from the figures of Section 7.2.2, which show the buckling of the infill panel, it is visible from square grid on the infill that the buckling wave lines are forming at nearly 45° at drifts larger than yield, which indicates that the tension field is actually forming at that angle.

Figure 8.13 and 8.14 show the variation in strain measurements across the infill plate of specimen SW-A-H to a drift of 0.40%, corresponding to 4.84mm relative displacement. The data in this plot is from the strain gauges shown in Figure 4.26, which are orientated at 45° from horizontal. As can be seen from the figure, the strain measurements from PWNUD, in upper north corner, and PWSLD, in lower south corner, are fairly uniform. Furthermore, it is also evident that the strain near the corner reached the yield before the strain in the middle attained the yield point. Thus, it can be realized that the entire plate actively initiate the dissipating energy from the corners of infill plate.

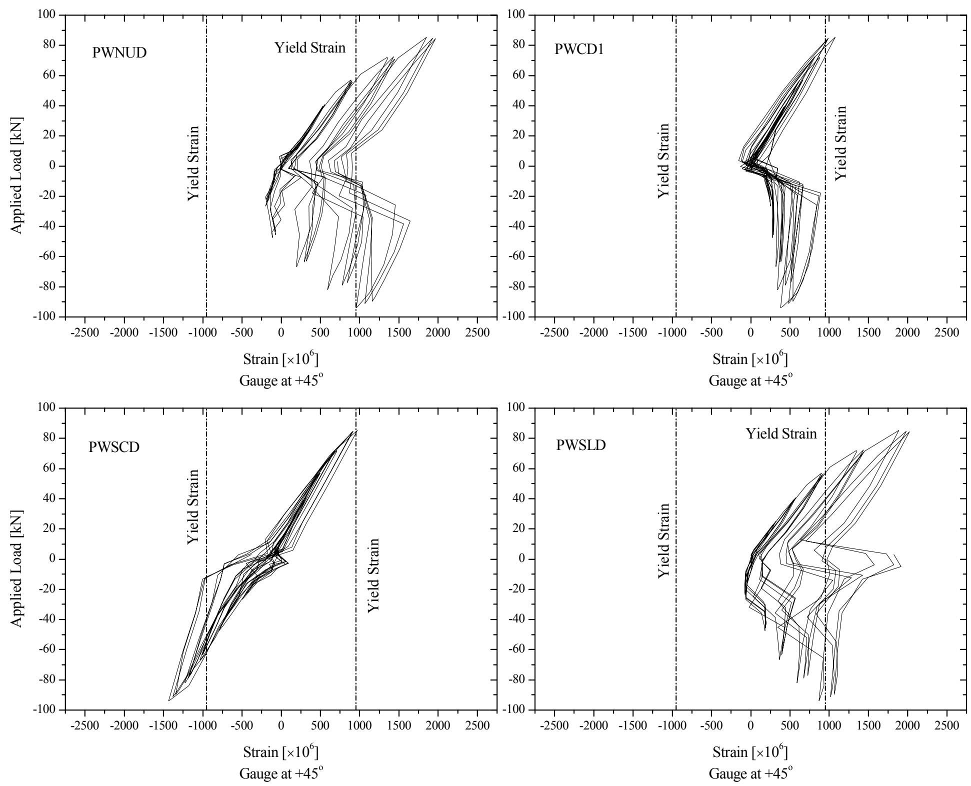

Figure 8.13: Variation of Strain across West Face of Infill Panel at +45° (SW-A-H)

Additionally, when the figure is examined, the strain measured in the same diagonal line such as the strain from PWSLD and PWSCD is not equal to each other. Therefore, the assumption reported by **Elgaaly and Liu (1997)** that the stress over the entire length of the tension field (or a strip) is equal to yield stress, while the strain varies is found to be acceptable. All gauges in Figure 8.13 and 8.14 were bounded on the west side of the specimen.

As can be noted from Figure 8.14, the strain across the infill reached the yield point. Hence, the whole infill actively contributed to dissipating energy.

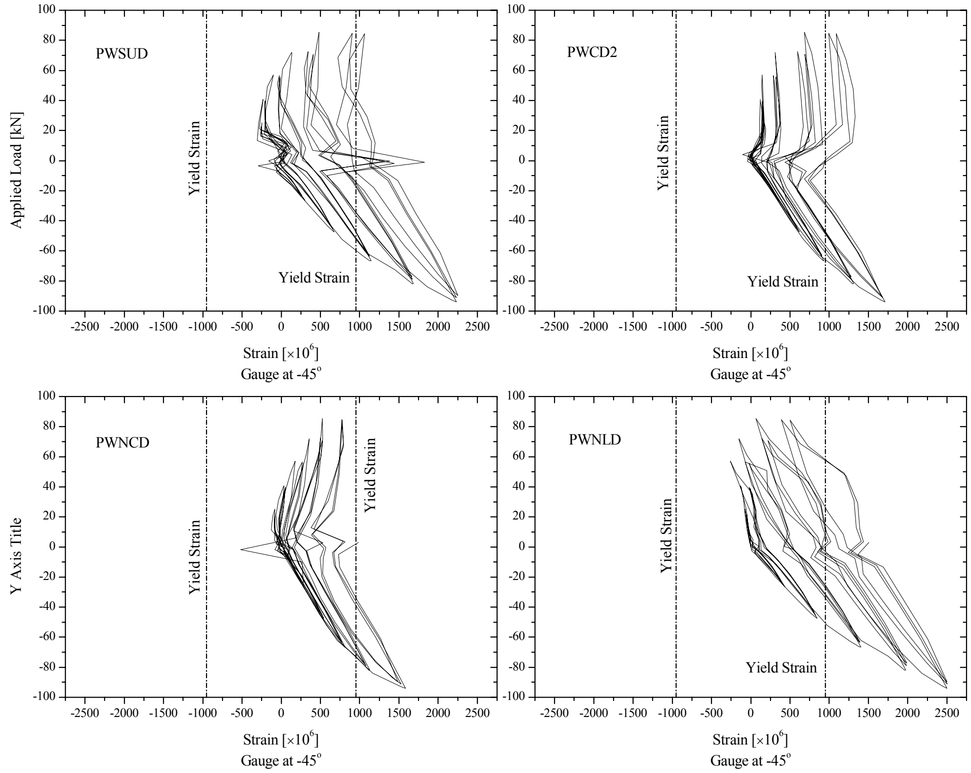

Figure 8.14: Variation of Strain across West Face of Infill Panel at -45° (SW-A-H)

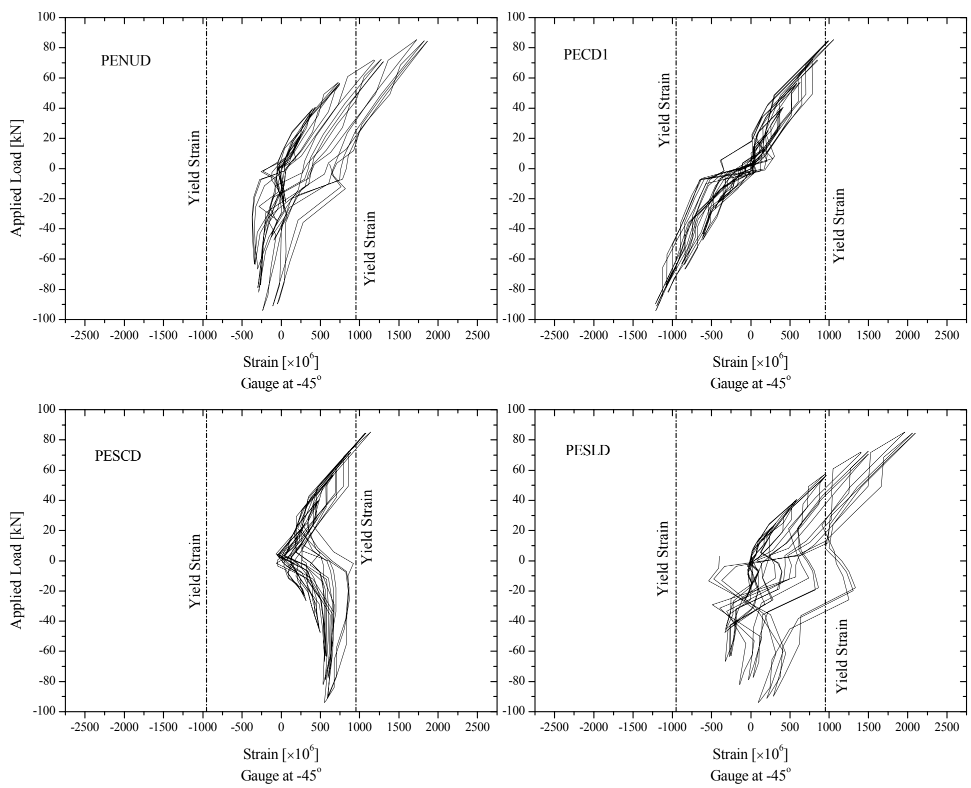

Figure 8.15: Variation of Strain across East Face of Infill Panel at -45° (SW-A-H)

In orientation of the gauges, the angle measured from the horizontal to gauge is positive if the turning direction is clockwise, otherwise it is negative.

Figures 8.15 and 8.16 also show the gauges, orientated at -45° and +45°, respectively, affixed to the east side of the infill panel. The data in these graphics are from the strain gauges shown in Figure 4.27. The infill has also a very important role in energy dissipation as can be noted from Figures 8.15 and 8.16. According to Figure 8.16, it is also evident that the measurements of strain from PESUD and PENLD have certainly uniformity. Moreover, the same situation is also valid between PECD2 and PENCD.

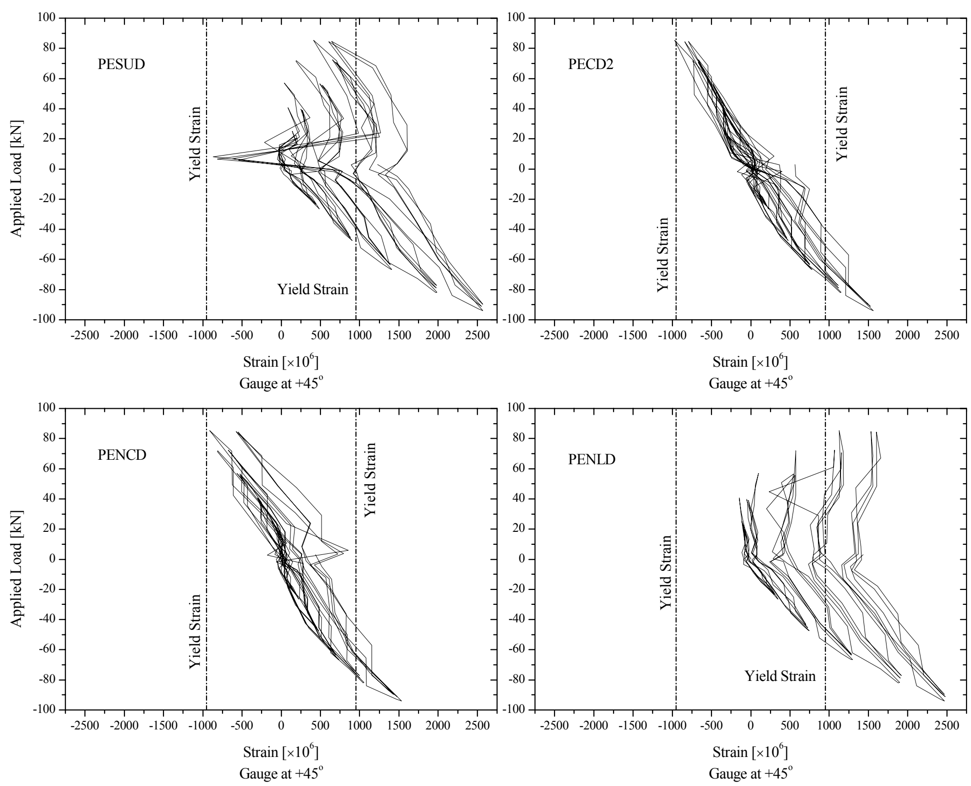

Figure 8.16: Variation of Strain across East Face of Infill Panel at +45° (SW-A-H)

The gauges used in Figures 8.13 and 8.15 are oriented to record tension strain when the specimen is loaded toward the positive direction (north) and the gauges considered in Figures 8.14 and 8.16 are oriented to do the same when the specimen is loaded toward the negative direction (south).

8.2.1 Comparison of the test and numerical analyses results

Figure 8.17 shows the cyclic response for specimen SW-A-H, superimposed with the pushover curves of SW-A-H from preliminary numerical model with a series of strip and finite element model.

As can be seen from the Figure 8.17, the ultimate load is reasonably predicted by the finite element model whereas it is underestimated by the strip model. Additionally, both finite element and strip model over-predicted the initial stiffness of the specimen. This is mostly attributed to the assumptions made in determining the moment-rotation curve of the beam-to-column joint. Additionally, bearing of the thin panel in front of the screws is not included in the TSPSW models. Therefore, the contribution of the bearing deformation to the elongation of the tension fields, on the other hand, to overall lateral displacement of TSPSW models is neglected.

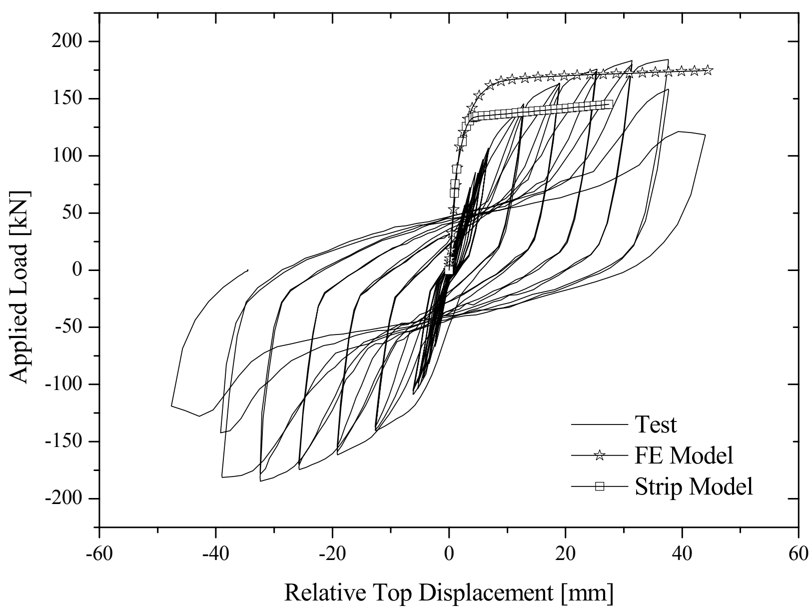

Figure 8.17: Comparison between Experimental and Numerical Results (SW-A-H)

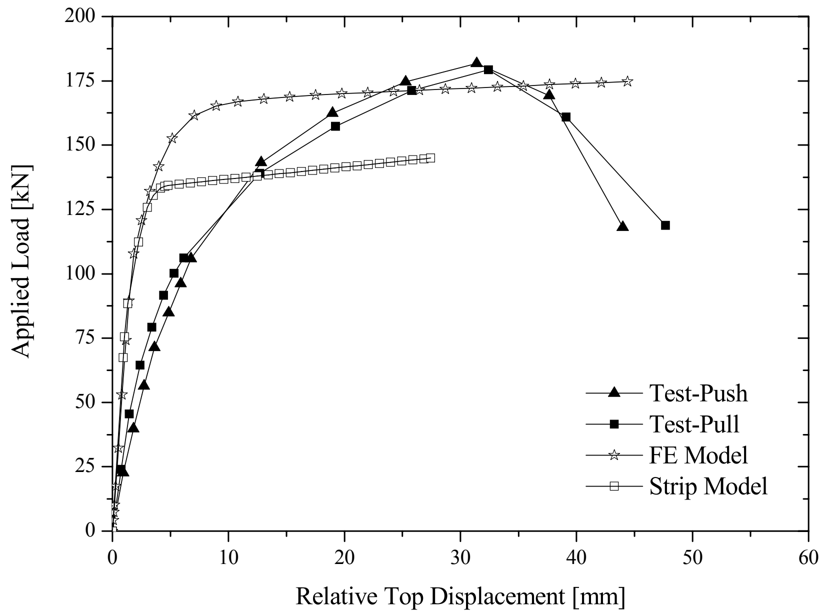

Figure 8.18: Comparison of Hysteresis Envelopes and Numerical Results (SW-A-H)

Load-displacement envelope curves of the specimen for both pushing and pulling direction with the pushover curves that superimposed are also shown in Figure 8.18.

As the Figure 8.18 is examined, the rapid post-ultimate strength degradation exhibited by the test specimen is not seen in the numerical results because plate tearing and local buckling observed near the end of the test were not included in the models.

Also, when compared the figures given in Section 7.2.2 with the Figure 8.19, which shows the deformed shape of the specimen SW-A-H near failure when subjected to monotonically increasing lateral displacements at the top, the deformed shapes obtained during testing are too difficult to depict by coarse finite element mesh used. More elements need to be used to represent these complex shapes. For clarity, the deformations in the figure are magnified three times.

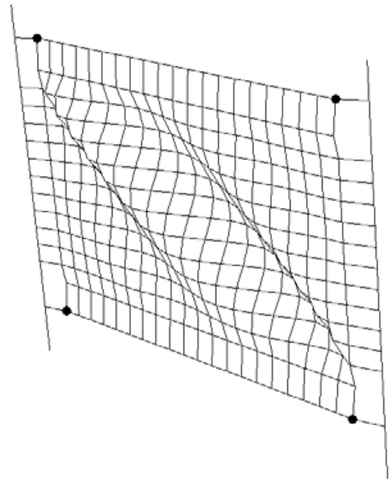

Figure 8.19: Deflected Shape of Finite Element Model (SW-A-H)

8.3 Specimen SW-B-H

Figure 8.20 shows the hysteresis for specimen SW-B-H, together with the hysteresis of BF-H. Despite the significant pinching observed in the hysteretic loops, if a negative half cycle that could not be performed due to the concerns mentioned before is assumed to be similar to positive half cycle done, the cyclic behavior of specimen SW-B-H was found to be ductile and also stable up to large drift levels as in the specimen SW-A-H. As can be seen from the figure, the maximum force attained in the test of SW-B-H is approximately 1.4 times that of specimen BF-H. Moreover, the infill panel contribution to the energy dissipation capability of the system is found to be acceptable. But, when compared the participation of the infill plates of the shear wall specimens, the contribution of the infill connected to the boundary frame on all edges will generally be more than the other. This discrepancy will comparatively be discussed in Section 8.6.

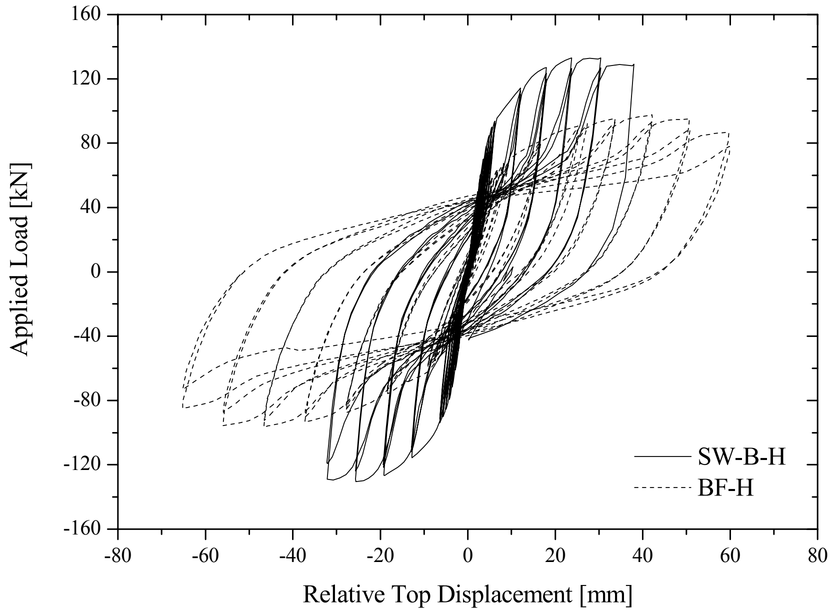

Figure 8.20: Comparison of Specimen SW-B-H and BF-H Hystereses

To examine the variation of the load capacity, the load-displacement envelopes of the specimen for pushing and pulling direction are plotted in Figure 8.21. The load and corresponding relative top displacements are calculated using the same method expressed in Section 8.2. Thus, all values computed are average of three values that were achieved at each displacement step. Table 8.8 gives the required forces in the pushing direction for the specimen at various drift levels in tabulated form. In this table, for comparison purpose, linear interpolation is again utilized in computing the required loads at the specified drift levels.

Table 8.8: Required Load at Each Drift Level in Pushing Direction (SW-B-H)

Drift [%]	Required Load [kN]
0.25	61.88
0.50	91.29
0.75	101.85
1.00	112.04
1.25	117.84
1.50	123.45
2.00	129.84

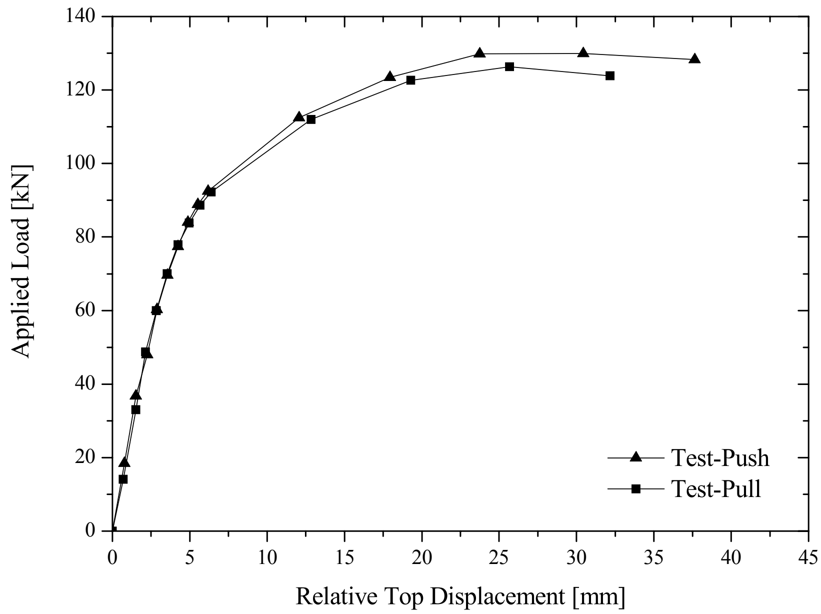

Figure 8.21: Envelopes of Specimen in Pushing and Pulling Direction (SW-B-H)

The variation of the initial stiffness with each displacement level is tabulated in Table 8.9 for pushing direction. In calculating the initial stiffness, polynomial curve fit through the appropriate data set is again used. Initial half cycle at each displacement step is also considered in this computation.

Table 8.9: The Variation of Initial Stiffness in Pushing Direction (SW-B-H)

Cycles	Δ/δ_y	Initial Stiffness [kN/mm]	Cycles	Δ/δ_y	Initial Stiffness [kN/mm]
1	0.13	19.643	22	0.89	7.173
4	0.25	17.436	25	1	6.767
7	0.37	16.713	28	2	5.887
10	0.47	12.452	31	3	4.349
13	0.58	9.867	34	4	2.676
16	0.69	9.066	36	5	1.779
19	0.79	7.507			

The energy dissipated per cycle at each displacement level is also listed in Table 8.10. The energy dissipation is computed using each complete cycle at each displacement increment and is the area enclosed by the load-relative displacement curve. At the last displacement step, a half cycle was able to be performed to prevent the measurement devices from damage due to entirely failure of the infill plate. Cycle 38, therefore, consists of a half hysteresis loop in positive (pushing) direction.

Table 8.10: Energy Dissipation per Cycle (SW-B-H)

Cycles	Dissipated Energy [kN×mm]	Cycles	Dissipated Energy [kN×mm]
1	2.225	19	110.991
2	2.784	20	72.506
3	2.788	21	67.918
4	9.417	22	142.342
5	8.469	23	93.158
6	8.671	24	85.844
7	26.491	25	175.694
8	18.979	26	124.276
9	13.535	27	124.926
10	37.658	28	1393.982
11	18.128	29	841.722
12	19.942	30	757.513
13	58.948	31	2310.184
14	29.409	32	1792.312
15	29.142	33	1659.577
16	80.471	34	3324.733
17	46.453	35	2901.389
18	39.665	36	4574.481
		37	4078.233

The cumulative energy dissipation of the specimen versus the cumulative number of cycles curve is shown in Figure 8.22. The cumulative dissipated energy is calculated as expressed in Section 8.2.

Additionally, to show the change of energy dissipation with number of cycle Figure 8.23 is also given. As can be noted from the figure, energy dissipation is suddenly increased after Cycle 27, corresponding to $\pm 1\delta_y$ displacement step. Before this cycle, the amount of energy dissipated does not seem to be appreciable.

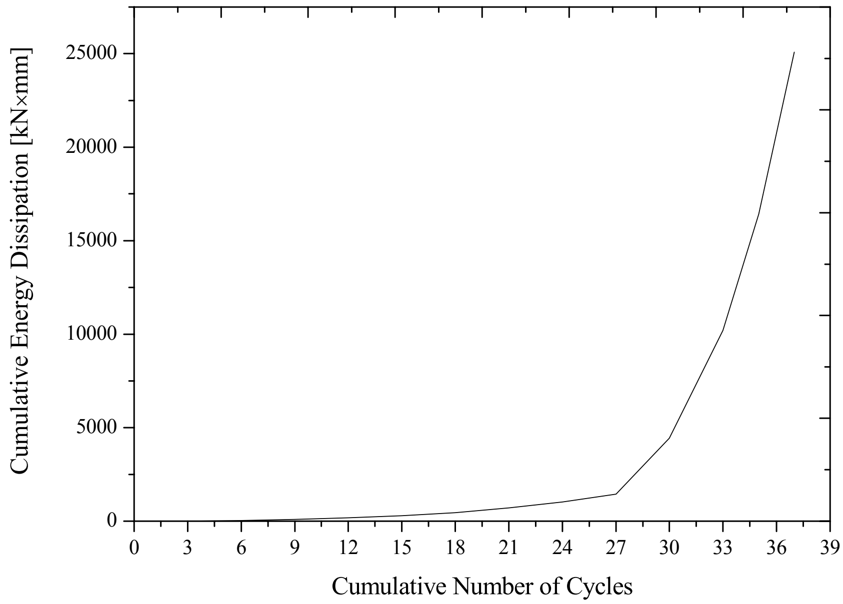

Figure 8.22: Cumulative Energy Dissipation (SW-H-B)

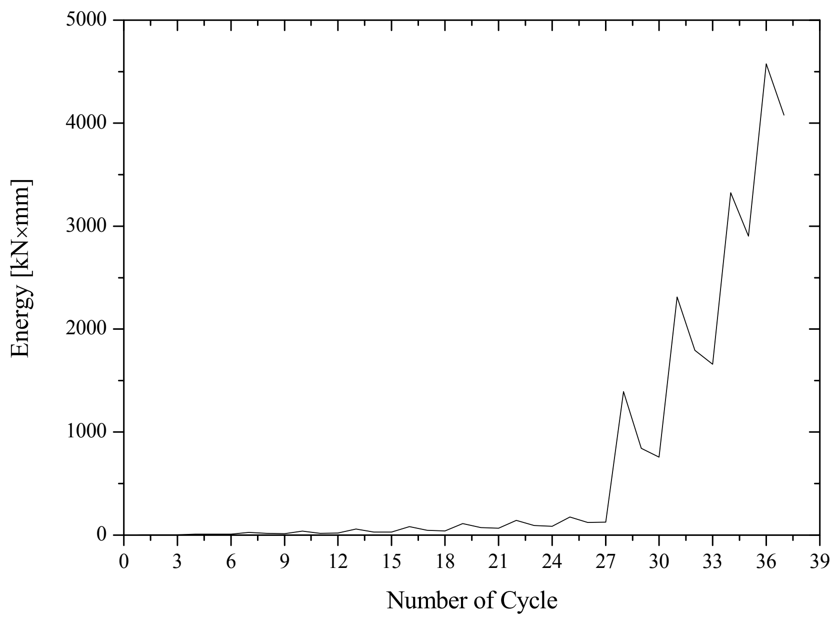

Figure 8.23: Energy Dissipation per Cycle (SW-B-H)

The magnitudes of the tensile principal strains and stresses, and their orientation with respect to vertical for three different levels are listed in Table 8.11, considering the strain gauges at the center cluster of the infill panel.

When the Table 8.11 is examined, the angles calculated from the strain gauges, PWCV, PWCD1 and PWCD2, at the center of the infill panel are generally between 41°and 53°. Also, that the initial predicted orientation of the principal stresses in the infill was 28° is not in agreement with the principal angles obtained from the strain measurements, which are from PWNCH, PWNCD and PWNCV on north and PWSCV, PWSCH and PWSCD on south sides from the infill center. In addition to this, the principal angles acquired using the strain from PWSCV, PWSCH and PWSCD are found to be different from the others. This is attributed to the possible error in affixing the gauges and the complex distribution of the strain over the infill due to the absence of the connections to the frame columns. The angles of 35° and 39° seem to be acceptable for the panel installed in this manner. All strain gauges that considered in this table were mounted on west face of the infill plate. In Table 8.11, the minus sign in front of the numbers that are included in column "Drift [%]" indicates the pulling direction.

Table 8.11: Principal Directions, Strains and Stresses (SW-B-H)

Strain gauges Considered	Drift [%]	α [°]	Principle Strain [mm/mm]	Principle Stress [MPa]
PWNCH PWNCD PWNCV	0.07	52	0.000209	31.79
	-0.06	-42	0.000160	24.15
	0.13	50	0.000455	76.91
	-0.14	-41	0.000382	54.73
	0.24	50	0.000747	131.63
	-0.24	-43	0.000574	84.84
PWCV PWCD1 PWCD2	0.07	45	0.000228	53.69
	-0.06	-53	0.000051	10.33
	0.13	53	0.000317	85.13
	-0.14	-41	0.000317	49.77
	0.24	46	0.000674	163.50
	-0.24	-43	0.000561	96.50
PWSCV PWSCH PWSCD	0.07	42	0.000241	46.73
	-0.06	-64 (min.) 26 (max.)	0.000113 0.000236	39.92 58.64
	0.13	42	0.000455	95.79
	-0.14	-35	0.000471	120.29
	0.24	41	0.000762	187.21
	-0.24	-39	0.000716	193.51

The orientation of the principal stresses at the center of the infill during elastic cycles is found to be slightly different than 45°. Furthermore, from the figures of Section 7.2.3, which show the buckling of the infill panel, it is visible from square grid on the infill that the buckling wave lines are forming at less than 45° from vertical at drifts larger than yield, which indicates that the tension field is actually forming at that angle.

Figure 8.24 and 8.25 show the variation in strain measurements across the infill plate of specimen SW-B-H to a drift of 0.41%, corresponding to 4.88mm relative displacement. The data in this plot is from the strain gauges shown in Figure 4.28, which are orientated at 45° from horizontal. As can be seen from the following figures, the strain measurements from PWNUD, in upper north corner, and PWSLD, in lower south corner, are reasonably uniform. Furthermore, it is also apparent that the strain near the corner reached the yield before the strain at the center of the infill attained the yield point as in the specimen SW-A-H. Therefore, it can be realized that the entire plate actively begins to dissipate energy from the corners of infill.

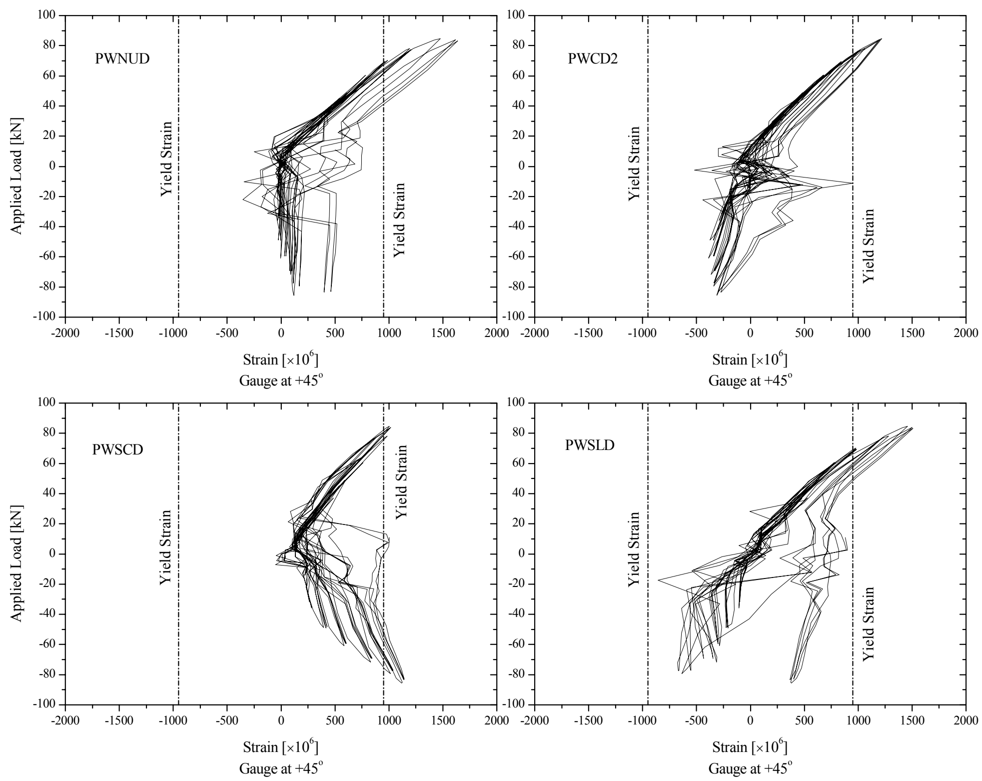

Figure 8.24: Variation of Strain across West Face of Infill Panel at +45° (SW-B-H)

Moreover, the strain measured in the same diagonal line such as the strain from PWSLD and PWSCD is not equal to each other. Therefore, the assumption reported by **Elgaaly and Liu (1997)** that the stress over the entire length of the tension field (or a strip) is equal to yield stress while the strain varies is again found to be acceptable for this type of TSPSW. All gauges in Figure 8.24 and 8.25 were bounded on the west side of the specimen.

As can be noted from Figure 8.24, it is shown that the strain across the infill reached the yield point. Hence, the infill entirely contributed to dissipating energy.

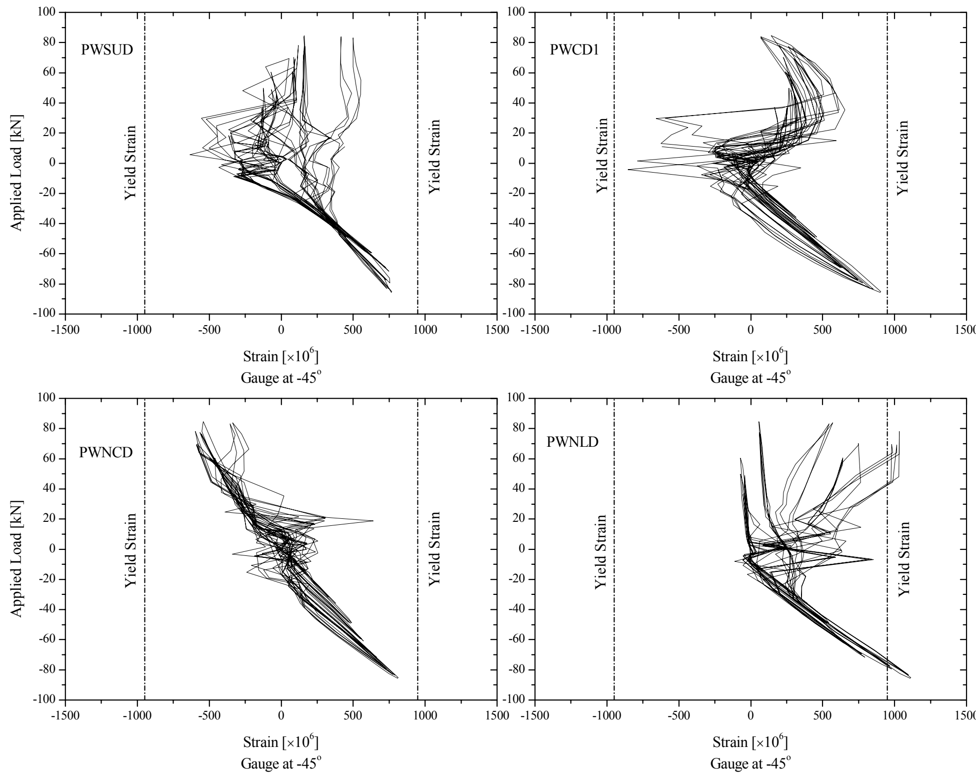

Figure 8.25: Variation of Strain across West Face of Infill Panel at -45° (SW-B-H)

Figures 8.26 and 8.27 also show the gauges, orientated at -45° and +45°, respectively, mounted on the east side of the infill panel. The data in these plots are from the strain gauges shown in Figure 4.29. In that step, it can be said that the infill has also an important role in energy dissipation. Nonetheless, as can be noted from Figures 8.26 and 8.27, it is shown that the yield strain is not reached. But, if it is thought that the principal angle of the stresses is less than 45°, the actual strain will somewhat be larger than yield. According to Figure 8.26, it is also evident that the measurements of strain from PENUD and PESLD have satisfactorily uniformity. However, the same situation is not also valid between PECD2 and PESCD.

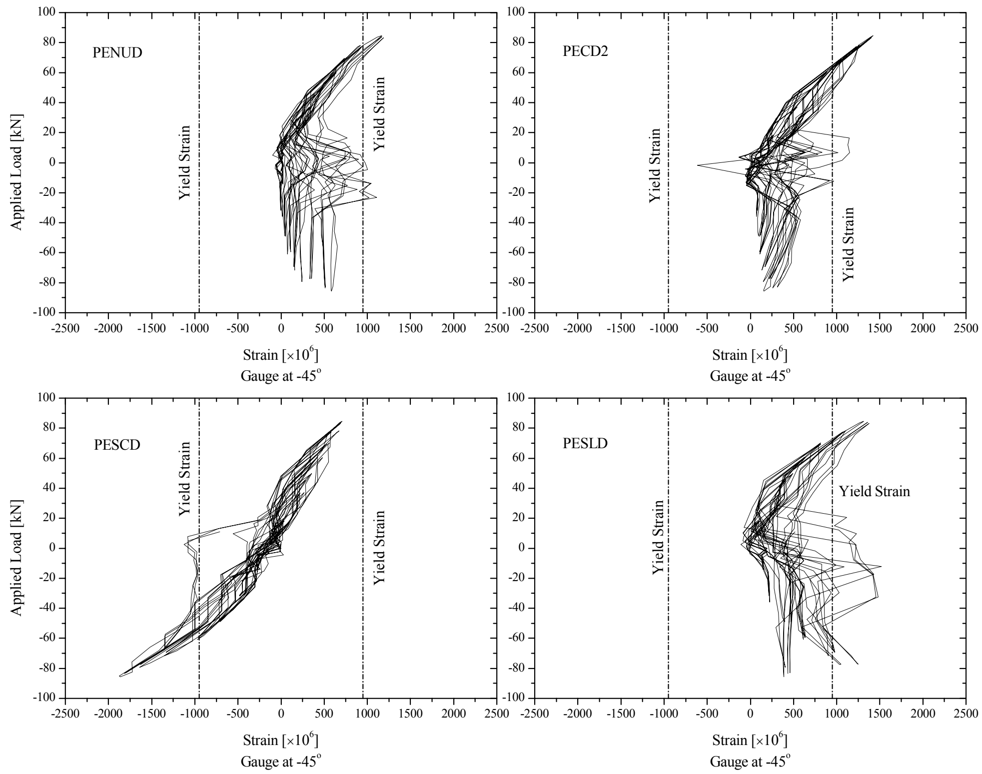

Figure 8.26: Variation of Strain across East Face of Infill Panel at -45° (SW-B-H)

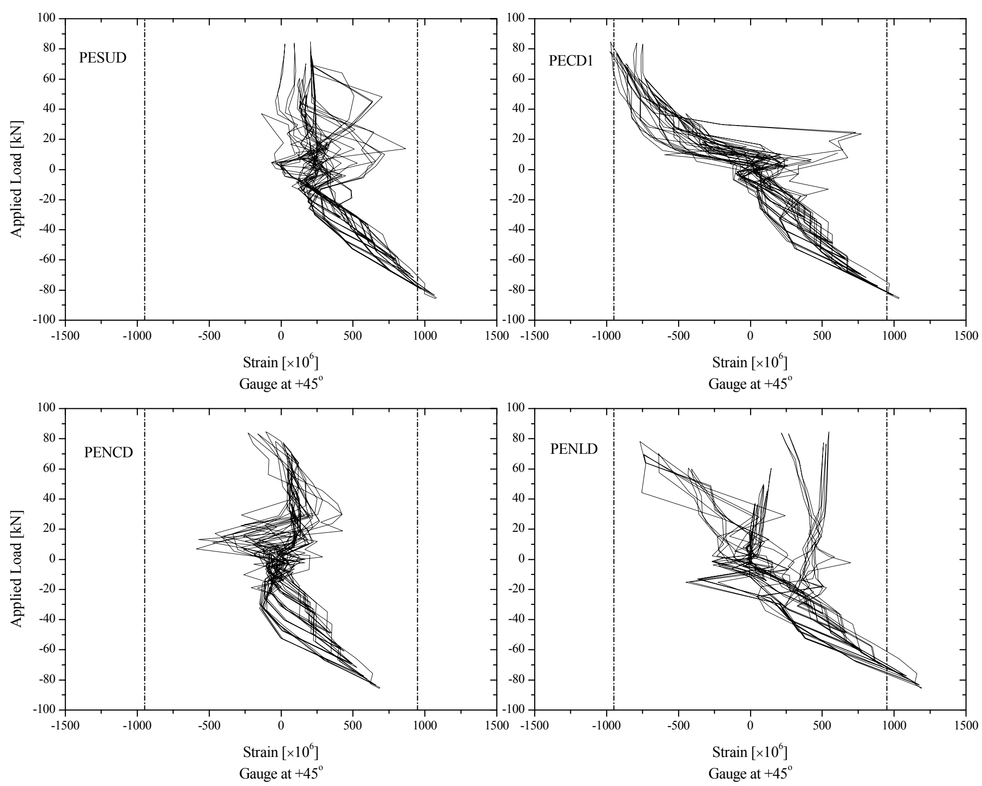

Figure 8.27: Variation of Strain across East Face of Infill Panel at +45° (SW-B-H)

8.3.1 Comparison of the test and numerical analyses results

The cyclic behavior of specimen SW-B-H is shown in Figure 8.28, superimposed with the pushover curves of SW-B-H from preliminary analytical model using a series of strip representing the infill panel and finite element models.

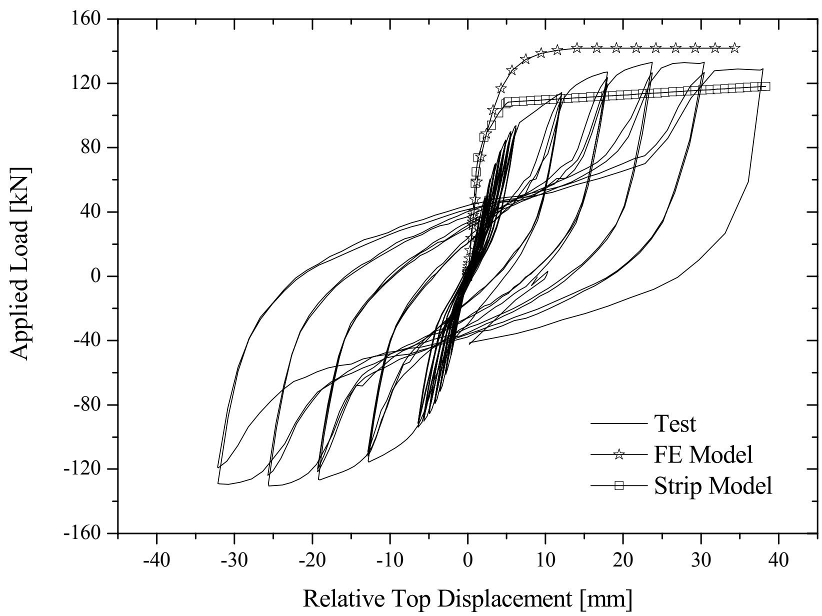

Figure 8.28: Comparison between Experimental and Numerical Results (SW-B-H)

As can be noted from above figure, the ultimate strength of the specimen from the finite element model is over-predicted by 6.6% whereas the strip model underestimated the ultimate strength by 10.6%. The initial stiffness of the specimen obtained from analytical model analyses is also overestimated. It is thought that the differences are induced by the assumptions made in determining the moment-rotation curve of the beam-to-column joint. Additionally, bearing of the infill panel in front of the screws is not included in the models. Due to very thin infill panel (0.50mm), bearing of the material in front the screws can occur at low load levels. Therefore, the panel-to-frame connection type affects the elastic stiffness, the initial yielding load and the stiffness after initial yielding. It can be noted that the bolted plate shear walls have smaller elastic stiffness and lower initial yielding load **(Elgaaly and Liu, 1997)**.

Load-displacement envelope curves of the specimen for both pushing and pulling direction with the pushover curves are also shown in Figure 8.29.

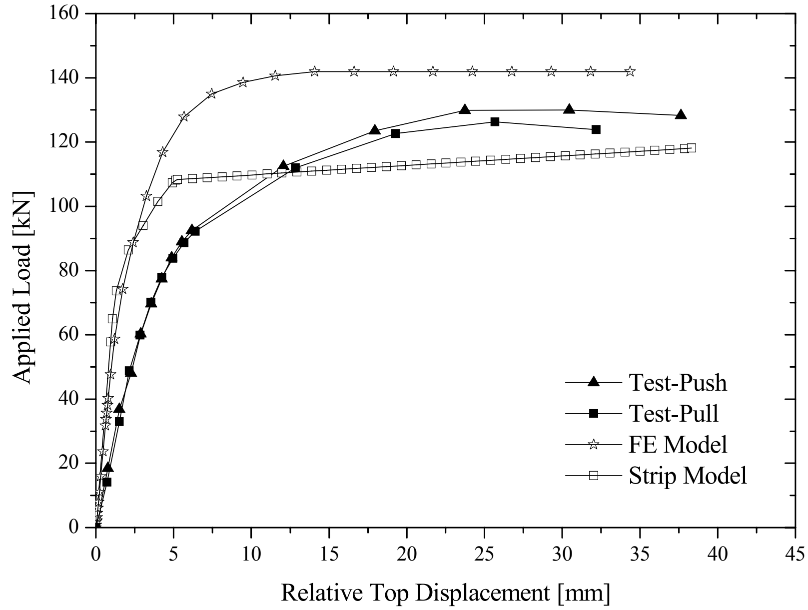

Figure 8.29: Comparison between Envelope of Cyclic Response and Numerical Results Curves (SW-B-H)

As the Figure 8.29 is examined, the rapid post-ultimate strength degradation exhibited by the test specimen is not observed compared to specimen SW-A-H. However, it should be aware that the last half cycle in negative direction was not performed.

Also, when compared the figures given in Section 7.2.3 with the Figure 8.30, which shows the deformed shape of the specimen SW-B-H near failure when subjected to monotonically increasing lateral displacements at the top, the deformed shapes obtained during testing are too difficult to depict by coarse finite element mesh used. More elements need to be used to represent these complex shapes. For clarity, the deformations in the figure are magnified three times.

When difficulties in obtaining convergence in the numerical analysis are encountered for n=1.5, an approximation of the ultimate strength is obtained even by taking n = 3.0. “n”, called a shape factor, is a parameter used for predicting the moment-rotation curve of beam-to-column connection.

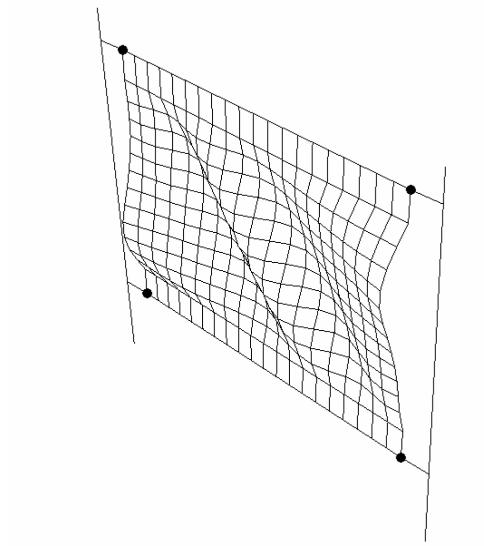

Figure 8.30: Deflected Shape of Finite Element Model (SW-B-H)

8.4 Proposed Improved Plate-Frame Interaction (IPFI) Method

The proposed model, shortly called IPFI, is fundamentally based on PFI (Plate-Frame Interaction Method) that was developed by **Sabouri-Ghomi et al. (2005)**. In this proposed method, the behavior of beam-to-column connections which are designed considering semi-rigid/partial strength joint approach is included. Eurocode3 is utilized in predicting the parameters such as initial rotational joint stiffness and bending moment resistance of the joint. The effect of the semi-rigid joint behavior is only accounted for obtaining the load versus top displacement curve of the bare frames.

In this proposed method, the load-displacement diagrams for the steel panel and for boundary frame can be obtained separately as given in **Sabouri-Ghomi et al. (2005)**. Then, by superimposing the two load-displacement diagrams that of the TSPSW system can be obtained. This expression is the principle of the proposed method. In the procedure of the improved method the specimen SW-B-H is firstly considered.

A typical shear load-displacement diagram of a steel panel of height h, width l, and thickness t is shown in Figure 8.31. In this figure, point A and point B correspond to the buckling limit and the yielding point of steel panel. Both points can be determined as given in the following.

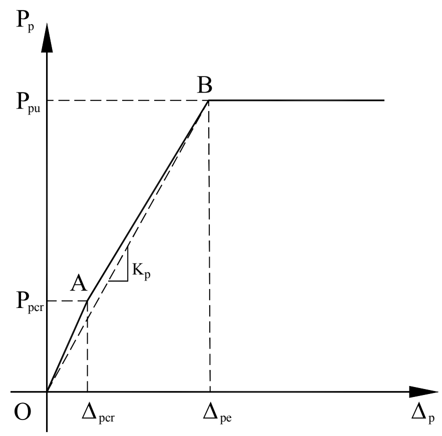

Figure 8.31: Shear Load-Displacement Curve of Infill Plate Only **(Sabouri-Ghomi et al., 2005)**

The critical shear force of the infill plate P_{pcr} is

$$P_{pcr} = \tau_{cr} \times l \times t \quad \textbf{(8.1)}$$

and critical shear displacement Δ_{pcr} is obtained from

$$\Delta_{pcr} = \frac{\tau_{cr}}{G} \times h \quad \textbf{(8.2)}$$

in which G: shear modulus of the infill plate material.

In the application of incomplete tension field theory to TSPSWs with the panel connected to beams only under the shear force, the distribution of the stresses in the panel can be categorized into three phases, namely, before, during and after buckling. The stress distributions corresponding to these stages are given in Figure 8.32. Mohr's circle that shows the stresses during the diagonal shear resistance is also drawn (Figure 8.32).

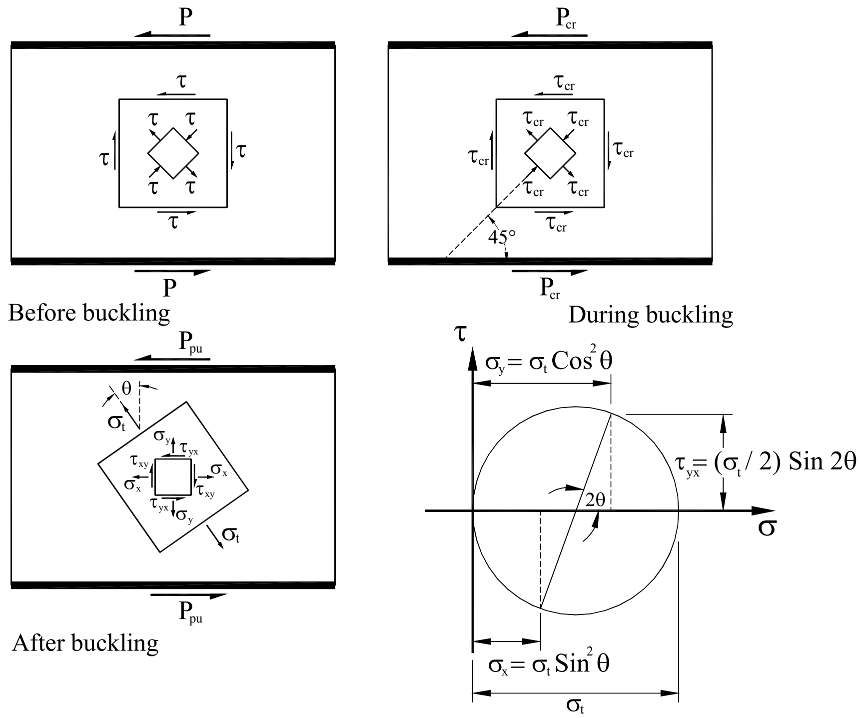

Figure 8.32: The Distribution of the Stresses in the Plate (adapted from **McGuire (1968)**)

As assumed, during the postbuckled stage, a tension field orientated at an angle θ with respect to the vertical gradually developes across the infill panel, as shown in Figure 8.33. This action is defined in **McGuire (1968)** as incomplete diagonal tension field.

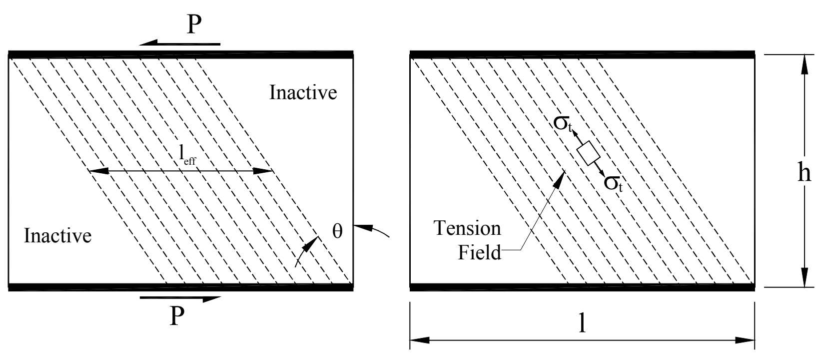

Figure 8.33: Incomplete Diagonal Tension Field (adapted from **McGuire (1968)**)

As a result, assuming the entire depth of the steel plate to be under uniform diagonal tension, this part of the resistance can be easily written as will be given soon. Before this, if σ_t denotes the value of the stress in the tension field at which yielding occurs, the total state of stress in the plate at yield, shown in Figure 8.33, is defined by

$$\sigma_x = \sigma_t \times \mathrm{Sin}^2\theta \tag{8.3}$$

$$\sigma_y = \sigma_t \times \mathrm{Cos}^2\theta \tag{8.4}$$

$$\tau_{xy} = \tau_{yx} = \tau_{cr} + \frac{1}{2} \times \sigma_t \times \mathrm{Sin}2\theta \tag{8.5}$$

By using Von Mises yield criterion, this stress distribution provides a lower bound for the strength of the web plate, provided that the beam members are strong enough to sustain the normal boundary forces associated with the tension field.

According to the Von Mises yield criterion, yielding of the plate occurs when

$$\left(\sigma_x - \sigma_y\right)^2 + \sigma_y^2 + \sigma_x^2 + 6 \times \tau_{xy}^2 - 2 \times \sigma^2 = 0 \tag{8.6}$$

Substituting Equations 8.3, 8.4 and 8.5 into 8.6 the value of σ_t at which yielding of the steel plate occurs is defined by

$$\sigma_t^2 + 3 \times \tau_{cr}^2 + 3 \times \tau_{cr} \times \sigma_t \times \mathrm{Sin}2\theta - \sigma^2 = 0 \tag{8.7}$$

The shear strength of the steel panel having incomplete diagonal tension field is now written by

$$P_{pu} = \tau_{xy} \times (l - h \times \tan\theta) \times t = \tau_{cr} \times l \times t + \frac{1}{2} \times \sigma_t \times \mathrm{Sin}2\theta \times (l - h \times \tan\theta) \times t \tag{8.8}$$

Also, substituting $l_{eff} = (l - h \times \tan\theta)$ into Equation 8.8, P_{pu} can be yield as (for the specimen SW-A-H, l_{eff} should be taken to be equal to l)

$$P_{pu} = \tau_{xy} \times l_{eff} \times t = \tau_{cr} \times l \times t + \frac{1}{2} \times \sigma_t \times \mathrm{Sin}2\theta \times l_{eff} \times t \tag{8.9}$$

The limiting elastic shear displacement Δ_{pe} is obtained by

$$\Delta_{pe} = \Delta_{pcr} + \Delta_{ppb} \tag{8.10}$$

Δ_{ppb} is determined by equating the work done by the postbuckled component of the shear forces to the strain energy of the incomplete tension field.

This leads to

$$\left(\frac{1}{4} \times \sigma_t \times \mathrm{Sin}2\theta\right) \times t \times (1 - h \times \tan\theta) \times \Delta_{ppb} = \frac{\sigma_t^2}{2 \times E} \times h \times t \times (1 - h \times \tan\theta) \tag{8.11}$$

thus,

$$\Delta_{ppb} = \frac{2 \times \sigma_t}{E \times \mathrm{Sin}2\theta} \times h \tag{8.12}$$

Substituting Δ_{ppb} from Equation 8.12 and Δ_{pcr} from Equation 8.2 in Equation 8.10 gives

$$\Delta_{pe} = \left(\frac{\tau_{cr}}{G} + \frac{2 \times \sigma_t}{E \times \mathrm{Sin}2\theta}\right) \times h \tag{8.13}$$

Having determined P_{pu} from Equation 8.8 and Δ_{pe} from Equation 8.13, point B is now defined in Figure 8.31.

In order to further simplify the calculations on the load-displacement diagram, a straight line can be used to connect the point O and point B. The slope of line OB in Figure 8.31, which is the stiffness of the steel plate, is given by

$$K_p = \frac{\left(\tau_{cr} \times 1 \times t + \frac{1}{2} \times \sigma_t \times \mathrm{Sin}2\theta \times (1 - h \times \tan\theta) \times t\right)}{\left(\frac{\tau_{cr}}{G} + \frac{2 \times \sigma_t}{E \times \mathrm{Sin}2\theta}\right) \times h} \tag{8.14}$$

As can be noted in Equation 8.13, the limiting elastic shear displacement Δ_{pe} is also independent of the panel width l, but dependent directly on the panel height h, as similar to complete tension field action **(Sabouri-Ghomi et al., 2005)**.

For one story ductile TSPSW, the idealization of bare frame deformed shape at yield is shown in Figure 8.34, the load-displacement diagram is shown in Figure 8.35. It is assumed that the beam-to-column connections are semi-rigid/partial strength and beams are subjected to double curvature bending with zero moment in the midspan section. If point C is determined in Figure 8.34, then the load-displacement diagram of the frame will be defined.

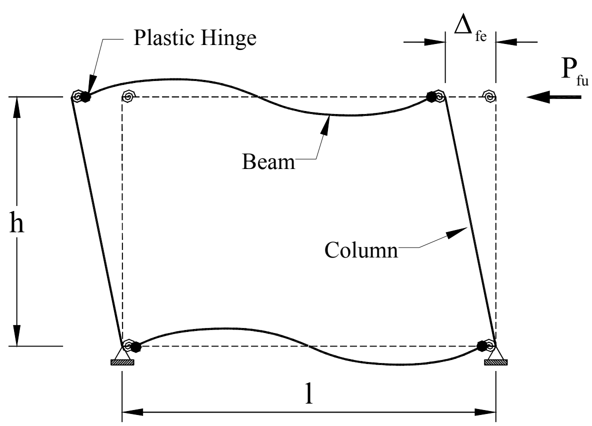

Figure 8.34: Bare Frame Idealization for IPFI Model

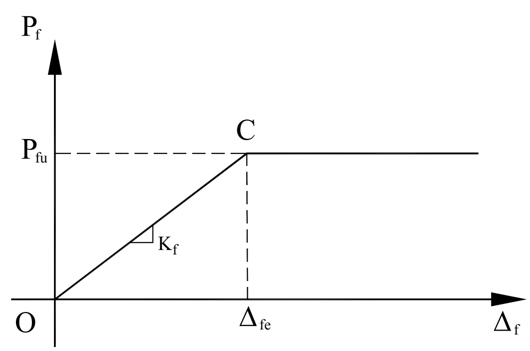

Figure 8.35: Load-Displacement Curve of Bare Frame

From Figure 8.34, the shear strength of the bare frame P_{fu} is

$$P_{fu} = \frac{4 \times M_{pcon}}{h} \tag{8.15}$$

The limiting elastic shear displacement of bare frame Δ_{fe} should be determined considering the semi-rigidity of the beam-to-column connections. As a result, Δ_{fe} can be given by (more details are available in Appendix C)

$$\Delta_{fe} = \left(\frac{M_{pcon} \times L \times h}{6 \times E \times I_b} \times \frac{\overline{K} \times (1 + \xi) + 12}{\overline{K}} \right) \tag{8.16}$$

in which

$$\overline{K} = \frac{K_{\varphi} \times l}{E \times I_b} \tag{8.17}$$

and

$$\xi = \frac{\dfrac{E \times I_b}{l}}{\dfrac{E \times I_c}{h}} \tag{8.18}$$

The slope of line OC in Figure 8.34, which is the stiffness of the frame, is

$$K_f = \frac{\dfrac{4 \times M_{pcon}}{h}}{\left(\dfrac{M_{pcon} \times l \times h}{6 \times E \times I_b} \times \dfrac{\overline{K} \times (1 + \xi) + 12}{\overline{K}} \right)} \tag{8.19}$$

To ensure that the plate dissipates more energy than the frame, it is suggested that the steel plate shear walls be designed in such a way that the following expression is satisfied **(Sabouri-Ghomi et al., 2005)**:

$$\Delta_{fe} > \Delta_{pe} \tag{8.20}$$

The load-displacement curve of the shear wall with semi-rigid beam-to-column joints can be obtained by superimposing the diagrams shown in Figure 8.31 and 8.35. Figure 8.36 shows the components of IPFI model load-displacement curve.

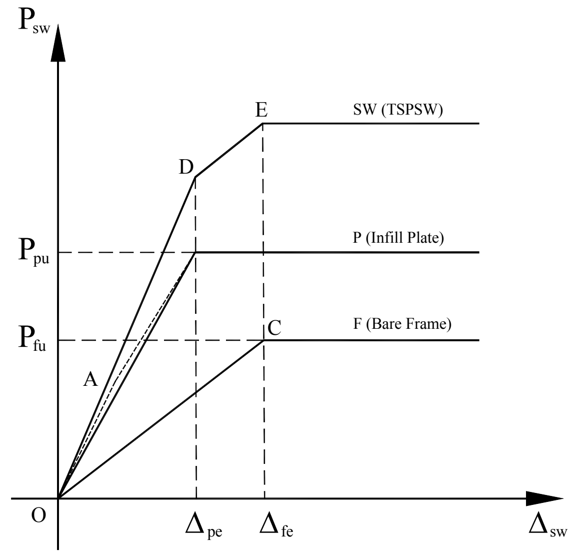

Figure 8.36: Load-Displacement Curves of the Components of a Shear Wall

8.4.1 Modification of shear load-displacement diagram of plate

In order to better represent the load-displacement behavior of the TSPSW systems and to account for the effect of the slippage and bearing deformations and stretching of the element shear load-displacement curve of the plate can be depicted by tri-linear curve approach instead of bilinear represention. Accordingly, the diagram given in Figure 8.31 is modified what is shown in Figure 8.37.

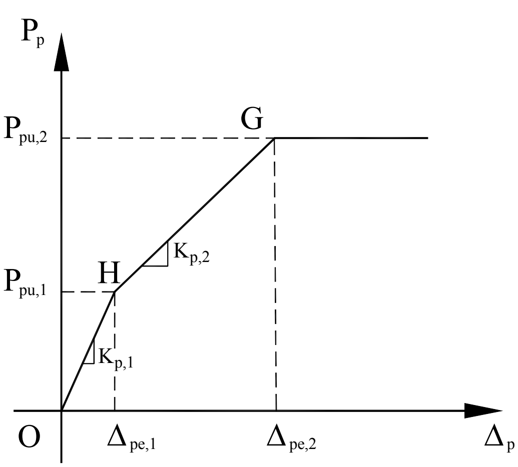

Figure 8.37: Proposed Shear Load-Displacement Curve of Infill Plate Only

For the purpose of this adaptation, two modification factors which are called C_1 and C_2 that will affect Δ_{pe} and P_{pu}, respectively are defined based on **Sabouri-Ghomi and Roberts (1991)** and **Sabouri-Ghomi et al. (2005)** and current test results that were obtained within this project. Initial yield displacement, $\Delta_{pe,1}$ and corresponding yield base shear, $P_{pu,1}$ can be calculated in the following;

$$\Delta_{pe,1} = \left(\frac{\tau_{cr}}{G} + \frac{2 \times \sigma_t}{E \times \mathrm{Sin}2\theta} \right) \times h \times C_1 \tag{8.21}$$

$$P_{pu,1} = \tau_{xy} \times l_{eff} \times t \times C_2 = \left(\tau_{cr} \times l \times t + \frac{1}{2} \times \sigma_t \times \mathrm{Sin}2\theta \times l_{eff} \times t \right) \times C_2 \tag{8.22}$$

The following values are suggested for these modifiers: $1.0 \le C_1 \le 2.0$ and $0.5 \le C_2 \le 1.0$. The researcher recognize that these values will need further refinement as more test results become available in the future. In general manner, these coefficients depend on the types of infill panel-to-boundary frame connection. This means that in case of welded plate shear walls C_1 and C_2 should be equal or close to 1.0 and in use of bolts or screws to connect the infill to the surrounding frame C_1 should be equal or close to 2.0 and C_2 should be selected as a value equal or close to 0.5.

Additionally, point G has to be defined to form the curve shown in Figure 8.37. For this purpose, based on the test results, it can be assumed that $\Delta_{pe,2}$ / $\Delta_{pe,1}$ is equal to 3.0~4.0. Thus, $\Delta_{pe,2}$ can be taken to be equal to $4 \times \Delta_{pe,1}$ for screwed (bolted) plate shear walls. The values close to 3.0 should be used for welded plate shear walls. Therefore, post-yield displacement $\Delta_{pe,2}$ and corresponding post-yield base shear $P_{pu,2}$ can easly be figured. In calculation of $P_{pu,2}$, it can be noted that full tension capacity of the plate should be taken into account. In this case, Figure 8.36 can be rearranged what is given in Figure 8.38. The value of 4.0 considered in proposed IPFI method leads to reasonable results as will be demonstrated in the following section. Initial stiffness ($K_{p,1}$) and reduced stiffness ($K_{p,2}$) can be written as given in the following equation.

$$K_{p,1} = \frac{P_{pu,1}}{\Delta_{pe,1}} \tag{8.23}$$

$$K_{p,2} = \frac{P_{pu,2} - P_{pu,1}}{\Delta_{pe,2} - \Delta_{pe,1}} \qquad \textbf{(8.24)}$$

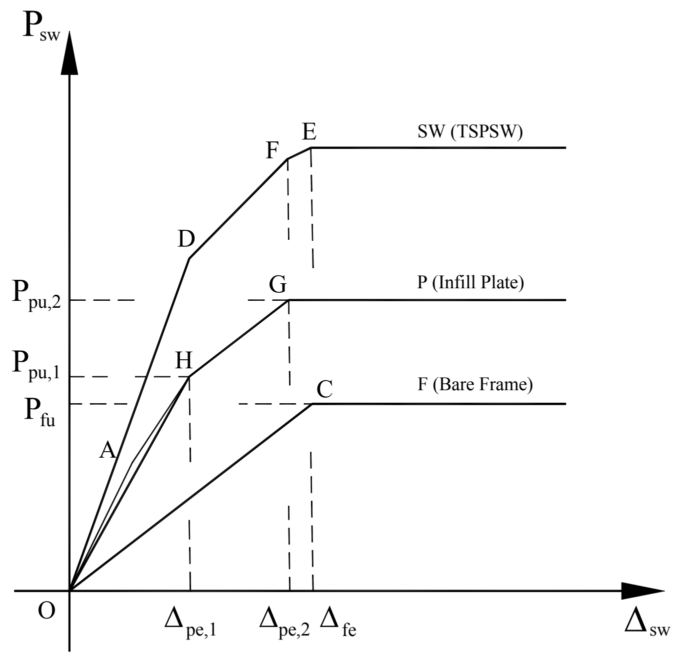

Figure 8.38: Load-Displacement Curves of the Components of a Shear Wall with Modified Infill Plate Contribution

8.4.2 Analytical studies on IPFI using test specimens

In this section, results from the implementation of the proposed IPFI method to the test specimens are compared with the corresponding test results in order to demonstrate the application and effectiveness of this method. As another analytical study, a value of R, response modification factor, is proposed based on the test results of SW-A-H and ATC-19 **(ATC-19, 1995)**. The detailed information about this is given in Appendix D.

This method can be implemented step by step as follows:

- use Equation 8.22 to calculate the initial shear strength of the steel panel in specimen SW-B-H due to incomplete diagonal tension field action assuming that θ = 35°, and assume that θ = 45° for the infill plate in specimen SW-A-H taking C_2 =0.8 for SW-B-H, C_2 =0.5 for SW-A-H and also τ_{cr} = 0.

- calculate the initial yield displacement, $\Delta_{pe,1}$ using Equation 8.21, assuming τ_{cr} be equal to zero because this value is not considerable for two types of the TSPSWs taking C_1 = 2.0 for both SW-B-H and SW-A-H.

- compute $\Delta_{pe,2}$ and $P_{pu,2}$ considering $\Delta_{pe,2}$ / $\Delta_{pe,1}$ = 4.0 and Equation 8.22 taking C_2 = 1.0 for both SW-B-H and SW-A-H under the assumption that full tension yield capacities of the plates are reached.

- to compute the shear strength of the bare frame, P_{fu}, use Equation 8.15, then

- the limiting elastic shear displacement of bare frame, Δ_{fe} can also be calculated utilizing Equation 8.16.

- as a result, draw the load-displacement curves of the components of the shear walls, bare frame and infill plate.

Two modification factors that affect the terms; Δ_{pe} and P_{pu} are included in order to acquire the trilinear approach that used for the new definition of the plate behavior. But, when this method is applied to the multi-story steel plate shear walls and also for better agreement between the results, it can be necessary to refine the modification factors for the terms in the equations as defined by **Sabouri-Ghomi et al. (2005)** to depict the real conditions of the TSPSW systems.

Thus, the load-deformation curve of a shear wall can easily be obtained by superposition of infill panel and bare frame load deformation diagrams, as shown in Figure 8.38.

Using implementation of IPFI method given above the load-displacement diagrams of the test specimens are obtained and shown in Figure 8.39~8.44.

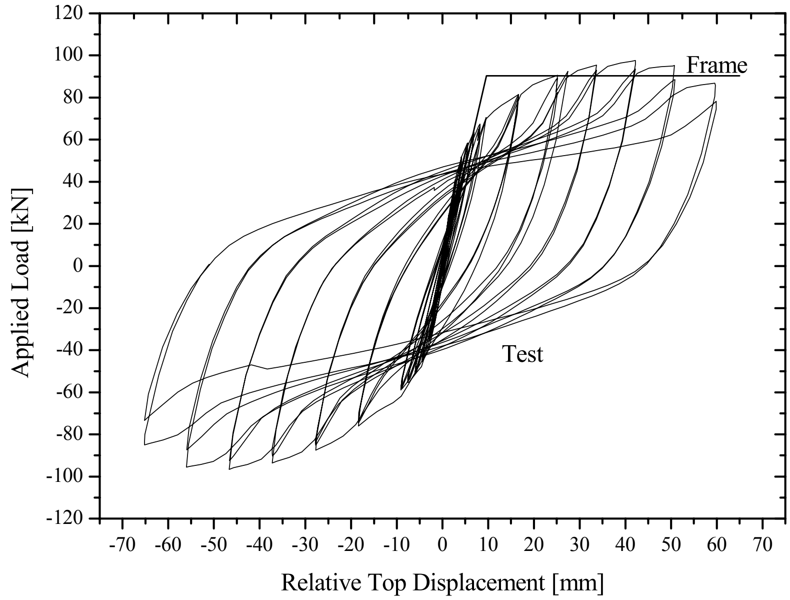

Figure 8.39: BF-H Hysteresis and Bare Frame Component of IPFI Model

As previously mentioned in Section 4.3.2.2, it should be remembered that the plastic moment capacity of the beam-to-column connections that were theoretically calculated in accordance with EC3 was increased by multiplying the value of 1.50. Thus, in calculating the the shear strength of the bare frame, P_{fu} the moment capacity value increased by 1.50 would be used.

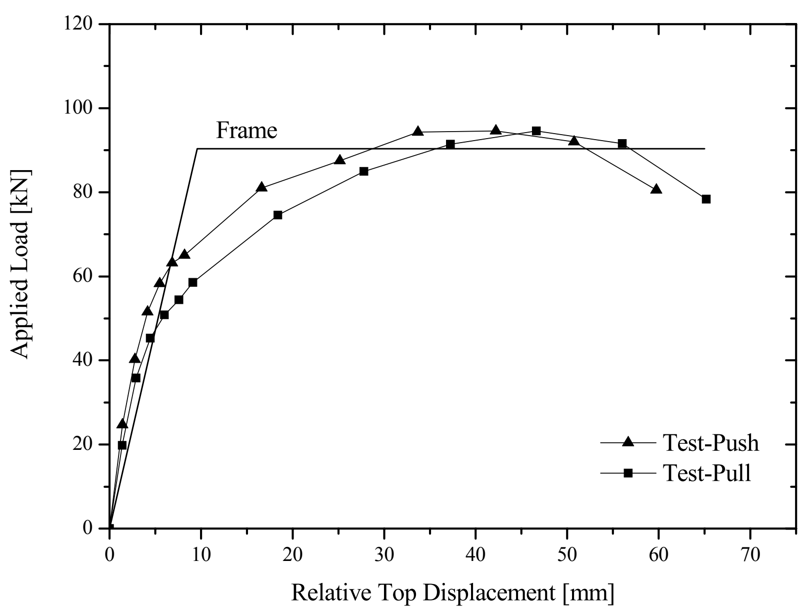

Figure 8.40: The Envelopes of BF-H Hysteresis and Bare Frame Component of IPFI Model

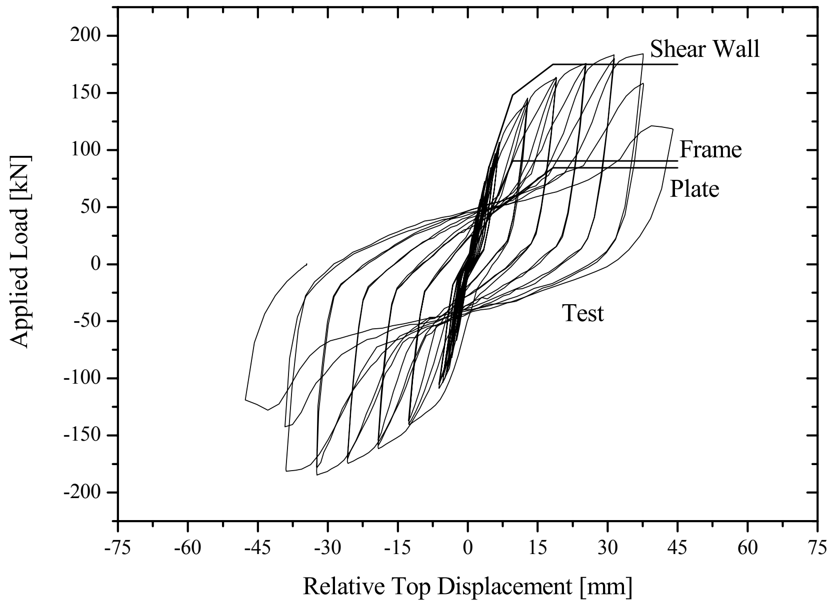

Figure 8.41: SW-A-H Hysteresis and Components of IPFI Model

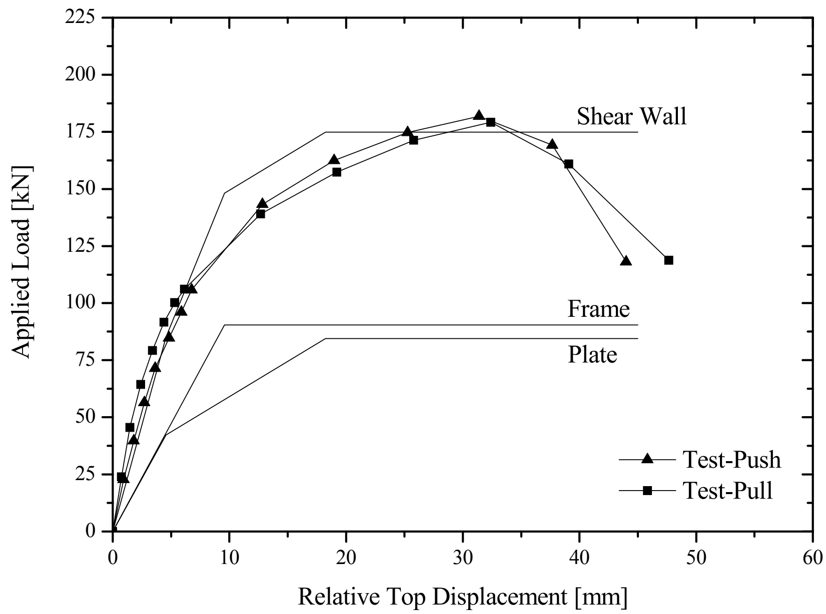

Figure 8.42: The Envelopes of SW-A-H Hysteresis and Components of IPFI Model

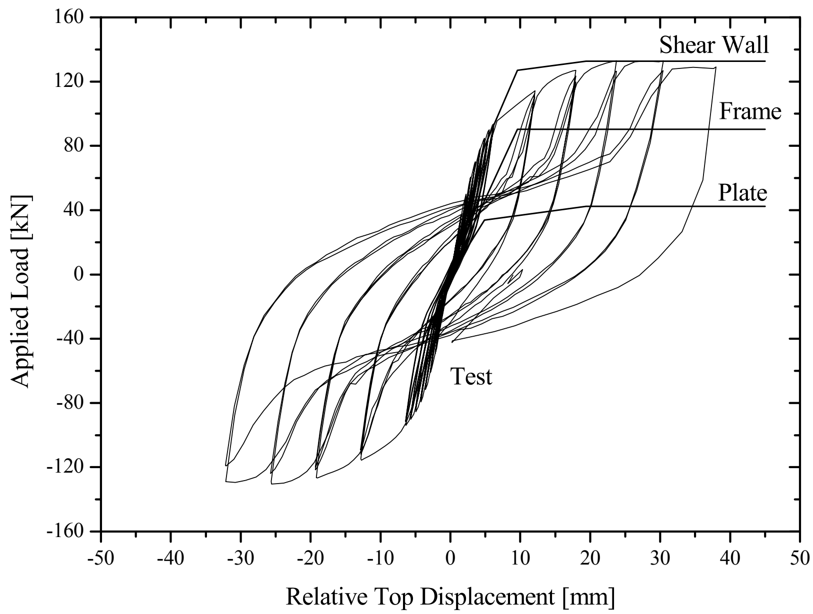

Figure 8.43: SW-B-H Hysteresis and Components of IPFI Model

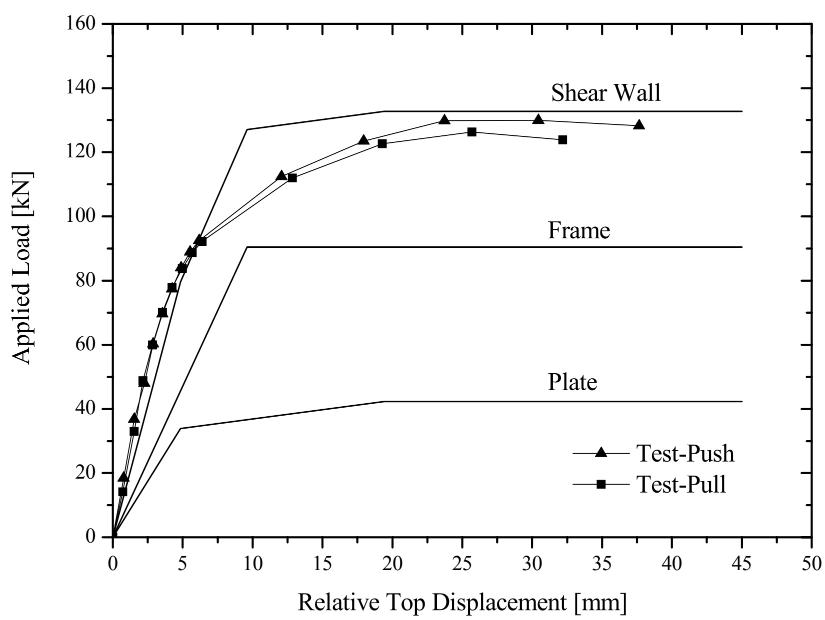

Figure 8.44: The Envelopes of SW-B-H Hysteresis and Components of IPFI Model

As above figures are examined the proposed method IPFI is able to depict the test results to a good degree of accuracy. Therefore, the ultimate strengths, initial stiffnesses, the yield displacements and the yield strengths of the specimens are able to be reasonably predicted by this proposed method. Some differences are attributed to the assumptions made in the Section 8.5 about the bare frame behavior and the fact that the infill panel dimensions (its height and width) are determined considering the centerlines of the columns and beams. Therefore, height and width of the infill panel taken into account are larger than actual dimensions of the panel. Additionally, in this method, the bearing strength of the thin panel in front of the screws used for the connection between infill panel and fish plates is taken into account using two modification factors. Thus, the contribution of the bearing and slippage deformations of the plate and the screws at the connections to the overall displacement of the specimens are only considered within the recommended values of these modifiers.

Consequently, this simplified modification of the plate behavior provides the structural designers with flexibility to predict the characteristics of TSPSW systems with semi-rigid beam-to-column connections. A significant advantage of this method is to be suitable for incorporation in practical seismic design provisions.

8.5 General Comparison of the Results and Discussion

In this section, three specimens are compared to each other. The comparisons are based on the detailed analyses of these specimens which were presented in previous section. The evaluation focuses on load capacity, differences in stiffness between specimens, energy dissipation and failure modes. The amount of energy dissipation is an important consideration in seismic design.

First, the load capacities of the specimens by comparing the maximum load corresponding to the specified drift levels are discussed. For this purpose, using the load required by specimen BF-H at each specified drift level as the basis of comparison, the ratio of the required loads between specimen BF-H, and the other specimens are listed in Table 8.12.

Table 8.12: Ratio of Required Load at Various Drift Levels

Drift [%]	SW-A-H / BF-H	SW-B-H / BF-H
0.25	1.44	1.47
0.50	1.62	1.52
0.75	1.80	1.53
1.00	1.91	1.55
1.25	1.92	1.51
1.50	1.94	1.50
2.00	1.99	1.50

Additionally, to demonstrate the contribution of the infill panel to the ultimate capacity of the TSPSW specimens, the ultimate load capacity of three specimens is compared to each other. Table 8.13 shows the ultimate load capacity of all specimens and the ratio of the ultimate load capacities of the shear wall specimens to that of specimen BF-H. The maximum load values attained throught the tests are considered in Table 8.13.

Table 8.13: Ultimate Load Capacity

Specimen	Ultimate Load Capacity [kN]	Ratio Definition	Ratio
BF-H	95.60	BF-H / BF-H	1.00
SW-A-H	183.50	SW-A-H / BF-H	1.92
SW-B-H	133.10	SW-B-H / BF-H	1.39

The stiffness and its change are also evaluated. Comparison of the stiffness values of the specimens is made using the envelopes of the specimen hystereses in pushing and pulling direction. In the envelope curves to use for obtaining initial stiffness of the specimens, the first five points that consist of the values at the cycle 1, 4, 7 and 10 are considered. Then, based on the comparison between the stiffness of specimen BF-H and the other specimens, the contribution from infill panel and frame are differentiated. The ratio of the initial stiffness of the shear wall specimens to that of specimen BF-H is tabulated in Table 8.14 and 8.15. Initial stiffness is also computed utilizing a polynomial curve fit.

Table 8.14: The Ratio of Initial Stiffness of the Specimens in Pushing

Specimen	Total Initial Stiffness [kN/mm]	Ratio Definition	Ratio
BF-H	17.818	BF-H / BF-H	1.00
SW-A-H	25.190	SW-A-H / BF-H	1.41
SW-B-H	26.838	SW-B-H / BF-H	1.51

Table 8.15: The Ratio of Initial Stiffness of the Specimens in Pulling

Specimen	Total Initial Stiffness [kN/mm]	Ratio Definition	Ratio
BF-H	15.532	BF-H / BF-H	1.00
SW-A-H	30.797	SW-A-H / BF-H	1.98
SW-B-H	22.746	SW-B-H / BF-H	1.46

As can be noted from the above tables, there is a considerable difference between the total initial stiffness of SW-A-H in pushing direction and that of SW-A-H in pulling direction. It is thougth that this difference is due to the out-of-plane deformation configuration of the infill panel. In pushing direction, the contribution of the infill panel is 41% in specimen SW-A-H whereas it is 51% in specimen SW-B-H. However, when Table 8.15 is examined, the initial stiffness of SW-A-H is approximately two times the initial stiffness of BF-H while SW-B-H's initial stiffness is about one and half times the BF-H's initial stiffness.

Energy dissipation, which is equal to the area enclosed by the load-displacement loops, is directly calculated from the load-displacement hysteresis curves. The cumulative dissipated energy and energy dissipation per cycle of each specimen is compared. For this purpose, the cumulative energy dissipation of the specimens is plotted versus the drift in Figure 8.43. Also, Figure 8.44 shows the energy dissipation per cycle of each specimen.

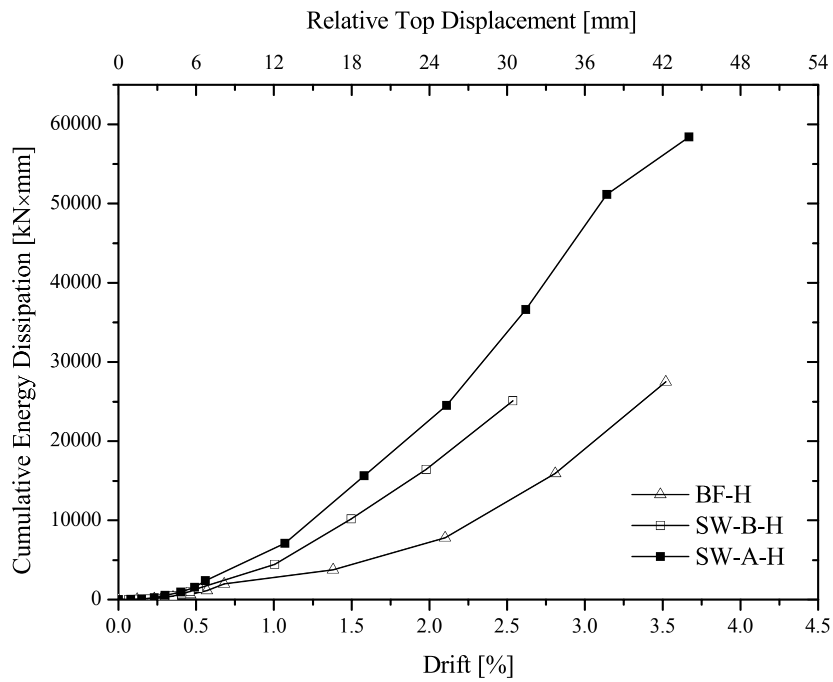

Figure 8.45: The Comparison of Cumulative Energy Dissipation

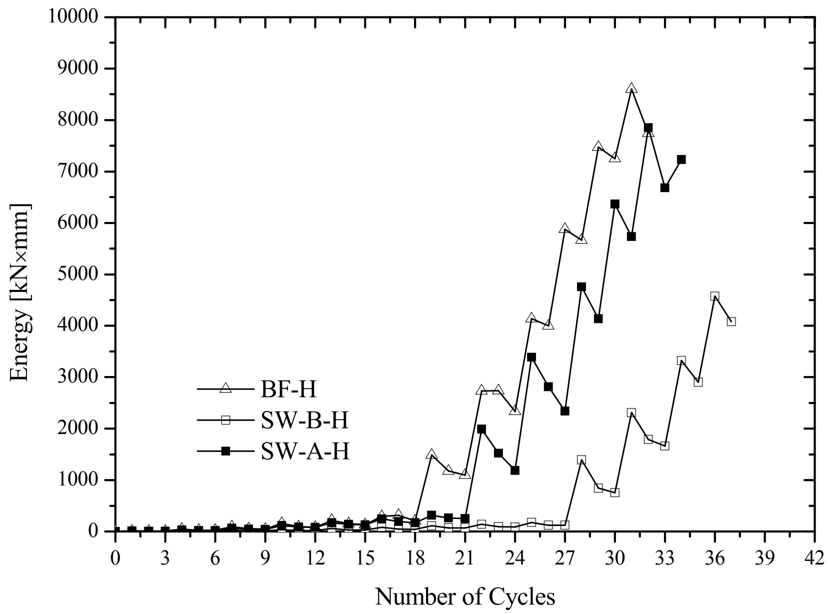

Figure 8.46: The Comparison of Energy Dissipation per Cycle

Because the displacement values at each step in deformation histories of the specimens are different from each other, the energy dissipation curves are plotted versus the drift ratio. It can be noted that since the amount of dissipated energy is very much loading path dependent and the specimens have different maximum drift at each displacement increment, the direct comparison of energy dissipation at the same condition can not be made. So, this comparison is made in graphical manner.

8.6 Summary

This research conducted consisted of four main components; design of test setup members and test specimens, numerical investigation of the specimens and finite element study, a physical testing programme and analytical study based on proposed methods.

Three specimens with single storey and bay, which included two TSPSWs (SW-A-H and SW-B-H) and a bare frame (BF-H) with semi-rigid beam-to-column connections were tested under a squence of loading intended to simulate a severe seismic event. Gravity loads were not applied to the columns. The cyclic deflection amplitudes were gradually increased according to the recommendations outlined in ATC-24 until significant degradation of the specimens was evident.

Prior to conducting the cyclic test of the specimens some ancillary tests included a series of material tests on the infill panels and beam end plates and self drilling screw connection tests that consist of five specimens were performed. In addition to this, a numerical study on simplified models, so-called strip models, of the test specimens was carried out.

For the specimens, three finite element models to use quadratic beam elements to represent the beams and columns and quadratic shell elements to model the infill panels were developed. An estimate of the initial out-of-flatness of the panels was also included. Material and geometric nonlinearities were taken into account in the models.

Additionally, the existing simplified method, panel-frame interaction method, which is originated by **Sabouri-Ghomi et al. (2005)** was improved considering the effect of the semi-rigid beam-to-column connection behavior and incomplete tension field action.

After the quasi-static tests and analytical investigations, the results from both the tests and numerical studies were assessed and comparatively discussed.

9. CONCLUSIONS AND RECOMMENDATIONS

In this thesis, four specimens in total, two frames without infill plates and two TSPSWs, were tested under cyclic loading in accordance with ATC-24. Additionally, the numerical method to predict the behavior of steel shear walls, which was originated by **Sabouri-Ghomi et al. (2002),** was improved considering the moment-rotation response of beam-to-column joints.

By evaluating the test results, examining and comparing the load capacity, stiffness, energy dissipation capacity, the findings and important points are given in the following section after a short summary of the study

9.1 Summary

The experimental research reported herein describes four cyclic tests that include 1/3 scale test specimens. Two specimens are thin steel plate shear walls and the rest are steel frames without infill panel. All specimens were tested under cyclic loading based on ATC-24 procedure. The main objective of the test was to compare the innovative TSPSW system which means the system with the infill plate connected to beams only to traditional one indicating the system with steel plate attached to the boundary frame on all edges.

The originality of this study is firstly to perform a cyclic test using steel shear wall specimen with 0.50mm thick infill plate attached to the surrounding frame on top and bottom edges only. With this experimental study, the performance of infill panel-to-boundary frame connection provided by self drilling screw under reversed load was also investigated.

Additionally, a theoretical investigation was carried out to acceptably predict the behavior of steel shear walls. For this purpose, the plate-frame interaction model that was originated by **Sabouri-Ghomi et al. (2002)** was considered and this method was improved taking the beam-to-column connections behavior into account based on the design concept of the semi-rigid joints. The findings from the tests, therotical and numerical investigations are summarized and the outcomes obtained from the research are presented below.

9.2 Conclusions

The analysis of SAP2000 model overestimates the initial stiffness of BF-H by 174%. However, the ultimate strength of the frame is under-predicted by 35%. This difference can be attributed to the following causes. The moment-rotation relationship for beam-to-column connections can not be not exactly defined in the model. Hence, the nonlinear behavior of the joints was described using appropriate plastic hinge definition, M3 in the joints. Also, the assumptions made in determining the moment-rotation curve for the semi-rigid beam-to-column joint with header end plate affect the behavior of the frame. The contribution of the bearing deformation at the infill panel-to-fish plates is not included in defining axial plastic hinges for the strips.

The finite element analysis utilizing ABAQUS over-predicts the initial stiffness of the specimen BF-H by 7.4% and gives a good prediction of its ultimate strength. The difference between the load-displacement curve from the numerical analysis and envelope curves from the test is due to moment-rotation model which were selected to represent the nonlinear behavior of the semi-rigid beam-to-column connection. The shape factor, n used in the formulation for the connection model especially has an effect on determining the path of the moment-rotation curve of the connection. As can be seen from Figure 8.8, if n is taken to be 1.5 instead of 3.0, the finite element model achieves good agreement with the cyclic test results.

The strip models that were developed for the preliminary numerical analyses of the shear wall specimens generally provided valuable information regarding the behavior of the shear wall systems. But, initial stiffness and yield base shear were overestimated by the strip model analyses. However, yield displacement values of the shear wall specimens were under-predicted by these simplified model analyses.

While the finite element models over-predict the initial stiffnesses of the shear wall specimens, the ultimate strength of the specimen SW-A-H is predicted well. However, the ultimate strength of the specimen SW-B-H is overestimated by 6.6%.

The differences between the analytical and the test results are attributed to the definition of the beam-to-column joints behavior in SAP2000 and the assumptions about prediction of the moment-rotation relationship for the beam-to-column connection type. As for the infill plate, the influence of the net sections on the edges of the infill plate is not included in the strip and finite element models. Therefore, the type of failure by tearing of the plate in the net section, which was encountered in the shear wall tests as well, is not considered. Additionally, the models do not cover the bearing effect of the infill plate material in the holes.

As indicated in **Elgaaly and Liu, (1995)**, the behavior of thin steel plate shear walls is governed by the tension field action and controlled by the boundary conditions. In this experimental research infill panel-to-boundary frame connection was provided by self drilling screws. Therefore, a screwed shear wall can have lower stiffness and initial yielding can occur at a lower load due to slippage and local deformations at the connections. Because the boundary condition at the panel-to-surrounding frame connection was not taken into account in the finite element models the initial stiffness, yield strength and corresponding displacement were over-predicted. Also, no failure caused by shearing of the screw occurred during the tests.

The moment capacity of the beam-to-column joint was obtained as 28.37kNm when the test results of specimen BF-H were evaluated. This value is about 1.5 times that value initially computed in accordance with EC3. Additionally, the initial assumption that the moment capacity was increased by multiplying 1.5 to account for a possible overstrength can be found appropriate.

An improved simple numerical model, IPFI method to account for the semi-rigidity of the beam-to-column joints, has been introduced and it has been demonstrated that the method is able to properly predict the behavior of the TSPSWs with semi-rigid beam-to-column connections. But, the plastic moment and stiffness of the beam-to-column joints should be obtained by using experimental methods or should be calculated in more detail. Additionally, the amplification factor can need to be used to account for the possible overstrength for the beam-to-column connections that form the frame. The value of 1.50 is used as the amplification factor in this research. However, within the research conducted, as such a value is not considered in the numerical analyses the ultimate strengths of the TSPSWs can be computed conservatively. In order to account for stretching, bearing and slippage deformations of the plate at the infill plate-to-boundary frame connections to better predict the behavior of the TSPSWs with semi-rigid partial strength beam-to-column connections some coefficients for the terms; Δ_{pe} and P_{pu} are used. However, the suggested modification factors of the improved method need further investigation for other types of plate configurations.

Also, to predict the cyclic behavior of a steel plate shear wall with semi-rigid beam-to-column connections, a hysteresis model that is given in detail in Appendix E was developed and gave a good prediction of the amount of energy dissipated.

When the maximum loads corresponding to the specified drift levels are compared the required loads at drift level of 1.0% for SW-A-H and SW-B-H are 1.91 and 1.55 times that for BF-H, respectively. Hence, the contribution of the infill plate to the ultimate shear strength of the frame is found to be considerable.

The initial stiffness of the specimen SW-A-H is approximately two times that of the BF-H when the envelope of the hysteresis loops in pulling direction is taken into account. The same value is 1.41 times the initial stiffness of the BF-H in pushing direction. As for the specimen SW-B-H, the initial stiffness is 1.50 times that of BF-H in both directions.

All specimens dissipate energy at nearly the same rate until 6.0mm which is relative top displacement (0.5% drift). After this point, energy dissipation of BF-H increases slightly as yielding progresses to other regions of the beam end plates. At 2.5% drift level, the energy dissipation of SW-A-H is approximately 2.8 times that of BF-H; similarly, the energy dissipated by SW-B-H is about 2.0 times that of BF-H.

If a steel building will be strengthen using shear wall systems, TSPSW system including the infill panels attached to the beams only can be used. Therefore, the premature failure due to buckling or yielding of the columns is prevented before the infill plate reachs its full capacity by yielding of the diagonal tension field. However, the base shear capacity of such shear wall systems is smaller than the traditional ones because of partial tension field action. But, the shear capacity as well as initial stiffness can be improved by using thicker infill panel provided that panel-to-boundary frame connection is designed in such a way the panel develops its full capacity by yielding of the diagonal tension field.

The use of thin steel plate shear walls to resist seismic forces is possible. Addition of a thin steel panel to a steel frame gives the system a substantial increase in stiffness, lateral load carrying capacity and energy absorption. The experimental results are shown that the entire infill panel of the shear wall specimen SW-A-H participated in dissipating energy. However, as expected initially, the contribution of the infill panel of the specimen SW-B-H to the dissipating energy is found to be acceptable. The TSPSW specimens utilizing flat infill panels and screwed connections to the surrounding frame were reasonably ductile and failures were the result of fractures (tears) in the net sections. Despite these fractures in the net sections which were occurred due to the presence of the screw holes, which appeared first at $-5\delta_y$ in the specimen SW-A-H, and at $4\delta_y$ in the specimen SW-B-H, the specimens did not suffer a significant loss of strength until 6 times the yield displacement. But, at the displacement level of $7\delta_y$, the shear force of SW-A-H was suddenly dropped by 34%.

9.3 Recommendations

The effect of the axial compression in the columns due to gravity loads in TSPSW systems where the infill panel is attached to the beams only should be investigated. In this experimental research, there were no axial compressive loads acting on the columns.

Test of specimens having infill panel attached to the beams only with stiffened openings should be performed. The effect of the variation of the stiffeners on the behavior of such shear walls should also be investigated.

The scaling effect should be studied. In this study, a 1/3 scaled frames were used for all specimens. This scale factor was applied to the storey height and bay only. The columns and beams were proportioned so as to remain elastic under the maximum possible loading. Additionally, in determining the infill panel thicknesses the actuator capacity became dominant rather than scale factor.

The infill panel-to-framing member connection is the most critical for the thin steel plate shear walls and should be investigated. In this research work, self drilling scews were utilized to provide the connection between panel-to-boundary frames. This type of connection may be economical, but not be practical because of application of a several number of screws.

To be able to accurately predict the behavior of the TSPSWs, nonlinear finite element models should be improved. For this purpose, ABAQUS/Explicit analysis technique can be utilized instead of ABAQUS/Standard using the elements supported by this technique.

REFERENCES

ABAQUS 6.4 Student Version, 2004. Hibbit, Karlsson, and Sorenson, Inc., Pawtucket, R.I.

Abbott, B. J. and Richard, R. M., 1975. Versatile elastic-plastic stress-strain formula, *Journal of Engineering Mechanics Division,* **101,** 511-515.

Agelidis, N. and Mansell, D. S., 1982. Seismic steel plate cores in tall buildings, *Civil Engineering Transactions of the Institution of Engineers,* Australia, CE24(1), 11-18.

Alinia, M. M. and Dastfan, M., 2006. Behavior of thin steel plate shear walls regarding frame members, *Journal of Constructional Steel Research,* **62,** 730-738.

Alinia, M. M. and Dastfan, M., 2007. Cyclic behavior, deformability and rigidity of stiffened steel shear walls, *Journal of Constructional Steel Research,* **63,** 554-563.

Astaneh-Asl, A., 2001. Seismic behavior and design of steel shear walls, Steel TIPS, University of California, Berkeley, California.

ATC-19, 1995. Structural response modification factors, *Applied Technology Council,* California.

ATC-24, 1992. Guidelines for cyclic seismic testing of components of steel structures, *Applied Technology Council,* California.

Basler, K., 1961. Strength of plate girders in shear, *Journal of the Structural Division,* **87,** ST7, 2967.

Berman, J. and Bruneau, M., 2003. Plastic analysis and design of steel plate shear walls, *Journal of Structural Engineering,* **129,** 1448-1456.

Berman, J. and Bruneau, M., 2004a. Plastic design and testing of light-gauge steel plate shear walls, *13th World Conference on Earthquake Engineering,* Vancouver, B.C. Canada**,** August 1-6.

Berman, J. and Bruneau, M., 2004b. Steel plate shear walls are not plate girders, *Engineering Journal,* Third Quarter**,** 95-106.

Berman, J. and Bruneau, M., 2005. Experimental investigation of light-gauge steel plate shear walls, *Journal of Structural Engineering,* **131,** 259-267.

Berman, J., Celik, O. C. and Bruneau, M., 2005. Comparing hysteretic behavior of light-gauge steel plate shear walls and braced frames, *Engineering Structures,* **27,** 475-485.

Bruneau, M. and Bhagwagar, T., 2002. Seismic retrofit of flexible steel frames using thin infill panels, *Engineering Structures,* **24,** 443-453.

Caccese, V., Elgaaly, M. and Chen, R., 1993. Experimental study of thin steel-plate shear walls under cyclic loading, *Journal of Structural Engineering,* **119,** 0573-0587.

Chen S. J. and Jhang C., 2006. Cyclic behavior of low yield point steel shear walls, *Thin Walled Structures,* **44,** 730-738.

Crisfield, M.A., 1981. A fast incremental/iterative solution procedure that handles snap-through, *Computer and Structures*, **13**, 55-62.

Dafalias, Y. F. and Popov E. P., 1976. Plastic internal variables formalism of cyclic plasticity, *Journal of Applied Mechanics,* **43,** 645-651.

Driver R., 1997. Seismic behavior of steel plate shear walls, *PhD Thesis*, University of Alberta, Edmonton, Canada.

Driver, R. G., Kulak, G. L., Elwi, A. E. and Kennedy, D. J. L., 1998a. FE and simplified models of steel plate shear wall, *Journal of Structural Engineering,* **124,** 0121-0130.

Driver, R. G., Kulak, G. L., Kennedy, D. J. L. and Elwi, A. E., 1998b. Cyclic test of four-story steel plate shear wall, *Journal of Structural Engineering,* **124,** 0112-0120.

Elgaaly, M. and Liu, Y., 1997. Analysis of thin-steel-plate shear walls, *Journal of Structural Engineering,* **123,** 1487-1496.

Elgaaly, M., 1998. Thin steel plate shear walls behavior and analysis, *Thin Walled Structures,* **32,** 151-180.

Elgaaly, M., 2000. Post-buckling behavior of thin steel plates using computational models, *Advances in Engineering Software,* **31,** 511-517.

Elgaaly, M., Caccese, V. and Du, C., 1993. Post-buckling behavior of steel-plate shear walls under cyclic loads, *Journal of Structural. Engeering*, **119,** 588-605.

Faella C., Piluso V. and Rizzano G., 2000. Structural Steel Semirigid Connections Theory, Design and Software, CRC Press LLC, Florida.

Goldberg, J. E. and Richard, R. M., 1963. Analysis of nonlinear structures, *Journal of Structural Division,* **89,** ST4.

Hitaka, T. and Matsui, C., 2003. Experimental study on steel shear wall with slits, *Journal of Structural Engineering,* **129,** 586-595.

Kraus, K., 1993. Photogrammetry, Fundamentals and Standard Processes, WB-Druck, 8959 Rieden, Germany.

Kuhn, P., Peterson, J. P. and Levin, L. R., 1952. A summary of diagonal tension, part I – methods of analysis, *Technical Note,* **2662,** National Advisory Committee for Aeronautics.

Liang, Q. Q., Uy, B., Wright, H. D. and Bradford, M. A., 2004. Local buckling of steel plates in double skin composite panels under biaxial compression and shear, *Journal of Constructional Steel Research,* **62,** 730-738.

Lubell, A. S., Prion, H. G. L., Ventura, C. E. and Rezai, M., 2000. Unstiffened steel plate shear wall performance under cyclic loading, *Journal of Structural Engineering,* **126,** 0453-0460.

McGuire, W., 1968. Structural Analysis and Design Series-Steel Structures, Prentice-Hall, Inc., Englewood Cliffs, N. J.

Mimura, H. and Akiyama, H., 1977. Load-deflection relationship of earthquake resistant steel shear walls with a developed diagonal tension field, *Trans., Arch. Inst. Of Japan,* Tokyo, Japan, 109-114 (in Japanese).

Moncarz, P. D. and Gerstle, K. H., 1981. Steel frames with nonlinear connections, *Journal of Structural Division,* **107,** 1427-1441.

Nakashima, M., 1995. Strain-hardening behavior of shear panels made of low yield steel I: Test, *Journal of Structural Engineering,* **121,** 1742-1749.

Nakashima, M., Iwai, S., Iwata, M., Takeuchi, T., Konomi, S., Akazawa, T. and Saburi, K., 1994. Energy dissipation behavior of shear panels made of low yield steel, *Earthquake Engineering and Structural Dynamics,* **23,** 1299-1313.

Powell, G. and Simpson J., 1981. Improved iterative strategy for nonlinear structures, *International Journal for Numerical Methods in Engineering*, **17**, 1455-1467.

Ramberg, W. and Osgood, W. R., 1943. Description of stress-strain curves by three parameters, *Technical Report,* **902,** National Advisory Committee for Aeronautics, Washington, DC.

Ramm, E., 1981. Strategies for tracing the nonlinear response near limit points, in *Nonlinear Finite Element Analysis in Structural Mechanics,* pp.68-89, Springer, New York.

Rezai M., 1999. Seismic behavior of steel plate shear walls by shake table testing, *PhD Thesis*, University of British Columbia, Vancouver, Canada.

Rezai, M., Ventura, C. E. and Prion, H. G. L., 2000. Numerical investigation of thin unstiffened steel plate shear walls, *Twelfth World Conference on Earthquake Engineering (12WCEE),* Auckland, New Zeland, January 30 – February 4.

Riks, E., 1979. An incremental approach to the solution of snapping and buckling problems, *International Journal of Solids and Structures*, **15**, 529-551.

Sabouri-Ghomi, S. and Roberts, T. M., 1991. Hysteretic characteristics of unstiffened plate shear panels, *Thin Walled Structures,* **12,** 145-162.

Sabouri-Ghomi, S. and Roberts, T. M., 1991. Nonlinear dynamic analysis of thin steel plate shear walls, *Computers & Structures,* **39,** 121-127.

Sabouri-Ghomi, S., Ventura, C. E. and Kharrazi, M. H. K., 2005. Shear analysis and design of ductile steel plate walls, *Journal of Structural Engineering,* **131,** 878-889.

SAP2000, Structural Analysis Program, Computers and Structures, Inc., Berkeley, California, USA.

SEAOC, 1999. Recommended lateral force requirements and commentary, *Structural Engineers Association of California*, Sacramento, CA.

Takahashi, Y., Takemoto, Y., Takeda, T. and Takagi, M., 1973. Experimental study on thin steel shear walls and particular bracings under alternative horizontal load, *IABSE Symposium, On Resistance and Ultimate Deformability of Structure Acted on by Well-Defined Repeated Loads,* Lisbon, Portugal, 185-191.

Thorburn, L. J. and Kulak, G. L., 1983. Analysis of steel plate shear walls, *Structural Engineering Report,* **107,** University of Alberta, Edmonton, Alta, Canada.

Timler, P. A. and Kulak, G. L., 1983. Experimental study of steel plate shear walls, *Structural Engineering Report,* **114,** University of Alberta, Edmonton, Alta, Canada.

Timler, P., Ventura, C. E., Prion, H. and Anjam, R., 1998. Experimental and analytical studies of steel plate shear walls as applied to the design of tall buildings, *The Structural Design of Tall Buildings,* **7,** 233-249.

Timoshenko, S. P., 1956. Strength of Materials; Part III, Advanced Theory and Problems, D. Van Nostrand Co., Princeton, New Jersey.

Tromposch, E. W. and Kulak, G. L., 1983. Cyclic and static behavior of thin panel steel plate shear walls, *Structural Engineering Report,* **145,** University of Alberta, Edmonton, Alta, Canada.

TS-138 EN 10002-1, 2004. Metallic materials-tensile testing-part 1: method of test at ambient temperature, *Turkish Standards Institute,* Ankara.

Vatansever, C. and Yardımcı, N., 2005. A numerical investigation of thin steel plate shear walls, *Steel Structures Symposium,* METU, Ankara, April 21-22, 113-125 (in Turkish).

Vatansever, C. and Yardımcı, N., 2007a. Analytical investigation of thin steel plate shear walls under lateral load, *2nd Steel Structures National Symposium,* Eskişehir, May 10-11, 17-27 (in Turkish).

Vatansever, C. and Yardımcı, N., 2007b. Numerical investigation of thin steel plate shear walls, *ECCOMAS Thematic Conference on Computational Methods in Structural Dynamics and Earthquake Engineering*, Rethymno, Crete, Greece, June 13–16.

Vatansever, C. and Yardımcı, N., 2007c. Analytical investigation of thin steel plate shear walls under monotonically increasing lateral loads, *Sixth National Conference on Earthquake Engineering,* Istanbul, October 16-20, 585-594 (in Turkish).

Vatansever, C., Yardımcı, N., Avşar Ö., Aydar U. and Şeker D. Z., 2007. The measurement of out-of-plane deformations of the infill panel in a steel plate shear wall by photogrametry, *The Union of Turkish National Photogrametry and Remote Sensing IV. Symposium*, İTÜ Ayazağa Campus, June 5-7 (in Turkish).

Vian, D., Lin, Y.-C., Bruneau, M. and Tsai, K.-C., 2003. Cyclic performance of low yield strength steel panel shear walls, *The Sixteenth KKCNN Symposium on Civil Engineering,* Korea**,** December 8-10, 2003.

Wagner, H., 1931. Flat sheet metal girders with very thin metal webs, part I – general theories and assumptions, *Technical Memorandum,* **604,** National Advisory Committee for Aeronautics.

Xue, M. and Lu, L.-W. 1994a. Interaction of infilled steel shear wall panels with surrounding frame members, *Proc. Struct. Stability Res. Council Annu. Tech. Session*, Bethlehem, Pa., 339-354.

Xue, M. and Lu, L.-W. 1994b. Monotonic and cyclic behavior of infilled steel shear panels, *Proc. 17th Czech and Slovak Int. Conf. on Steel Struct.and Bridges,* Bratislava, Slovakia.

Zhao, Q. and Astaneh-Asl, A., 2004. Cyclic behavior of traditional and innovative composite shear walls, *Journal of Structural Engineering,* **130,** 271-284.

APPENDIX A

The experimental testing and observations of the specimen BF-F is described in this section. Observations made regarding the performance of the specimen during testing will be given in the following sections.

A.1 Specimen BF-F

Specimen BF-F, shown in Figure A.1, is a moment-resisting frame with semi-rigid beam-to-column joints which is composed of flush end plates. All dimensions of the specimen are the same as the other test specimens.

Figure A.1: Specimen BF-F

The cyclic behavior of the specimen BF-F, shown in Figure A.2, is generally characterized by hysteresis loops that are pinched. When this response is compared with that of the specimen BF-H the hysteresis loops of BF-H are more open than those of BF-F. This can be attributed to large out-of-plane deformations of the top beam south end at the large load levels.

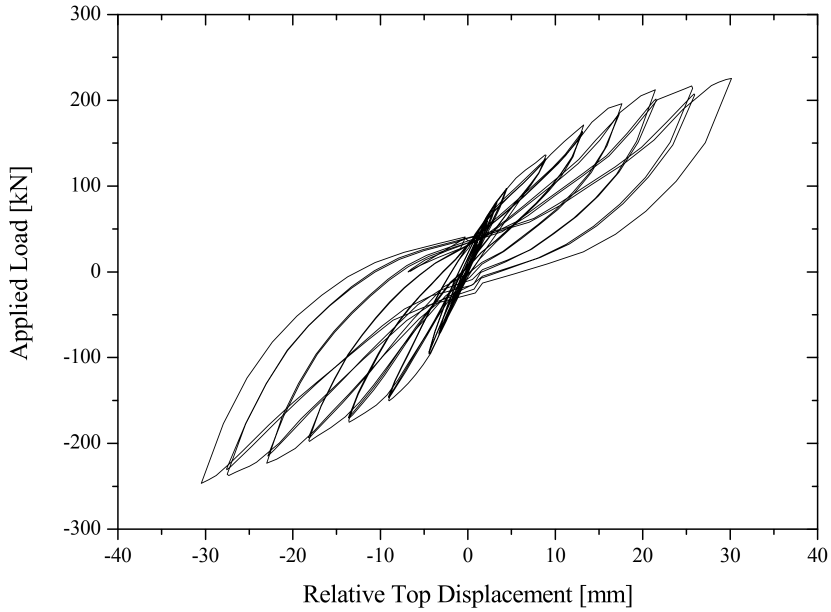

Figure A.2: Hysteresis Curves for BF-F

In order to show the load capacity, the load-deflection envelopes of the specimen for pushing and pulling direction are plotted in Figure A.3. As can be seen from the figure, applied load reached the actuator capacity value of 250kN in pulling direction. At this stage, test was stopped to prevent the loading system from any damage.

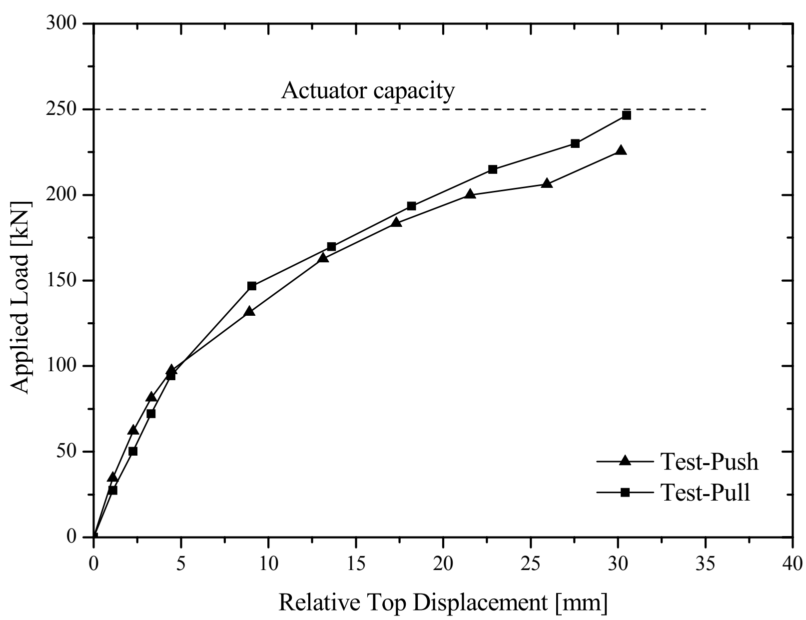

Figure A.3: Envelopes of Specimen BF-F

The loads and corresponding relative displacements in the envelope curves were the values that were attained in each second cycle at each displacement level. The ultimate loads that were reached at end of the test in the pushing and pulling directions are 225.5kN and 246.5kN, respectively. The difference between these load values is due to large out-of-plane deformations that were mainly observed during pushing. The maximum out-of-plane deformation value is approximately 20mm.

A.1.1 Experimental observations

Until the Cycle 10 (5.75mm top displacement, 0.37% drift) specimen BF-F showed completely linear behavior. At the Cycle 10, a gap not more than 2.0mm between the upper edge of the south end plate of the bottom beam and the column flange was observed (Figure A.4).

Figure A.4: Gap between the Beam End Plate and Column Flange
(Specimen BF-F, Cycle 10 and Top Disp. of -5.74mm)

Based on the extrapolation of the shape of the load-deflection hysteresis curve obtained at a top displacement of 5.75mm and load value of 96.8kN and the numerical analysis results from the nonlinear model of the specimen, this displacement was determined to be the experimentally obtained yield point for the specimen BF-F.

Up to Cycle 20, there was no any noticeable failure occurred in the beam-to-column joints. However, the gabs between beam end plates and column flanges became larger and reached approximately 5.0mm. Figure A.5 shows the gab between upper edge of the south end plate of the lower beam and the column flange at the Cycle 19.

Figure A.5: Gap between the Beam End Plate and Column Flange
(Specimen BF-F, Cycle 19 and Top Disp. of 23.20mm)

At the Cycle 20 (22.88mm top displacement, 1.44% drift), loud sound coming from the specimen was suddenly heard., the reason of this sound could not be found up to the Cycle 23 although several inspections were carried out. The load value of 183.5kN in pushing and 193.4kN in pulling direction were obtained. But, no drop of load was observed at this stage. At the Cycle 23, it was recognized that the sound was due to the bolt failure by damaging threads in the upper south joint. This bolt failure is shown in Figure A.6.

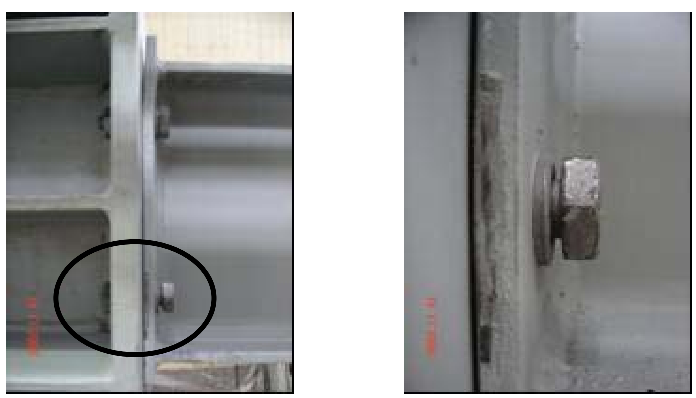

Figure A.6: Failure Bolt at the East Side of the Bottom Bolt-Row
(Specimen BF-F, Cycle 23 and Top Disp. of -34.35mm)

After the Cycle 23, the maximum gab of 8.0mm between the beam end plate and column flange was obtained at the bottom north joint as is shown in Figure A.7.

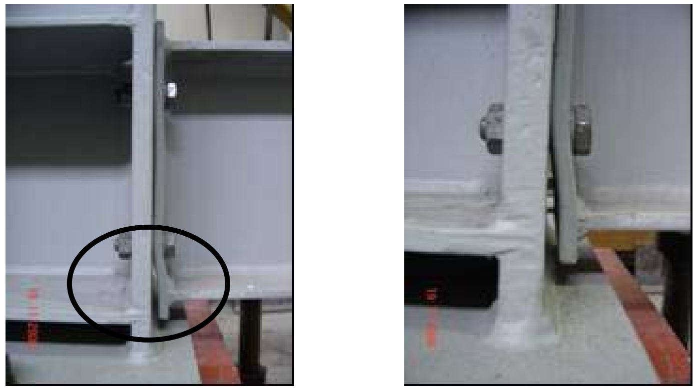

Figure A.7: Gap between the Beam End Plate and Column Flange
(Specimen BF-F, Cycle 25 and Top Disp. of -37.60mm)

The maximum applied load that was attained at the last cycle (Cycle 25) was 246.5kN. Therefore, test was terminated due to the attainment of the actuator capacity and large out-of-plane deformations of the top beam.

APPENDIX B

This section includes the results obtained from the Eurocode 3 procedure by the computer codes to be developed to compute the basic parameters of the beam-to-column connections, with flush end plates and header plates. In calculating the parameters of the intial stiffness and the plastic moment capacity of the joint, the calculation procedure is fundamentally based on Eurocode 3. Additionally, the contribution of the component of the end plate in bending to these fundamental variables is calculated considering the **Faella et al. (2000)**.

B.1 Semi-Rigid Beam-to-Column Joint with Flush End Plate

```
          ********* Initial Rotational Stiffness *********

Bolt row lever arms
--------------------
h( 1 )[mm] =  209.900
h( 2 )[mm] =  49.900

Column flange in bending for joint rotational stiffness
-------------------------------------------------------
Kcfbec[N/mm]=   12087190.000
beffcfbmin1[mm]= 144.827

Column web in tension for joint rotational stiffness
----------------------------------------------------
beffcwt( 1 )[mm] = 0.000
beffcwt( 2 )[mm] = 0.000
Kcwtec[N/mm] =     ∞ (due to stiffeners)

End-plate in bending for joint rotational stiffness
---------------------------------------------------
mep[mm] =          39.675
m2[mm] =           38.012
beffep1ec[mm]=     249.282
beffep2ec[mm]=     222.177
```

```
beffepminec[mm]=   222.177
Kepbec[N/mm]=      623497.100

Bolts in tension for joint rotational stiffness
-----------------------------------------------
Kb( 1 )[N/mm]= 1082401.673
Kb( 2 )[N/mm]= 1082401.673

Column web in shear for joint rotational stiffness
--------------------------------------------------
Avc[mm2] =    4109.443
Kcws[N/mm] =  ∞ (due to stiffeners)

Column web in compression for joint rotational stiffness
--------------------------------------------------------
beffcwc1[mm] =     257.171
beffcwc2[mm] =     253.685
beffcwcminec[mm] = 253.685
Kcwc[N/mm] =       ∞ (due to stiffeners)

Beam flange in compression for joint rotational stiffness
---------------------------------------------------------
Kbfc[N/mm] =       ∞ (as given in EC3)

Beam web in tension for joint rotational stiffness
--------------------------------------------------
Kbwt[N/mm] =       ∞ (as given in EC3)
```

Joint rotational stiffness

Kphi[kN*m/rad] =   16877.486

For alfa =   5.600

```
            ********* Joint Flexural Resistance *********

Column web in shear for flextural resistance
--------------------------------------------
VcwsRd[kN] =  576.539
FcwsRd[kN] =  576.539
```

```
Column web in compression for flextural resistance according to EC
-----------------------------------------------------------------
beffcwc1[mm] =      257.171
beffcwc2[mm] =      253.685
beffcwcminec[mm] = 253.685
omega1 =            0.921
omega2 =            0.764
omega =             0.921
lamdawc =           0.000
roec =              1.000
FcwcRdec[kN] =      578.384

Beam flange and web in compression
----------------------------------
MbRd[kNm] =    130.680
FbfcRd[kN] =   503.002

Bolts in tension for joint flexural resistance according to EC
-------------------------------------------------------------
dr[mm] =     14.131
Ar[mm2] =    156.828
BtRd[kN]=    141.146
FbtRd[kN]=   282.291

Column web in tension for flextural resistance according to EC
-------------------------------------------------------------
mc[mm] =            23.050
ec[mm] =            92.500
eep[mm] =           35.000
ecmin[mm] =         28.813
beffcwt1ec[mm] =    144.827
beffcwt2ec[mm] =    207.825
beffcwtminec[mm] = 144.827
omega1 =            0.921
omega2 =            0.764
omega =             0.921
lamdawc =           0.000
roec =              1.000
FcwtRdec[kN] =      378.293
```

```
Column flange in tension for flextural resistance according to EC
-----------------------------------------------------------------
n[mm]=              28.813
ew[mm]=             7.575
beffcft1ec[mm] =    144.827
beffcft2ec[mm] =    207.825
beffcftminec[mm] =  144.827
Mpcft1Rdec[kNm] =   3167.376
Mpcft2Rdec[kNm] =   3167.376
FcftRd1ec[kN] =     729.203
FcftRd2ec[kN] =     278.973
FcftRdminec[kN] =   278.973

End-plate in tension for flextural resistance according to EC
-------------------------------------------------------------
nep[mm]=            35.000
beffept1ec[mm] =    249.282
beffept2ec[mm] =    222.177
beffeptminec[mm] =  222.177
Mpept1Rdec[kNm] =   1675.772
Mpept2Rdec[kNm] =   1675.772
FeptRd1ec[kN] =     200.686
FeptRd2ec[kN] =     177.192
FeptRdminec[kN] =   177.192

Beam web in tension for flextural resistance according to EC
------------------------------------------------------------
beffbwtminec[mm]=   222.177
FbwtRdec[kN] =      395.920
```

Moment resistance of the joint according to EC

FRdmin[kN]=   177.192

MjRd[kNm] =   37.193

MjRde[kNm] = 24.795

B.2 Semi-Rigid Beam-to-Column Joint with Header Plate

```
          ********* Initial Rotational Stiffness *********

Bolt row lever arms
-------------------
h( 1 )[mm] =      179.500
h( 2 )[mm] =       19.500

Column flange in bending for joint rotational stiffness
-------------------------------------------------------
Kcfbec[N/mm]=   12087190.000
beffcfbmin1[mm]= 144.827



Column web in tension for joint rotational stiffness
----------------------------------------------------
beffcwt( 1 )[mm] = 144.827
beffcwt( 2 )[mm] = 144.827
Kcwtec[N/mm] =     1119780.291

End-plate in bending for joint rotational stiffness
---------------------------------------------------
mep[mm] =         38.543
m2[mm] =          39.400
beffepec(1)[mm]= 242.174
beffepec(2)[mm]= 181.087
beffepec(3)[mm]= 197.923
beffepec(4)[mm]= 128.961
beffepminec[mm]= 128.961
Kepbec[N/mm]=   417937.400

Bolts in tension for joint rotational stiffness
-----------------------------------------------
Kb( 1 )[N/mm]= 1146622.105
Kb( 2 )[N/mm]= 1146622.105

Column web in shear for joint rotational stiffness
--------------------------------------------------
Avc[mm2] =    4109.443
Kcws[N/mm] =  ∞ (due to stiffeners)
```

```
Column web in compression for joint rotational stiffness
--------------------------------------------------------
beffcwc1[mm] =     257.171
beffcwc2[mm] =     238.685
beffcwcminec[mm] = 238.685
Kcwc[N/mm] =       ∞ (due to stiffeners)

Beam flange in compression for joint rotational stiffness
--------------------------------------------------------
(No component and contribution)
```

Joint rotational stiffness

Kphi[kN*m/rad] = 7598.050

For alfa =   8.000

```
            ********* Joint Flexural Resistance *********

Column web in shear for flextural resistance
--------------------------------------------
VcwsRd[kN] =  576.539
FcwsRd[kN] =  576.539

Column web in compression for flextural resistance according to EC
------------------------------------------------------------------
beffcwc1[mm] =     257.171
beffcwc2[mm] =     238.685
beffcwcminec[mm] = 238.685
omega1 =           0.921
omega2 =           0.764
omega =            0.921
lamdawc =          0.541
roec =             1.000
FcwcRdec[kN] =     555.563

Bolts in tension for joint flexural resistance according to EC
--------------------------------------------------------------
dr[mm] =    14.131
Ar[mm2] =   156.828
BtRd[kN]=   141.146
FbtRd[kN]=  282.291
```

```
Column web in tension for flextural resistance according to EC
--------------------------------------------------------------
mc[mm] =           23.050
ec[mm] =           92.500
eep[mm] =          35.000
ecmin[mm] =        28.813
beffcwt1ec[mm] =   144.827
beffcwt2ec[mm] =   207.825
beffcwtminec[mm] = 144.827
omega1 =           0.921
omega2 =           0.764
omega =            0.921
lamdawc =          0.541
roec =             1.000
FcwtRdec[kN] =     378.293

Column flange in tension for flextural resistance according to EC
-----------------------------------------------------------------
n[mm]=             28.813
ew[mm]=            7.575
beffcft1ec[mm] =   144.827
beffcft2ec[mm] =   207.825
beffcftminec[mm] = 144.827
Mpcft1Rdec[kNm] =  3167.376
Mpcft2Rdec[kNm] =  3167.376
FcftRd1ec[kN] =    729.203
FcftRd2ec[kN] =    278.973
FcftRdminec[kN] =  278.973

End-plate in tension for flextural resistance according to EC
-------------------------------------------------------------
nep[mm]=           35.000
beffept1ec[mm] =   242.174
beffept2ec[mm] =   181.087
beffept3ec[mm] =   197.923
beffept4ec[mm] =   128.961
beffeptminec[mm] = 128.961
Mpept1Rdec[kNm] =  972.691
Mpept2Rdec[kNm] =  0.000
FeptRd1ec[kN] =    100.946
FeptRd2ec[kN] =    160.798
FeptRdminec[kN] =  100.946
```

```
Beam web in tension for flextural resistance according to EC
------------------------------------------------------------
beffbwtminec[mm]=  128.961
FbwtRdec[kN] =     229.809
```

Moment resistance of the joint according to EC
--

FRdmin[kN]=   100.946

MjRd[kNm] =   18.120

MjRde[kNm] = 12.080

APPENDIX C

In this section, the detailed information about Δ_{fe}, limiting elastic shear displacement of the frame, is included. In obtaining the formulation of this variable, semi-rigidity of the beam-to-column connections is also considered. Addditionally, it is assumed that the beams are subjected to double curvature bending with zero moment in the midspan section under the lateral load at the top.

C.1 Substructure and Derivation of φ

To simplify the procedure a subassemblage, as shown in Figure C.1, which has been extracted from the actual frame and which comprises the half of the top and bottom beams and a column is utilized. This model is believed to be representative of the actual frame failing in global mode.

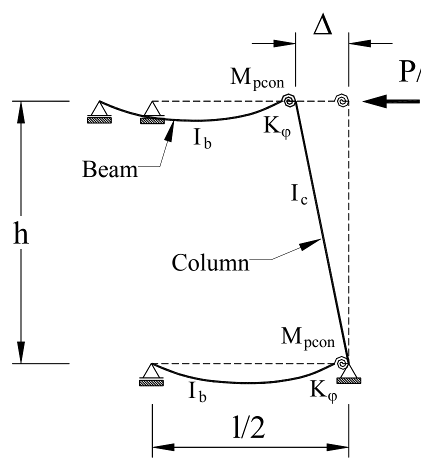

Figure C.1: Simplified Model

The element stiffness coefficient, m_{φ} for the beam, shown in Figure C.2, with the elastic support against rotation at its one end and the roller support at the other end is obtained as given below.

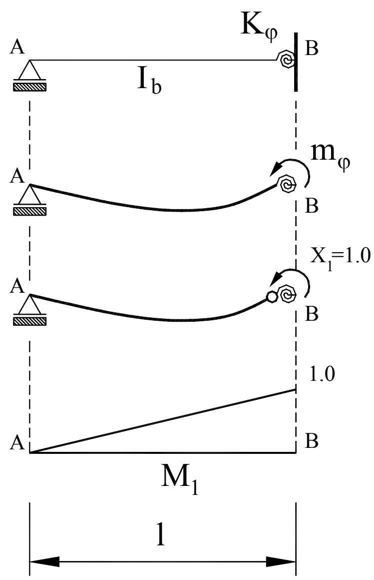

Figure C.2: Beam Element and Unit Displacement at B

Using the force method considering the connection rigidity and above moment diagram;

$$X_1 = m_\varphi = \frac{1}{\dfrac{L}{3EI_b} + \dfrac{1}{K_\varphi}} \tag{C.1}$$

Let's initially take,

$$A = \frac{L}{3EI_b} + \frac{1}{K_\varphi} \tag{C.2}$$

Taking the half of the frame (Figure C.1) into account; $L = L/2$

$$\overline{K} = \frac{K_\varphi L}{EI_b} \tag{C.3}$$

According to EC3 one of the simplest idealizations possible for beam-to-column joints is the elastic-perfectly plastic one. Since the load-deflection response of the specimens is predominantly governed by the nonlinear behavior of the beam-to-column joints the similar approach can be used for the bare frame idealization.

Hence, in accordance with EC3, the half of the initial stiffness of the joint can be taken into account in bare frame idealization for IPFI. Thus, substituting $K_\varphi = K_\varphi / 2$ into Equation C.2,

$$m_\varphi = \frac{6EI_b}{L} \times \frac{\overline{K}}{\overline{K}+12} = \frac{1}{A} \qquad \textbf{(C.4)}$$

The study of the substructure (Figure C.1) subjected to the horizontal force of P/2 applied at the top level provides the following relationship, Equation C.5.

Using the slope deflection method, the linear equations can be written in a matrix form as,

$$\begin{bmatrix} \frac{1}{A}+\frac{4EI_c}{h} & \frac{2EI_c}{h} & \frac{6EI_c}{h^2} \\ \frac{2EI_c}{h} & \frac{1}{A}+\frac{4EI_c}{h} & \frac{6EI_c}{h^2} \\ \frac{6EI_c}{h^2} & \frac{6EI_c}{h^2} & \frac{12EI_c}{h^3} \end{bmatrix} \times \begin{bmatrix} \varphi_1 \\ \varphi_2 \\ \Delta \end{bmatrix} = \begin{bmatrix} 0 \\ 0 \\ \frac{P}{2} \end{bmatrix} \qquad \textbf{(C.5)}$$

in which φ_1, φ_2 are unknown rotations at the joints and δ is the unknown lateral displacement.

For the simplicity of the calculation, assuming that $\varphi_1 = \varphi_2$, then Equation C.5 can be written as,

$$\begin{bmatrix} \frac{1}{A}+\frac{6EI_c}{h} & \frac{6EI_c}{h^2} \\ \frac{6EI_c}{h^2} & \frac{6EI_c}{h^3} \end{bmatrix} \times \begin{bmatrix} \varphi \\ \Delta \end{bmatrix} = \begin{bmatrix} 0 \\ \frac{P}{4} \end{bmatrix} \qquad \textbf{(C.6)}$$

From Equation C.6 and taking, $\xi = \dfrac{\frac{EI_b}{1}}{\frac{EI_c}{h}}$, φ and Δ can be calculated as

$$\varphi = -\frac{Ph}{4} \times \frac{L}{6EI_b} \times \frac{\overline{K}+12}{\overline{K}} \qquad \textbf{(C.7)}$$

$$\Delta = \frac{Ph}{4} \times \frac{Lh}{6EI_b} \times \frac{\overline{K}(1+\xi)+12}{\overline{K}} \tag{C.8}$$

After calculation of φ and Δ, using m_φ and φ M_{con} can be formulated as

$$M_{con} = \frac{6EI_b}{L} \times \frac{\overline{K}}{\overline{K}+12} \times \left(-\frac{Ph}{4} \times \frac{L}{6EI_b} \times \frac{\overline{K}+12}{\overline{K}} \right) \tag{C.9}$$

Hence,

$$M_{con} = -\frac{Ph}{4} \tag{C.10}$$

C.2 Formulation of Δ_{fe}

At the onset of failing the frame with the plastic moments at the joints (connection sections), namely at the stage of $\Delta = \Delta_{fe}$ and $M = M_{pcon}$, using the Equations C.8 and C.10 limiting elastic shear displacement of the frame can be formulated as

$$\Delta_{fe} = \left(\frac{M_{pcon} Lh}{6EI_b} \times \frac{\overline{K}(1+\xi)+12}{\overline{K}} \right) \tag{C.11}$$

APPENDIX D

This section deals with the R factor, response modification factor, which is proposed for the TSPSWs whose infill panels are connected to the beams and columns on their edges. For the purpose of this, ATC-19 is primarily considered.

Currently, the UBC-97, IBC-2000 as well as Turkish Seismic Code-2007 do not give any value of R for steel plate shear walls. However, the Canadian code discusses only unstiffened relatively thin steel plate shear walls welded along their boundaries to beams and columns (**Astaneh-Asl, 2001**).

There is no specific research which has been done on identifying all variables affecting R. But, by studying the data from performance of structures during earthquakes, test results and analytical studies, it seems that R factor depends on basically ductility, overstrength, period of vibration and redundancy in the system (**ATC-19, 1995**).

D.1 Tentatively Proposed Values of R by Astaneh-Asl (2001)

The proposed design coefficients and factors for four seismic-resisting systems with steel plate shear walls are listed in Table D.1.

Table D.1: Proposed Design Coefficients and Factors for Steel Plate Shear Wall Seismic Force-Resisting Systems

Basic Seismic Force-Resisting System	Response Modification Factor, R	System Overstrength Factor, Ω_o	Deflection Amplification Factor, C_d
Unstiffened steel plate shear walls inside gravity carrying steel frame with simple beam-to-column connections	6.5	2.0	5
Stiffened steel plate shear walls inside gravity carrying steel frame with simple beam-to-column connections	7.0	2.0	5
Dual system with special steel moment frames and unstiffened steel plate shear walls	8.0	2.5	4
Dual system with special steel moment frames and stiffened steel plate shear walls	8.5	2.5	4

D.2 Values of R

According to ATC-19, R is splitted into three factors that account for contributions from reserve strength, ductility and redundancy, as follows:

$$R = R_S \times R_\mu \times R_R \qquad \textbf{(D.1)}$$

in which,

R_S: the period-dependent strength factor,

R_μ: the period-dependent ductility factor,

R_R: redundancy factor,

D.2.1 Strength factor (R_S)

The maximum lateral strength of a building will generally exceed its design strength. The factor is used to amplify seismic forces in design of specified structural elements and their connections to adjoining elements (**SEAOC, 1999**). Such use of this factor is adopted by Turkish Seismic Code-2007. A method for evaluating the reserve strength of a building follows.

$$R_S = \frac{V_o}{V_d} \qquad \textbf{(D.2)}$$

where,

V_o: the base shear force at the roof displacement corresponding to the limiting state of response,

V_d: the design base shear,

In design of the test specimen SW-A-H, design base shear force was taken to be equal to V_o (load capacity of actuator). Then, an assumption is required to establish R_S factor. This factor can be taken as 2.0 for the specimen SW-A-H by considering semi-rigid beam-to-column connections and screw connections used to attach the infill panel to beams and columns.

D.2.2 Ductility factor (R_μ)

Displacement ductility ratio at the system level is used to determine the ductility factor. It must be recognized that the ductility factor is a measure of the nonlinear response of the complete framing system and not components of the framing system **(ATC-19, 1995)**.

The evaluation of ductility factor is based on Newmark and Hall (1982) given in **ATC-19 (1995)**. According to this research, the relationship that can be used to estimate the ductility factor, R_μ for elasto-plastic SDOF systems as follows:

for periods below 0.03 seconds:

$$R_\mu = 1.0 \tag{D.3}$$

for periods between 0.12 and 0.50 seconds:

$$R_\mu = \sqrt{2\mu - 1} \tag{D.4}$$

for periods exceeding 1.00 seconds:

$$R_\mu = \mu \tag{D.5}$$

in which,

μ: the displacement ductility ratio which is generally defined as the ratio of limit state displacement (Δ_m) to yield displacement (Δ_y).

When this method is applied to the specimen SW-A-H an assumption is again needed due to the fact that a system is not considered. In experimental and analytical studies that were conducted within this research are included structural components such as steel bare frames and TSPSWs. However, the period is generally larger than 1.0 for a multi-storey steel buildings using TSPSWs as a lateral load-resisting system. Therefore, for the specimen SW-A-H, R_μ can be taken to be equal to μ.

D.2.3 Redundancy factor (R_R)

A redundant seismic framing system should be composed of multiple vertical lines of framing, each designed and detailed to transfer seismic-induced internal forces to the foundation **(ATC-19, 1995)**

Degree of redundancy of a structure can be considered at two levels **(Astaneh-Asl, 2001)**:

a) at the global structural level by studying how many lateral force resisting systems there are in the structure and how well they are distributed in the plan and over the height of the structure,
b) at the local level of lateral load resisting system itself by studying how much redundancy and force distribution capability the lateral force resisting system has within a given story and over the height.

It is repoted by **Astaneh-Asl (2001)** that tests of one to four–story steel plate shear wall systems have indicated that steel shear walls have very high degree of redundancy by the fact that infill panels are highly indeterminate systems. During the test of SW-A-H, at Cycle $6\delta_y$, although 140mm long tear of the infill panel occurred in upper north corner, no strength degradation was observed and the wall was still carrying the applied load.

Hence, it is assumed that the specimen SW-A-H has excellent redundancy and R_R is equal to1.0.

D.3 Proposed Value of R for TSPSWs

When we consider the information given above, the value that is calculated as given in Equation D.1 can be assigned to value of R.

Overstrength factor, $R_S = 2.0$

Redundancy factor, $R_R = 1.0$

In determining the ductility factor, displacement ductility ratio of the specimen SW-A-H is taken into account. In order to obtain this value, the pushover curve from the calibrated nonlinear finite element model is considered. The nonlinear response of the specimen is idealized using equal-energy method. The application of this method is shown in Figure D.1.

The ultimate displacement value of 31.40mm is experimentally obtained. This value is the peak displacement attained in the cyclic test of the specimen SW-A-H.

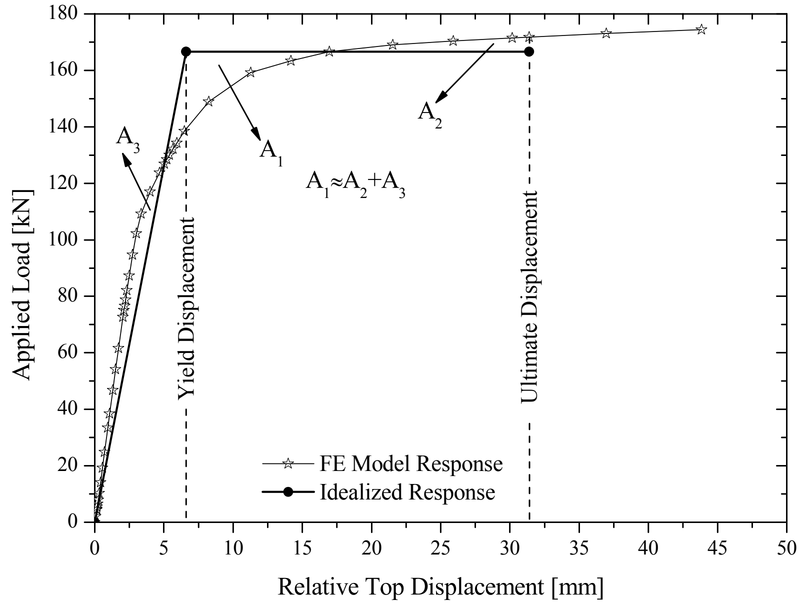

Figure D.1: Idealization of Pushover Curve for Specimen SW-A-H

If the drift ratio is limited to 1.5%,

Ductility factor, $R_{\mu} = \mu = \dfrac{18.00}{6.61} \cong 2.72$

If the drift limit state is removed, on the other hand, the maximum lateral displacement is equal to the displacement corresponding to the limit state,

Ductility factor, $R_{\mu} = \mu = \dfrac{31.40}{6.61} \cong 4.75$

Therefore,

$R = 2.0 \times 2.72 \times 1.0 \cong 5.4$ (when drift limit state considered)

$R = 2.0 \times 4.75 \times 1.0 \cong 9.5$ (when drift limit state not considered)

The latter value is found to be higher than those proposed by **Astaneh-Asl (2001)**. For the reasons and under the assumptions mentioned above, these values for R are approximate only. Much additional study and full system analysis are needed before values of R can be rationally assigned to new systems. When we consider the infill panels connected to the boundary frames by screws or bolts, it is very clear that the failure will occur in such a way that infill plate fractures in net section. Therefore, it can be suggested that small values should be assigned to response modification factors, R for such thin steel plate shear walls.

APPENDIX E

A theoretical hysteresis curve is proposed based fundamentally on the test results and researches conducted by **Mimura and Akiyana (1977)**, **Tromposch and Kulak (1987)** and **Driver et al. (1998a)**.

The load-displacement responses of the bare frame and infill plate which are considered in developing the theoretical hysteresis curves for SW-A-H and SW-B-H specimens are given in Figure E.1 and E.2, respectively.

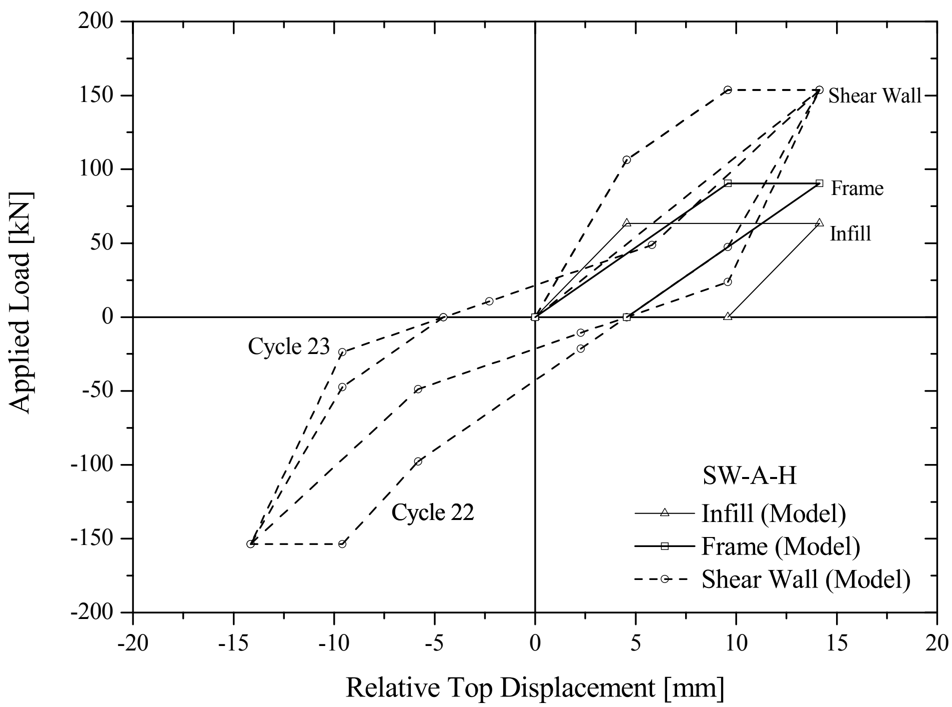

Figure E.1: Components of Proposed Hysteresis Curve for SW-A-H

In Figure E.1 and E.2, the load-displacement behavior of the infill panel under the shear force is represented by bilinear curve for the simplicity. Additionally, to better predict the energy dissipation per cycle it is assumed that $C_1 = 2.0$ and $C_2 = 0.75$ for the infill plate of SW-A-H and that $C_1 = 1.50$ and $C_2 = 0.70$ for that of SW-B-H.

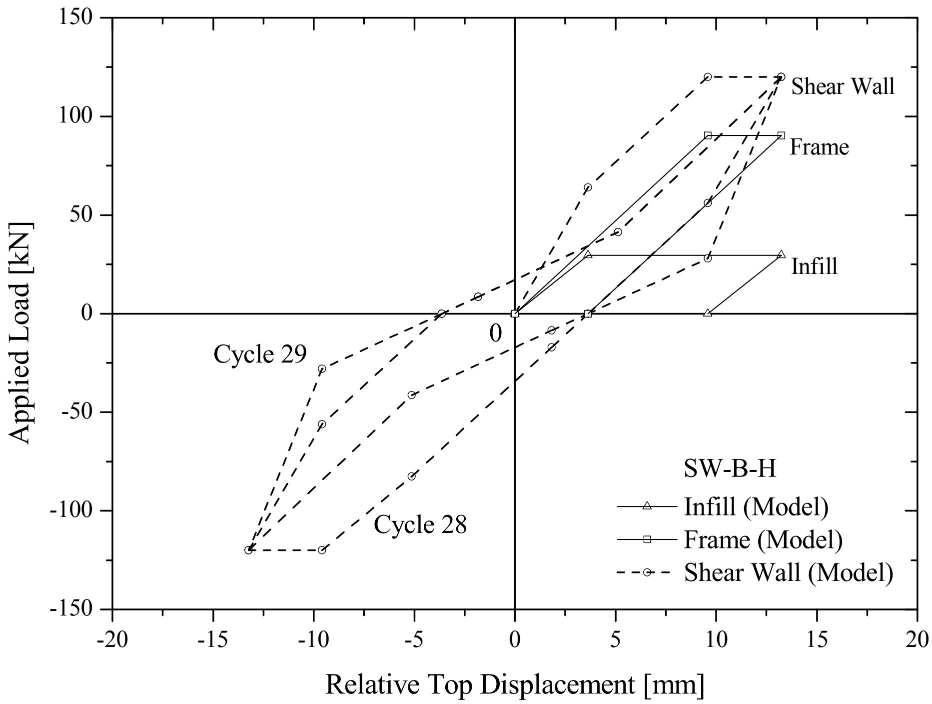

Figure E.2: Components of Proposed Hysteresis Curve for SW-B-H

The parameters of the proposed hysteresis curve for TSPSW specimens are shown in the Figure E.3.

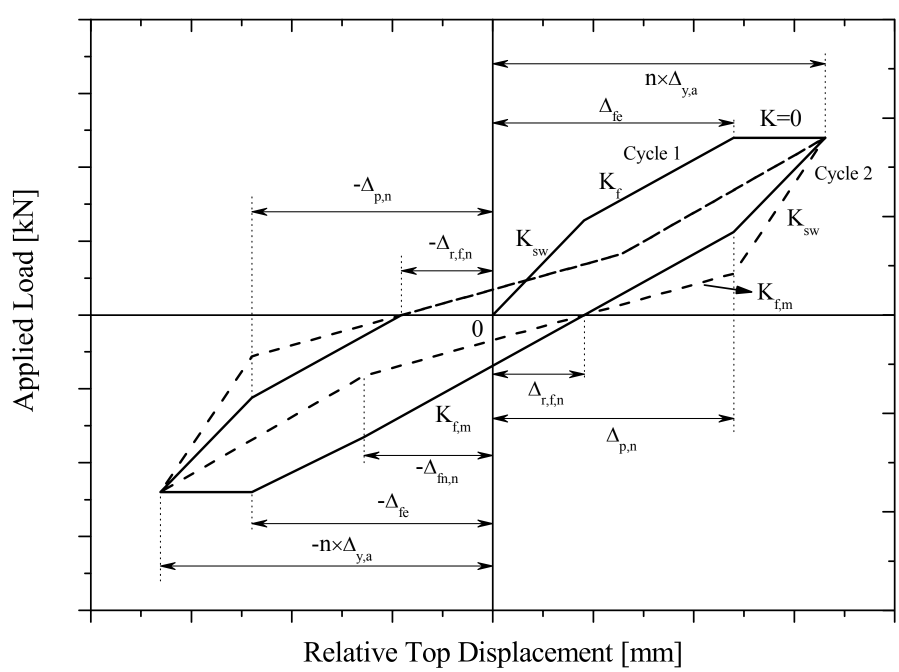

Figure E.3: Parameters of the Proposed Hysteresis Curve

These parameters can be computed as follows for specimen SW-A-H:

$$K_{f,m} = (1.0 \sim 0.20) \times K_f$$

The parameter $K_{f,m}$ for each specified cycle can be defined in the following based on the test results.

$K_{f,m} = 1.0 \times K_f$ for the first cycle at $2\times\Delta_{y,a}$

$K_{f,m} = 0.50 \times K_f$ for the second cycle at $2\times\Delta_{y,a}$

$K_{f,m} = 0.40 \times K_f$ for the second cycle at $3\times\Delta_{y,a}$

$K_{f,m} = 0.30 \times K_f$ for the second cycle at $4\times\Delta_{y,a}$

$K_{f,m} = 0.30 \times K_f$ for the second cycle at $5\times\Delta_{y,a}$

$K_{f,m} = 0.20 \times K_f$ for the second cycle at $6\times\Delta_{y,a}$

Other parameters can be expressed that,

K_{sw}: $K_f + K_p$

K_{sw}: initial stiffness of the shear wall

$$\Delta_{y,a} = \frac{\Delta_{pe} + \Delta_{fe}}{2}$$

$\Delta_{y,a}$: Average of infill and frame yield displacements

$\Delta_{p,2} = \Delta_{r,p,0}$; n = 2, (for the cycle at $2\times\Delta_{y,a}$)

$\Delta_{p,2}$: displacement of infill at cycle $2\times\Delta_{y,a}$

$\Delta_{r,p,0}$: residual displacement of infill at cycle $2\times\Delta_{y,a}$

n: the number of displacement steps after the cycle of $1\times\Delta_{y,a}$

$$\Delta_{r,p,0} = \Delta_t - \frac{P_{pu}}{K_p};\ \Delta_t = n \times \Delta_{y,a}$$

$\Delta_{p,n} = \Delta_{p,(n-1)} + \Delta_{y,a}$; n = 3,….., n

$\Delta_{r,f,2} = \Delta_{r,f,0}$; n = 2, (for the cycle at $2\times\Delta_{y,a}$)

$$\Delta_{r,f,0} = \Delta_t - \frac{P_{fu}}{K_f}\,;\ \Delta_t = n \times \Delta_{y,a}$$

$$\Delta_{r,f,n} = \Delta_{r,f,(n-1)} + 0.5 \times \Delta_{y,a}\,;\ n = 3,\ldots.., n$$

$$\Delta_{fn,2} = 0.5 \times \Delta_{r,f,2} + 0.5 \times \Delta_{y,a}$$

$$\Delta_{fn,n} = 0.5 \times \Delta_{r,f,n} + 0.5 \times \Delta_{y,a}\,;\ n = 3,\ldots.., n$$

The parameters of the proposed hysteresis curve for SW-B-H are similar to those given for SW-A-H. The expressions that are different from those shown above can be calculated in the following.

$$K_{f,m} = (1.0 \sim 0.15) \times K_f$$

The parameter $K_{f,m}$ for each specified cycle can be defined in the following based on the test results.

$K_{f,m} = 1.0 \times K_f$ for the first cycle at $2\times\Delta_{y,a}$

$K_{f,m} = 0.50 \times K_f$ for the second cycle at $2\times\Delta_{y,a}$

$K_{f,m} = 0.25 \times K_f$ for the second cycle at $3\times\Delta_{y,a}$

$K_{f,m} = 0.20 \times K_f$ for the second cycle at $4\times\Delta_{y,a}$

$K_{f,m} = 0.15 \times K_f$ for the second cycle at $5\times\Delta_{y,a}$

$\Delta_{r,f,2} = \Delta_{r,f,0}$; n = 2, (for the cycle at $2\times\Delta_{y,a}$)

$$\Delta_{r,f,0} = \Delta_t - \frac{P_{fu}}{K_f}\,;\ \Delta_t = n \times \Delta_{y,a}$$

$$\Delta_{r,f,n} = \Delta_{r,f,(n-1)} + \Delta_{y,a}\,;\ n = 3,\ldots.., n$$

The comparisons which are made between some specified test cycles and the proposed hysteresis curves for TSPSW specimens are shown in the Figure E.4~E.20.

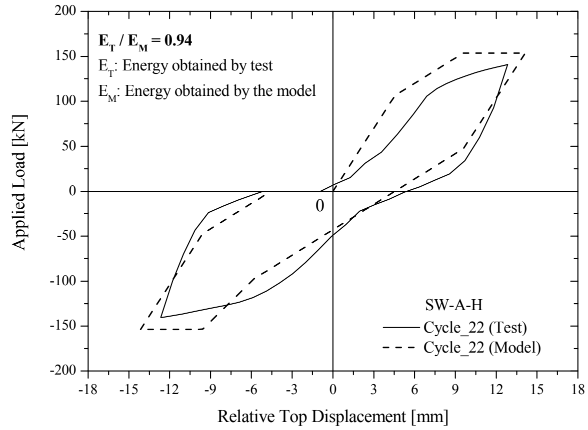

Figure E.4: Cycle 22 of SW-A-H

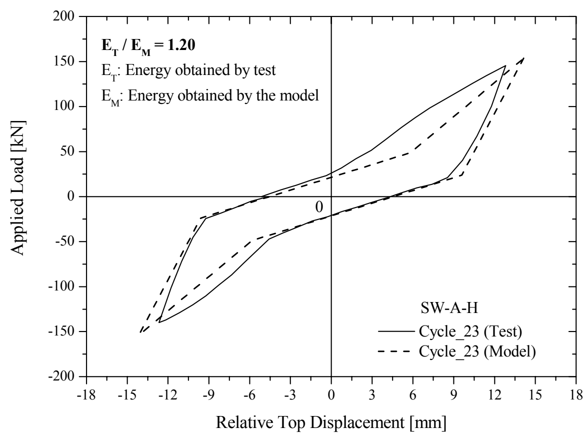

Figure E.5: Cycle 23 of SW-A-H

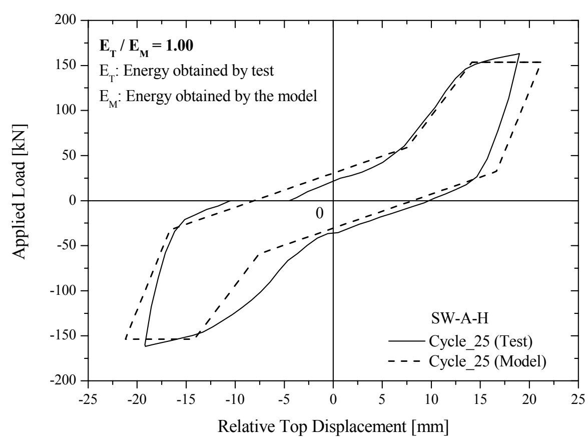

Figure E.6: Cycle 25 of SW-A-H

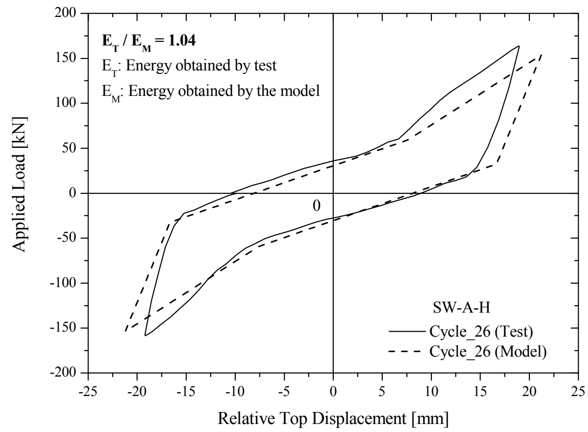

Figure E.7: Cycle 26 of SW-A-H

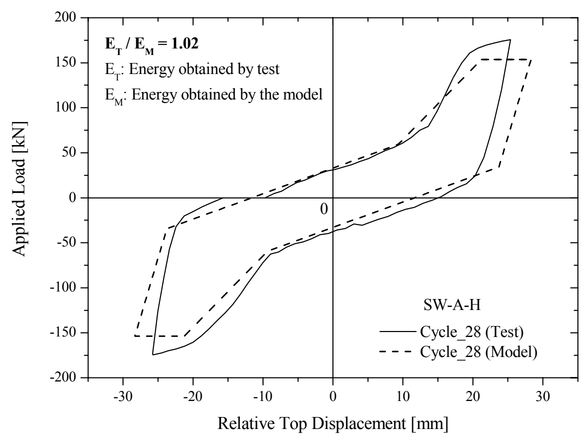

Figure E.8: Cycle 28 of SW-A-H

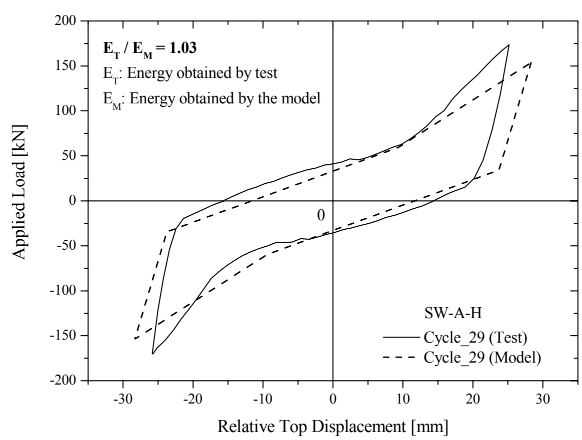

Figure E.9: Cycle 29 of SW-A-H

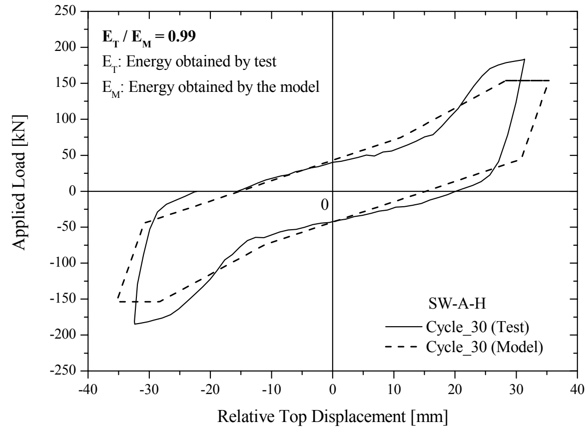

Figure E.10: Cycle 30 of SW-A-H

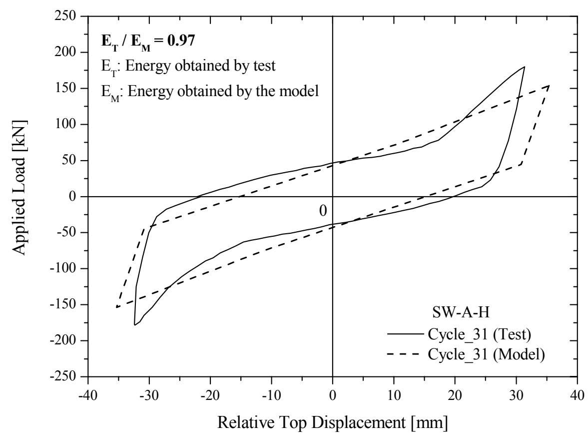

Figure E.11: Cycle 31 of SW-A-H

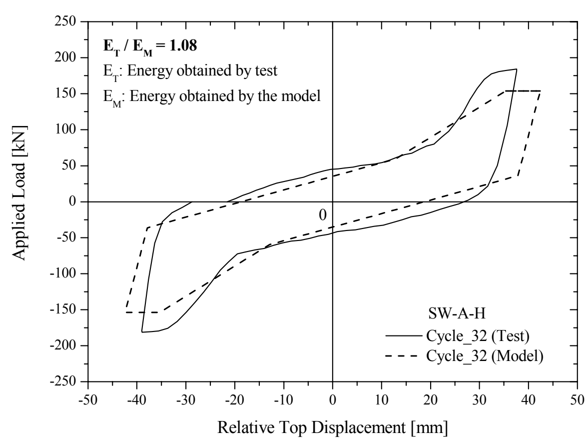

Figure E.12: Cycle 32 of SW-A-H

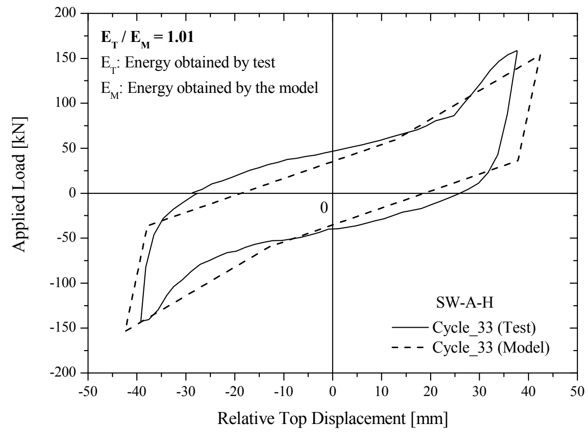

Figure E.13: Cycle 33 of SW-A-H

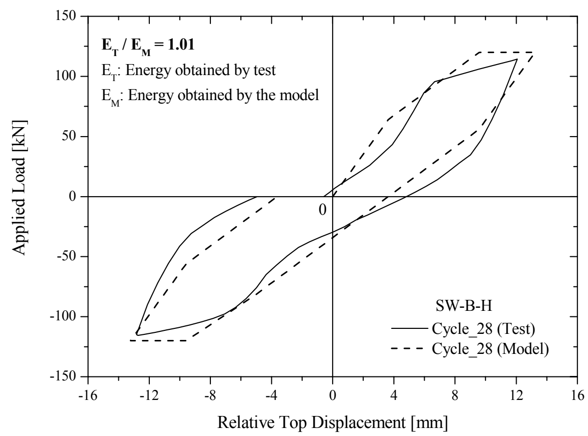

Figure E.14: Cycle 28 of SW-B-H

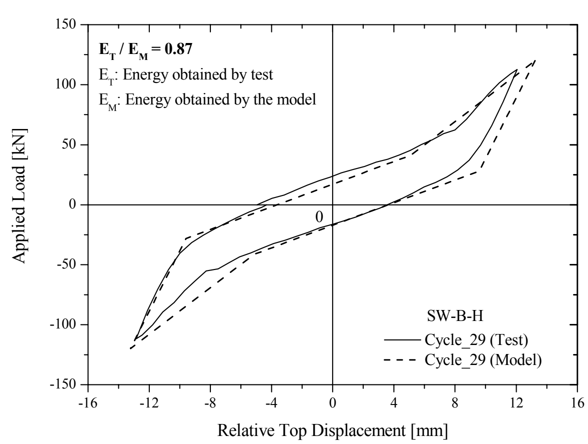

Figure E.15: Cycle 29 of SW-B-H

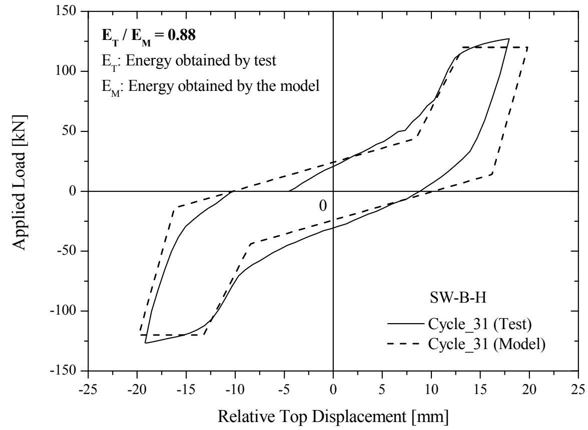

Figure E.16: Cycle 31 of SW-B-H

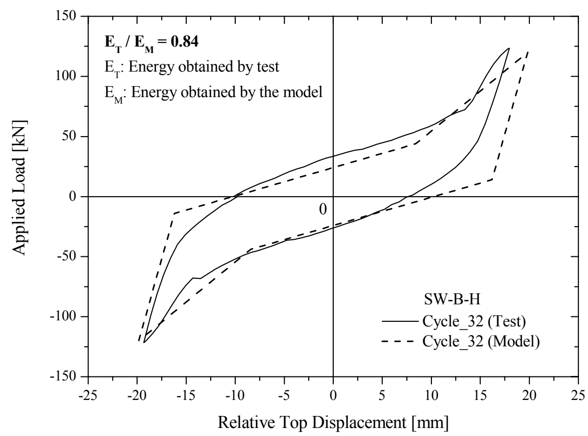

Figure E.17: Cycle 32 of SW-B-H

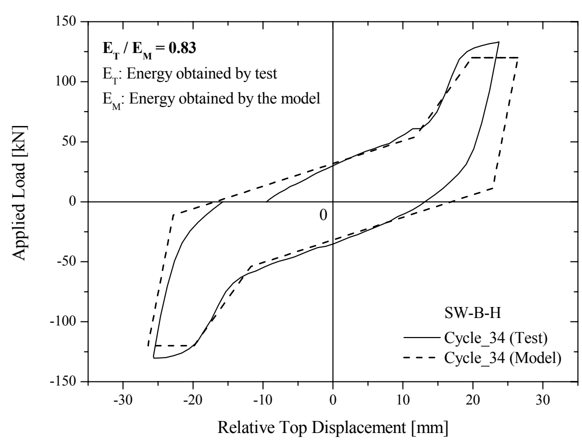

Figure E.18: Cycle 34 of SW-B-H

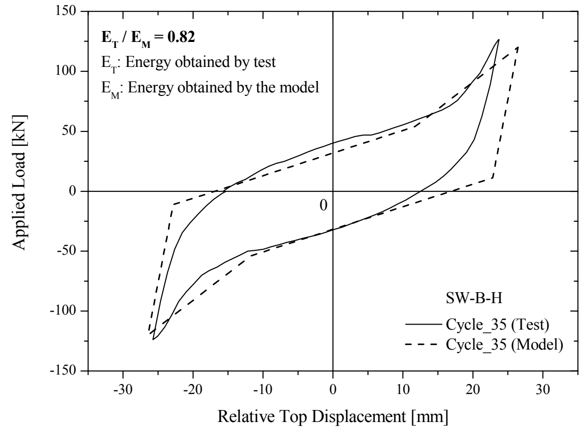

Figure E.19: Cycle 35 of SW-B-H

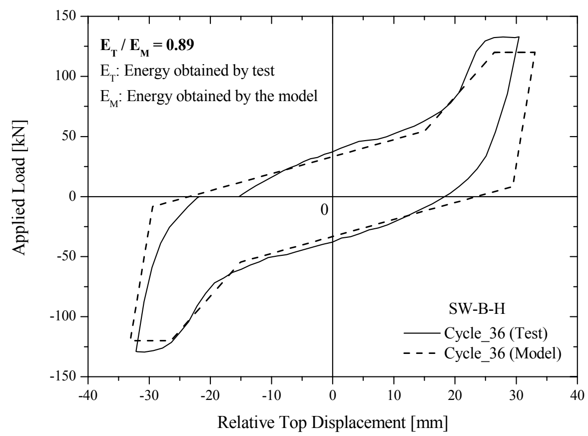

Figure E.20: Cycle 36 of SW-B-H

BIOGRAPHY

Cüneyt Vatansever was born in Bursa, on November 01, 1974. He attended the primary school in Bursa, and concluded his primary education in Bursa in 1986. He continued his high school education in Bursa Atatürk High School, and graduated from the high school in 1992.

In September, 1992, he was enrolled as an undergraduate student at the Technical University of Yıldız (YTU), Division of Civil Engineering. He received the Bachelor of Science degree in Civil Engineering Program from the YTU in August, 1996. After graduation, he was enrolled as a graduate student at the Istanbul Technical University (ITU), Division of Civil Engineering. He was awarded the Master of Science degree in Civil Engineering program from the ITU Institute of Science and Technology in July, 2000. In the same year, he started his doctorate at the same program. He is currently working as a research and teaching assistant in Division of Civil Engineering of ITU, Faculty of Civil Engineering.